Analysis of the Asc1p/RACK1 microenvironment in *Saccharomyces cerevisiae* using proximity-dependent Biotin Identification (BioID) and high-resolution mass spectrometry

Dissertation

for the award of the degree

"Doctor rerum naturalium"

of the Georg-August-Universität Göttingen

within the doctoral program "Molecular Biology of Cells"

of the Georg-August-University School of Science (GAUSS)

submitted by

Nadine Opitz
née Smolinski

from Peine

Göttingen 2016

Thesis Committee

Dr. Oliver Valerius
Department of Molecular Microbiology and Genetics
Institute of Microbiology and Genetics, Georg-August-University Göttingen

Prof. Dr. Heike Krebber
Department of Molecular Genetics
Institute of Microbiology and Genetics, Georg-August-University Göttingen

Dr. Achim Dickmanns
Department for Molecular Structural Biology
Institute of Microbiology and Genetics, Georg-August-University Göttingen

Members of the Examination Board

Referee: Dr. Oliver Valerius
Department of Molecular Microbiology and Genetics
Institute of Microbiology and Genetics, Georg-August-University Göttingen

2nd Referee: Prof. Dr. Heike Krebber
Department of Molecular Genetics
Institute of Microbiology and Genetics, Georg-August-University Göttingen

Further members of the Examination Board

Prof. Dr. Gerhard Braus
Department of Molecular Microbiology and Genetics
Institute of Microbiology and Genetics, Georg-August-University Göttingen

Prof. Dr. Rolf Daniel
Department of Genomic and Applied Microbiology
Institute of Microbiology and Genetics, Georg-August-University Göttingen

Prof. Dr. Kai Heimel
Department of Molecular Microbiology and Genetics
Microbial Cell Biology
Institute of Microbiology and Genetics, Georg-August-University Göttingen

Dr. Hans Dieter Schmitt
Department of Neurobiology
Project Group Membrane Transport in Yeast
Max Planck Institute for Biophysical Chemistry, Göttingen

Date of oral examination: 19th October 2016

I hereby declare that the doctoral thesis entitled "Analysis of the Asc1p/RACK1 microenvironment in *Saccharomyces cerevisiae* using proximity-dependent Biotin Identification (BioID) and high-resolution mass spectrometry" has been written independently and with no other sources and aids than quoted.

_____

Nadine Opitz

Parts of this work are published in

Smolinski, N., and Valerius, O. (2016). Nachbarschaftsstudien am Ribosom: *proximity dependent biotin identification.* BIOspektrum *22*, 134–136.

Opitz, N., Schmitt, K., Hofer-Pretz, V., Neumann, B., Krebber, H., Braus, G.H., Valerius, O. (2017). Capturing the Asc1p/RACK1 microenvironment at the head region of the 40S ribosome with quantitative BioID in yeast. Mol. Cell. Proteomics, doi: 10.1074/mcp.M116.066654.

Acknowledgement - Danksagung

Mein erster und besonderer Dank gilt Dr. Oliver Valerius für die engagierte Betreuung dieser Arbeit. Wertvolle Diskussionen sowie gemeinsame Überlegungen zu immer neuen Herausforderungen dieses Projektes haben wesentlich zum Gelingen dieser Arbeit beigetragen. Vielen Dank für die vielseitige Unterstützung und das entgegengebrachte Vertrauen.

Prof. Dr. Gerhard Braus danke ich für die Möglichkeit in einem anregenden Arbeitsumfeld in der *Abteilung für Molekulare Mikrobiologie und Genetik* promovieren zu können. Darüber hinaus möchte ich mich für Ideen und Ratschläge im Rahmen der Progress Reports bedanken.

Meinen Thesis Committee Mitglieder Prof. Dr. Heike Krebber und Dr. Achim Dickmanns danke ich für hilfreiche Anregungen und Gedanken zur Weiterentwicklung meiner Projekte und die angenehme Atmosphäre bei den Thesis Committee Meetings. Außerdem möchte ich mich bei Prof. Dr. Heike Krebber und der *Abteilung für Molekulare Genetik* für die nette Zusammenarbeit und Hilfestellungen u.a. bei der Dichtegradientenzentrifugation bedanken.

Des Weiteren danke ich Dr. Hans Dieter Schmitt und Dr. Sabrina Beckmann für die Anregung zum BioID-Experiment und für die Bereitstellung des *birA**-Plasmids.

Ein großer Dank gilt allen Mitgliedern des Labors 115. Dr. Kerstin Schmitt danke ich für die enge und ergiebige Zusammenarbeit und für die Unterstützung insbesondere in der finalen Phase meiner Doktorarbeit. Des Weiteren danke ich Verena Hofer-Pretz für die hervorragende technische Unterstützung in den ersten drei Jahren, sowie Ute Neef für die engagierte technische Assistenz im letzten Jahr dieser Arbeit. Bei Anika Kühn möchte ich mich für hilfreiche Anregungen und Ratschläge insbesondere zu methodischen Fragestellungen bedanken. Ich danke euch für die unbeschwerte Zeit im Labor und für eure Freundschaft. Außerdem danke ich allen Masterstudenten, die mit ihren Laborrotationen und Masterarbeiten dieses Projekt unterstützt haben.

Darüber hinaus möchte ich mich bei allen Mitgliedern der *Abteilung für Molekulare Mikrobiologie und Genetik* für die große Hilfsbereitschaft bei den kleinen und großen Herausforderungen des Alltags und das damit verbundene angenehme Arbeitsklima bedanken. Den Mitarbeitern der Göttinger Graduiertenschule für Neurowissenschaften, Biophysik und Molekulare Biowissenschaften (GGNB) danke ich für die hervorragende Organisation und die vielseitigen Hilfestellungen.

Ich möchte mich außerdem herzlich bei meiner Familie für ihre Unterstützung und das stetige Interesse an meiner Arbeit bedanken. Maik danke ich von Herzen für das große Verständnis und unzählige Ermutigungen während der letzten vier Jahre. Danke für deinen grenzenlosen Rückhalt und dein Vertrauen in mich.

Table of Contents

I

List of Figures

List of Tables

List of Supplementary Figures

List of Supplementary Tables

Abstract

The conserved ribosome-associated Asc1 protein of *Saccharomyces cerevisiae* forms a seven bladed β-propeller and binds to the head region of the 40S ribosomal subunit in close proximity to the mRNA exit tunnel. Asc1p is considered a scaffold protein organizing the local microenvironment near the area of translation initiation at the ribosome to link mRNA translation with cellular signaling. In this study, proteins in the direct proximity of Asc1p were discovered with the *in vivo* protein labeling technique *proximity-dependent Biotin IDentification* (BioID) in combination with high-resolution mass spectrometry. The RNA polymerase II degradation factor Def1p and the ribosomal clamping factor Stm1p as well as mRNA-binding proteins and translational/transcriptional regulators appeared as Asc1p-proximal proteins during exponential cell growth. In addition to mRNA-binding proteins close to Asc1p at exponential growth such as Scp160p, Sro9p and Gis2p, mild heat stress increasingly attracts further mRNA-binding proteins, namely Hek2p, New1p, and Psp2p into the Asc1p proximity. Phenotypes caused by the synthetic deletion of the *SCP160* or *STM1* gene in *asc1⁻* cells also revealed genetic interactions. Additionally, proteins required for mRNP granule formation and activity reflect Asc1p's impact on P-body homeostasis. Starvation for glucose caused severe changes in the Asc1p-neighborhood: Ribosomal proteins of the small and the large ribosomal subunit, and the ubiquinone biosynthetic enzyme Coq5p accumulated in the Asc1p proximity and replaced most of the proteins present during exponential growth. These changes might reflect a general aggregation of ribosomes at glucose starvation, and might indicate a channeling of translation capacities towards mitochondria. The Asc1$^{R38D\ K40E}$ protein variant was described to be ribosome-binding compromised, however, was revealed here as capable to bind the ribosome *in vivo*. Additional proximal proteins suggest either a subpopulation of Asc1$^{R38D\ K40E}$p apart from the ribosome or spatial flexibility of the protein at the ribosome. To study physical Asc1p-protein interactions in further detail, *ASC1* alleles were constructed for the site-specific incorporation of the photo-reactive amino acid Bpa as cross-linker into the Asc1 protein at different sites. Future *in vitro* cross-linking experiments of these Asc1^{Bpa}p variants with some of the identified proximal proteins will lead to detailed knowledge about the nature of the interactions. Overall, the Asc1p microenvironment suggests that the β-propeller not only coordinates protein biosynthesis with cellular signaling, but beyond that synchronizes these processes with nuclear mRNA synthesis.

1. Introduction

1.1 Scaffold proteins in cellular signaling and complex organization

Scaffold proteins are mediators of protein-protein interactions and function as organizers of multiprotein complex assemblies (Pan et al., 2012; Vondriska et al., 2004). Through the regulation of protein proximities, scaffolds promote or prevent posttranslational modifications of their nearby proteins and control their activities and the status of whole protein complexes (reviewed in Pan et al., 2012). Hence, scaffold proteins have a major impact on cellular signaling. They fine-tune signal transmission in a spatiotemporal manner by arranging components of signaling cascades, e.g. kinases or phosphatases and their substrates, in a way that enables directed signal wiring (Fig. 1A; reviewed in Elion, 2001; Shaw and Filbert, 2009). The *Saccharomyces cerevisiae* Ste5 protein is considered as a scaffold prototype in cellular schmitsignaling and as such regulates the <u>mi</u>togen <u>a</u>ctivated <u>p</u>rotein <u>k</u>inase (MAPK) cascade of the pheromone response pathway. Pheromone sensing by a seven-transmembrane receptor initiates the mating pathway and mobilizes the heterotrimeric G-protein composed of the Gα-subunit Gpa1p and the Gβ/γ-heterodimer Ste4p/Ste18p (see also Fig. 5). Dissociation of the Gβ/γ-heterodimer from the Gα-subunit thereupon activates the MAPK cascade consisting of Ste20p (MAP4K), Ste11p (MAP3K), Ste7p (MAP2K) and the MAPK Fus3p. Ste5p scaffolds the phosphorylation cascade by the sequential arrangement of Ste11p, Ste7p and Fus3p (Fig. 1A, see also Fig. 5; reviewed in Dohlman, 2002; Elion, 2001).

Additionally to the spatial organization of cascade participants, a scaffold protein can influence complex activity by an allosteric inhibition of a catalytic binding partner within the assembly. The accessory recruitment of further interacting proteins or a modification of the scaffold itself subsequently inverses the inhibitory effect (Fig. 1B; Bhattacharyya et al., 2006; reviewed in Pan et al., 2012). In general, posttranslational modifications, like phosphorylation, ubiquitylation, sumoylation or lipidation, affect the structural and physical properties of a scaffold, and thereby dynamically coordinate the binding affinity for specific interaction partners according to spatial and temporal requirements (Fig. 1C; reviewed in Pan et al., 2012). Lipid modifications, e.g. by phosphoinositides, are prevalently used to target scaffold proteins with their associated interaction partners to membranes, like plasma membranes, and Golgi or nuclear membranes (Fig. 1D; reviewed in Cho, 2006; Lemmon and Ferguson, 2000). Additionally, scaffold proteins can guide protein assemblies to further subcellular localizations, e.g. into the nucleus, the Golgi apparatus, endosomes and mitochondria (reviewed in Shaw and Filbert, 2009). Thus, scaffold proteins play a major role within eukaryotes in the cellular response to external and internal stimuli by regulating the functional interplay of protein

assemblies in terms of space, time, and protein complex activity. Accordingly, scaffolds are crucial for fundamental processes as diverse as gene expression, protein synthesis and turnover, metabolism, and membrane and cytoskeleton dynamics (Pan et al., 2012).
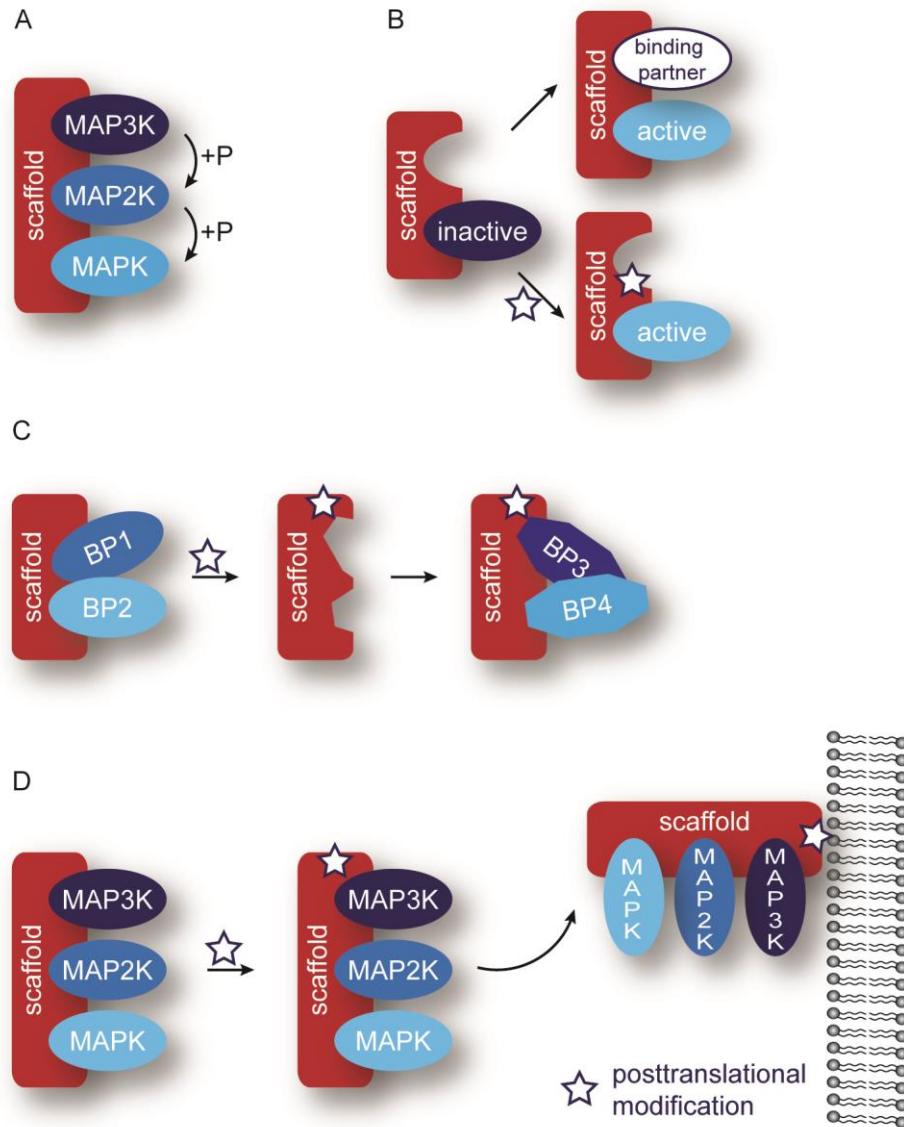
Fig. 1: Scaffold proteins fulfill versatile functions. (A) Scaffold proteins can serve as binding platforms that provide proximity between components of phosphorylation cascades (+P) and thereby facilitate signal propagation. (B) The association of a catalytic protein to a scaffold can influence its activity, an effect that can be reversed by the additional interaction of the scaffold with another binding partner or by posttranslational modification of the scaffold. (C) Posttranslational modifications influence the structural and physical properties of a scaffold protein and thereby regulate the dynamic interactions with specific binding partners (BP). (D) Scaffolds can target their associated proteins to specific subcellular localizations, e.g. lipidations guide scaffold proteins and their binding partners to membranes.

Scaffold proteins feature multiple protein binding domains, which enable the simultaneous interaction with various proteins for complex assembly (reviewed in Vondriska et al., 2004). There are hundreds of different domains that can specify a protein's binding capacities (http://smart.embl-heidelberg.de/). The WD40 domain is one of the most prominent protein interaction domains in scaffold proteins, typically without own catalytic activity (Stirnimann et al., 2010). One domain consists of several WD40 repeats which, are composed of 44 to 66 amino acids with a glycine-histidine dipeptide in the N-terminal region and a tryptophan-aspartate (WD) motif at the C-terminus (reviewed in Stirnimann et al., 2010; Xu and Min, 2011). The most common WD40 protein architecture is characterized by a seven-bladed β-propeller, which provides an adequate surface for protein-protein interactions (Stirnimann et al., 2010). In *S. cerevisiae* - the eukaryotic model organism used in this study - 105 proteins are so far identified as WD40 repeat containing proteins with in total 543 WD40 domains (http://smart.embl-heidelberg.de). These proteins are involved in transcription, RNA processing, mRNA translation, protein degradation, intracellular trafficking and cytoskeleton assembly, and couple these processes to cellular signaling events.

1.2 The WD40 protein Asc1

The Gβ-like Asc1 protein of *S. cerevisiae* belongs to the family of WD40 proteins and consists of seven WD40 repeats (Fig. 2A; Chantrel et al., 1998). Crystallization of recombinant *S. cerevisiae* Asc1p expressed in *Escherichia coli* revealed one single WD40 domain that folds into a seven-bladed β-propeller, the most common WD40 architecture characteristic for Gβ-like proteins (Coyle et al., 2009; Stirnimann et al., 2010). In contrast to canonical Gβ-proteins, Asc1p lacks an N-terminal extension, which is supposed to be required for Gγ-binding. Each blade of the WD40 propeller comprises four anti-parallel β-sheets labeled strands A-D, which are interconnected by loops (Fig. 2B; Stirnimann et al., 2010; Tarnowski et al., 2014). One blade, however, does not correspond to one WD40 repeat. Instead, strands A-C from one repeat and strand D from the following together complete one propeller blade (Fig. 2B; Smith et al., 1999; Stirnimann et al., 2010; Tarnowski et al., 2014). The loops connecting strands B and C within one blade, and strands D and A of two adjacent blades, form the top surface of the overall structure, whereas the loops A-B and C-D are located at the opposite site (Coyle et al., 2009; Tarnowski et al., 2014). Thus, the scaffold structure provides three major surfaces for protein-protein or protein-RNA interactions: the top, the bottom and the circumference of Asc1p (Fig. 2A; Coyle et al., 2009; Smith et al., 1999). Additionally, the central hole was described as putative binding area for small molecules (Tarnowski et al., 2014; Yatime et al., 2011).
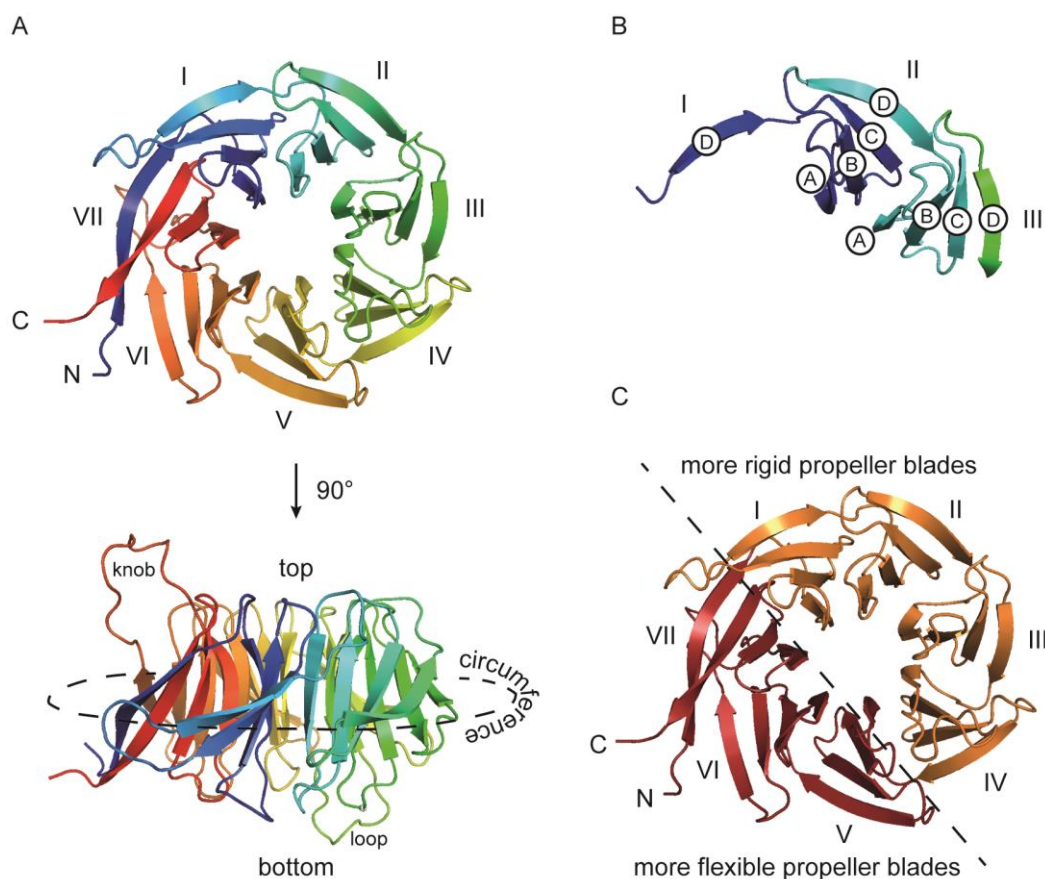
Fig. 2: The WD40 protein Asc1. (A) The Asc1 protein consists of seven WD40 repeats that form a Gβ-like seven-bladed β-propeller. A 90° horizontal rotation of the protein structure shows the top, bottom and circumference of the protein – surfaces available for protein-protein or protein-RNA interactions. The surface additionally features a loop insertion between blades III and IV and a knob-like structure between blades VI and VII. (B) One propeller blade consists of four antiparallel β-sheets, labeled A-D, in which β-sheets A-C belong to one WD40 repeat and β-sheet D to the adjacent repeat. All β-sheets belonging to one WD40 repeat are colored equally. (C) The protein can be divided into two parts: the more rigid blades I-IV (colored in orange), and a rather flexible area comprising blades V-VII including the knob-like structure (colored in red). The Asc1p crystal structure data derive from the entry 3FRX (Coyle et al., 2009) of the *Research Collaboratory for Structural Bioinformatics Protein Data Bank* (RCSB PDB; http://www.rcsb.org/pdb/home/home.do) and were used for visualization with the *PyMOL Molecular Graphics System* software.

The 3D-structure of the Asc1p propeller moreover features two particular insertions: a loop at the bottom between blades III and IV and a knob-like structure at the top between blades VI and VII providing additional protruding surfaces for protein-protein or protein-RNA interactions (Fig. 2A; Coyle et al., 2009). The structured knob is highly flexible (Fig. 2C) as demonstrated by hydrogen-deuterium exchange studies, whereas most of the internal B-C

hairpins comprising the B-C turns as well as adjacent peptides of blades B and C are the most rigid features of the propeller and consequently required to maintain the overall Gβ-like structure (Tarnowski et al., 2014). In total, blades V-VII contain more flexible regions compared to the remaining four propeller blades I-IV (Fig. 2C; Tarnowski et al., 2014). Since blades IV-VII are considered the major binding surface for dynamic protein interactions, this argues for a correlation between structural flexibility and protein association (Tarnowski et al., 2014). The N- and C-termini of the proteins are expelled from the propeller and converge in a Velcro-like manner (Coyle et al., 2009; Tarnowski et al., 2014). Importantly, it was demonstrated that upon homodimer formation (see also chapter 1.5.3) Asc1p undergoes structural alterations (Tarnowski et al., 2014). Thus, upon ligand binding new surfaces might be exposed for further interactions.

1.3 Asc1p: A ribosomal scaffold protein

The 319 amino acids of the highly conserved Asc1 protein are encoded by a nucleotide sequence of 957 base pairs situated on two exons (Chantrel et al., 1998). The *ASC1* gene is located on chromosome XIII and covers in total 1230 base pairs. An intron of 273 base pairs bearing the *SNR24* gene interrupts the *ASC1* coding sequence at position 538 (Chantrel et al., 1998). The *SNR24* gene encodes the small nucleolar RNA (snoRNA) U24, which is involved in nucleolar ribosome maturation (Kiss-László et al., 1996; Qu et al., 1995). It contains a C/D-box motif and anneals to the 28S pre-rRNA, thereby mediating its site specific 2'-O-methylation (Kiss-László et al., 1998; Qu et al., 1995). The interruption of the *ASC1* open reading frame (ORF) by one or more introns is conserved among species with varying numbers and positions within the *ASC1* coding sequence (Choi et al., 2003; Liu et al., 2010; Müller et al., 1995; Wang et al., 2003). In *S. cerevisiae* only 3.7% of all genes bear an intron, whereas this applies to 66% of all ribosomal genes (Link et al., 1999). Asc1p is equally abundant as ribosomal proteins (Ghaemmaghami et al., 2003; Kleinschmidt et al., 2006; Kulak et al., 2014; Link et al., 1999) and its gene expression is co-regulated with genes encoding ribosomal proteins, e.g. by the transcription factors Fhl1p and Ifh1p that associate to many ribosomal gene promotors in *S. cerevisiae* (Kleinschmidt et al., 2006). In accordance with this, Asc1p co-migrates with 40S ribosomal subunits in sucrose gradients, and the association of the β-propeller with 40S proteins is resistant to elevated salt concentrations as described for integral ribosomal proteins (Chantrel et al., 1998; Inada et al., 2002; Link et al., 1999). Asc1p is not present at the 40S pre-ribosome, which is exported from the nucleus into the cytoplasm for maturation, but is bound to the 80S-like ribosome, a non-translating intermediate during the

final steps of 40S maturation (Strunk et al., 2012). Thus, Asc1p is considered a core constituent of ribosomes, although it is only encoded by one allele, in contrast to most other ribosomal proteins, which are encoded by two isogenes (Kleinschmidt et al., 2006; Link et al., 1999). Crystallizations of the *S. cerevisiae* 80S ribosome and the *Tetrahymena thermophila* 40S subunit, as well as cryo-EM reconstruction studies on *Thermomyces lanuginosus* and *S. cerevisiae* 40S and 80S structures located Asc1p to the exposed head region of the 40S ribosome in direct proximity to the mRNA exit tunnel (Fig. 3; Ben-Shem et al., 2011; Rabl et al., 2011; Sengupta et al., 2004). The top surface of Asc1p is oriented to the ribosome interface, where it physically interacts with the ribosomal proteins Rps3, Rps16 and Rps17 (Fig. 3; Ben-Shem et al., 2011; Rabl et al., 2011; Sengupta et al., 2004). The C-terminus of Rps3p converges Asc1p as a highly flexible, unstructured arm (Ben-Shem et al., 2011; Rabl et al., 2011). Furthermore, the ribosome facing site of Asc1p contacts helices 39 and 40 of the 18S rRNA with an area of positively charged amino acids (Coyle et al., 2009). The Asc1p bottom is not involved in ribosome association and exposed for additional protein-protein interactions (Fig. 3; Ben-Shem et al., 2011; Sengupta et al., 2004). Thus, as a scaffold protein, Asc1p can be considered as a contact site of the ribosome for further cellular constituents.
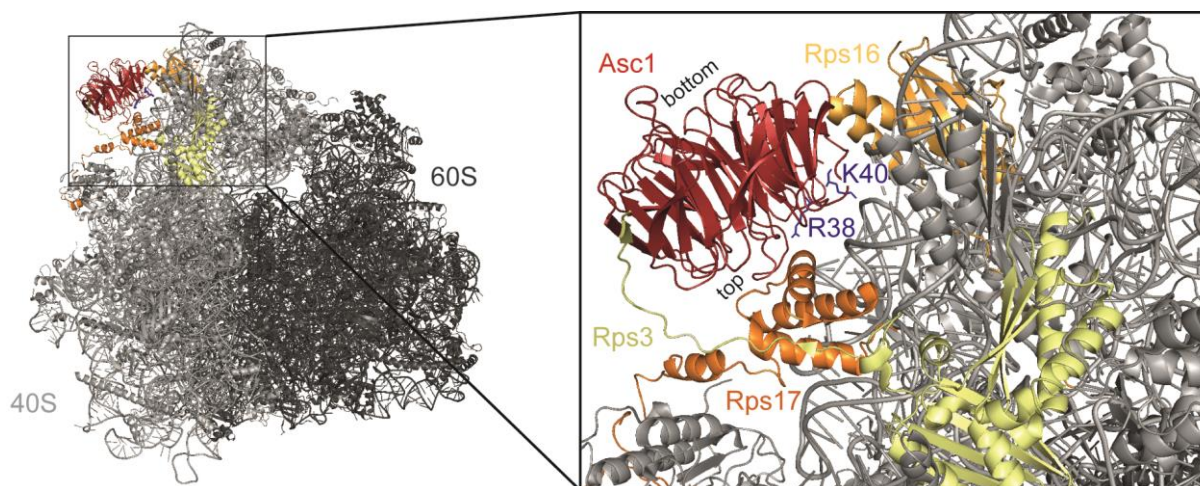
Fig. 3: Asc1p locates to the 40S ribosomal subunit. The scaffold Asc1p is an integral ribosomal protein and locates to the head region of the 40S ribosomal subunit. At this exposed position it physically interacts with the ribosomal proteins Rps3, Rps16 and Rps17. Asc1p moreover contacts helices 39 and 40 of the 18S ribosomal RNA with an area of positively charged amino acids including residues Arg38 (R38) and Lys40 (K40), whose exchange to negatively charged Asp and Glu, respectively, affects the affinity of Asc1p to ribosomes. The crystal structure data of the *S. cerevisiae* 80S ribosome derives from the PDB entry 4V88 (Ben-Shem et al., 2011) and was used for visualization with the *PyMOL Molecular Graphics System* software.

Immunofluorescence and centrifugation studies localized the Asc1 protein to the cytoplasm and to the cytosolic part of membranes (Baum et al., 2004; Chantrel et al., 1998). In contrast to its ribosome-associated localization during exponential growth, a ribosome-free cytosolic localization of an Asc1p sub-population was suggested in stationary yeast cells (Baum et al., 2004). Whether this reflects an *in vivo* situation, or an artefact of ultracentrifugation, or as suggested by Nilsson et al. (2004) results from an over-stoichiometric Asc1p to ribosome level, remained elusive. An artificial Asc1p variant was used to analyze the importance of its ribosome association for functionality (Coyle et al., 2009). Within the crystal structure of Asc1p the area that contacts the rRNA includes the residues Arg38 and Lys40 and is characterized by a high degree of stability implying that ribosome-binding is of major importance for Asc1p (Tarnowski et al., 2014). The *asc1^{R38D K40E}* mutant, hereafter referred to as *asc1^{DE}*, features the exchange of Arg38 and Lys40 to negatively charged Asp and Glu, respectively, resulting in repelling forces between the protein and the negatively charged phosphate backbone of the 18S rRNA, which are thought to diminish the binding affinity of Asc1^{DE}p to the ribosome (Coyle et al., 2009). Ultracentrifugation of *asc1^{DE}*-derived protein extracts in sucrose density gradients confirmed reduced ribosome-binding of the mutated version (Coyle et al., 2009). However, the DE mutation exerts only a minor impact on Asc1p-dependent phenotypes rather suggesting *in vitro* separation of Asc1^{DE}p from ribosomes through centrifugation (Coyle et al., 2009; Schmitt et al., 2017).

1.4 Asc1p/RACK1 is highly conserved among eukaryotic species

S. cerevisiae Asc1p is an integral ribosomal protein, however, it is not present in mitochondrial ribosomes (De Silva et al., 2015). Consistently, *ASC1* is not encoded in bacterial or archaeal genomes (Dresios et al., 2006). *ASC1*/Asc1p is highly conserved throughout eukaryotes, ranging from the single cell yeast over filamentous fungi, plants, and arthropods to vertebrates including mammals. The *S. cerevisiae* Asc1p amino acid sequence shares 54% identity with *Homo sapiens* RACK1, and 47% with the *Arabidopsis thaliana* RACK1A variant. Additionally, the structural organization of *S. cerevisiae* Asc1p as a seven bladed β-propeller reveals a high degree of conservation to its orthologues Gib2p from *Cryptococcus neoformans*, and RACK1 from *A. thaliana*, *T. thermophila* and human (Fig. 4; Coyle et al., 2009; Ero et al., 2015; Rabl et al., 2011; Ruiz Carrillo et al., 2012; Ullah et al., 2008). The comparison of *S. cerevisiae*, *A. thaliana* and *H. sapiens* Asc1p/RACK1 regarding their structural dynamics revealed only minor differences between these species (Tarnowski et al., 2014).

Fig. 4: Asc1p is highly conserved throughout the eukaryotic kingdom. Asc1p and its orthologues Gib2p from *C. neoformans*, RACK1A from *A. thaliana* and RACK1 from *H. sapiens* show a high degree of conservation at the structural level. The crystal structure data of the Asc1p orthologues derive from the PDB entries 3FRX (*S. cerevisiae*; Coyle et al., 2009), 4D6V (*C. neoformans*; Ero et al., 2015), 3DM0 (*A. thaliana*; Ullah et al., 2008) and 4AOW (*H. sapiens*; Ruiz Carrillo et al., 2012) and were used for visualization with the *PyMOL Molecular Graphics System* software.

Also functional homologies of the different Asc1p orthologues were revealed among eukaryotes. Most Asc1p/RACK1 orthologues were identified as ribosomal proteins (Chang et al., 2005; Ero et al., 2015; Link et al., 1999; Shor et al., 2003). Consistently, mammalian RACK1 is able to substitute for *S. cerevisiae* Asc1p in a Δ*asc1* strain at the 40S ribosomal subunit of yeast ribosomes (Gerbasi et al., 2004). Furthermore, *A. thaliana* RACK1, *Neurospora crassa* CPC2 and rat RACK1 complement phenotypes of Asc1p-depleted yeast cells (Guo et al., 2011a; Hoffmann et al., 1999) and deletion of *cpc2* in *Schizosaccharomyces pombe* was complemented by the expression of *Trypanosomas brucei* and *Rattus norvegicus* RACK1 (McLeod et al., 2000; Rothberg et al., 2006).

1.5 Asc1p/RACK1 interacts with proteins attributed to a broad range of molecular functions

The first study on *S. cerevisiae* Asc1p identified the deletion of the *ASC1* ORF as suppressor of the growth defect of a *hap1⁻ (cyp1⁻) hem1⁻* strain, hence its name as "Absence of growth Suppressor of Cyp1 1" (Chantrel et al., 1998). In the unicellular budding yeast, Asc1p is dispensable for growth in general (Chantrel et al., 1998). Still, an *ASC1* deletion strain exhibits an enlarged cell size and a decelerated growth rate (Link et al., 1999; Valerius et al., 2007). Especially when challenged with stressing growth conditions, Δ*asc1* strains show severe defects as e.g. the inability of diploid cells to develop pseudohyphae and the absence of invasive growth of haploid cells upon nutritional deprivations (Valerius et al., 2007). Cell wall integrity is disturbed in Asc1p-depleted cells (Melamed et al., 2010; Rachfall et al., 2013; Valerius et al., 2007), and they show an increased sensitivity to pheromone and osmotic stress (Chasse et al., 2006; Melamed et al., 2010). Asc1p is further required to maintain the respiratory capacity and to cope with elevated temperatures (Auesukaree et al., 2009; Rachfall et al., 2013; Sinha et al., 2008).

Mammalian RACK1 was first characterized in a screen for protein kinase C (PKC) interacting proteins using a rat brain cDNA library and was named according to its presumed function as "Receptor for Activated C Kinase 1" (Ron et al., 1994). Ever since, the protein was assigned to multiple cellular functions. In general, the function of a scaffold protein is tightly coupled to its interaction partners (Vondriska et al., 2004). In total, 78 proteins are listed in the *Saccharomyces Genome Database* (SGD; http://www.yeastgenome.org/) as physical Asc1p interaction partners, and also its orthologues from other species are reported to interact with a myriad of proteins (reviewed in Gandin et al., 2013a; Islas-Flores et al., 2015). This is in accordance with the broad impact of Asc1p/RACK1 on cellular functions, which are summarized in the following sections.

1.5.1 Asc1p/RACK1 affects translation via protein-protein interactions with important translational regulators

As a core component of ribosomes the Asc1/RACK1 protein affects translation in multiple ways. Asc1p-depleted *S. cerevisiae* cells exhibit an increased overall translational activity, which was also demonstrated in an *in vitro* translation assay, indicative of a repressive impact of Asc1p on global translation (Chiabudini et al., 2014; Gerbasi et al., 2004). Furthermore, the translation of rather specific messages is affected in cells lacking Asc1p (Sezen et al., 2009; Thompson et al., 2016). Similarly, deletion of *cpc2* in *S. pombe* affects the biosynthesis of

specific proteins, however, decreases the overall translational activity by 18% (Núñez et al., 2009; Shor et al., 2003). In *A. thaliana*, which possesses three *RACK1* gene copies, a *rack1a rack1b* double deletion mutant shows a reduced amount of 60S subunits and impaired 80S monosome assembly as well as an increased sensitivity to the protein biosynthesis inhibitor anisomycin (Guo et al., 2011a). In contrast, an accumulation of monosomes can be observed in heterozygous *Rack1* mice, which goes along with decreased rates of translation (Volta et al., 2013). Despite the effects of Asc1p/RACK1-depletion on global translation it can be assumed that Asc1p/RACK1 is dispensable for translation in general. The protein is not required for viability of yeast cells and lethality during embryogenesis in higher eukaryotes does not occur before gastrulation in RACK1-deficient mice or larvae formation in fruit flies (Kadrmas et al., 2007; Volta et al., 2013). Moreover, inhibition of RACK1 in human cells and in *Drosophila melanogaster* has no effect on their viability (Majzoub et al., 2014). Therefore, Asc1p/RACK1 is rather implicated in the decoding of specific transcripts, presumably in response to particular developmental programs and external cues. Protein expression is tightly regulated at multiple steps as diverse as transcription, mRNA stability and localization, and translation initiation and elongation. Furthermore, mRNA-binding proteins and mRNA silencing elements like miRNAs control the translation of a transcript. The Asc1/RACK1 protein affects many of these stages by differential protein interactions as outlined in the following sections.

1.5.1.1 Asc1p/RACK1 binds and affects translation initiation factors

Translation initiation is a tightly regulated step in protein biosynthesis and an important stage for transcript selection (Sonenberg and Hinnebusch, 2009). It is controlled by numerous proteins which makes it a highly susceptible stage for signal-dependent regulation (Sonenberg and Hinnebusch, 2009). In accordance with this, Asc1p/RACK1, which is also an important player in cellular signaling (see chapter 1.5.2), interacts with different e̲ukaryotic translation i̲nitiation f̲actors (eIFs). An early step in translation initiation is the formation of the 43S p̲re-i̲nitiation c̲omplex (PIC): The methionyl initiator tRNA (Met-tRNA$_i$) interacts with GTP-bound eIF2 to form the t̲ernary c̲omplex (TC). The TC joins the 40S ribosomal subunit together with and promoted by eIF1, eIF1A, eIF3 and eIF5 (reviewed in Hinnebusch and Lorsch, 2012). The eIF3 multiprotein complex consists of six subunits in yeast and 13 subunits in mammals and is thus the largest initiation factor in translation (reviewed in Hinnebusch and Lorsch, 2012). In *S. cerevisiae*, Asc1p was suggested to interact with eIF3/b (Prt1p) and eIF3/c (Nip1p; Gavin et al., 2002; Kouba et al., 2012a), and Asc1p-depletion results in a decreased 40S binding affinity of the eIF3 complex indicating that Asc1p might support eIF3 ribosome localization (Kouba et

al., 2012a). Furthermore, eIF3 is regulated by dynamic posttranslational modifications of its subunits (Farley et al., 2011), and phosphorylation of several eIF3 subunits was revealed to be affected by Asc1p-depletion (Schmitt et al., 2017). Moreover, eIF3 supports binding of mRNAs to the 40S ribosome. It cooperates with the eIF4F complex, comprising eIF4A, eIF4E and eIF4G. The integrity of mRNA is ensured by eIF4E, which binds to the intact cap structure of an mRNA, and by the poly(A)-binding protein (PABP) (reviewed in Hinnebusch and Lorsch, 2012). Mammalian RACK1 binds the cap-binding protein eIF4E in complex with PKCβII, which phosphorylates eIF4E in a RACK1-dependent manner (Ruan et al., 2012). eIF4G mediates the closed loop formation by interacting with both eIF4E and PABP (reviewed in Hinnebusch and Lorsch, 2012). Yeast Asc1p co-purifies with eIF4G and is required for its efficient phosphorylation (Gavin et al., 2002; Schmitt et al., 2017). The RNA helicase eIF4A removes mRNA secondary structures and allows efficient AUG recognition (reviewed in Hinnebusch and Lorsch, 2012). Depletion of Asc1p in *S. cerevisiae* leads to increased phosphorylation of eIF4A (Schmitt et al., 2017; Valerius et al., 2007). For Gib2p of *C. neoformans* a physical interaction with eIF4A was demonstrated (Wang et al., 2014). After the AUG-Met-tRNA$_i$ pairing is established the eIF2-bound GTP is hydrolyzed and eIF2-GDP dissociates for complex regeneration (reviewed in Hinnebusch and Lorsch, 2012). *S. cerevisiae* Asc1p affects the phosphorylation status of eIF2α and eIF2β, which are required for start codon recognition and GDP to GTP exchange (Schmitt et al., 2017; Valerius et al., 2007).

Mammalian RACK1 serves as scaffold for activated PKCβII, an interaction that plays a crucial role in 80S ribosome assembly. RACK1 associates with PKCβII and eIF6, thereby mediating phosphorylation of eIF6 by PKC, which is required for the release of eIF6 from the 60S subunit and subsequent subunit joining (Ceci et al., 2003). A physical interaction of RACK1 with eIF6 is conserved in *A. thaliana*, however, the plant is missing a PKC homolog (Guo et al., 2011a). Interestingly, in contrast to other initiation factors, Asc1p/RACK1 stays at the ribosome during mRNA translation (Gerbasi et al., 2004). This implicates that Asc1p/RACK1 is not only involved in initiation, but might also affect translation elongation, re-initiation and/or termination. Consistently, RACK1 bridges the interaction between eEF1A2 and the c-Jun N-terminal kinase (JNK) required for the phosphorylation of the elongation factor at ribosomes in HEK293 (human embryonic kidney) cells (Gandin et al., 2013b). Also *T. brucei* RACK1 co-purifies with eEF1A (Choudhury et al., 2011; Regmi et al., 2008). In the budding yeast, Asc1p affects the phosphorylation status of the elongation factor eEF3 and the termination factor eRF3 (Schmitt et al., 2017). Together, this shows the broad impact of Asc1p/RACK1 on mRNA translation at multiple stages.

1.5.1.2 Asc1p/RACK1 interacts with mRNA-binding proteins

mRNA-binding proteins are crucial for the transport and/or the subsequent localized translation of bound transcripts at the ribosome. The *S. cerevisiae* Asc1 protein physically interacts with the K̲ h̲omology (KH)-domain containing mRNA-binding protein Scp160 and is involved in the association of Scp160p to ribosomes (Baum et al., 2004). Consistently, Scp160p shows a decreased affinity to mono- and polysomes in Asc1p-depleted cells (Baum et al., 2004). Asc1p and Scp160p were described as parts of a complex called SESA (S̲my2p, E̲ap1p, S̲cp160p, and A̲sc1p), which additionally features the glycine-tyrosine-phenylalanine (GYF)-domain protein Smy2 and the translational repressor and eIF4E-binding protein Eap1 (Sezen et al., 2009). Together, these proteins control the translation of the *POM34* mRNA, which encodes a protein required for spindle pole body duplication (Sezen et al., 2009). Besides the *POM34* mRNA, Scp160p associates to further mRNAs, among them mRNAs encoding polarity factors and mating pathway factors like *SRO7*, *FUS3* or *ASH1* to regulate their localized translation at bud and shmoo tips (Irie et al., 2002; Gelin-Licht et al., 2012). The interaction of Asc1p with Scp160p at the ribosome might locate the associated mRNAs to the area of translation initiation. Accordingly, mammalian RACK1 was identified as component of m̲essenger r̲ibo̲nucleo̲protein (mRNP) complexes at the synapse (Angenstein et al., 2002). RACK1 physically interacts with the two paralogous La-related mRNA-binding proteins LARP4 and LARP4B and within the same complex with the poly(A)-binding protein PABP1, however, probably in an indirect manner (Angenstein et al., 2002; Mattijssen and Maraia, 2015). Although LARP4B arose from LARP4 gene duplication, both proteins function independently and associate to a different subset of mRNAs (Mattijssen and Maraia, 2015).

In neuronal cells, ribosome-associated RACK1 interacts with the mRNA-binding protein ZBP1 (Ceci et al., 2012). β-actin mRNA is bound by ZBP1 and is transported in ribonucleic-protein complexes (RNA granules) to its final destination in a translationally repressed manner (Ceci et al., 2012). These RNA granules contain eukaryotic translation initiation factors as well as 40S ribosomal subunits. RACK1 binds both ZBP1 and the tyrosine kinase Src, and mediates ZBP1 phosphorylation through Src, which results in the release and subsequent localized translation of the β-actin mRNA (Ceci et al., 2012). Similarly, RACK1 controls the phosphorylation status of the mRNA-binding protein SAM68 which specifically associates to 3'-u̲ntranslated r̲egions (UTRs) of selected mRNAs (Miller et al., 2004). RACK1 positively affects the mRNA-binding ability of SAM68 by inhibiting Src phosphorylation activity (Mamidipudi et al., 2007). Thus, RACK1 can regulate the translation of SAM68 associated mRNAs.

In the fission yeast *S. pombe*, the Asc1p/RACK1 homologue Cpc2p interacts with the mRNA-binding protein Nrd1p, an association that cooperatively controls the translation of *ste11* mRNA (Jeong et al., 2004; Oowatari et al., 2011). Nrd1p functions as negative regulator of sexual differentiation through the translational repression of Ste11p-regulated transcripts (Jeong et al., 2004). Thus, Cpc2p affects sexual differentiation by the translational control of specific transcripts (Jeong et al., 2004; Oowatari et al., 2011). Additionally, *S. pombe* Cpc2p regulates the translation of *rpl25* mRNA through decreased recruitment of the mRNA to polysomes (Shor et al., 2003). Accordingly, the ribosomal scaffold Asc1p/RACK1 controls protein synthesis of rather specific mRNAs in different eukaryotic organisms.

1.5.1.3 Asc1p/RACK1 affects mRNP granule formation and is a constituent of mRNP granules in higher eukaryotes

As mentioned above RACK1 regulates the translation of β-actin mRNA in neurons, which is transported in a translationally repressed manner within RNA granules to its final destination for localized translation (Ceci et al., 2012). Similarly, the sequestration of mRNAs into mRNP granules inhibits protein synthesis at a posttranscriptional level mostly as a response to challenging growth conditions (reviewed in Buchan and Parker, 2009). There are two distinct mRNP structures, namely stress granules and processing bodies (P-bodies), which can partially overlap (reviewed in Decker and Parker, 2012). Stress granules contain stalled translation pre-initiation complexes, meaning mRNAs with their associated mRNA-binding proteins, as well as 40S ribosomal subunits with translation initiation factors (reviewed in Buchan and Parker, 2009). P-bodies lack ribosomal subunits and eIFs, but additionally contain mRNA degrading enzymes (reviewed in Decker and Parker, 2012). Thus, these structures cooperatively control the translation and decay of existing transcripts.

As a ribosomal protein, human RACK1 co-migrates with the 40S subunit into stress granules under challenging growth conditions, like arsenite treatment or hypoxia, thereby affecting cellular apoptosis (Arimoto et al., 2008). Moreover, human RACK1 was identified as an *O*-linked *N*-acetylglucosamine modified protein upon arsenite treatment (Ohn et al., 2008). This modification is required for nutritional sensing and stress responses in metazoans and is considered as major modification of stress granule and P-body constituents (Ohn et al., 2008). Consistently, their study confirmed the presence of human RACK1 in stress granules (Ohn et al., 2008). *S. cerevisiae* Asc1p has not been identified as mRNP granule component, but Asc1p-depleted cells fail to form P-bodies specifically upon replication stress in response to hydroxyurea (Tkach et al., 2012). *S. pombe* Cpc2p associates to the mRNA-binding protein

Nrd1p, a stress granule component during glucose deprivation and arsenite stress (Oowatari et al., 2011; Satoh et al., 2012). Absence of Cpc2p in arsenite stressed cells results in a significant decrease of stress granules (Satoh et al., 2012). Also this effect depends on particular stress condition (Satoh et al., 2012).

1.5.1.4 Asc1p/RACK1 mediates translational arrest and is required for co-translational quality control

As soon as translation is initiated and ongoing, the nascent peptide is constantly monitored. A missing or premature stop codon, inhibitory mRNA structures and the presence of polybasic stretches within the nascent polypeptide chain result in stalled elongation complexes and aberrant proteins. Co-translational quality control systems recognize these aberrant proteins as well as translational arrests. They react to these events at an early stage resulting in mRNA and nascent peptide degradation if necessary (reviewed in Lykke-Andersen and Bennett, 2014). Poly(A) stretches within mRNAs as well as poly-basic peptide sequences stall elongation, the latter due to their affinity to the negatively charged exit tunnel (Lu and Deutsch, 2008).

Ribosome-associated Asc1p is required for the translational arrest at polybasic peptide sequences and rare mRNA codons to promote co-translational polypeptide degradation (Brandman et al., 2012; Kuroha et al., 2010; Letzring et al., 2013; Matsuda et al., 2014). Consistently, the read-through of mRNA sequences encoding polybasic stretches is significantly enhanced in Asc1p-depleted cells (Letzring et al., 2013). Arrested ribosomes recruit the ribosome quality control (RQC) complex, consisting amongst others of the E3 ubiquitin ligase Ltn1p, which mediates proteasomal degradation of the nascent peptide in an Asc1p-dependent manner (Brandman et al., 2012; Letzring et al., 2013; Matsuda et al., 2014). Asc1p further supports the endonucleolytic cleavage of the aberrant mRNA (Kuroha et al., 2010). The WD40 protein additionally protects yeast cells from substantial harms, since Asc1p-depletion results in frame-shifting at rare CGA codons with a rate of 40% (Wolf and Grayhack, 2015). In HEK293T cells, RACK1 is suggested to recruit the serine/threonine kinase JNK to the ribosome and to mediate the phosphorylation of the translation elongation factor eEF1A2, which in turn associates with misfolded newly synthesized peptides mediating their subsequent ubiquitylation for proteasomal degradation (Gandin et al., 2013b). Hence, Asc1p/RACK1 not only affects the translation of specific mRNAs, but is also involved in the co-translational degradation of aberrant peptides.

1.5.2 Asc1p/RACK1 is a major player in cellular signaling

Asc1p/RACK1 interacts with numerous players of signaling pathways in various eukaryotic organisms. As a ribosomal protein Asc1p/RACK1 was attributed a function as a molecular link between cellular signaling and translation. However, it not only links signals to the translational machinery, but also mediates the cross-talk between different signaling pathways, which is outlined in the following sections.

1.5.2.1 Asc1p/RACK1 interacts with components of the cAMP/PKA signaling pathway

Asc1p is a Gβ-like protein, but is missing the N-terminal coiled-coil domain that is required for Gγ-binding and thus characteristic for canonical Gβ-subunits. Still, in *S. cerevisiae* Asc1p was described to function as Gβ-subunit in the cAMP/PKA pathway for glucose signaling (Zeller et al., 2007). It physically interacts with the glucose receptor-associated Gα-protein Gpa2 (Fig. 5) specifically in its GDP-bound form and inhibits the guanine nucleotide exchange (Zeller et al., 2007). The G-protein controls the activity of the adenylate cyclase Cyr1p which produces cAMP upon pathway activation. cAMP subsequently activates the protein kinase A (PKA) resulting in the activation of the transcription factor Flo8p and others required for invasive and pseudohyphal growth (Fig. 5). The physical interaction between Asc1p and Cyr1p causes decreased cAMP production upon glucose stimulation (Fig. 5; Zeller et al., 2007). In contrast, the Asc1p orthologue Gib2p in *C. neoformans* positively regulates cAMP levels. Like Asc1p, Gib2p functions as the Gβ-subunit in cAMP signaling (Palmer et al., 2006). It physically interacts with the Gα-subunit Gpa1p and additionally with the Gγ proteins Gpg1p and Gpg2p. Furthermore, a direct interaction with the downstream signaling target Smg1p was observed (Palmer et al., 2006).

Further components of the cAMP/PKA signaling pathway are phosphodiesterases required to lower cAMP levels by breaking phosphodiester bonds within the second messenger. Human RACK1 specifically interacts with the PDE4 isoform PDE4D5 (Steele et al., 2001; Yarwood et al., 1999). This interaction enhances the binding affinity of PDE4D5 to cAMP in membrane fractions of HEK293 cells (Bird et al., 2010). Via binding to RACK1 PKCα can phosphorylate and activate PDE4D5 (Bird et al., 2010) demonstrating that RACK1 mediates a cross-talk between cAMP and PKC signaling.
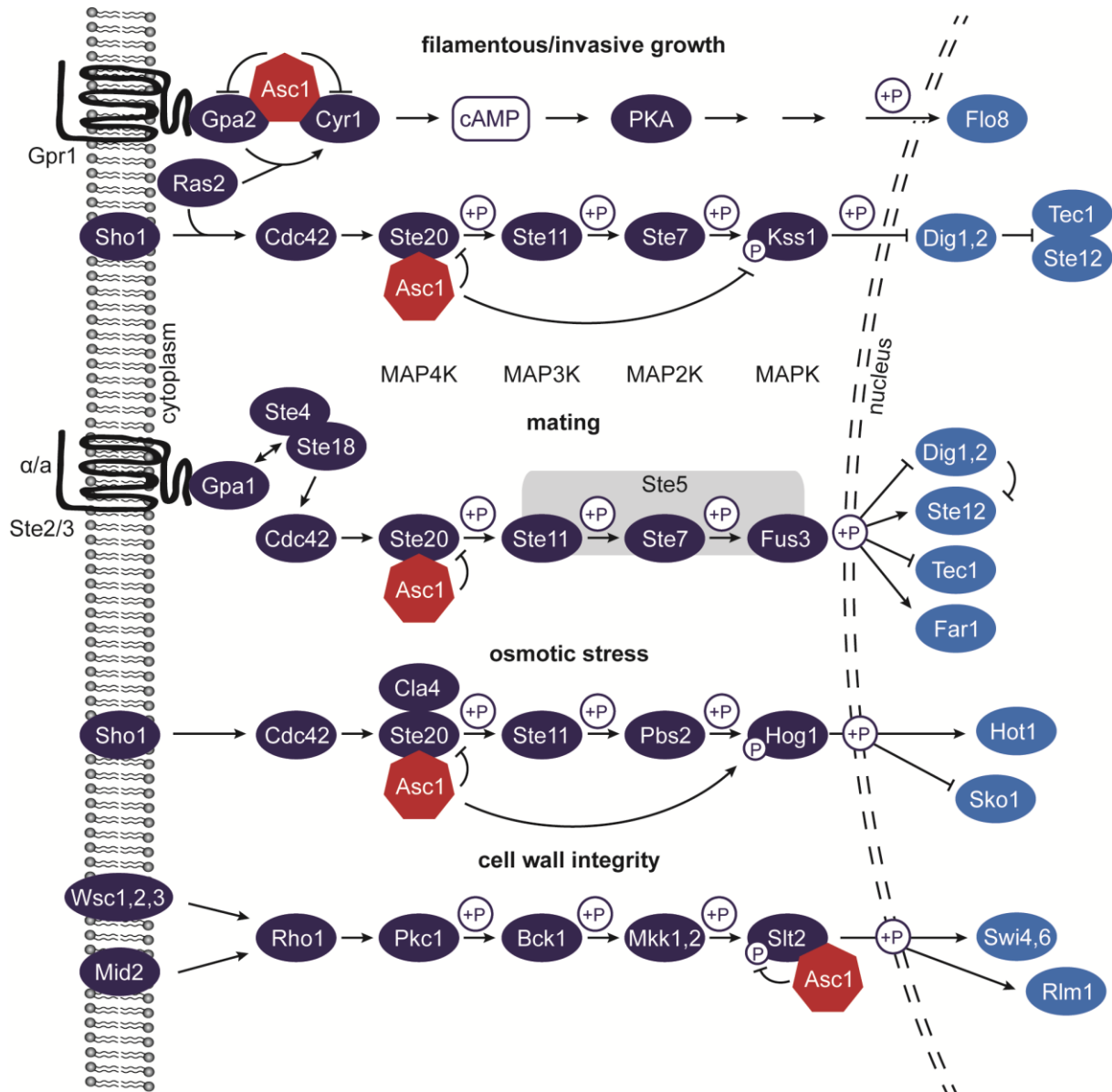
Fig. 5: Asc1p interacts with components of the *S. cerevisiae* cAMP/PKA pathway and MAPK cascades. The Asc1 protein physically interacts with the Gα-subunit Gpa2p and with the adenylate cyclase Cyr1p of the glucose response pathway. Thereby, it negatively affects cAMP signaling. Asc1p further binds the MAP4K Ste20p of the MAPK pathway responding to starvation and influences Kss1p (MAPK) phosphorylation. Both pathways regulate pseudohyphal and invasive cell growth. The MAP4K Ste20p is also part of the mating and osmotic stress response pathway. Asc1p-depletion results in a decreased phosphorylation level of the osmotic stress MAPK Hog1p. Within the cell wall integrity pathway an interaction of Asc1p with the MAPK Slt2p was described and Slt2p-phosphorylation is increased in Asc1p-depleted cells. Pathway information were obtained from Breitkreutz et al., 2010, Schmitt et al., 2017, Zeller et al., 2007, and the *KEGG database* (http://www.genome.jp/kegg).

1.5.2.2 Asc1p/RACK1 influences MAPK pathways by differential protein-protein interactions

Asc1p/RACK1 is implicated in several MAPK cascades and physically interacts with components of these pathways in different organisms. The signal transduction pathway regulating cell wall integrity in *S. cerevisiae* comprises the yeast protein kinase C (Pkc1p) and a downstream MAPK module including the MAPK Slt2p (Fig. 5). Asc1p physically interacts with the MAPK and its absence results in Slt2p hyperphosphorylation (Fig. 5; Breitkreutz et al., 2010; Chasse et al., 2006). Accordingly, cell wall integrity is disturbed in cells lacking Asc1p (Rachfall et al., 2013; Valerius et al., 2007). Furthermore, Asc1p binds Ste20p which locates upstream of the MAPKs Fus3p, Kss1p and Hog1p controlling the pheromone response pathway, invasive/pseudohyphal growth and the osmotic stress response, respectively (Fig. 5; Zeller et al., 2007). Asc1p depletion causes an increase in Kss1p phosphorylation and a significant reduction in Hog1p phosphorylation at sites required for its activity (Fig. 5; Schmitt et al., 2017; Zeller et al., 2007). Accordingly, Asc1p-depletion results in diminished adhesion and pseudohyphae formation and increased sensitivity against osmotic stress (Melamed et al., 2010; Valerius et al., 2007).

In *A. thaliana*, RACK1 functions as scaffold protein in a similar manner as the yeast Ste5 protein. RACK1 scaffolds the MAPK module that answers to pathogen-secreted proteases. It interacts with the MAP3K MEKK1, the redundant MAP2Ks MKK4 and MKK5, and the MAPKs MPK3 and MPK6 and facilitates their communication (Cheng et al., 2015). Furthermore, RACK1 interacts with AGB1, the Gβ-protein of this pathway, and thus links the G-protein to the downstream MAPK cascade (Cheng et al., 2015).

In human COS-7 and HEK293 cells, RACK1 interacts with the MAP3K MTK1, which regulates apoptosis via its downstream targets p38 and JNK in response to different types of stress (Arimoto et al., 2008). Activation of MTK1 requires the formation of a MTK1-homodimer, which leads to MTK1 autophosphorylation. In the absence of stress, RACK1 keeps MTK1 in a dimeric, however, inactive form. Thereby, it facilitates the subsequent activation as soon as stress conditions appear (Arimoto et al., 2008). As mentioned above, distinct stresses like arsenite or hypoxia cause RACK1 to move into stress granules (Arimoto et al., 2008). Thus, these stress conditions impede MTK1 activation due to RACK1-MTK1 dissociation (Arimoto et al., 2008).

The extracellular signal-regulated kinase (ERK) is a MAPK that responds to extracellular stimuli, such as integrin-mediated signals. RACK1 was identified as interaction partner not only for ERK1 and ERK2, but also for the corresponding MAP2Ks Raf-1 and B-Raf and the

MAP3Ks MEK1 and MEK2 indicating a scaffolding function of RACK1 for this cascade (Vomastek et al., 2007). Accordingly, the absence of RACK1 results in decreased pathway activation in response to integrin in REF52 fibroblasts (Vomastek et al., 2007). Moreover, ERK signaling controls the transcription and stability of c-Jun, a regulator of RACK1 transcription, which suggests a connection to the JNK signaling pathway (Lopez-Bergami et al., 2007). RACK1 is indeed engaged in the JNK pathway, a stress-activated MAPK pathway. It interacts with the JNK-specific MAP2K MKK7 in human hepatocellular carcinoma cells (Guo et al., 2013). This interaction increases the phosphorylation of both MKK7 and the MAPK JNK and facilitates the interaction between MKK7 and the corresponding MAP3K (Guo et al., 2013). RACK1 was also shown to interact with JNK itself (López-Bergami et al., 2005). Furthermore, RACK1 represents a functional and physical link between JNK and PKC signaling as it functions as molecular bridge between both kinases and thus enables the phosphorylation of JNK at Ser129 through PKC. This modification seems to enhance in turn the phosphorylation of JNK by its two MAP2Ks MKK7 and MKK4 (López-Bergami et al., 2005). The other way around, sufficient MKK4/MKK7 protein levels are required to allow for PKC-dependent JNK phosphorylation (López-Bergami et al., 2005).

1.5.3 Asc1p/RACK1 forms Gβ-homo- and heterodimers

The seven-bladed β-propeller structure is known from Gβ-subunits of heterotrimeric G-proteins and is highly conserved for Asc1/RACK1 proteins in eukaryotes. The WD40 propeller provides a large surface to bridge protein-protein interactions. Some proteins, however, share the same binding site on the scaffold suggesting that their interaction with Asc1p/RACK1 would be mutually exclusive. RACK1 interacts with the _N_-methyl-_D_-aspartate (NMDA) receptor (NMDAR) subunit NR2B and with the Fyn kinase, which in turn phosphorylates NMDAR. Both were reported to bind RACK1 at the same site in a non-exclusive, but simultaneous manner (Thornton et al., 2004; Yaka et al., 2002). This observation first suggested the presence of RACK1-homodimers, which was confirmed to be formed in cells of the rat brain with the dimerization site mapped to WD4 (Thornton et al., 2004). Furthermore, the RACK1-homodimer mediates the degradation of hypoxia-inducible factor 1 (HIF1), the oxygen-dependent master regulator of transcription (Liu et al., 2007a). RACK1 competes with HSP90 for HIF1α-binding and bridges the interaction of HIF1α with Elongin-C as part of a E3 ubiquitin ligase complex, thereby promoting HIF1α ubiquitylation and proteasomal degradation (Liu et al., 2007a). Again, HIF1α and Elongin-C share the same binding site at the β-propeller, and thus RACK1-homodimerization is required to bridge the interaction (Liu et al., 2007b, 2007a).

Also in the plant *A. thaliana* and in the slime mold *Dictyostelium discoideum* evidence for dimer formation was reported (Omosigho et al., 2014; Sabila et al., 2016).

In yeast, *in vivo* formation of an Asc1p-homodimer has not been demonstrated, however, a crystal structure of an Asc1p-homodimer was resolved (Fig. 6; Yatime et al., 2011). This structure mapped the dimer interface to blade 4 of the β-propeller and illustrates a distinct structural reconstruction within this area (Yatime et al., 2011). The two inner β-strands of blade 4, B and C, protrude from the propeller core, whereas β-strands A and D of both monomers build a shared new propeller blade (Fig. 6; Yatime et al., 2011). The two propeller surfaces are shifted to each other by an angle of approximately 90°C and present an enlarged and renewed scaffolding surface for further protein interactions (Fig. 6; Tarnowski et al., 2014; Yatime et al., 2011). Besides Asc1p/RACK1 homodimerization, the protein was also described to build heterodimers with further WD40/Gβ-like proteins. RACK1 associates to G-protein-coupled receptor (GPCR)-uncoupled Gβ/γ-complexes in NIH3T3 and COS-7 cells (Chen et al., 2004, 2005a; Dell et al., 2002). In brain cells, a trimolecular complex consisting of RACK1, Gβ and the NMDAR subunit NR2B was observed, suggesting a cross-talk between G-protein signaling and the NMDA ion channel (Thornton et al., 2004). In the plant *A. thaliana*, RACK1 binds the Gβ-protein AGB1, and also *D. discoideum* Rack1 interacts with Gβ *in vitro* (Cheng et al., 2015; Omosigho et al., 2014).
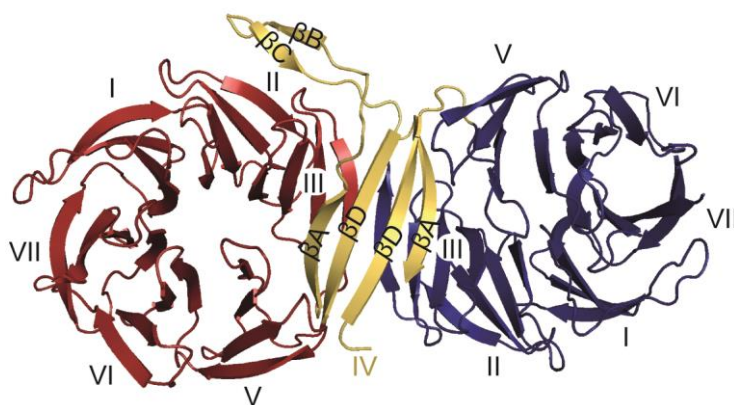
Fig. 6: The Asc1p-homodimer. The crystal structure of the Asc1p-homodimer shows a structural rearrangement of the propeller blades four of both monomers. The βB- and βC-sheets are expelled from the propeller core and the βA- and βD-sheets form a shared fourth propeller blade. β-sheets B and C from the second monomer are not resolved. The two monomers are rotated to each other by 90°. The crystal structure data of the *S. cerevisiae* Asc1p-homodimer derive from the PDB entry 3RFH (Yatime et al., 2011) and were used for visualization with the *PyMOL Molecular Graphics System* software.

1.6 Asc1p in other eukaryotes

As mentioned above the Asc1 protein is highly conserved throughout the eukaryotic kingdom. It shares a high degree of similarity to its orthologues from other eukaryotes on the amino acid sequence and quarternary structure level. Asc1p/RACK1 was studied in various eukaryotic systems, which is outlined in the following sections.

1.6.1 Asc1p in yeasts and filamentous fungi

The Asc1p orthologue Cpc2p of the fission yeast *S. pombe* is required for cell cycle coordination and sexual differentiation. Accordingly, Δ*cpc2* cells exhibit a defect in G_1 arrest for subsequent conjugation and meiosis, a prominent delay in G_2/M transition and concomitantly elongated cell size (Jeong et al., 2004; McLeod et al., 2000; Núñez et al., 2010; Won et al., 2001). Moreover, Cpc2p-depleted cells show an altered response to varying environmental stimuli including osmotic, oxidative, and cell wall stress (Núñez et al., 2009; Won et al., 2001). Deletion of *ASC1* in the human pathogen *Candida albicans* also affects developmental processes in this fungus. Upon environmental stimuli the ascomycete switches from the unicellular yeast form to hyphal structures, which are crucial for *C. albicans* virulence. As a result of Asc1p-depletion the fungus fails to form filaments, which goes along with decreased pathogenicity in a systemic mouse infection model (Kim et al., 2010; Liu et al., 2010). Furthermore, CpcB, the Asc1p orthologue in *Aspergilli*, supports conidial germination in both *Aspergillus nidulans* and *Aspergillus fumigatus* (Kong et al., 2013). It is further required for sexual development of *A. nidulans* and hyphal growth and pathogenicity especially in the opportunistic pathogen *A. fumigatus* (Cai et al., 2015; Kong et al., 2013). In the basidiomycete and human pathogen *C. neoformans* the Asc1p orthologue Gib2p functions as Gβ-subunit for the Gα-protein Gpa1p and is thus required for cAMP signaling, which is a central regulator of virulence of the fungus (Palmer et al., 2006; Wang et al., 2014). Accordingly, virulence of Gib2p-depleted cells in infected mice was significantly reduced (Ero et al., 2015). Deletion of Rak1 in *Ustilago maydis*, a basidiomycete that causes the corn smut disease, results in aberrant growth and colony morphology, defects in cell wall integrity, and reduced filament formation subsequently leading to a defect in cell fusion, which in turn affects virulence in maize (Wang et al., 2011).

1.6.2 RACK1 in plant physiology

A plant Asc1p/RACK1 orthologue was first identified in *Nicotiana tabacum* BY2 cells (Ishida et al., 1993). Meanwhile, RACK1 was found in numerous plant organisms including *Oryza sativa*, *A. thaliana*, *Phaseolus vulgaris*, *Zea mays*, and many more (Islas-Flores et al., 2009; Iwasaki et al., 1995; van Nocker and Ludwig, 2003; Yu et al., 2014). In contrast to fungal or animal organisms, several plant genomes possess more than one *RACK1* gene copy. In *A. thaliana*, RACK1 is encoded by three alleles, *RACK1A*, *RACK1B* and *RACK1C*, and *O. sativa* contains two copies (Chen et al., 2006; Zhang et al., 2014). In plant organisms, RACK1 is ascribed an important role in the control of hormonal responses. Expression of the RACK1 orthologue in tobacco is induced by auxin treatment and similarly, OsRACK1 and ZmRACK1 expression is regulated by different hormones (Ishida et al., 1993; Nakashima et al., 2008; Yu et al., 2014). Furthermore, RACK1 significantly influences the cellular response to hormones. *A. thaliana* RACK1 acts as negative regulator of the abscisic acid (ABA) pathway (Guo et al., 2009, 2011a). Intriguingly, ABA treatment and *rack1a* and *rack1b* double deletion have a similar effect on gene expression of a specific subset of genes (Guo et al., 2011a). Also, RACK1 plays a particular role in the plant immune response. OsRACK1 physically interacts with the Rac1 immune complex and is accordingly involved in the immune defense against potential threats (Nakashima et al., 2008). Within the plant kingdom a total of 138 proteins has been reported to interact with RACK1 in different species (Islas-Flores et al., 2015). This variety goes along with multiple cellular processes affected in different organisms. Plant RACK1 is involved in translation, plant development, and stress responses (Chen et al., 2006; Guo et al., 2009, 2011b, 2011a; Zhang et al., 2014). These processes finally affect the overall organism in terms of seed germination, flowering and leaf production (Chen et al., 2006; Zhang et al., 2014).

1.6.3 RACK1 in metazoan organisms

The Asc1/RACK1 protein is also studied in several metazoan model organisms. In the nematode *Caenorhabditis elegans* RACK1 mediates axon pathfinding and is required for lamellipodia and filopodia formation (Demarco and Lundquist, 2010). In the fruit fly *D. melanogaster*, a dynamic RACK1 expression pattern with a significant increase during early developmental stages, was observed in different tissues implying particular importance of the protein during embryogenesis (Kadrmas et al., 2007; Vani et al., 1997). Still, the protein is present at all developmental stages and was further attributed to gamete production and oogenesis in female flies (Kadrmas et al., 2007). Also in *Xenopus laevis* Rack1 is differentially

expressed in different tissues and at varying developmental stages, hinting to a major role in cellular differentiation (Kwon et al., 2001). It interacts with Ptk7, which controls planar cell polarity, and thus coordinates neural tube closure (Wehner et al., 2011). The *Danio rerio* Rack1 protein physically interacts with Vangl2, a protein that is required for planar cell polarity, and targets it to the cellular membrane. Therefore, zebrafish RACK1 is implicated in gastrulation (Li et al., 2011).

The RACK1 protein is highly expressed in various kinds of mammalian tissues, among others in brain, kidney, liver or spleen cells, and it shows a dynamic expression pattern according to developmental requirements in a cell type specific manner (Chou et al., 1999; Padanilam and Hammerman, 1997; Ron et al., 1994). RACK1 is highly expressed in embryonic mouse brains, but decreases at post-natal stages (Ashique et al., 2006). Similarly, RACK1 is significantly reduced in aged rat brains compared to their younger counterparts (Pascale et al., 1996). Furthermore, RACK1 expression is up-regulated in injured cells (Padanilam and Hammerman, 1997). Together, this implicates an important role for RACK1 in development. Accordingly, RACK1 is crucial for viability at early developmental stages, more precisely during gastrulation in mice (Volta et al., 2013). The protein is mainly located in the cytosol, but was also found in the nucleus (He et al., 2010; Rigas et al., 2003; Robles et al., 2010). A high number of putative interaction partners hints to the versatility of biological processes RACK1 is involved in, though it can be assumed that the specific interactions and processes are cell context specific (Gandin et al., 2013a). RACK1 is implicated in protein translation (see 1.5.1), signaling (see 1.5.2), and transcription (see 1.7). Furthermore RACK1 interacts with a multitude of proteins of the intracellular transport machinery and regulates cytoskeletal organizations and focal adhesion assemblies (see 1.7; Doan and Huttenlocher, 2007; Hermanto et al., 2002; Kiely et al., 2006, 2008). Since RACK1 is further involved in neuronal responses, it is not surprising that neurodegenerative diseases, e.g. Alzheimer's disease, were connected to RACK1 (Battaini et al., 1999). Its function in cell proliferation and spreading connects RACK1 tightly with different types of cancer (Serrels et al., 2010). It was declared as prognostic indicator of breast cancer and was further identified to be involved in several other kinds of cancer (Cao et al., 2010; Li and Xie, 2015).

1.7 RACK1 affects further molecular mechanisms in higher eukaryotes

In the preceding chapters the impact of Asc1p/RACK1 on several cellular processes in yeast and further eukaryotic organisms was described in detail. The scaffold contributes to translational control in multiple ways and is a major player in cellular signaling. In eukaryotes other than the baker's yeast, further molecular mechanisms and cellular processes are described to be affected by the scaffold Asc1p/RACK1, which are summarized in the following paragraphs and in Tab. 1.

According to its name, the mammalian Asc1p orthologue RACK1 functions as receptor for activated protein kinase C (Ron et al., 1994). In mammals, 11 PKC isoforms are described, classified as classical (α, βI, βII, γ), novel (δ, ε, η, θ) and atypical (ζ, ι/λ) PKCs (Mukherjee et al., 2016). RACK1 was reported to interact with several PKC isoforms (Liedtke et al., 2002; Robles et al., 2010; Rosdahl et al., 2002; Wehner et al., 2011), an interaction that stabilizes PKC in its active conformation (Ron et al., 1994). The great diversity of PKC isoforms requires a high degree of regulation, which is mediated in part by RACK1. Furthermore, PKC signaling is tightly connected to other signaling pathways, e.g. Src signaling (Chang et al., 2001). Amongst others, RACK1 binds several Src-family kinases, in this case, however, the interaction inhibits kinase activity (Chang et al., 1998; Yaka et al., 2002).

As described in chapter 1.5.1, Asc1p/RACK1 is involved in translational regulation at multiple stages. In plants and animals, RACK1 additionally mediates mRNA silencing (Jannot et al., 2011; Otsuka et al., 2011; Speth et al., 2013). Fine-tuning of mRNA translation is mediated by short non-coding RNAs, namely microRNAs or miRNAs, which are able to silence messages by complementary base pairing with these mRNAs (Carthew and Sontheimer, 2009). After miRNA processing the mature miRNA associates with multiple proteins, amongst others the Argonaute (AGO) protein. Together, they form the miRNA-induced silencing complex (miRISC), which subsequently controls transcript silencing or degradation via complementary base pairing (Carthew and Sontheimer, 2009). RACK1 interacts with different components of the miRNA processing machinery and of the miRISC in different eukaryotic organisms as summarized in Tab. 1, and thus further impacts translational regulation at a posttranscriptional level.

Additionally, RACK1 affects gene expression at a transcriptional level as it is able to shuttle into the nucleus in mammalian cells. Since RACK1 has no nuclear entry or export sequence, the translocation of the scaffold protein is most probably aided by its interaction partners. Within the nucleus, RACK1 physically interacts with various transcriptional regulators and thereby impacts the transcription of specific genes (Tab. 1).

Tab. 1: Molecular mechanisms affected by RACK1 in plant and metazoan organisms. The functions of specific RACK1 protein interactions in eukaryotes are summarized and assigned to the processes these interactions contribute to.

Process	Organism	RACK1 interactor		Observation/function	Reference
mRNA silencing	human, *C. elegans*	miRISC		RACK1 bridges the interaction of miRISC with translating ribosomes and with mRNAs.	Jannot et al., 2011
	human	KSRP AGO2		RACK1 is needed for miRNA recruitment into the miRISC.	Otsuka et al., 2011
	A. thaliana	SERRATE AGO1		RACK1 is involved in miRNA maturation and transcript silencing.	Speth et al., 2013
Protein kinase regulation	human, rat, rabbit, chinese hamster, frog	PKCβII and further PKC isoforms		RACK1 stabilizes the activated conformation of serine and threonine kinases and shuttles activated PKCβII to subcellular localizations. RACK1 couples PKCβII to ribosomes for translational control.	Grosso et al., 2008a, 2008b; Ron et al., 1994, 1995, 1999; Sharma et al., 2013
	human	Src-family tyrosine kinases	Src	RACK1 is phosphorylated by Src and binds Src and inhibits the activity.	Chang et al., 1998, 2001, 2002
	mouse, rat		Fyn	RACK1 inhibits Fyn activity and bridges the association of Fyn with the NMDAR. After cAMP/PKA pathway activation Fyn dissociates from RACK1 and phosphorylates NMDAR.	Yaka et al., 2002, 2003
Translocation into the nucleus	mouse	PKCα		RACK1 shuttles rhythmically into the nucleus and promotes BMAL1 phosphorylation. It affects transcription of circadian genes.	Robles et al., 2010
	human, rat, mouse	14-3-3ζ, (scaffold protein)		RACK1 binds chromatin at the BDNF promoter upon cAMP/PKA pathway activation resulting in chromatin remodeling and BDNF transcription.	He et al., 2010; Neasta et al., 2012; Yaka et al., 2003
	human	androgen receptor (transcription factor)		RACK1 affects androgen receptor phosphorylation resulting in transcriptional regulation of its target genes.	Kraus et al., 2006; Rigas et al., 2003
Ion channel and receptor binding	human, rat	GABA$_A$		RACK1 promotes PKC-dependent GABA$_A$-subunit phosphorylation.	Brandon et al., 1999, 2002; Feng et al., 2001
	rat	NMDA receptor		RACK1 regulates NMDAR phosphorylation by Fyn kinase and impacts channel activity.	Yaka et al., 2002
	mink, chick	PTPμ		RACK1 interacts with PTPμ primarily during cell-cell contact.	Mourton et al., 2001; Rosdahl et al., 2002
	human, mouse	IGF-IR		RACK1 scaffolds the complex formation with further signaling proteins at the IGF-I receptor for downstream signaling in adhesive cells.	Kiely et al., 2002, 2005; Zhang et al., 2006
	human	β-integrin		RACK1 interacts with β-integrin after phorbol ester treatment resulting in cell adhesion.	Liliental and Chang, 1998
Focal adhesion	human	PP2A		RACK1 binds PP2A at IGF-IR and dissociates after IGF-I stimulation leading to PP2A inactivation.	Kiely et al., 2006, 2008
	human	c-Abl		RACK1 is phosphorylated by c-Abl enabling RACK1-FAK interaction. RACK1 regulates FAK phosphorylation.	Kiely et al., 2009

Tab. 1: Continued.

Process	Organism	RACK1 interactor	Observation/function	Reference
Focal adhesion	human	paxillin	RACK1 affects paxillin phosphorylation and dynamics.	Doan and Huttenlocher, 2007; Mamidipudi et al., 2004
	human, chinese hamster	Src	RACK1 binds and regulates Src kinase at focal adhesions.	Cox et al., 2003; Doan and Huttenlocher, 2007
	rat	ERK	RACK1 targets active ERK to focal adhesions in response to FAK activation.	Vomastek et al., 2007
	human	talin and vinculin	RACK1 interacts with vinculin in adhesive and with talin in floating cells.	de Hoog et al., 2004
	mouse	PDE4D5	RACK1 bridges the interaction of the phosphodiesterase PDE4D5 and FAK.	Serrels et al., 2010

At cellular membranes RACK1 interacts with cytoplasmic tails of various receptors and ion channels (Tab. 1) and is thus involved in the intracellular response to extracellular cues. The focal adhesion complex is a multiprotein complex that provides a physical link between the extracellular matrix via integrins to the cytoskeleton which allows the cell to respond to mechanical signals. This complex consists of integrins, which are directly attached to the extracellular matrix at the outer surface of the cell, and of multiple scaffold proteins that connect the integrins to actin and various downstream signaling pathways. Although RACK1 is not present in mature adhesions, the scaffold is essentially involved in the assembly of this complex and physically interacts with multiple compounds or mediates their posttranslational modification within focal adhesions (Tab. 1). Accordingly, RACK1 silencing results in insufficient focal adhesion assembly and disturbed focal adhesion disassembly (Cox et al., 2003; Doan and Huttenlocher, 2007; Onishi et al., 2007).

1.8 Aim of the study

This study aimed to characterize the microenvironment of the Asc1 protein associated to the head region of the 40S ribosomal subunit and its changes in response to different growth conditions. To this end, the *in vivo* protein labeling technique *proximity-dependent Biotin IDentification*, short *BioID*, was established for the yeast *S. cerevisiae* and applied in combination with *stable isotope labeling with amino acids in cell culture* (SILAC) for quantitative liquid chromatography-mass spectrometry (LC-MS) analysis. Asc1p was described as a mediator between cellular signaling and ribosomal translation and might thus organize the neighborhood of proteins in a spatiotemporal manner depending on environmental

stimuli. Proteins proximal to Asc1p were sought for during exponential growth, and the dynamics of this neighborhood were studied in response to mild heat shock and glucose starvation. Synthetic deletions of genes encoding Asc1p proximal proteins together with the *asc1*⁻ allele were phenotypically characterized for possible genetic interactions. The Asc1$^{R38D\ K40E}$ protein variant was reported as ribosome-binding deficient inferred from its low abundance in polysome fractions after sucrose density gradient ultracentrifugation. Yet, expected *asc1*⁻ phenotypes were not observed for *asc1$^{R38D\ K40E}$* strains, hinting either to Asc1p's proper function without ribosome-binding or to an experimental artefact separating the protein from polysomes only during ultracentrifugation. Proximity analyses with BioID were performed to characterize its microenvironment and to clarify the *in vivo* situation of Asc1$^{R38D\ K40E}$p. To further characterize physical interactions between Asc1p and proximal proteins identified with BioID, the incorporation of the UV-inducible artificial amino acid Bpa into Asc1p was prepared for future *in vitro* cross-link experiments with recombinantly purified proteins. Altogether, at the example of the ribosomal Asc1 protein, this study aimed for a better understanding of how the proximity of a scaffold protein appears and changes in dependence of different environmental stimuli or amino acid exchanges within the protein that alter the anchorage of the scaffold protein to its destined site at the ribosome.

2. Materials and Methods

Figures presented in this work were generated with the Adobe Illustrator and Adobe Photoshop Elements CS6 software (Adobe Systems, San Jose, California, USA). Text editing and data processing and presentation was executed with Microsoft Word and Microsoft Excel 2010 (Microsoft, Redmond, Washington, USA).

2.1 *S. cerevisiae* strains and their construction

The *S. cerevisiae* strains used in this work are of the Σ1278b background and are listed in Tab. 2. For gene knock-outs generated in this work the plasmid pUG72 (Gueldener et al., 2002) was used as template to produce a *loxP-URA3-loxP* cassette by polymerase chain reaction (PCR). Primers with overhangs homologous to the 5'- and 3'-flanking regions of the respective genes were employed and the resulting PCR-products were inserted into the genome of the RH2817, RH3263 or RH3510 strain by homologous recombination. Oligonucleotides used as primers are listed in Tab. S1. Transformants were selected on medium without uracil and were confirmed by PCR and Southern hybridization.

Tab. 2: *S. cerevisiae* strains used in this work. For single and double mutant strains at least two individual clones were generated and are listed with individual strain identifiers.

Strain	Genotype	Reference
RH2817	*MATα, ura3-52, trp1::hisG*	Valerius et al., 2007
RH3263	*MATα, ura3-52, trp1::hisG, leu2::hisG, Δasc1::LEU2*	Valerius et al., 2007
RH3510	*MATα, ura3-52, trp1::hisG, asc1-loxP SNR24*	Rachfall et al., 2013
RH3493	*MATα, ura3-52, trp1::hisG, Δarg4::loxP, Δlys1::loxP*	Schmitt et al., 2017
RH3494	*MATα, ura3-52, trp1::hisG, leu2::hisG, Δasc1::LEU2, Δarg4::loxP, Δlys1::loxP*	Schmitt, 2015
RH3653 RH3654 RH3655	*MATα, ura3-52, trp1::hisG, Δstm1::URA3*	This work
RH3656 RH3657 RH3658	*MATα, ura3-52, trp1::hisG, leu2::hisG, Δasc1::LEU2, Δstm1::URA3*	This work
RH3659 RH3660	*MATα, ura3-52, trp1::hisG, asc1-loxP SNR24, Δstm1::URA3*	This work

Tab. 2: Continued.

Strain	Genotype	Reference
RH3661 RH3662 RH3663	*MATα, ura3-52, trp1::hisG, Δgis2::URA3*	This work
RH3664 RH3665 RH3666	*MATα, ura3-52, trp1::hisG, leu2::hisG, Δasc1::LEU2, Δgis2::URA3*	This work
RH3667 RH3668	*MATα, ura3-52, trp1::hisG, asc1-loxP SNR24, Δgis2::URA3*	This work
RH3669 RH3670 RH3671	*MATα, ura3-52, trp1::hisG, Δscp160::URA3*	This work
RH3672 RH3673	*MATα, ura3-52, trp1::hisG, leu2::hisG, Δasc1::LEU2, Δscp160::URA3*	This work
RH3674 RH3675	*MATα, ura3-52, trp1::hisG, asc1-loxP SNR24, Δscp160::URA3*	This work
RH3676 RH3677 RH3678	*MATα, ura3-52, trp1::hisG, Δhek2::URA3*	This work
RH3679 RH3680 RH3681	*MATα, ura3-52, trp1::hisG, asc1-loxP SNR24, Δhek2::URA3*	This work
RH3682 RH3683	*MATα, ura3-52, trp1::hisG, Δdef1::URA3*	This work

2.2 Bacterial strain and plasmid constructions

The *E. coli* DH5α strain (F', *Φ80dlacZΔM15*, Δ(*lacZYA-argF*), *U169*, *deo*R, *rec*A1, *end*A1, *hsd*R17, (rK⁻, mK⁺), *sup*E44, λ-, *thi*-1, *gyr*A96, *rel*A1; Woodcock et al., 1989) was used for plasmid generation and amplification. Plasmids used in this study are listed in Tab. 3. Oligonucleotides used as primers for plasmid generation are listed in Tab. S1. For the generation of a plasmid encoding an *ASC1-birA** fusion gene (see also Fig. 8A), the *ASC1*-containing high-copy number plasmid pME2624 served as backbone. This plasmid was linearized by PCR with a forward primer annealing downstream of the *ASC1* ORF and a reverse primer annealing to the 3'-end of the *ASC1* ORF excluding the stop codon. The reverse primer featured a large overhang containing a 36 base pair linker sequence and a sequence complementary to the first 20 base pairs of the *birA** gene after the start codon. The *birA** allele

containing the point mutation R118G was amplified from plasmid pRS313 (kindly provided by Dr. H. D. Schmitt, Max Planck Institute of Biophysical Chemistry, Göttingen) without its start codon. The reverse primer contained a sequence complementary to the plasmid backbone. The linearized plasmid backbone and the *birA** fragment were fused by homologous recombination using the *In-Fusion® HD Cloning Kit* (#639650, Clontech, Mountain View, California, USA). The coding sequence of the *ASC1-birA** fusion was verified by DNA sequencing and the plasmid was named pME4478. Similarly, a plasmid expressing the mere *birA** was constructed (see also Fig. 8B): Plasmid pME2624 was linearized by PCR with the forward primer annealing downstream of the *ASC1* ORF and a reverse primer annealing to the plasmid backbone upstream of the *ASC1* ORF with a 20 bp overhang complementary to the *birA** gene. The *birA** allele including the ATG start codon was amplified from plasmid pRS313 and fused with the linearized plasmid backbone by homologous recombination. The coding sequence of *birA** was verified by DNA sequencing and the plasmid was named pME4480. A plasmid encoding an *asc1^{DE}-birA** fusion was generated by site directed mutagenesis (see also Fig. 8C). The mutated *asc1^{DE}* allele features two amino acid exchanges: R38D and K40E. To insert these substitutions within the *ASC1-birA** allele, pME4478 bearing the *ASC1-birA** fusion gene was used as template. With a complementary primer pair carrying the two mutations in its central part, the *ASC1-birA** plasmid was fully amplified resulting in the *asc1^{DE}-birA** vector. The template DNA was removed by *Dpn*I treatment which exclusively digests methylated DNA, and thus only the parental vectors. The resulting plasmid was verified by DNA sequencing and termed pME4479. To obtain plasmid pME4481 *ASC1* and its native promoter were amplified from pME4364 with oligonucleotides that generated a *Sac*I and an *Xho*I site for restriction digestion and cloning into pME2789. Plasmids bearing *asc1* mutant alleles with codons exchanged to the amber stop codon for the incorporation of the artificial photoreactive amino acid ρ-b̲enzoyl-p̲henyl̲a̲lanine (Bpa) were also generated by site directed mutagenesis using pME2834 and pME2624 as templates. The *asc1* alleles were confirmed by DNA sequencing and are named pME4174-pME4181, pME4183, pME4185, pME4186 and pME4482-pME4525.

Tab. 3: Plasmids used in this work.

Plasmid	Description	Reference
pUG72	*AmpR, pUC_{ori}, loxP::URA3::loxP*	Gueldener et al., 2002
pME2787	*MET25Prom, CYC1Term, URA3*, 2 μm	Mumberg et al., 1994
pME2789	*GAL1Prom, CYC1Term, TRP1, CEN/ARS*	Mumberg et al., 1994

Tab. 3: Continued.

Plasmid	Description	Reference
pME2791	*GAL1Prom, CYC1Term, URA3, CEN/ARS*	Mumberg et al., 1994
pME2624	pME2787 with *ASC1*	Our collection
pME2834	pME2787 with *ASC1-Strep*	Our collection
pME4364	pME2791 with *ASC1* with its native promoter (500 bp)	Schmitt et al., 2017
pHK1249	*EDC3Prom, URA3, CEN/ARS*; *EDC3-mCH*	Buchan et al., 2008
pESC Yrs	*ADH1Prom, TRP1, 2 µm,* TyrRS/tRNA$_{CUA}$	Chin et al., 2003
pRS313	*PGK1Prom, CYC1Term, HIS3, CEN/ARS, birA^{R118G}* (based on van Werven and Timmers, 2006)	H. D. Schmitt (MPI-BPC)
pME4478	*MET25Prom, CYC1Term, URA3, 2 µM, ASC1-birA**	This work
pME4479	*MET25Prom, CYC1Term, URA3, 2 µM, asc1^{DE}-birA**	This work
pME4480	*MET25Prom, CYC1Term, URA3, 2 µM, birA**	This work
pME4481	pME2789 with *ASC1* with its native promoter (500 bp)	This work
pME4174	pME2787 with *asc1^{P30Amber}-Strep*	This work
pME4175	pME2787 with *asc1^{D51Amber}-Strep*	This work
pME4176	pME2787 with *asc1^{F54Amber}-Strep*	This work
pME4177	pME2787 with *asc1^{A75Amber}-Strep*	This work
pME4178	pME2787 with *asc1^{A95Amber}-Strep*	This work
pME4179	pME2787 with *asc1^{K118Amber}-Strep*	This work
pME4180	pME2787 with *asc1^{K137Amber}-Strep*	This work
pME4181	pME2787 with *asc1^{Q139Amber}-Strep*	This work
pME4183	pME2787 with *asc1^{T209Amber}-Strep*	This work
pME4185	pME2787 with *asc1^{P267Amber}-Strep*	This work
pME4186	pME2787 with *asc1^{Q299Amber}-Strep*	This work
pME4482	pME2787 with *asc1^{N17Amber}-Strep*	This work
pME4483	pME2787 with *asc1^{K62Amber}-Strep*	This work
pME4484	pME2787 with *asc1^{K107Amber}-Strep*	This work
pME4485	pME2787 with *asc1^{K129Amber}-Strep*	This work
pME4486	pME2787 with *asc1^{N148Amber}-Strep*	This work
pME4487	pME2787 with *asc1^{N174Amber}-Strep*	This work
pME4488	pME2787 with *asc1^{N196Amber}-Strep*	This work
pME4489	pME2787 with *asc1^{Q237Amber}-Strep*	This work
pME4490	pME2787 with *asc1^{R275Amber}-Strep*	This work

Tab. 3: Continued.

Plasmid	Description	Reference
pME4491	pME2787 with $asc1^{F278Amber}$-*Strep*	This work
pME4492	pME2787 with $asc1^{Y281Amber}$-*Strep*	This work
pME4493	pME2787 with $asc1^{H288Amber}$-*Strep*	This work
pME4494	pME2787 with $asc1^{N17Amber}$	This work
pME4495	pME2787 with $asc1^{P30Amber}$	This work
pME4496	pME2787 with $asc1^{F54Amber}$	This work
pME4497	pME2787 with $asc1^{K62Amber}$	This work
pME4498	pME2787 with $asc1^{I67Amber}$	This work
pME4499	pME2787 with $asc1^{A75Amber}$	This work
pME4500	pME2787 with $asc1^{K87Amber}$	This work
pME4501	pME2787 with $asc1^{A95Amber}$	This work
pME4502	pME2787 with $asc1^{K107Amber}$	This work
pME4503	pME2787 with $asc1^{K118Amber}$	This work
pME4504	pME2787 with $asc1^{K129Amber}$	This work
pME4505	pME2787 with $asc1^{K137Amber}$	This work
pME4506	pME2787 with $asc1^{Q139Amber}$	This work
pME4507	pME2787 with $asc1^{N148Amber}$	This work
pME4508	pME2787 with $asc1^{K161Amber}$	This work
pME4509	pME2787 with $asc1^{D165Amber}$	This work
pME4510	pME2787 with $asc1^{N174Amber}$	This work
pME4511	pME2787 with $asc1^{F186Amber}$	This work
pME4512	pME2787 with $asc1^{N196Amber}$	This work
pME4513	pME2787 with $asc1^{T209Amber}$	This work
pME4514	pME2787 with $asc1^{A226Amber}$	This work
pME4515	pME2787 with $asc1^{K228Amber}$	This work
pME4516	pME2787 with $asc1^{Q237Amber}$	This work
pME4517	pME2787 with $asc1^{E239Amber}$	This work
pME4518	pME2787 with $asc1^{N248Amber}$	This work
pME4519	pME2787 with $asc1^{T258Amber}$	This work
pME4520	pME2787 with $asc1^{P267Amber}$	This work
pME4521	pME2787 with $asc1^{R275Amber}$	This work
pME4522	pME2787 with $asc1^{F278Amber}$	This work

Tab. 3: Continued.

Plasmid	Description	Reference
pME4523	pME2787 with *asc1*^{Y281Amber}	This work
pME4524	pME2787 with *asc1*^{H288Amber}	This work
pME4525	pME2787 with *asc1*^{Q299Amber}	This work

2.3 Cultivation of microorganisms

2.3.1 Cultivation of *S. cerevisiae* cells

Yeast strains were cultivated at 30°C in yeast extract peptone dextrose medium (YEPD; 1% yeast extract, 2% peptone, 2% glucose) or yeast nitrogen base minimal medium (YNB; 0.15% yeast nitrogen base without amino acids and ammonium sulfate, 0.5% ammonium sulfate, 2% glucose) with the respective supplements. Liquid cultures were cultivated on a shaker at approximately 100 rpm and solid medium was supplied with 2% agar. L-arginine (20 mg/l), L-lysine HCl (30 mg/l), L-tryptophan (20 mg/l) and uracil (20 mg/l) were supplemented if required. For differential protein labeling according to the SILAC approach 50 mg/l differentially labeled L-arginine and L-lysine were added to the growth medium ($^{13}C_6$-L-arginine HCl (#201203902), $^{13}C_6$ $^{15}N_4$-L-arginine HCl (#201603902), 4,4,5,5-D_4-L-lysine HCl (#211103912), $^{13}C_6$-L-lysine HCl (#211203902); Silantes GmbH, München, Germany). The optical density (OD) of cell cultures was determined by photometrical measurement at 600 nm. The culture volume required for inoculation of main cultures was calculated according to the following formula:

$$V_i = V_m \cdot OD_m \cdot e^{-\mu \cdot \Delta t}/OD_p$$

with V_i = inoculation volume in ml, V_m = volume of main culture in ml, OD_m = desired OD_{600} of main culture, OD_p = OD_{600} pre-culture, μ = growth rate (0.29/h), and Δt = growth time in h.

2.3.2 Cultivation of *E. coli* cells

E. coli cells were cultivated in lysogeny broth liquid medium (LB; 1% tryptone, 0.5% yeast extract, 1% NaCl) supplemented with 100 μg/ml ampicillin for selection with shaking or on agar plates containing 2% agar. Cultures were grown at 37°C.

2.4 DNA-extraction from microorganisms

2.4.1 Isolation of genomic DNA from *S. cerevisiae*

The isolation of genomic DNA from *S. cerevisiae* was performed according to Hoffman and Winston (1987). After overnight cultivation of *S. cerevisiae* strains in 10 ml YEPD medium cells were collected by centrifugation at 3,000 rpm for 3 min and washed with 500 μl H_2O. Cell lysis was obtained by vigorous shaking for 5 min at 4°C in 200 μl lysis buffer (2% Triton X-100, 1% sodium dodecyl sulfate (SDS), 100 mM NaCl, 10 mM Tris pH 8.0, 1 mM EDTA), 200 μl phenol:chloroform:isoamylalcohol mix (25:24:1; #A156.2, Carl Roth GmbH & Co. KG, Karlsruhe, Germany) and in the presence of an equal amount of glass beads. After centrifugation at 13,000 rpm for 5 min the aqueous phase was transferred to a fresh reaction tube. 200 μl phenol:chloroform:isoamylalcohol (25:24:1) were added, the sample was mixed and centrifuged again at 13,000 rpm for 5 min. The resulting aqueous phase was transferred to a new reaction tube and mixed with 1 ml ice-cold 100% ethanol. For efficient precipitation the samples were incubated at -20°C for at least 10 min. Nucleic acids were sedimented by centrifugation at 13,000 rpm for 5 min at 4°C and resuspended in 400 μl H_2O. For RNA degradation 3 μl RNaseA (10 mg/ml) were supplied and the sample was incubated at 37°C for 10 min. Afterwards 10 μl 4 M ammonium acetate and another 1 ml ice-cold ethanol were added to precipitate DNA. The sediment was dried at room temperature and the DNA was dissolved in 50 μl H_2O.

2.4.2 Isolation of plasmid DNA from *E. coli*

Plasmid DNA was isolated from 5 ml *E. coli* overnight cultures with the *QIAPrep Spin Miniprep Kit* (#27106, QIAGEN GmbH, Hilden Germany) according to the manufacturer's instructions.

2.5 Cloning techniques

2.5.1 Polymerase chain reaction

Polymerase chain reactions (PCRs) were performed according to Saiki et al. (1985). Depending on the intended application of the resulting PCR product different DNA polymerases were applied. Amplification of DNA for genomic integration by homologous recombination or plasmid generation was performed with the *KOD* DNA polymerase (#71085-3, Merck, Darmstadt, Germany) or the *Phusion* High-Fidelity DNA Polymerase (#F-530L, Thermo Fisher Scientific, Waltham, Massachusetts, USA). Amplification of rather long DNA fragments like whole plasmid backbones was done with the *Q5® Hot Start High Fidelity* DNA Polymerase

(#M0494S, New England Biolabs, Frankfurt am Main, Germany). Analytical PCRs for strain or plasmid confirmation were done with the *Taq* DNA polymerase (#EP0404, Thermo Fisher Scientific) or the *Pfu* DNA polymerase (#EP0572, Thermo Fisher Scientific). All polymerases were used according to the manufacturer's instructions. Oligonucleotides were obtained from Eurofins MWG Operon (Ebersberg, Germany).

2.5.2 Agarose gel electrophoresis

DNA fragments were mixed with 10x DNA loading dye (10% Ficoll 400, 0.2% bromphenol blue sodium salt, 0.2% xylene cyanol, 200 mM EDTA, pH 8.0) in a 1:10 ratio and samples were loaded on horizontal 1% agarose gels. Agarose was dissolved in TAE buffer (40 mM tris-acetate, 20 mM acetic acid, 2 mM EDTA, pH 8.3) and supplemented with 0.5 µg/ml ethidium bromide. DNA fragments were separated electrophoretically in TAE-buffer at 90 V and visualized with the *Gel iX20 Imager* (Intas Science Imaging Instruments, Göttingen, Germany) at 254 nm. The *GeneRuler 1 kb DNA Ladder* (#SM0311, Thermo Fisher Scientific) was used as reference to estimate the size of DNA fragments. For DNA extraction from agarose gels respective DNA bands where excised from the gel and DNA was purified with the *QIAquick Gel Extraction Kit* (#28706, QIAGEN GmbH) according to the manufacturer's instructions.

2.5.3 Restriction digestion of DNA

DNA restriction digestions were performed with type II restriction endonucleases and their suitable digestion buffers (Thermo Fisher Scientific) in a total volume of 20 µl according to the manufacturer's instructions. Samples were incubated at 37°C for 3 h or overnight.

2.5.4 Ligation of DNA

To ligate DNA fragments obtained by restriction digestion linearized plasmid DNA was mixed with an excess of the respective insert DNA, 1 µl T4 DNA ligase (#EL0016, Thermo Fisher Scientific) and 2 µl of the supplied 10x ligase buffer in a total volume of 20 µl and incubated at room temperature for 10 min before transformation of *E. coli* cells. Alternatively, linearized plasmid backbones and insert fragments with respective overhangs were fused by homologous recombination using the *In-Fusion® HD Cloning Kit* (#639650, Clontech) according to the manufacturer's instructions.

2.5.5 DNA sequencing

DNA sequencing was carried out by the *Göttingen Genomics Laboratory* (G2L, Göttingen, Germany) with 100 ng of DNA and 5 pmol of the respective primer or by the *Seqlab Sequencing Laboratories Göttingen GmbH* (Göttingen, Germany) with 720-1200 ng of DNA and 30 pmol of the respective primer.

2.6 Transformation of microorganisms

2.6.1 Transformation of *S. cerevisiae*

Transformation of *S. cerevisiae* cells was carried out according to the lithium acetate method (Ito et al., 1983). Yeast cells were pre-cultured overnight and 700-800 µl of this cell suspension were used to inoculate the 10 ml YEPD main culture that was subsequently cultivated for another 4-6 h. The cells were collected by centrifugation at 3,000 rpm for 3 min and resuspended in 10 ml lithium acetate/TE buffer (0.1 M lithium acetate, 10 mM Tris-HCl, 1 mM EDTA, pH 8.0). The cell suspension was incubated 15-20 min on a shaker for genomic integration of linear DNA fragments. For transformation with plasmid DNA no further incubation was required. The cells were harvested by centrifugation at 3,000 rpm for 3 min, the supernatant was discarded, and the cells were resuspended in the residual liquid. Each 200 µl of the cell suspension were transferred to two 1.5 ml reaction tubes and 20 µl preheated (65°C) single stranded salmon sperm DNA (10 mg/ml in TE buffer, pH 8.0) were added. Plasmid DNA or linear DNA fragments for chromosomal integration were added to one of the samples, the other one served as negative control and was not supplied with DNA. Both samples were mixed with 800 µl 50% PEG 4000 (in lithium acetate/TE buffer), incubated at 30°C for 30 min, and exposed to heat shock at 42°C for 25 min. The cells were collected by centrifugation at 7,000 rpm for 30 sec and resuspended in 1 ml YEPD medium. The samples were incubated at 30°C on a shaker for 1 h or 3 h for plasmid transformation or chromosomal integration of linear DNA fragments, respectively. The cells were sedimented by centrifugation at 4,000 rpm for 30 sec and resuspended in the residual liquid. The cell suspension was dispersed on solid selective media and incubated for 3 days at 30°C.

2.6.2 Preparation of competent *E. coli* cells

Competent *E. coli* cells were generated according to Inoue et al. (1990). DH5α cells were cultivated at 20°C in 250 ml super optimal broth (SOB) medium (2% tryptone, 0.5% yeast extract, 10 mM NaCl, 2.5 mM KCl, 10 mM MgCl$_2$, 10 mM MgSO$_4$) while shaking at 200 rpm for approximately 24 h until an OD$_{600}$ of 0.6. The cells were incubated on ice for 10 min and

collected by centrifugation at 2,500 x g for 10 min at 4°C. The cell sediment was dissolved in 80 ml transformation buffer (TB; 10 mM HEPES, 15 mM CaCl$_2$, 55 mM MnCl$_2$, 250 mM KCl, pH 6.7) and incubated on ice for further 10 min. The cells were collected by centrifugation at 2,500 x g for 10 min at 4°C and resuspended in 20 ml TB. 1.4 ml DMSO were added and the cells were incubated on ice for 10 min. Small aliquots were frozen in liquid nitrogen and stored at -80°C.

2.6.3 Transformation of *E. coli*

200 µl competent *E. coli* DH5α cells were thawed on ice and mixed with 20 µl of a prepared ligation reaction (see 2.4.4) or 1 µl intact plasmid DNA (see 2.3.2). The samples were incubated for 30 min on ice, followed by a 90 sec heat shock at 42°C. Cells were chilled on ice for another 3 min and mixed with 800 µl LB medium. After incubation for 1 h at 37°C on a shaker the cells were collected by centrifugation at 5,000 rpm for 2 min. The supernatant was discarded and the cells were resuspended in the remaining liquid. The cell suspension was dispersed on solid selective medium and incubated overnight at 37°C.

2.7 Southern hybridization

The verification of correct locus integration of linear DNA fragments into the yeast genome was done by Southern hybridization experiments performed according to Southern (1975). Whole genomic DNA of *S. cerevisiae* was fragmented by restriction digestion overnight, and the resulting fragments were heated to 65°C for 10 min and electrophoretically separated on a 1% agarose gel at 70 V for 10 min, followed by approximately 2 h at 90 V. The gel was washed for 10 min in 0.25 M HCl, for 25 min in 0.5 M NaOH/1.5 M NaCl and 30 min in 1.5 M NaCl/0.5 M Tris, pH 7.5. By capillary blotting for 2-3 h or overnight the DNA was transferred from the gel to the nylon *Hybond-N Membrane* (#RPN203N, GE Healthcare, München, Germany). The membrane was dried at 75°C for 7 min, and UV-exposure for 3 min per side cross-linked the DNA to the membrane. Prehybridization buffer (0.5 M NaCl, 4% Blocking reagent; #NIP552, GE Healthcare), pre-heated to 55°C, was added to the membrane and incubated for at least 30 min at 55°C. The labeled DNA-probe was generated according to the manufacturer's instructions with the *AlkPhos Direct Labeling Reagents* (#RPN3680, GE Healthcare) and added to the membrane for hybridization overnight at 55°C. The membrane was washed twice for 10 min at 55°C with the first wash buffer (2 M urea, 0.1% SDS, 50 mM sodium phosphate, pH 7, 150 mM NaCl, 1 mM MgCl$_2$, 0.2% Blocking reagent), followed by washing twice with the second wash buffer (50 mM Tris base, 100 mM NaCl, 2 mM MgCl$_2$,

pH 10) for 5 min each at room temperature. For signal detection the membrane was covered with 1 ml *CDP-Star^{TM} Detection Reagent* (#RPN3682, GE Healthcare), incubated for 5 min and finally exposed to the *Amersham Hyperfilm^{TM}-ECL^{TM}* (#28906836, GE Healthcare).

2.8 Protein analyses

2.8.1 Preparation of whole protein extracts from *S. cerevisiae*

For inoculation of a 50 ml main culture two sequential 10 ml YNB pre-cultures were cultivated at 30°C, the first one overnight, the second subsequently for approximately eight hours. The latter was used to inoculate the main culture, which was in turn grown overnight to an OD_{600} of 0.8 unless stated otherwise. Cells were collected by centrifugation at 3,000 rpm for 3 min at 4°C and washed in 2.5 ml ice-cold breaking buffer (100 mM Tris-HCl, pH 7.5, 200 mM NaCl, 5 mM EDTA, 20% glycerol) or 1xStrep buffer (10 mM HEPES, pH 7.9, 10 mM KCl, 1.5 mM $MgCl_2$) if protein purification with Strep-Tactin® columns was intended. Cells were collected again at 3,000 rpm for 3 min and resuspended in 500 µl breaking buffer containing 1 *cOmplete^{TM}* protease inhibitor cocktail tablet (#11836145001, Roche Diagnostics, Mannheim, Germany) per 50 ml and 0.5% β-mercaptoethanol, or in 500 µl 1x Strep buffer with 1 *cOmplete^{TM}* protease inhibitor cocktail tablet per 50 ml, 0.5 mM DTT and 0.5 mM PMSF. In case of phospho-protein analyses 1 *PhosSTOP^{TM}* phosphatase inhibitor cocktail tablet (#04906837001, Roche Diagnostics) per 10 ml, 1 mM NaF, 8 mM β-glycerol phosphate, and 0.5 mM sodium vanadate were added. Cell lysis was carried out with the *Retsch MM400* (Retsch GmbH, Haan, Germany) with a frequency of 30 sec^{-1} for 4 min in the presence of glass beads (∅ 0.25 to 0.50 mm). For denaturing cell lysis the sample was mixed thoroughly with 4% SDS on a shaker for 5 min and heated to 65°C for 5 min. After centrifugation at 13,000 rpm for 15 min at room temperature the protein containing supernatant was transferred to a fresh 1.5 ml reaction tube. Protein concentrations were determined with the *BCA reagent* (#23224 and #23228, Thermo Fisher Scientific) according to the manufacturer's instructions.

2.8.2 Enrichment of biotinylated proteins and peptides with Strep-Tactin® columns

For the enrichment of biotinylated proteins, denatured by SDS, *Strep-Tactin® Sepharose®* gravity flow columns with 1 ml column bed volume (#2-1202-001, IBA GmbH, Göttingen, Germany) were used at room temperature. Buffers were degassed to avoid the formation of air bubbles within the Sepharose bed. The whole protein sample was applied to the column, the column bed was washed with 50 ml 1x washing buffer (#2-1003-100, IBA GmbH) containing 0.4% SDS and the biotinylated proteins were eluted with 1x washing buffer containing 10 mM

biotin. *Strep-Tactin*® spin columns (#2-1850-010, IBA GmbH) were used for the purification of biotinylated peptides according to the manufacturer's instructions. Peptides were eluted in three steps with each time 150 µl of 1x washing buffer containing 10 mM biotin.

2.8.3 Chloroform methanol precipitation

Extraction of proteins by chloroform methanol precipitation was performed according to Wessel and Flügge (1984). Aliquots of 100 µl each of a protein sample were transferred into 1.5 ml reaction tubes and sequentially supplied with 400 µl of methanol, 100 µl of chloroform and 300 µl of H_2O. After the addition of H_2O the samples were vigorously shaken for 10 min and centrifuged at 10,000 rpm for 3 min at 4°C. The water induces phase separation and precipitated proteins locate to the interphase. The upper aqueous layer was carefully removed and additional 300 µl of methanol were added to the lower phase. The samples were mixed and then centrifuged at 13,000 rpm for 10 minutes at 4°C. The supernatant was gently removed and the protein pellet was dried and resolved in urea/thiourea.

2.8.4 SDS-polyacrylamide gel electrophoresis

SDS-polyacrylamide gel electrophoresis (SDS-PAGE) was performed according to Laemmli (1970). Protein extracts were supplied with protein loading dye (3x stock: 0.25 M Tris-HCl, pH 6.8, 15% β-mercaptoethanol, 30% glycerol, 7% SDS, 0.3% bromphenol blue) and denatured at 65°C for 10 min. Proteins were separated electrophoretically on a 12% SDS-gel in electrophoresis buffer (25 mM Tris-base, 250 mM glycine, 0.1% SDS, 0.34% EDTA) at 100 V for at least 10 min, followed by separation at 200 V until sufficient separation. The SDS gel consisted of a running gel (375 mM Tris, pH 8.8, 12% acrylamide/bisacrylamide 37.5:1 (*Rotiphorese*® *Gel 30*, #3029.1, Carl Roth GmbH Co. KG), 2 mM EDTA, 0.1% SDS) and a stacking gel (125 mM Tris, pH 6.8, 5% acrylamide/bisacrylamide (37.5:1), 2 mM EDTA, 0.1% SDS). The *PageRuler*^{TM} *Prestained Protein Ladder* (#26616, Thermo Fisher Scientific) was used as reference for molecular weight estimation.

2.8.5 Western blot analyses

Western blot experiments were performed according to Burnette (1981). SDS-PAGE separated proteins were electro-blotted onto nitrocellulose membranes (*Amersham*^{TM} *Protran*® *Western blotting membrane*, #GE10600002, Sigma-Aldrich, München, Germany) in *Mini-Trans-Blot-Electrophoretic-Cells* (Bio-Rad Laboratories GmbH, München, Germany) in transfer buffer (25 mM Tris-base, 200 mM glycine, 0.02% SDS and 20% methanol) for 1.5 h at 100 V or

overnight at 30 V and 4°C. For visualization of total protein levels membranes were stained with Ponceau Red (0.2% PonceauS, 3% trichloroacetic acid) for at least 5 min, washed with H_2O and photographed with the *FUSION-SL-4* (PEQLAB Biotechnology GmbH, Erlangen, Germany). Staining was removed by washing in phosphate buffered saline (PBS; 8 mM Na_2HPO_4, 2 mM NaH_2PO_4, 150 mM NaCl) or Tris buffered saline (TBS; 150 mM Tris, 150 mM NaCl, pH 7.2-7.4) with or without milk, depending on the following blocking reagent. Membranes were blocked for at least 1 h or overnight at 4°C in PBS either with 2-5% milk or with 1% bovine serum albumin (BSA), or TBS with 5% BSA and subsequently incubated for at least 2 h at room temperature or overnight at 4°C with the primary antibody. The antibodies were diluted in the respective blocking solution as follows: polyclonal rabbit anti-Asc1p (generated from affinity purified Asc1p by Davids Biotechnologie GmbH, Regensburg, Germany), 1:5,000 in 5% milk with 0.1% Tween 20; polyclonal rabbit anti-Rps3p (kindly provided by Prof. Dr. H. Krebber, Georg-August University Göttingen, Germany), 1:3,000 in 2% milk with 0.1% Tween 20; polyclonal phospho-p38 MAPK (Thr180/Tyr182; #9211, Cell Signaling Technology, Danvers, Massachusetts, USA), 1:500 in 5% BSA with 0.1% Tween 20 in TBS. After three 10 min washing steps in PBS the secondary antibody, peroxidase-coupled goat anti-rabbit (#G21234, MoBiTec, Göttingen, Germany), was added, diluted 1:2,000 in PBS with 5% milk and incubated with the membrane at room temperature for 1 h. *Pierce*^{TM} *High Sensitivity Streptavidin-HRP* (#21130, Thermo Fisher Scientific) was directly added to the membrane after blocking in 1% BSA, diluted 1:5,000 in 1% BSA with 0.1% Tween, and incubated for 1 h. The membranes were washed three times with PBS for each 10 min and incubated 1 min in freshly prepared *Enhanced Chemiluminescence* solution, consisting of 20 ml 100 mM Tris-HCl, pH 8.5 with 100 µl 2.5 mM luminol, 44 µl 40 µM paracumaric acid and 6.15 µl of 30% H_2O_2. Chemiluminescent signals were detected with the *FUSION-SL-4* and protein signals were quantified according to total protein levels with the help of the *BIO-1D Software Version 15.01* (Vilber Lourmat, Eberhardzell, Germany).

2.8.6 Colloidal coomassie staining

Proteins separated on SDS-gels were stained with colloidal Coomassie G250 according to Kang et al. (2002). Following SDS-PAGE the gel was shaken in fixing solution (40% ethanol, 10% acetic acid) for 1 h and subsequently washed twice with H_2O for 10 min. The gel was incubated overnight in Coomassie G250 staining solution (0.1% Coomassie Brilliant Blue G250, 5% aluminium sulfate-(14-18)-hydrate, 10% methanol, 2% ortho-phosphoric acid). The solution was prepared as follows: Aluminum sulfate was dissolved in H_2O and methanol was

added afterwards. Coomassie Brilliant Blue G250 was dissolved in the solution and phosphoric acid was added. To remove Coomassie particles after staining the gel was washed with H_2O, to reduce the staining it was incubated in fixing solution and subsequently washed twice with H_2O.

2.8.7 Trypsin digest of proteins

Protein digestion with trypsin was performed according to Shevchenko et al. (1996). Gel bands or lanes were cut into small pieces of approximately 2 mm and transferred into 1.5 ml *Protein LoBind Tubes* (#0030108116, Eppendorf, Hamburg, Germany). Approximately 30 µl acetonitrile were added to the gel pieces. The volume was adjusted to the amount of gel, since the gel pieces should be fully covered with acetonitrile. The samples were incubated for 10 min under constant shaking and the acetonitrile was removed. The gel pieces were dried for 10 min in the *Savant SPDIIIV SpeedVac concentrator* (Thermo Fisher Scientific). 150 µl 10 mM DTT were added and the samples were incubated at 56°C for 1 h. The DTT solution was removed and the gel pieces were covered with 150 µl 55 mM iodoacetamide dissolved in 100 mM NH_4HCO_3. The samples were incubated for 45 min in the dark. The iodoacetamide was removed and the gel pieces were washed with 100 mM NH_4HCO_3 followed by washing with acetonitrile. Both wash steps were performed under constant shaking and repeated twice. The gel pieces were dried in the *SpeedVac concentrator* for 10 min and subsequently covered with sufficient trypsin digestion buffer (#37283.01, SERVA Electrophoresis, Heidelberg, Germany). The samples were incubated for 45 min on ice and excessive trypsin digestion buffer was removed. The gel pieces were covered with 25 mM NH_4HCO_3, and the samples were incubated overnight at 37°C. The liquid was collected by centrifugation at 13,000 rpm and transferred to a fresh 1.5 ml *Protein LoBind Tube*. Peptides were extracted from the gel by the sequential incubation with 20 mM NH_4HCO_3 for 10 min and three times with a 50% acetonitrile, 5% formic acid mixture for each 20 min. Incubations were performed under constant shaking and the liquid was collected by centrifugation and transferred into the new *LoBind Tube* after each step. The collected supernatant was completely dried in the *SpeedVac concentrator*. The peptide pellet was resolved in 20 µl sample buffer (2-5% acetonitrile, 0.1% formic acid) for further purification. The purification with the C18 <u>s</u>top <u>a</u>nd <u>g</u>o <u>e</u>xtraction (stage) tips was performed according to Rappsilber et al. (2003) and Rappsilber et al. (2007). Small disks were obtained from a C18 *Solid phase extraction Disk* (#2215, 3M, Neuss, Germany) and at least two of them were pushed into a 100-200 µl pipette tip on top of each other. The C18 column material was equilibrated with 100 µl methanol with 0.1% formic acid, followed by 100 µl 70% acetonitrile with 0.1% formic acid and washed twice with 100 µl H_2O with 0.1% formic acid.

After the addition of each solvent the stage tips were centrifuged with the help of an adaptor in 2 ml reaction tubes at 13,000 rpm for 2 min. The peptide sample was loaded and incubated on the stage tip for 5 min, followed by centrifugation at 4,000 rpm for 5 min. To increase the yield, the flow-through was loaded again and the stage tips were centrifuged at 4,000 rpm for 5 min once more. The C18 material was washed twice with 100 µl H_2O with 0.1% formic acid, each time followed by centrifugation at 10,000 rpm for 2 min. For peptide elution 60 µl 70% acetonitrile with 0.1% formic acid were applied onto the column, incubated on the stage tip for 5 min, and centrifuged at 4,000 rpm for 5 min. This peptide solution was dried completely in the *SpeedVac concentrator* and resolved in the sample buffer for LC-MS analyses.

2.8.8 Liquid chromatography-mass spectrometry analyses

LC-MS analysis for protein identification and SILAC-based protein quantification was performed with an *Orbitrap Velos Pro^{TM} Hybrid Ion Trap-Orbitrap* mass spectrometer. 1-5 µl of peptide solutions were loaded and washed on an *Acclaim$^®$ PepMAP 100* pre-column (#164564, 100 µm x 2 cm, C18, 3µm, 100 Å, Thermo Fisher Scientific) with 100% loading solvent A (98% H_2O, 2% acetonitrile, 0.07% trifluoracetic acid (TFA)) at a flow rate of 25 µl/min for 6 min. Peptides were separated by reverse phase chromatography on an *Acclaim$^®$ PepMAP RSLC* column (75 µm x 25 cm (#164536) or 50 cm (#164540), C18, 3 µm, 100 Å, Thermo Fisher Scientific) with a gradient from 98% solvent A (H_2O, 0.1% formic acid) and 2% solvent B (80% acetonitrile, 20% H_2O, 0.1% formic acid) to 42% solvent B for 95 min and to 65% solvent B for the following 26 min at a flow rate of 300 nl/min. Peptides eluting from the chromatographic column were on-line ionized by nanoelectrospray at 2.4 kV with the *Nanospray Flex Ion Source* (Thermo Fisher Scientific). Full scans of the ionized peptides were recorded within the Orbitrap FT analyzer of the mass spectrometer within a mass range of 300-1850 m/z at a resolution of 30,000 or in case of SILAC-based experiments 60,000. Collision-induced dissociation (CID) fragmentation of data-dependent top-ten peptides was performed with the *LTQ Velos Pro* linear ion trap. For data acquisition and programming the *XCalibur 2.2* software (Thermo Fisher Scientific) was used. Protein identification and SILAC-based quantification was performed with the *MaxQuant 1.5.1.0* software (Cox and Mann, 2008). A *UniProt*-derived *S. cerevisiae*-specific database (http://www.uniprot.org, Proteome ID UP000002311, 6721 entries, download 2014) was used for database search with the Andromeda algorithm and with the program's default parameters. As the digestion mode trypsin/P was used, maximum missed cleavage sites were set to three, carbamidomethylation of cysteins was considered as fixed modification, acetylation of the N-terminus, oxidation of methionines, and

biotinylation of lysines were set as variable modifications. For SILAC-based experiments Arg6 and Lys4 or Arg10 and Lys8 were set as *medium* or *heavy* isotopic peptide labels, respectively. *Match between runs*, *FTMS requantification* and *FTMS recalibration* were enabled. The mass tolerance was 4.5 ppm for precursor ions and 0.5 Da for fragment ions. The decoy mode was revert with a false discovery rate of 0.01. Subsequent data processing and statistical analysis were performed with the *Perseus 1.5.1.0* software. For the identification of proteins and their biotinylated lysine residues also the *Proteome Discoverer^TM 1.4* software was used. Database searches were performed with the *SequestHT* and *Mascot* search algorithms against a *S. cerevisiae*-specific protein database (SGD, 6110 entries including common contaminants, S288C_ORF_database release version 2011, Stanford University). The digestion mode was set to trypsin and the maximum of missed cleavage sites to two or three in case biotinylated lysine residues were expected. Carbamidomethylation of cysteins was set as fixed modification, oxidation of methionines and biotinylation of lysines were set as variable modifications (if required). The mass tolerance was 10 ppm for precursor ions and 0.6 Da for fragment ions. The decoy mode was revert with a false discovery rate of 0.01.

2.8.9 Proximity-dependent biotin identification

BioID was modified from Roux et al. (2012). For the comparison of three strains or conditions in one BioID experiment, cells were cultivated individually in 200 ml YNB medium with the required amino acids including 50 mg/l of stable isotope labeled amino acids, and with 10 µM D-biotin (#47868, Sigma-Aldrich) until an OD_{600} of 0.8 was reached. When comparing growth conditions all three cultures were cultivated equally until an OD_{600} of 0.6 or 0.7 was reached. At this point heat stress was triggered by shifting the cells to 37°C or starvation was induced by washing and shifting the cells to YNB medium with or without glucose. Biotin was added 10-15 min after stress induction and the cells were cultivated for 1 h. Before gathering cells, a 20 ml aliquot was taken from each culture and used for visualization of biotinylated proteins with Streptavidin-HRP. Cells were harvested by centrifugation and resuspended in 15 ml Strep-buffer each. The three cell suspensions were combined in a 1:1:1 ratio according to the optical densities of the cultures. Cell lysis was obtained in 1x Strep-buffer as described in 2.7.1. The protein crude extract was split into two parts: About 60 µg were used as proteome standard and were directly separated by SDS-PAGE. The remaining crude extract was used for biotin affinity capture as described in 2.7.2. The proteins of the eluate were precipitated by chloroform-methanol extraction and separated by SDS-PAGE. This gel lane and the proteome lane were each cut into 10 pieces and subjected to tryptic digestion followed by LC-MS analysis.

2.8.10 Sucrose density gradient centrifugation

For sucrose density gradient centrifugation *S. cerevisiae* cells were cultivated overnight in 200 ml YNB medium until an optical density of approximately 0.8 was reached. Cells were incubated with 100 µg/ml cycloheximide for 15 min on ice and collected by centrifugation at 3,000 rpm for 3 min at 4°C. The cell sediment was resuspended in washing buffer (20 mM HEPES-KOH, pH 7.5, 10 mM KCl, 2.5 mM $MgCl_2$, 1 mM EGTA) and transferred to a 2 ml screw cap reaction tube. After additional centrifugation the collected cells were resuspended in an equal amount of lysis buffer (20 mM HEPES-KOH, pH 7.5, 10 mM KCl, 2.5 mM $MgCl_2$, 1mM EGTA, 1 mM DTT, 100 µg/ml cycloheximide, 1 *cOmplete*^{TM} EDTA-free protease inhibitor cocktail tablet (#4693132001, Roche Diagnostics) per 50 ml), and glass beads were added equally. Mechanical cell lysis was performed with the *Fast-Prep-24* (MP Biomedicals, Illkirch, France) which was employed twice for 20 s at 5.0 m/s. The cell debris was collected by centrifugation at 13,000 rpm for 5 min at 4°C and the supernatant was transferred to a fresh reaction tube. Centrifugation and transfer to new tubes was repeated until the supernatant was clear. The OD_{260} of a 1:100 dilution was determined with the *NanoDrop 2000* (Thermo Fisher Scientific). The volume that equals an OD_{260} of 15 was calculated and loaded onto a 7-47% sucrose gradient, generated with the *Gradient Master 108* (BioComp Instruments, Fredericton, Canada). The sucrose gradients were centrifuged at 40,000 rpm for 2 h 50 min at 4°C in a TH-641 rotor in a *Sorvall WX80* ultracentrifuge (Thermo Fisher Scientific) and fractions were collected with the *Foxy Jr. Fraction Collector* (Optical Unit Type 11, Absorbance detector UA-6, Teledyne Isco, Lincoln, Nebraska, USA). To this end a 60% sucrose solution was pumped into the bottom of the gradient tube. The absorbance was measured at 254 nm for polysome profiling. Proteins from the collected fractions were precipitated with trichloracetic acid for subsequent Western blot analyses.

2.8.11 Trichloracetic acid precipitation

1 volume of a 20% trichloracetic acid (TCA) solution were added to 1 volume of a protein sample. The sample was incubated at 4°C overnight and centrifuged at maximum speed for 1 h at 4°C. The supernatant was removed by pipetting and the sediment was washed twice with 1 ml ice-cold 80% acetone. The samples were centrifuged after each wash step for 20 min at 13,000 rpm at 4°C. The supernatant was removed and the pellet was dried and resolved in 3x protein loading dye and boiled at 95°C for 5 min.

2.9 Phenotypical analyses

2.9.1 Drop dilution assay

Yeast cells were pre-cultured overnight in 10 ml YNB medium with the respective amino acids and subsequently cultivated for approximately 4 h in fresh 10 ml YNB medium until an optical culture density of approximately 0.6 was reached. The cultures were diluted in YNB medium with the respective amino acids to an OD_{600} of 0.1 and 10-fold dilution series were prepared. 20 µl of each dilution were dropped on YNB agar plates, and 10 µl were applied on YEPD plates. For the analysis of cell wall integrity YNB or YEPD medium was supplemented with 125 µg/ml congo red. Respiratory capacity was investigated on YNB or YEP medium containing 2% glycerol as sole non-fermentable carbon source. Osmotic stress was induced on YNB or YEPD medium containing 60-75 mM NaCl. The translational fitness was analyzed on YNB medium with the translation inhibitors canavanine (600 ng/ml) or cycloheximide (0.025-0.15 µg/ml). After 3 to 5 days of incubation at 30°C or 37°C to investigate heat sensitivity the plates were photographed with the *Gel iX20 Imager* (Intas Science Imaging Instruments).

2.9.2 Adhesion assay

Yeast cells were patched on YNB agar plates containing 10 mM 3-amino-1,2,4-triazole (3-AT) and incubated at 30°C for 3 days. Non-adhesive cells were removed by gentle washing under a constant stream of water. Plates were photographed before and after washing.

2.10 Fluorescence microscopy

Yeast cells were pre-cultured overnight in 10 ml YNB minimal medium supplemented with the respective amino acids. 10 ml main cultures were inoculated to an optical density of approximately 0.2 and cultivated for further 4 h. To induce heat stress the cultures were shifted to 37°C and incubated 1h before microscopy. To cause glucose starvation the cells were washed in YNB medium without glucose and cultivated in glucose-free YNB medium for 15-30 min. Fluorescence microscopy was performed with a Zeiss Axio Observer.Z1 microscope (Zeiss, Oberkochen, Germany) with a CSU-X1 A1 confocal scanner unit (Yokogawa, Musashino, Japan) and a QuantEM:512SC digital camera (Photometrics, Tucson, Arizona, USA). A 100x oil objective was used for magnification and a RFP filter (s561R) for mCherry visualization. Data acquisition and processing was done with the SlideBook 6.0 software (Intelligent Imaging Innovations, Denver, Colorado, USA). For quantification at least 400 cells were counted per strain and replicate.

3. Results

3.1 Analysis of the proteinaceous Asc1p-neighborhood with BioID

The highly conserved Gβ-like Asc1 protein provides a scaffold with a surface for protein-protein interactions at the 40S ribosomal subunit (Rabl et al., 2011; Sengupta et al., 2004). The exposed position at the head region of ribosomes in close proximity to factors of the translation initiation process (Rabl et al., 2011) hints to a regulative function as transition unit communicating signaling events to and from the translational machinery. Asc1p might be required for the dynamic organization of local microenvironments at ribosomes, and thus might precisely synchronize functional protein interactions for translational control and cellular signaling. Numerous high throughput studies list Asc1p to co-purify with a variety of baits in affinity purification assays (http://www.yeastgenome.org). Here, an *in vivo* approach was favored to capture the molecular microenvironment of Asc1p: *Proximity-dependent Biotin IDentification*, short BioID, was employed to inventory Asc1p-neighboring proteins and thus potential interactors. BioID is an *in vivo* protein labeling technique developed in the lab of Brian Burke (Roux et al., 2012). This approach makes use of an *E. coli* biotin protein ligase, namely BirAp, which selectively biotinylates acetyl-CoA carboxylase at a short recognition sequence in its natural environment. The exchange of an arginine at position 118 to glycine (BirA^{R118G}, hereafter referred to as BirA*) renders the enzyme target-unspecific resulting in the promiscuous biotinylation of primary amines in a proximity-dependent manner. For protein biotinylation BirA*p forms an activated biotin, biotinoyl-5'-AMP, from biotin and ATP that stays associated with the ligase until an appropriate lysine residue is accessible (Chapman-Smith and Cronan, 1999; Lane et al., 1964). Fused to a protein of interest, BirA*p hence labels proteins within reach of the bait with biotin. The covalent modification is subsequently used to enrich the marked proteins via the strong interaction of biotin with streptavidin. Finally, the identity of these proteins can be determined by mass spectrometry (MS).

Our bait Asc1p was C-terminally fused with the promiscuous biotin ligase BirA*p to identify its proteinaceous neighbors during exponential growth and to monitor changes in its proximity at challenging growth conditions. Asc1p-depleted cells exhibit a growth defect in response to glucose deprivation and at elevated temperatures among others. Thus, both conditions were chosen in this study to analyze the dynamics in the Asc1p-neighborhood. The Asc1$^{R38D\ K40E}$p (short Asc1^{DE}p) variant shows a decreased ribosome-binding affinity during ultracentrifugation of cell extracts in sucrose density gradients (Coyle et al., 2009). To get a comprehensive view on the *in vivo* localization and the proteinaceous neighbors of the mutated protein, it was also fused to BirA*p in this work.

3.1.1 Overexpression of plasmid-borne *ASC1-birA** and *asc1^{DE}-birA** provides wild type-like Asc1 protein levels

The Asc1 protein is a constituent of the small ribosomal subunit and physically contacts the ribosomal proteins Rps3, Rps16 and Rps17, as well as helices 39 and 40 of the ribosomal 18S RNA (Fig. 7; Ben-Shem et al., 2011; Rabl et al., 2011). Both Asc1p termini converge at the ribosome-averted site (Ben-Shem et al., 2011; Coyle et al., 2009) and are therefore available for the fusion to the promiscuous biotin ligase BirA*p. For the intended BioID analyses, however, the sequential arrangement of both fusion constituents is of particular importance: A fusion construct that places BirA*p N-terminally of Asc1p might result in the formation of a functional biotin ligase prior to the translation of the complete fusion construct. This would probably lead to an increased labeling of proteins involved in the BirA*-Asc1p biosynthesis. Thus, a C-terminal *ASC1-birA** fusion gene was generated, which forms the mature biotin ligase at the end of the fusion protein biosynthesis. Intended to allow a rather flexible movement of BirA*p, the fusion was bridged by four Gly-Ser-Ser repeats as a linker (Fig. 7).
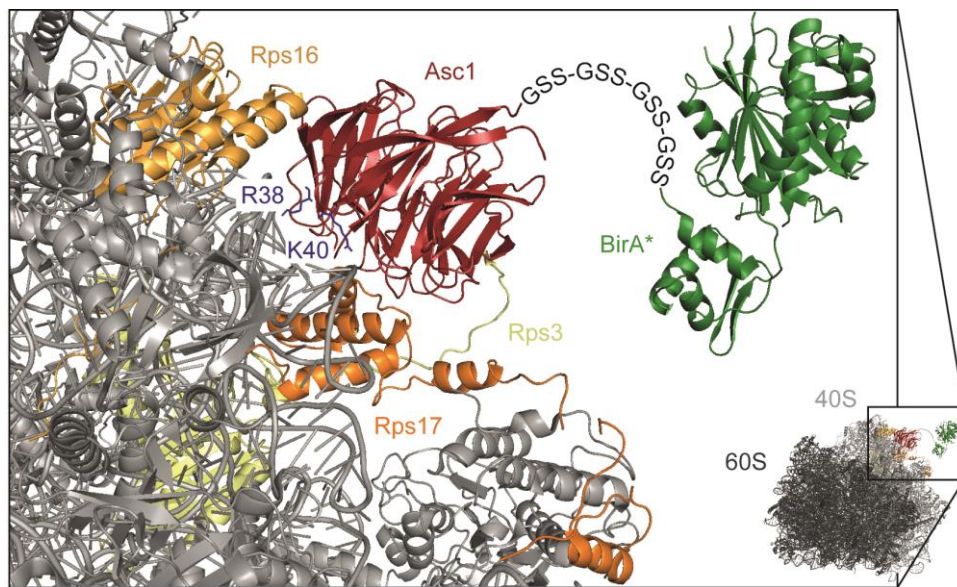
Fig. 7: Asc1-BirA*p at the head of the 40S ribosomal subunit. The Asc1 protein is a constituent of the 40S ribosomal subunit and interacts physically with the ribosomal proteins Rps3, Rps16 and Rps17. Amino acid residues Arg38 (R38) and Lys40 (K40) contribute to ribosome-binding and their exchange to Asp or Glu, respectively, weakens ribosome-association. The BirA* protein is fused to the C-terminus of Asc1p and Asc1^{DE}p via four repeats of a Gly-Ser-Ser (GSS) linker sequence. Due to the ribosome-averted orientation of the Asc1p C-terminus, ribosome-binding of the fusion proteins should not be sterically compromised. The crystal structure data of the *S. cerevisiae* 80S ribosome and the *E. coli* BirA protein derive from the PDB entries 4V88 (Ben-Shem et al., 2011) and 1BIB (Wilson et al., 1992) and were combined to model the fusion protein with the *PyMOL Molecular Graphics System* software.

For the construction of the *ASC1-birA** gene fusion, a high-copy number plasmid bearing the wild type (wt)-*ASC1* gene (pME2624) was amplified and linearized by whole-vector PCR. This reaction with specific oligonucleotides as primers (see Tab. S1) removed the *ASC1* stop codon and simultaneously added a sequence encoding the Gly-Ser-Ser repeats of the linker and an overhang for homologous recombination with *birA** (Fig. 8A). The *birA** gene was amplified from plasmid pRS313 (kindly provided by Dr. Hans Dieter Schmitt, Max Planck Institute for Biophysical Chemistry, Göttingen) without its start codon and supplied with a sequence complementary to the plasmid backbone (Fig. 8A). The linearized plasmid backbone and the *birA** fragment were finally fused by homologous recombination with *In-Fusion*® *Cloning* (Fig. 8A; Benoit et al., 2006).
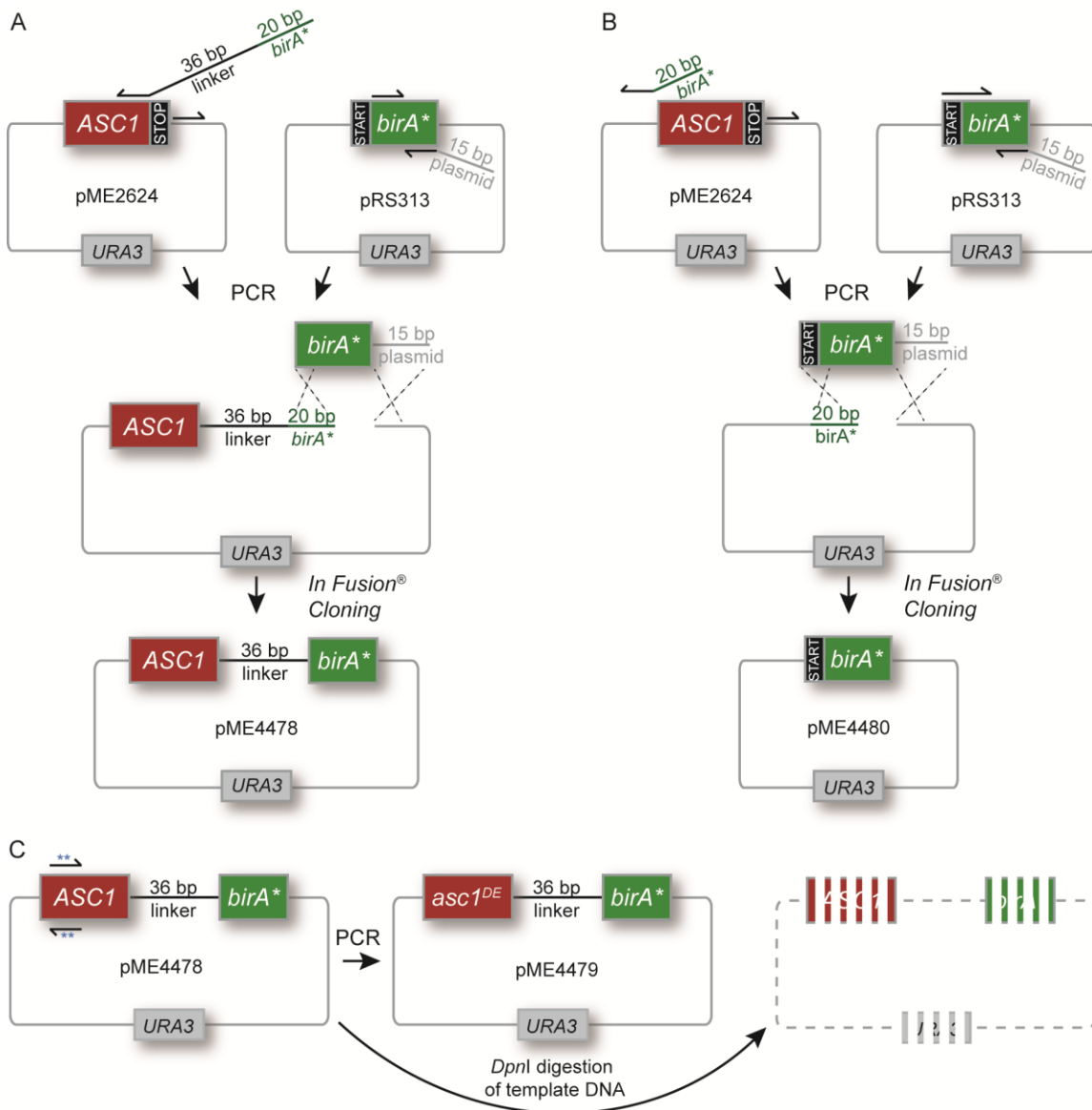
Fig. 8: Generation of *ASC1-birA**, *birA** and *asc1^{DE}-birA** encoding high-copy number plasmids.
(A) The 2 μ wt-*ASC1* plasmid (pME2624) was amplified and linearized by whole-vector PCR with a primer pair that was designed to remove the *ASC1* stop codon and to generate an overhang at the 3'-end

of the *ASC1* gene containing a sequence that encodes a fourfold Gly-Ser-Ser linker and 20 base pairs (bp) homologous to the 5'-end of *birA** (without its start codon). During amplification of the *birA** gene from plasmid pRS313 a sequence of 15 bp complementary to the plasmid backbone was added at the 3'-end, and the start codon was eliminated. The linearized *ASC1* plasmid and the *birA** fragment were fused by homologous recombination resulting in pME4478. (B) Cloning of the mere *birA** into the high-copy number plasmid was realized by linearization of the wt-*ASC1* plasmid (pME2624) by whole-vector PCR using primers that eliminated the *ASC1* ORF and added a homologous overhang of 20 bp for recombination with *birA**. During amplification of the *birA** ORF from pRS313 15 bp complementary to the plasmid backbone were supplied at the 3'-end. The linearized plasmid and the *birA** fragment were fused by homologous recombination resulting in pME4480. (C) The exchange of Arg38 and Lys40 to Asp and Glu, respectively, within the *ASC1-birA** fusion gene was achieved by site-directed mutagenesis. The *ASC1-birA** plasmid (pME4478) was amplified with a complementary primer pair with the two mutated codons in their center resulting in the *asc1^{DE}-birA** vector (pME4479). Parental plasmid DNA was removed by *Dpn*I treatment, which exclusively digests methylated DNA derived from *E. coli*.

A high-copy number plasmid bearing the mere biotin ligase *birA** used as a negative control in all BioID experiments was constructed in a similar way: The wt-*ASC1* plasmid (pME2624) was amplified as linear fragment by whole-vector PCR with a primer pair that omitted the complete *ASC1* ORF and generated overlapping regions for homologous recombination with *birA** (Fig. 8B). The *birA** ORF including its start codon was amplified from pRS313 and supplied with additional base pairs at the 3'-end complementary to the plasmid backbone (Fig. 8B). Thus, after homologous recombination the *ASC1* ORF was replaced by the *birA** coding sequence (pME4480; Fig. 8B).

To investigate the proteinaceous neighborhood of the ribosome-binding compromised Asc1^{DE}p variant, an *asc1^{DE}-birA** fusion was generated for subsequent BioID analyses. The *asc1^{DE}* mutant is characterized by two amino acid exchanges: Arg38 and Lys40 are replaced by negatively charged Asp and Glu, respectively. Site-directed mutagenesis was applied to exchange these two residues within the *ASC1-birA** fusion gene. A complementary primer pair bearing the two mutated codons was used to fully amplify the *ASC1-birA** containing plasmid (pME4478) by whole-vector PCR yielding in the *asc1^{DE}-birA** vector (pME4479; Fig. 8C). The resulting mixture of parental plasmid DNA and the desired modified vector was subjected to *Dpn*I treatment which exclusively cleaves methylated DNA and thereby removes the template (Fig. 8C).

Western blotting and subsequent visualization of the Asc1p-variants with an Asc1p-specific antibody demonstrated that overexpression of the plasmid-borne *ASC1-birA** and *asc1^{DE}-birA** fusions in a Δ*asc1* strain background provided wt-like Asc1 protein levels (Fig. 9A).

Sequence coverage of BirA*p: 78.5%

```
        1          11         21         31         41         51
  1 MKDNTVPLKL IALLANGEFH SGEQLGETLG MSRAAINKHI QTLRDWGVDV FTVPGKGYSL
 61 PEPIQLLNAK QILGQLDGGS VAVLPVIDST NQYLLDRIGE LKSGDACIAE YQQAGRGGRG
121 RKWFSPFGAN LYLSMFWRLE QGPAAAIGLS LVIGIVMAEV LRKLGADKVR VKWPNDLYLQ
181 DRKLAGILVE LTGKTGDAAQ IVIGAGINMA MRRVEESVVN QGWITLQEAG INLDRNTLAA
241 MLIRELRAAL ELFEQEGLAP YLSRWEKLDN FINRPVKLII GDKEIFGISR GIDKQGALLL
301 EQDGIIKPWM GGEISLRSAE K
```

peptides identified   position of amino acid exchange

Fig. 9: Expression of plasmid-borne *ASC1-birA** and *asc1^{DE}-birA** provides wt-like Asc1 protein levels and increases protein biotinylation. (A) Expression of the Asc1-BirA* and the Asc1^{DE}-BirA* fusion proteins (~70 kDa) from high-copy number plasmids (pME4478 or pME4479, respectively) in the Δ*asc1* strain background (RH3263) provides wt-like Asc1p levels. Proteins were detected in Western blot experiments using an Asc1p-specific antibody and were normalized according to the Ponceau staining of the complete lane (shown is a section of the lane). (B) Protein biotinylation, detected with HRP-coupled streptavidin, was elevated in strains expressing Asc1-BirA*p, Asc1^{DE}-BirA*p and the mere BirA* protein in comparison to the wt-*ASC1* and Δ*asc1* strains. All strains were cultivated overnight in the presence of 10 µM biotin. The amount of biotinylated proteins was normalized according to the Ponceau staining of the complete lanes. (C) Expression of the mere BirA* protein in the wt-*ASC1* strain (RH2817) was verified by LC-MS analysis.

Expression of *birA** in a wt-*ASC1* strain background was verified by LC-MS analysis. The whole cell extract of this strain was separated by SDS-PAGE and gel pieces comprising the area around 35 kDa were digested with trypsin. A database search with the *SequestHT* search engine of the Proteome Discoverer™ software against a *S. cerevisiae*-specific protein database including the mutated *E. coli*-derived BirA* protein identified the biotin ligase with 18 unique peptides, 945 peptide sequence matches (PSMs) and a sequence coverage of 78.5% in two independent LC-MS runs (Fig. 9C). The amino acid at position 118, whose exchange renders the ligase target-unspecific (R118G), was not covered. The cultivation of the three strains expressing a fused or unfused BirA* protein in the presence of elevated biotin levels resulted in a remarkable increase of overall biotinylation compared to equally cultivated wt-*ASC1* and Δ*asc1* strains visualized using HRP-coupled streptavidin (Fig. 9B). Thus, BirA*p-mediated protein biotinylation is functional and suitable for subsequent BioID analyses in *S. cerevisiae*.

3.1.2 Asc1-BirA*p and Asc1^{DE}-BirA*p complement Δ*asc1* phenotypes

The Asc1p orthologue of higher eukaryotes, RACK1, is essential for viability already during early embryogenesis (Volta et al., 2013). The *S. cerevisiae* Asc1 protein on the contrary is dispensable for yeast growth in general (Chantrel et al., 1998; Giaever et al., 2002). Nevertheless, the scaffold is likewise essential for developmental processes and required for yeast cells to cope with diverse environmental stresses (Melamed et al., 2010; Rachfall et al., 2013; Valerius et al., 2007). It is involved in translational control and supports several signal transduction pathways, including the cell wall integrity pathway (Parsons et al., 2004; Rachfall et al., 2013; Schmitt et al., 2017; Valerius et al., 2007). Asc1p-depleted cells are highly sensitive against the translational inhibitors canavanine and cycloheximide (Parsons et al., 2004; Schmitt et al., 2017). Canavanine is a non-proteinogenic amino acid that is incorporated into proteins instead of the structurally highly similar amino acid arginine resulting in aberrant proteins. Cycloheximide inhibits translation elongation by blocking mRNA translocation. Asc1p-depleted cells further exhibit a growth defect at elevated temperature (37°C or above) or on medium containing an exclusive non-fermentable carbon source, the latter implicating decreased respiratory capacity (Auesukaree et al., 2009; Rachfall et al., 2013; Sinha et al., 2008). An impairment of the cell wall integrity pathway is apparent by an augmented sensitivity of Asc1p-depleted cells against congo red, which disturbs cell wall integrity through interacting with microfibrils, and by non-adhesive growth on agar surfaces during amino acid starvation (Rachfall et al., 2013; Valerius et al., 2007).

Expression of the *ASC1-birA** gene fusion from a high-copy number plasmid in the Δ*asc1* strain complemented these phenotypes (Fig. 10): The heat response at 37°C and the respiratory competence on plates containing 2% glycerol as exclusive and non-fermentable carbon source were restored in Δ*asc1* cells transformed with the *ASC1-birA** plasmid. Furthermore, the fusion protein rescued the sensitivity to congo red and complemented adhesive growth on agar plates containing the histidine analogue 3-amino-1,2,4-triazole (3-AT), which induces histidine starvation. The growth defect of Asc1p-depleted cells caused by the translational inhibitors canavanine and cycloheximide was partially complemented by the *ASC1-birA** fusion. In summary, the fusion to the biotin ligase BirA*p does not compromise the functionality of Asc1p in general demonstrating that it can adopt Asc1p's role in Δ*asc1* cells.
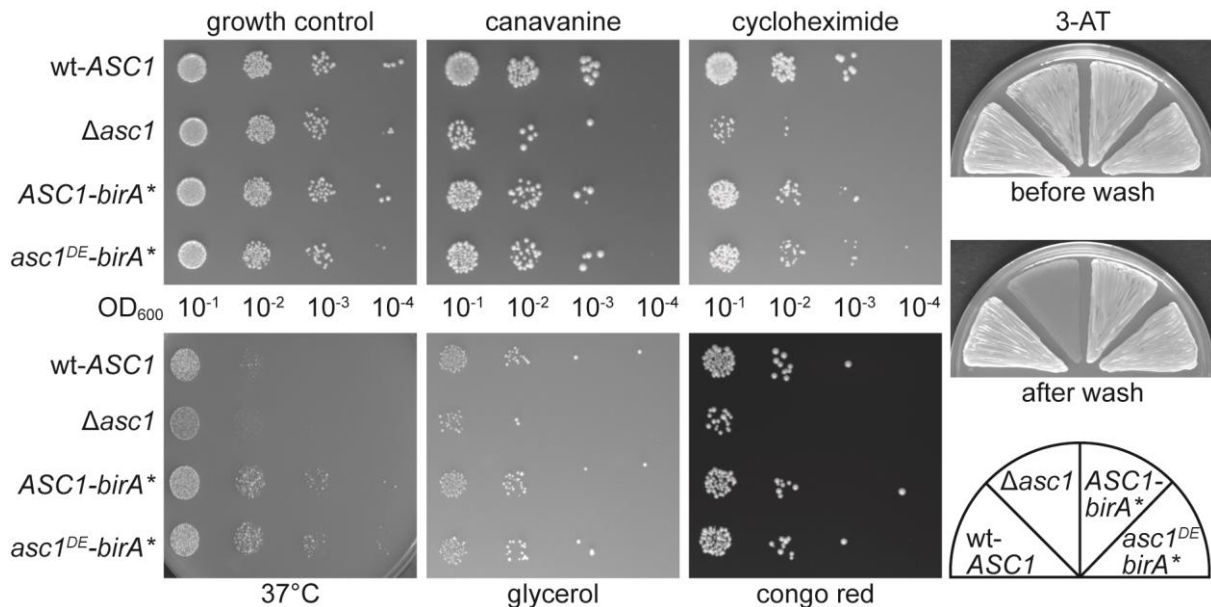
Fig. 10: Asc1-BirA*p and Asc1^{DE}-BirA*p complement Δ*asc1* phenotypes. For drop dilution assays 20 µl of 10-fold dilution series of wt-*ASC1*, Δ*asc1*, *ASC1-birA** and *asc1^{DE}-birA** cell suspensions were spotted on YNB agar plates containing the translation inhibitors canavanine (600 ng/ml) or cycloheximide (0.15 µg/ml). Cells were also dropped on YNB plates with 2% glycerol as sole and non-fermentable carbon source and on YNB medium with the cell wall-disturbing drug congo red (125 µg/ml). One YNB agar plate was incubated at 37°C instead of 30°C to score for heat sensitivity and another YNB agar plate was used for growth control. All plates were photographed after three to five days of growth. Adhesive growth upon amino acid starvation (histidine starvation) was induced with 1 mM 3-AT and scored after three days of growth by gentle washing. *ASC1-birA** and *asc1^{DE}-birA** were expressed from high-copy number plasmids in the Δ*asc1* strain background. The wt-*ASC1* and Δ*asc1* strains were transformed with an appropriate empty vector (pME2787).

The R38D K40E mutation within Asc1p was initially described to cause ribosome-binding deficiency, since the Asc1^{DE} protein had a decreased affinity to ribosomes during ultracentrifugation in sucrose density gradients (Coyle et al., 2009). Due to the assumption that Asc1p's exposed position at the ribosome has a major impact on its cellular function, phenotypes similar to a Δ*asc1* strain were expected for the *asc1^{DE}* strain (Coyle et al., 2009). In contrast, this mutant strain exhibits only mild phenotypes, e.g. a slightly increased sensitivity to cycloheximide (Coyle et al., 2009; Schmitt et al., 2017). Consistently, the *asc1^{DE}-birA** strain showed impaired growth on plates containing cycloheximide (Fig. 10). Apart from that it complemented the phenotypes of the Δ*asc1* strain mentioned above (Fig. 10). In total, the *asc1^{DE}-birA** strain behaves as it was described for the *asc1^{DE}* strain and is consequently suitable to investigate the proteinaceous neighborhood of the ribosome-binding compromised mutated protein.

3.1.3 The Asc1-BirA* fusion protein authentically locates to the 40S ribosomal subunit

The ability of the Asc1-BirA* fusion protein to functionally complement Δ*asc1*-phenotypes implicates that it authentically locates to the 40S ribosomal subunit. Consistently, the ribosome-averted orientation of the Asc1p C-terminus suggests that ribosome-binding of the fusion protein is sterically possible (Fig. 7). By ultracentrifugation of equal amounts of wt-*ASC1* and *ASC1-birA** cell extracts in sucrose density gradients and subsequent Western blot experiments the distribution of Asc1p and Asc1-BirA*p within the different ribosomal fractions was monitored (Fig. 11A and B). Small amounts of wt-Asc1p were detected in the ribosome-free fraction, most of it, however, located to the 40S and higher fractions. The Asc1-BirA* fusion protein behaved similar: It co-migrated with the 40S, monosomal and polysomal fractions. In comparison to the wt-protein a slightly increased amount of the fusion protein was detected in the non-ribosomal fraction (Fig. 11A). The migration of the small ribosomal subunit was monitored with an Rps3p-specific antibody in Western blot experiments (kindly provided by Prof. Dr. Heike Krebber, Georg-August-University Göttingen). These data provide evidence that Asc1-BirA*p also spatially complements Asc1p-depletion and is suitable to monitor the Asc1p microenvironment *in vivo*.

As mentioned above, the Asc1^{DE} protein behaves differently during ultracentrifugation (Coyle et al., 2009). To exclude an impact of the BirA*p fusion on the migration of the Asc1^{DE} protein in sucrose density gradients during ultracentrifugation, also *asc1^{DE}-birA** cell extracts were separated by ultracentrifugation. As expected, also the fusion protein with the R38D and K40E exchanges extensively shifted to the ribosome-free fractions of the profile (Fig. 11A). Only

minor amounts of the fusion proteins were detected in the higher ribosomal fractions. Thus, the Asc1^{DE}p variant exhibits a decreased affinity to ribosomes during ultracentrifugation independent of its fusion to the biotin ligase BirA*p.
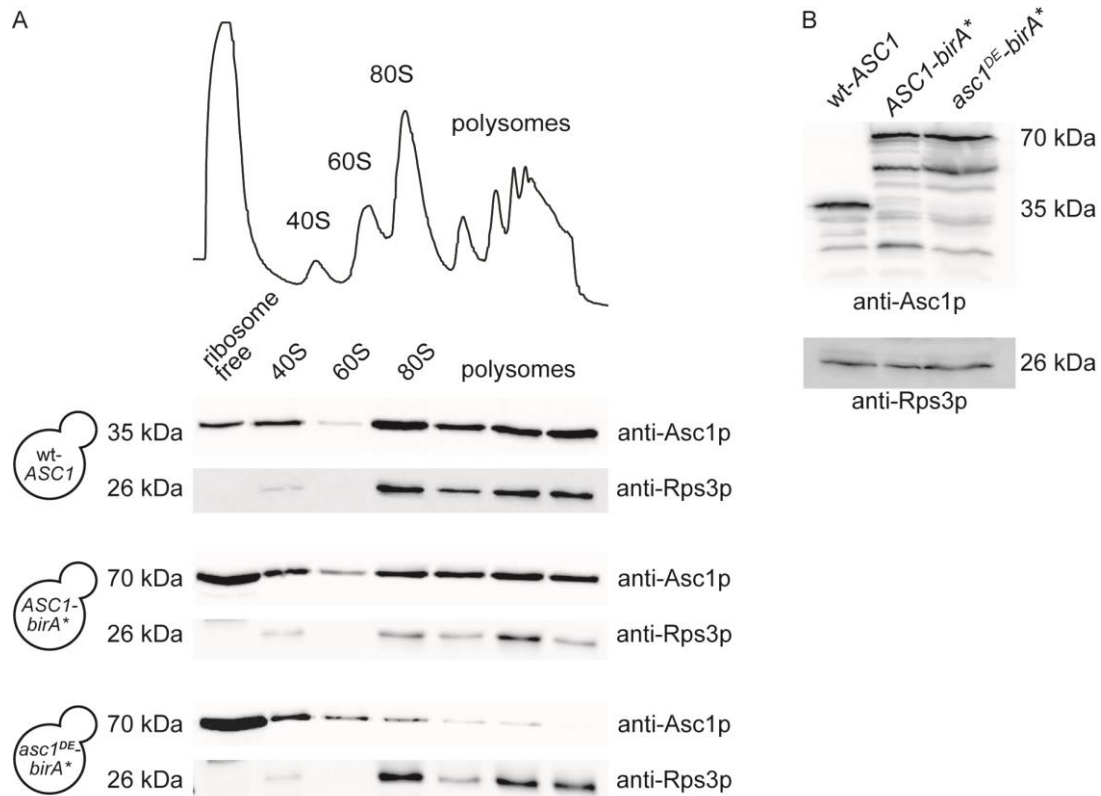
Fig. 11: Asc1-BirA*p associates with translating ribosomes, whereas Asc1^{DE}-BirA*p shifts to the ribosome-free fraction during ultracentrifugation in sucrose density gradients. (A) The ribosome-binding ability of the Asc1-BirA* and Asc1^{DE}-BirA* fusion proteins in comparison to wt-Asc1p was visualized by sucrose density gradient centrifugation followed by Western blot analysis with an Asc1p-specific antibody. The abundances of the different Asc1p variants in the non-ribosomal fraction, and in the fractions containing the 40S and 60S subunits as well as the 80S monosomes and polysomes revealed ribosome-binding of the Asc1-BirA* protein, but ribosome-dissociation of the Asc1^{DE}-BirA*p variant during ultracentrifugation. The distribution of Rps3p within these fractions was visualized with an Rps3p-specific antibody as marker for the migration of the small ribosomal subunit. The ribosome profile of the wt-*ASC1* strain is depicted representatively. (B) Equal amounts of protein extract were loaded onto the three sucrose gradients. As an input control the same amounts were compared by Western blotting and visualized with the Asc1p- and Rps3p-specific antibodies.

3.1.4 Extended cultivation times after biotin supply increase the overall protein biotinylation efficiency

For the intended BioID analyses Asc1p-proximal proteins are supposed to be labeled with biotin *in vivo*. The yeast *S. cerevisiae*, however, cannot accomplish *de novo* biotin synthesis and thus depends on biotin supply from the environment. *S. cerevisiae* cells are able to realize the last steps of the biotin formation from the precursors 7-keto-8-aminopelargonic acid (KAPA), 7,8-diaminopelargonic acid (DAPA) or desthiobiotin (DTB; Ohsugi and Imanishi, 1985). The uptake of KAPA and DAPA is accomplished by the plasma membrane permease Bio5p (Phalip et al., 1999). Biotin or its derivate DTB are imported by the vitamin H transporter Vht1p (Stolz et al., 1999). For efficient labeling of Asc1p-neighboring proteins by the fused biotin ligase BirA*p, sufficient biotin has to be readily available during cultivation. Different amounts of biotin were tested to determine the optimal biotin concentration for efficient protein biotinylation. The wt-*ASC1* and *ASC1-birA** strains were individually cultivated in the presence of 10 nM, 100 nM, 1 µM, 10 µM or 100 µM biotin or without biotin as negative control and total biotinylated proteins were visualized using Streptavidin-HRP after Western blotting (Fig. 12A). Without the additional supply of biotin to the growth medium there is no obvious difference in overall protein biotinylation between the wt-*ASC1* strain and the strain containing the foreign biotin ligase BirA*p. Cultivation overnight in the presence of 10 nM to 100 µM biotin results in increased protein biotinylation in the *ASC1-birA** strain compared to the wild type control (Fig. 12A). The higher the amount of biotin in the *ASC1-birA** cultures the more biotinylation occurs. This applies at least until 10 µM biotin. 100 µM biotin did not result in any further increase (Fig. 12A). Hence, for *in vivo* protein labeling with biotin, 10 µM of the vitamin were supplied in all following BioID experiments.

To determine the time required for sufficient protein biotinylation, Asc1-BirA*p-containing cultures were grown with biotin for 15, 30, 60 and 120 min or overnight or in the absence of biotin as negative control (Fig. 12B). Cultivation in the presence of biotin for 15 min did not significantly affect the biotinylation level of proteins. 30 and 60 min incubation with biotin had a mild effect (factor 1.3) on overall biotinylation. After 120 min post biotin supply protein biotinylation was increased by a factor of 1.6, however, the strongest effect was observed after overnight incubation with biotin. Therefore, for BioID experiments cell cultures were incubated with biotin overnight, if applicable.
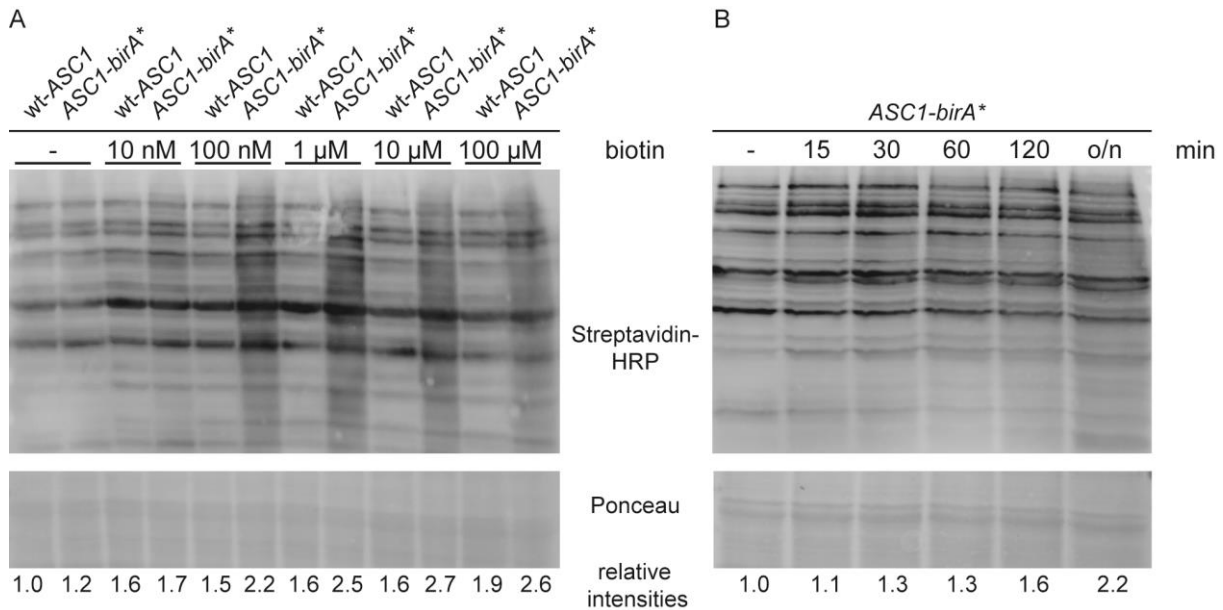
Fig. 12: Overnight incubation with high amounts of biotin increases protein biotinylation. (A) The wt-*ASC1* strain and the Δ*asc1* strain expressing plasmid-borne *ASC1-birA** were cultivated in the presence of different amounts of biotin (10 nm - 100 µM) or without biotin (-). Whole protein extracts were blotted onto a nitrocellulose membrane and biotinylated proteins were visualized with HRP-coupled streptavidin. The amount of biotinylated proteins was normalized to the whole protein level visualized by Ponceau staining. (B) The Δ*asc1* strain expressing plasmid-borne *ASC1-birA** was cultivated in the presence of 10 µM biotin for 15 - 120 min or overnight (o/n), or without biotin (-) as reference. Biotinylated proteins were visualized using HRP-coupled streptavidin and normalized to the level of total Ponceau-stained proteins.

3.1.5 Biotinylated proteins elute efficiently from Strep-Tactin® columns with concentrated biotin

The affinity of biotin to avidin or its bacterial homologue streptavidin is one of the strongest non-covalent occurring interactions in nature. With the BioID approach interacting and proximal proteins of Asc1p are supposed to be labeled *in vivo* with biotin and this modification is subsequently used to purify the biotinylated proteins via streptavidin. Strep-Tactin® is an engineered streptavidin derivate specifically designed to bind the eight amino acid Strep-tag®, an affinity tag for protein purification and detection (Voss and Skerra, 1997). The modification improves binding of the Strep-tag® to Strep-Tactin®, however, the affinity of biotin to the modified streptavidin is decreased. This facilitates the purification and especially the elution of biotinylated proteins via and from Strep-Tactin®. Gravity flow Strep-Tactin® Sepharose® columns with a bed volume of 1 ml were employed for all BioID experiments in this study. For

the elution of Strep-tagged proteins from Strep-Tactin® Sepharose® columns six elution steps with each 500 µl of a buffer containing the biotin derivate DTB is suggested. As visualized in Fig. 13, DTB is, however, not sufficient to release biotinylated proteins derived from an *ASC1-birA**-expressing strain cultivated in the presence of biotin from the Strep-Tactin® column efficiently. In contrast, elution with a buffer containing 10 mM biotin replaced the majority of biotinylated proteins. Thus, in the following BioID experiments biotinylated proteins were eluted from Strep-Tactin® Sepharose® columns with 10 mM biotin in six elution steps, and all six fractions were pooled and used for the following LC-MS analysis.
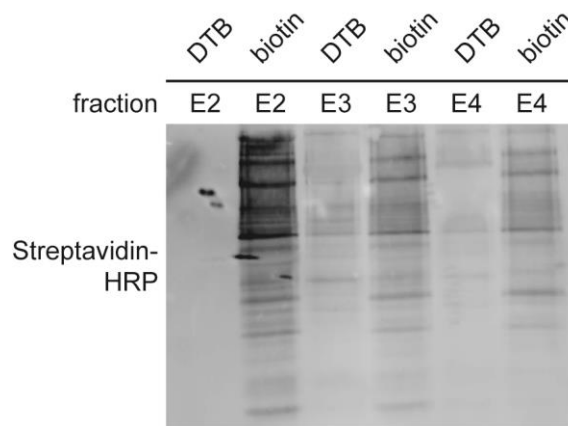
Fig. 13: High excess of biotin is required to elute biotinylated proteins efficiently from Strep-Tactin®. The elution capacity of DTB and biotin was compared and is shown for elution steps 2-4. The protein extract from an Asc1-BirA*p-expressing strain cultivated overnight in the presence of 10 µM biotin was equally distributed on both columns. Released biotinylated proteins are visualized with Streptavidin-HRP after Western blotting.

3.1.6 The integration of control cultures for accurate quantification of BioID-mediated protein enrichments is feasible using SILAC

For the identification of proteins located in the Asc1p-neighborhood with BioID, *ASC1-birA**-expressing cells were cultivated in the presence of biotin overnight yielding in the covalent biotinylation of Asc1p-interacting and proximal proteins in reach of the fused biotin ligase BirA*p (Fig. 14A). Cell lysis was performed under denaturing conditions to avoid co-purifications during Strep-Tactin® enrichment. Thus, primarily biotinylated proteins were captured with the stationary chromatographic Strep-Tactin® phase and eluted with excessive biotin in a total volume of 3 ml from columns with 1 ml bed volume (Fig. 14A). Proteins of the combined eluates were precipitated and separated by SDS-PAGE in one single gel lane. The proteins in this lane were in-gel digested with trypsin for bottom-up LC-MS analysis (Fig. 14A).
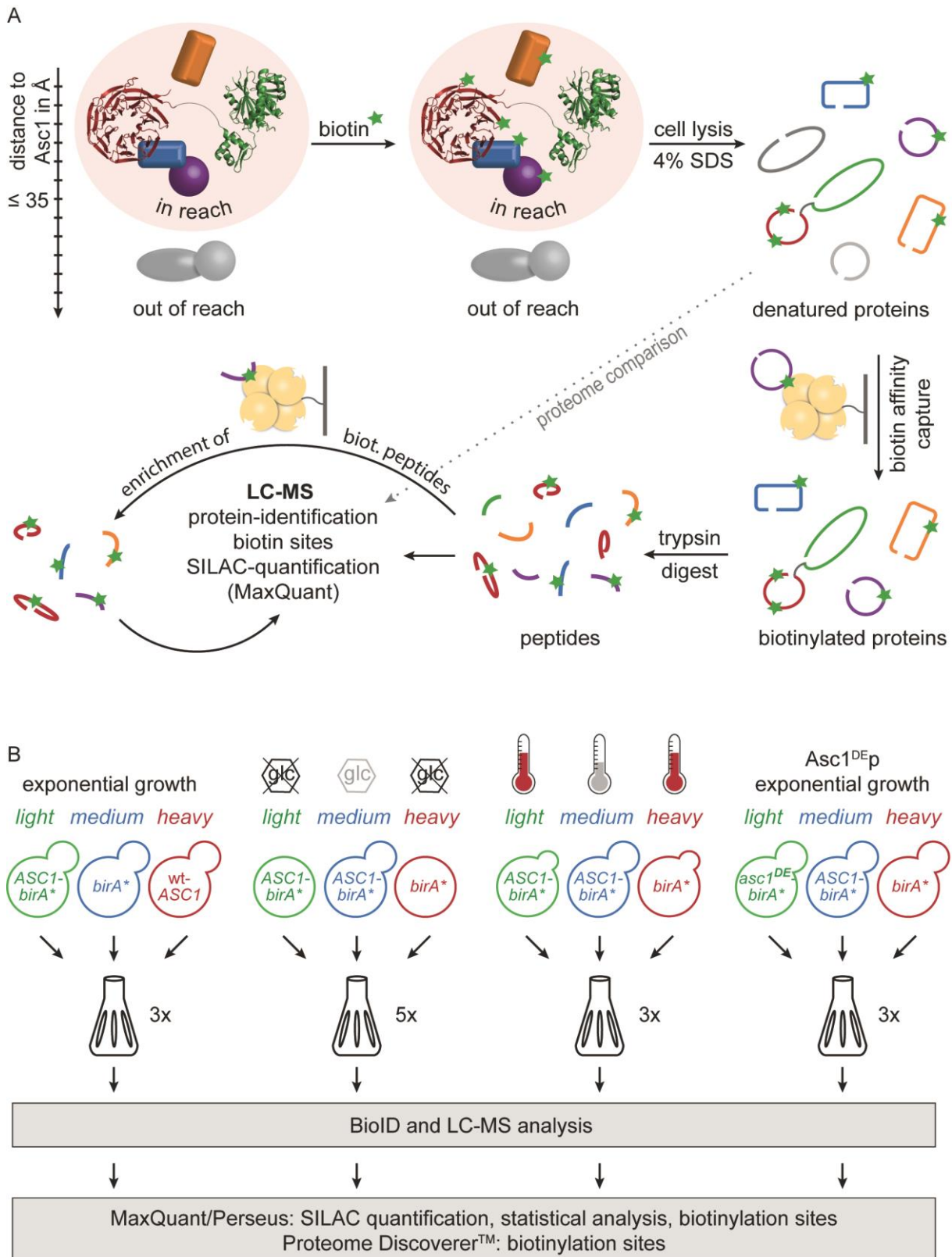
Fig. 14: SILAC-BioID: Enrichment-quantification against controls. (A) Biotin was used by the Asc1-BirA* fusion protein as substrate to covalently biotinylate proteins in reach (up to approximately 35 Å). After cell lysis in the presence of 4% SDS, biotinylated proteins were enriched via biotin affinity capture and afterwards digested with trypsin. The resulting peptides were subjected to LC-MS analysis for protein identification and for the determination of biotinylated lysine residues. SILAC quantification

was done with the MaxQuant software (Cox and Mann, 2008). Additional database searches with the Proteome Discoverer™ software enhanced the identification of biotinylation sites. To improve the coverage of biotinylated peptides, half of the peptide solution was subjected to additional biotin affinity capture and subsequent LC-MS analysis. Peptide samples without biotin affinity capture were also analyzed by LC-MS. The resulting proteome values were used to normalize affinity capture SILAC ratios against total protein abundances. (B) All four BioID experiments were done with triple SILAC to quantitatively compare cells of three different cultures in one batch. The neighborhood of Asc1-BirA*p was determined by the quantitative comparison with the *birA** and wt-*ASC1* strains as negative controls. Alterations in the Asc1p-neighborhood upon glucose starvation (see chapter 3.1.8) and heat stress (37°C; see chapter 3.1.9) were determined against *ASC1-birA** at exponential growth (2% glucose, 30°C) as reference and *birA** at stress as negative control. One replicate of the "heat stress" BioID experiment was performed with a label swap, which is not indicated in the scheme. The neighborhood of Asc1^{DE}-BirA*p was investigated against *ASC1-birA** as reference and *birA** as negative control (see chapter 3.1.10). Yeast strains were individually cultivated in the presence of 10 μM biotin and were labeled with lysine and arginine isotope variants as indicated. All genes were expressed from high-copy number plasmids in a Δ*arg4* Δ*lys1* strain background to ensure exclusive incorporation of the labeled amino acids into all proteins. The number of biological replicates is indicated for each experiment.

Protein identification based on the obtained LC-MS/MS2 raw data files was achieved by database searches with the Andromeda search algorithm of the MaxQuant software (Cox and Mann, 2008) using a *S. cerevisiae*-specific protein database. Besides the mere protein identification, biotinylated lysine residues within the proteins were determined in case the modified peptides were covered. To increase the relative abundance of biotinylated peptides and thus their coverage, half of the peptide mixture was used for a second Strep-Tactin® enrichment followed by LC-MS analysis (Fig. 14A). Biotinylated lysine residues identified by additional database search with the *SequestHT* and *Mascot* search engines of the Proteome Discoverer™ software were also further considered.

A discrimination between Asc1-BirA*p-specific and -unspecific enrichments of proteins was achieved by the quantitative comparison of *ASC1-birA**-derived proteins to proteins of negative control strains with stable isotope labeling with amino acids in cell culture (SILAC; Ong et al., 2002). With a triple SILAC approach three individual strains or cultures were directly compared in one batch (Fig. 14B). Two negative control strains were considered (Fig. 14B): 1) A wt-*ASC1* strain revealed naturally biotinylated proteins. 2) A wt-*ASC1* strain expressing an unfused BirA* protein revealed biotinylations and subsequent enrichments caused by BirA*p independent of Asc1p and its localization. Both strains additionally enabled the exclusion of

proteins that were non-specifically enriched by the Strep-Tactin® Sepharose® column. Like the *ASC1-birA** allele, both wt-*ASC1* and *birA** were expressed from high-copy number plasmids. All plasmids were expressed in yeast strains auxotrophic for arginine and lysine ($\Delta arg4 \, \Delta lys1$), which exclusively incorporate labeled arginine and lysine into all proteins during overnight cultivation. Proteins of the *ASC1-birA**, *birA** and wt-*ASC1* strains were differentially labeled with *light* (Arg^0 and Lys^0), *medium* (Arg^6 and Lys^4) or *heavy* (Arg^{10} and Lys^8) amino acids, respectively (Fig. 14B). After cultivation and labeling, a similar number of cells from all three strains was pooled and further processed in one batch according to the BioID workflow (Fig. 14B). Database search with the Andromeda search engine of the MaxQuant software results in quantitative SILAC protein ratios, which describe the relative abundance of an identified protein within the enrichment sample derived from one strain compared to another. Further data processing and filtering of the SILAC ratios was done with the Perseus software (Tab. S2; Cox and Mann, 2008). Besides LC-MS data analysis with MaxQuant/Perseus, also the Proteome Discoverer™ software (search algorithms *SequestHT* and *Mascot*) was used for database searches against a *S. cerevisiae*-specific database. The resulting data were mainly considered for the identification of further biotin sites.

Additionally to the protein sample derived from the Strep-Tactin® enrichment, an aliquot of the whole cell extract taken prior to the biotin affinity capture was separated by SDS-PAGE, in-gel digested with trypsin and analyzed by LC-MS as input control (Fig. 14A). The resulting SILAC ratios reveal variations in total cellular abundances and were used to normalize the effects of the biotin enrichment.

Four different BioID analyses were performed as indicated in Fig. 14B: (1) The Asc1p-neighborhood was monitored in cells growing exponentially, alterations in the Asc1p-neighborhood during (2) glucose starvation and (3) heat stress were examined, and (4) proteinaceous neighbors of the ribosome-binding compromised $Asc1^{DE}$ protein were recorded. All SILAC-based BioID experiments were performed in three or five biological replicates to account for statistical values (Fig. 14B). The level of overall protein biotinylation in each culture was visualized in Western blot experiments with Streptavidin-HRP (Fig. S1). In the following chapters the term "SILAC ratio" refers to protein ratios with the value of the strain/condition of interest (in Fig. 14B labeled in green) in the numerator and the value of the respective negative control or reference strain in the denominator.

3.1.7 Identification of Asc1p-proximal proteins at exponential growth with BioID

Biotin affinity capture of proteins derived from the cell pool of three cultures followed by LC-MS analysis and subsequent database search resulted in the initial identification of more than 2,000 proteins. In the end, however, only those proteins that were biotinylated and subsequently enriched to a greater extend from the *ASC1-birA** strain in comparison to the negative control strains were considered as putative Asc1p-neighbors. A significant enrichment, and thus neighborhood, was defined by log$_2$ SILAC enrichment ratios ≥ 0.26 ($\triangleq 20\%$) against the *birA** control strain in at least four out of six biological replicates, and by log$_2$ SILAC enrichment ratios ≥ 1 ($\triangleq 100\%$) against the wt-*ASC1* control strain in at least two out of three biological replicates. The three additional *ASC1-birA*/birA** SILAC ratios were obtained from the BioID analysis with the ribosome-binding compromised Asc1^{DE}p variant as bait (see chapter 3.1.10). The Asc1^{DE}p-BioID experiments used the *ASC1-birA** strain and the *birA** strain as reference and negative control strains, respectively, and thus supplied three additional *ASC1-birA*/birA** ratios.

With these thresholds 40 proteins were identified as putative Asc1p-neighbors in exponentially growing cells (Tab. 4, or in more detail in Tab. S3). Statistical significance within the three or six repetitions was assessed with a two-sample t-test with a p-value of 0.05. The resulting candidates can be divided into 4 sub-groups: 18 proteins were proteome-corrected and had at least one identified biotinylated lysine residue. Further eight candidates were likewise normalized, but a biotin site was not found. Additional nine proteins were identified with at least one biotin site, but without a proteome value for normalization. For the remaining five candidates neither a biotin site nor a proteome value was found. Still, due to the significant enrichment of these proteins upon biotin affinity capture they were further considered as putative Asc1p-neighbors. Statistical significance of candidates without a proteome reference was determined with a one-sample t-test with a p-value of 0.05.

Among the 18 highest scoring putative Asc1p-neighbors known physical interaction partners like the mRNA-binding protein Scp160 and the ribosomal protein Rps3 were verified (Baum et al., 2004; Sezen et al., 2009; Ben-Shem et al., 2011). Moreover, the enrichment of Asc1p itself supports the high degree of reliance of this approach. Additionally, Asc1p was reported to co-purify with further putative neighbors identified with BioID, namely Rps26Ap, Ubp3p, Bre5p and Nob1p (Ho et al., 2002; Ossareh-Nazari et al., 2010; Schütz et al., 2014). Rps26p is encoded by two alleles, namely *RPS26A* and *RPS26B*. The specific enrichment of Rps26Ap as Asc1p-neighboring protein can be suggested from the identification of a biotinylated Rps26Ap-specific peptide from the very C-terminus of the protein.

Tab. 4: Asc1p-neighbors during exponential growth. Proteins that were enriched from cells of the *ASC1-birA** strain with a log$_2$ SILAC-ratio ≥ 0.26 against the *birA** negative control in at least 4 out of 6 replicates and against the wt-*ASC1* negative control with a log$_2$ SILAC-ratio ≥ 1 in at least 2 out of 3 replicates were considered as Asc1p-neighbors. The ratios were normalized against the respective proteome value (if available). A two-sample t-test (or one-sample t-test if no proteome value was available) with a p-value of 0.05 indicated the enrichment as statistically significant. Standard deviations (SD) and the number of identified biotinylation sites are listed. The colors represent the values of the mean SILAC ratios. SILAC quantification and statistical analyses were performed with the MaxQuant/Perseus software. Biotinylated lysine residues were identified with the MaxQuant/Perseus and the Proteome Discoverer™ software. Exceptions of the described thresholds are indicated as follows: $^{2/6}$ only two valid values available from six replicates; ^{T} p-value above the threshold in the t-test; ^{o} one clear outlier was not considered for the calculation of mean and standard deviation.

protein	enriched /*birA**		enriched /wt-*ASC1*		number of biotin sites
	ratio	SD	ratio	SD	
proteome-corrected and biotin site(s) identified					
Def1	3.22	0.37	3.38	0.06	9
Rps26A	3.10	0.28	4.57	0.27	2
Pbp4	2.91$^{2/6}$	0.49	5.08	0.09	5
Scp160	2.84	0.14	6.72	0.74	4
Asc1	2.84	0.58	4.77	0.45	15
Sro9	2.00	0.29	3.84	0.26	5
Lsm12	1.30	0.15	4.62	0.67	2
Ubp3	1.23$^{3/6}$	0.17	3.08	0.51	2
Rps20	0.81	0.19	6.65	1.33	5
Rps3	0.78	0.04	2.55	0.07	3
Stm1	0.68	0.17	3.66	0.34	14
Cdc33	0.66	0.65	2.96	2.26^T	2
Gis2	0.61	0.19	3.81	0.45	1
Spt5	0.61	0.24	2.35	0.17	1
Rpg1	0.54	0.61	1.01	2.10^T	1
Mbf1	0.53	0.26	4.85	0.42	3
Pob3	0.50	0.21	2.79	0.26	1
Rps2	0.37	0.16	1.72	0.24	1
proteome-corrected, but no biotin site identified					
Coq5	1.76	2.90^T	3.55	1.31	-
Atp7	1.25	0.37	2.23	0.06	-
Cnb1	1.06$^{3/6}$	0.41	2.08	0.33	-
Pst2	1.02	0.11	4.14	0.32	-
Not3	0.65$^{2/6}$	0.27	2.55	0.69	-
Pbp1	0.64	0.30	3.03	0.69	-
Xrn1	0.62	0.22	2.70	0.07	-
Nan1	0.32$^{3/6}$	0.29^T	1.37	0.71	-
no proteome value, but biotin(s) site identified					
Syh1	1.64	0.11	2.73	0.16	3
Hel2	1.64	0.66	1.67	0.09^T	1
Bre5	1.01^o	0.17^o	3.55	0.41	3
Ubp2	0.68	0.39	1.42	0.05	2
Nob1	0.67	0.37	3.25	0.34	1
Smy2	0.62	0.82^T	3.24	0.36	2
Slf1	0.44	0.18	2.19	0.45	1

Tab. 4: Continued.

protein	enriched /birA*		enriched /wt-ASC1		number of biotin sites
	ratio	SD	ratio	SD	
no proteome value, but biotin site(s) identified					
Hsm3	0.43	0.60[T]	2.79	0.20	1
Eap1	0.27[o]	0.20[o]	1.93	0.44	1
neither proteome value nor biotin site identified					
Shs1	1.65	0.24	2.84	0.11	-
Rim11	1.37	0.33	2.58	0.95[T]	-
Nab6	0.65[3/6]	0.36[T]	1.82	0.20	-
Yor385W	0.50	0.32	2.34	0.57	-
Ypk1	0.36	0.43[T]	2.49	0.58	-

0	0.5	1.0	> 1.5

The strongest BioID-mediated enrichment relative to the *birA** control strain was observed for the RNA polymerase II degradation factor Def1p, followed by the ribosomal protein Rps26A and the mRNA-binding proteins Scp160 and Sro9. Pbp4p, a Pbp1p-binding protein, was highly enriched in the Asc1p-neighborhood and a strong candidate although only quantification values from two replicates were available. Biotinylation at five different lysine residues additionally indicated Asc1p proximity of Pbp4p. The highest biotinylation in number was observed for Def1p, for Asc1p itself, and for the ribosome clamping factor Stm1p, with nine, fifteen or fourteen identified biotinylated lysine residues, respectively (positions of biotinylated lysine residues are listed in Tab. S4).

The 40 candidates were grouped according to their molecular functions (Fig. 15). A non-exclusive assignment to these groups demonstrates an enrichment of proteins with mRNA-binding activity (e.g. Scp160p, Sro9p, Gis2p) and proteins that generally associate to ribosomes (e.g. Cdc33p, Rpg1p, Eap1p). Many of the Asc1p-neighbors are characterized as mRNP granule components (e.g. Pbp1p, Pbp4p, Lsm12p) or are involved in the regulation of ubiquitylation (e.g. Def1p, Ubp3p, Hel2p) or translation (e.g. Stm1p, Rpg1p, Cdc33p). Also, proteins that function in mRNA-processing were identified in the Asc1p-neighborhood. Together, these data reveal an accumulation of factors involved in mRNA translation, mRNA stability, and gene transcription within the microenvironment of Asc1p, hinting to a role of Asc1p as expansive modulator of gene expression.
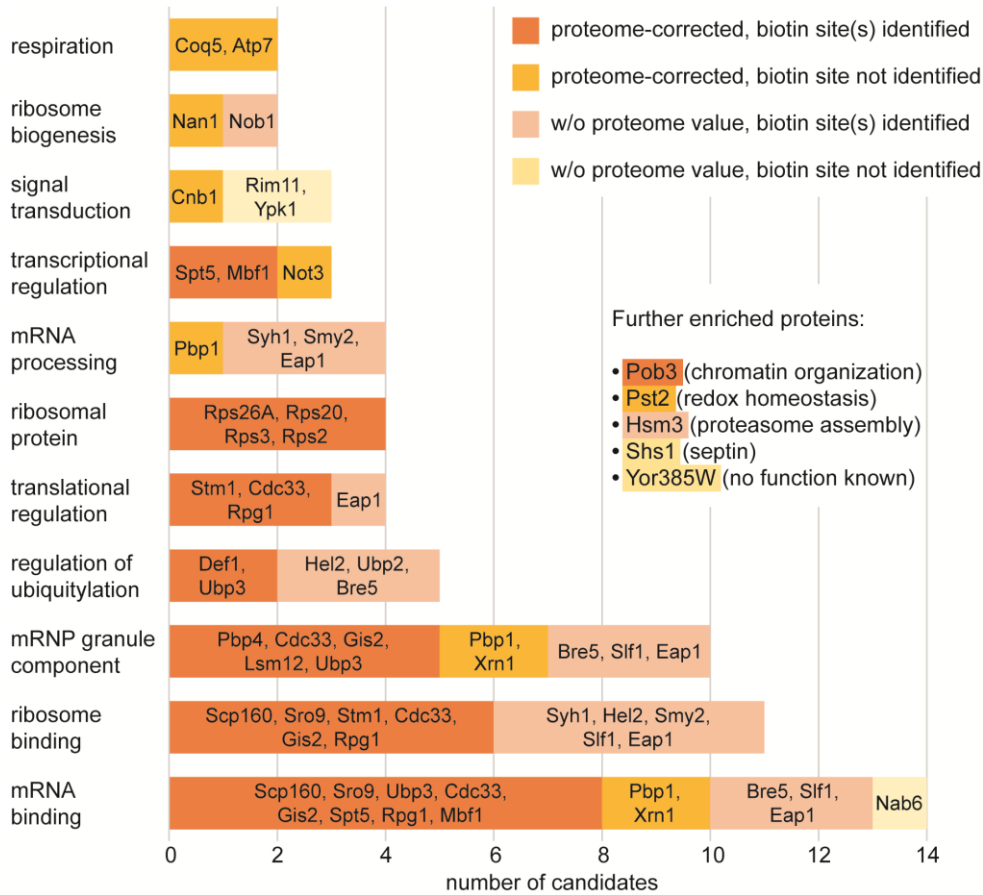
Fig. 15: Functional grouping of Asc1p-neighbors. In total, 40 proteins were identified in the Asc1p-vicinity and assigned to groups of molecular functions in a non-exclusive manner. The number of proteins per group is indicated in the x-axis. The number of potential Asc1p-neighbors per group with or without proteome value, and with or without identified biotin site is reflected by the respective colors. Corresponding candidates are listed.

3.1.8 The Asc1p-neighborhood remodels upon glucose starvation

Since BioID proved to be an adequate *in vivo* tool to study a protein's microenvironment, alterations in the vicinity of Asc1p were analyzed upon differential environmental stimuli. The effect of glucose deprivation on the Asc1p-neighborhood was monitored in *ASC1-birA** cells starved for glucose in comparison to *ASC1-birA** cells cultivated in the presence of 2% glucose as reference. As negative control the *birA** strain was equally grown in the absence of glucose to expose Asc1p-independent enrichments (Fig. 14B). Prior to inducing glucose deprivation the three strains were grown exponentially until an optical culture density of 0.7. To particularly label starvation-specific Asc1p-neighboring proteins, biotin was only supplemented 15 minutes after cell transfer to the glucose-free medium. The culture was then incubated for one further hour to achieve efficient biotinylation for the following affinity capture experiment. The *birA**

negative control strain was treated equally, the *ASC1-birA** reference strain, however, was shifted to medium with 2% glucose instead. The triple SILAC experiment with these three strains/conditions was performed in five independent biological replicates. LC-MS/MS2 data processing was performed as described in Tab. S5. SILAC ratios of the total proteome without biotin affinity capture with the exponentially grown *ASC1-birA** strain in the denominator confirmed the glucose shortage, since glucose transporters Hxt6p/Hxt7p and Hxt2p, and the hexokinase Hxk1p among others were highly upregulated during starvation (Tab. S6).

Besides the expected changes on the whole proteome level, the Asc1-BirA*p microenvironment was also significantly altered upon glucose deprivation. BioID-captured enrichment of a protein within the Asc1p-neighborhood upon starvation was defined by a $\log_2$ SILAC enrichment ratio ≥ 0.26 against the reference culture and the negative control. 29 proteins passed this threshold and were considered as glucose starvation-specific Asc1p-neighbors (Tab. 5, and in more detail in Tab. S7; biotin site positions are listed in Tab. S8).

Among them, twelve ribosomal proteins of both the small and large ribosomal subunits, e.g. Rpl18p, Rpl23p and Rps5p, were identified. Also proteins implicated in amino acid metabolism, e.g. Lys9p and Thr1p specifically enriched in the proximity of Asc1p in response to glucose starvation (Fig. 16B). Coq5p, a protein involved in the ubiquinone biosynthesis and hence cellular respiration showed the strongest enrichment in the Asc1p-neighborhood during glucose starvation. This protein was identified as Asc1p-neighbor already during exponential growth in the presence of glucose, however, to a considerably lesser extent.

Other proteins that were found as Asc1p-neighbors during exponential growth leave the head region of the ribosome at starvation ($\log_2$ SILAC ratio ≤ -0.26 and thus orange to red background color in Tab. 5). Due to the degree of reliability only proteome-corrected candidates are further considered in the following paragraph, however, additional candidates that were identified without a proteome value for normalization are listed in Tab. S7. In total, 15 Asc1p-neighbors identified with BioID at exponential growth were significantly less enriched by biotin affinity capture from cells suffering from glucose shortage including the mRNA-binding proteins Scp160, Sro9 or Gis2, as well as translational regulators (e.g. Stm1p or Rpg1p) and further high-scoring candidates (e.g. Def1p or Mbf1p; Fig. 16A). This is in accordance with decreased rates of translation initiation during glucose starvation. The accumulation of ribosomal proteins in the Asc1p-neighborhood implies a replacement of the mRNA-binding proteins, Def1p, Stm1p and others in favor of an aggregation of ribosomal subunits during carbon source deprivation.

Tab. 5: Changes in the Asc1p-neighborhood during glucose starvation. Proteins that were enriched via BioID from *ASC1-birA** cells cultivated in the absence of glucose with a $\log_2$ SILAC ratio ≥ 0.26 against the *ASC1-birA** reference strain (2% glucose) were considered as starvation-specifically enriched in the Asc1p-neighborhood; proteins with a $\log_2$ SILAC ratio ≤ -0.26 were considered as migrated from the Asc1p-neighborhood in response to glucose starvation. A $\log_2$ SILAC ratio ≥ 0.26 against the *birA** negative control strain was required in both cases in at least three out of five biological replicates. The ratios were normalized against the respective proteome value. A two-sample t-test with a p-value of 0.05 indicated the enrichment as statistically significant. Standard deviations (SD) and the number of identified biotinylation sites are listed. Proteins that were identified as Asc1p-neighbors during exponential growth are listed in bold. Ribosomal proteins that were starvation-specifically enriched are marked with an asterisk. The colors represent the values of the mean SILAC ratios. SILAC quantification and statistical analyses were performed with the MaxQuant/Perseus software. Biotinylated lysine residues were identified with the MaxQuant/Perseus and the Proteome Discoverer™ software. Exceptions of the described thresholds are indicated as follows: [T] p-value above the threshold in the t-test.

protein	enriched /ASC1-birA*		enriched /birA*(-glc)		number of biotin sites
	ratio	SD	ratio	SD	
proteome-corrected and biotin site(s) identified					
Rpl12*	0.55	0.45	0.57	0.53	1
Eft1	0.37	0.35	0.32	0.32	1
Lsm12	-0.32	0.07	0.99	0.08	1
Rpa190	-0.47	0.21	0.35	0.09	1
Rps20	-0.49	0.08	0.85	0.13	4
Stm1	-0.70	0.07	0.87	0.16	6
Rpg1	-0.90	0.16	1.42	0.39	2
Sro9	-1.11	0.20	2.57	0.68	2
Psp2	-1.14	0.28	0.81	0.46	3
Asc1	-1.50	0.18	1.90	0.52	13
Bre5	-1.50	0.16	1.67	0.41	1
Def1	-1.53	0.75	3.34	0.90	5
Pbp4	-1.70	0.22	2.85	0.46	1
Scp160	-1.76	0.20	2.50	0.56	3
proteome-corrected, but no biotin site identified					
Coq5	5.67	1.41	5.61	1.36	-
Fpr1	1.01	0.53	0.72	0.45[T]	-
Rpl18*	0.97	0.77	0.60	0.70[T]	-
Sec26	0.96	0.87	0.66	0.79[T]	-
Shb17	0.95	0.48	0.70	0.55	-
Cpr1	0.88	0.64	0.66	0.64[T]	-
Rpl23*	0.86	0.58	0.54	0.51	-
Chc1	0.81	0.81[T]	0.57	0.57[T]	-
Lys9	0.74	0.63[T]	0.56	0.44[T]	-
Thr1	0.73	0.73[T]	0.62	0.63[T]	-
Act1	0.71	0.55	0.52	0.55[T]	-
Rps5*	0.70	0.50	0.53	0.51[T]	-
Rps11	0.68	0.50	0.52	0.45	-
Ura2	0.67	0.69	0.60	0.68[T]	-
Rps4*	0.59	0.42	0.35	0.33[T]	-

Tab. 5: Continued.

protein	enriched /ASC1-birA*		enriched /birA* (-glc)		number of biotin sites
	ratio	SD	ratio	SD	
proteome-corrected, but no biotin site identified					
Sah1	0.58	0.54	0.34	0.44^T	-
Rps14*	0.55	0.44	0.44	0.51^T	-
Ura6	0.54	0.41	0.54	0.47	-
Tif11	0.54	0.30	0.53	0.44^T	-
Rpl9A*	0.51	0.41	0.32	0.42^T	-
Rpl10*	0.50	0.34	0.48	0.43	-
Rpl11*	0.46	0.38	0.34	0.34^T	-
Adi1	0.44	0.25	0.65	0.46	-
Rpl1*	0.43	0.31	0.31	0.31^T	-
Rps0*	0.40	0.27	0.54	0.40	-
Mvd1	0.36	0.34^T	0.27	0.28	-
Pex11	0.35	0.17	0.30	0.20^T	-
Hek2	-0.28	0.08^T	0.56	0.19	-
Bfr1	-0.55	0.09	0.30	0.07	-
Ret2	-0.69	0.31	0.25	0.24	-
Dia1	-0.81	0.30	0.52	0.12	-
Ccr4	-0.83	0.15	0.27	0.32^T	-
Xrn1	-0.93	0.15	0.40	0.14	-
Srp1	-0.95	0.49	0.45	0.28	-
Gis2	-1.10	0.26	0.34	0.15	-
His6	-1.33	0.99	0.31	0.47^T	-
Shs1	-1.54	0.17	0.91	0.23	-
Mbf1	-1.64	0.24	0.46	0.14	-
Spt5	-1.90	0.33	0.52	0.39	-
New1	-2.43	0.42	0.35	0.43^T	-
Ent3	-2.79	0.12	0.64	0.16	-

```
< -1.5   -1.0    -0.5     0     0.5    1.0    > 1.5
```

The Asc1-BirA* protein itself is also less enriched after glucose depletion (Tab. 5, Fig. 16A). Its total cellular abundance as well as biotinylation in general, however, was not affected by glucose starvation. Consistently, all known naturally biotinylated proteins in yeast, like the acetyl-CoA carboxylase Acc1p, the pyruvate carboxylases Pyc1p/Pyc2p or the mitochondrial acetyl-CoA carboxylase Hfa1p, were equally enriched from cells starved from glucose as from cells grown exponentially (Tab. S9). Thus, the decreased enrichment of Asc1-BirA*p during glucose deprivation hints to an impeded accessibility of Asc1-BirA*p for self-biotinylation, which might result from a modified arrangement of ribosomes. In summary, glucose deprivation leads to significant alterations in the Asc1p microenvironment, including a concentration of ribosomal proteins, and a migration of mRNA-binding proteins and translational regulators away from the scaffold suggesting a structural rearrangement of ribosomes during starvation.
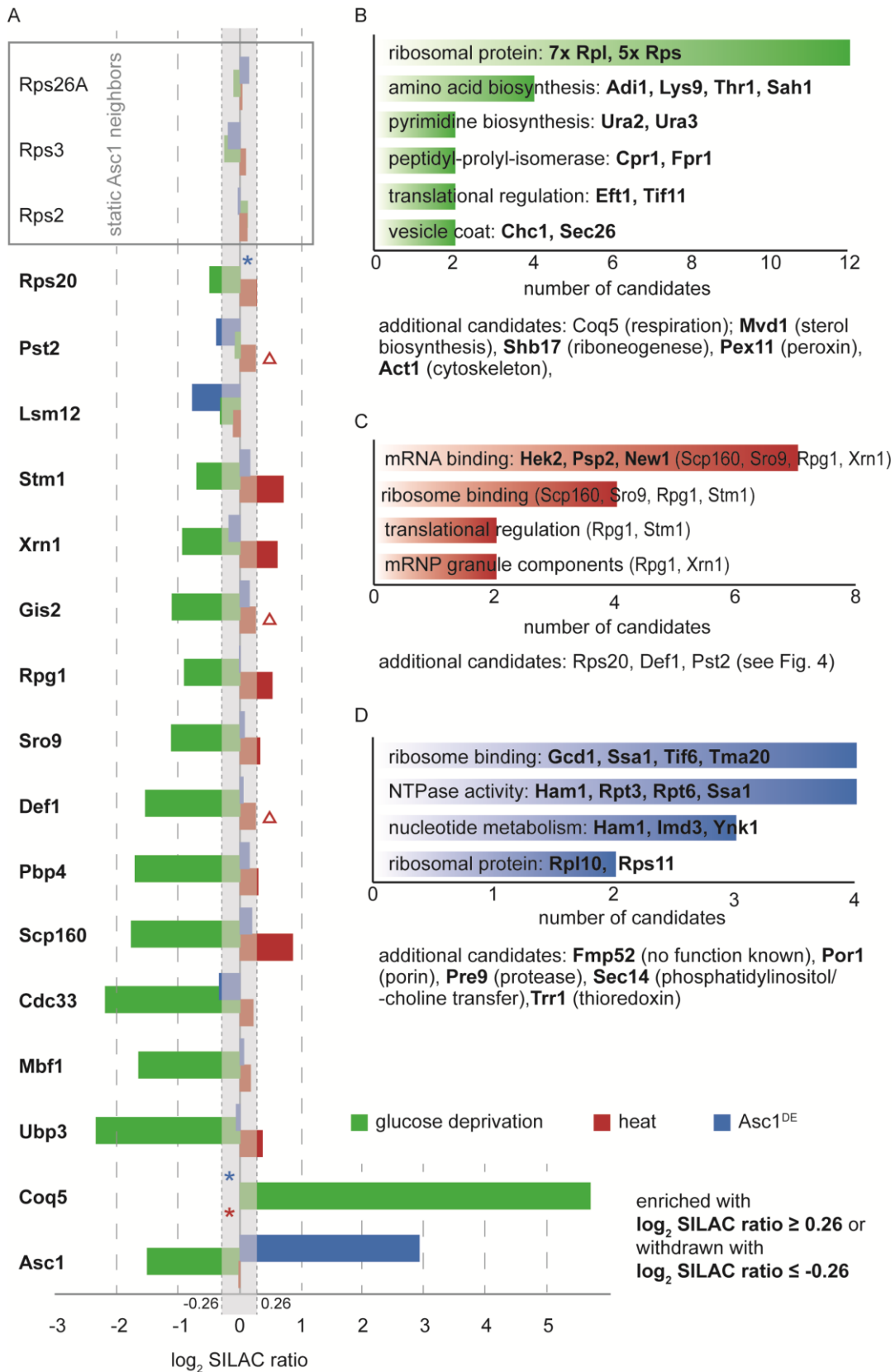
Fig. 16: Dynamics within the proteinaceous neighborhood of Asc1p. (A) The bar chart depicts changes in the Asc1-BirA*p neighborhood in cells during glucose deprivation and mild heat stress (37°C) and due to the R38D K40E exchange relative to the neighborhood of Asc1-BirA*p during exponential growth (2% glucose, 30°C). 19 proteins identified as Asc1p-neighbors during exponential

growth are listed on the left. The bars represent the mean value of $\log_2$ SILAC enrichment ratios of the *ASC1-birA**-strain starved for glucose (green), cultivated at 37°C (red) or of the *ASC1^{DE}-birA**-strain (blue) relative to the wt-*ASC1-birA** strain (2% glucose, 30°C). Proteins were considered as dynamic Asc1p-neighbors if $\log_2$ SILAC ratios were outside -0.26 and 0.26. Stable Asc1p-neighbors, independent of the tested growth conditions or the DE-exchange, are listed at the top within the gray box ($\log_2$ SILAC ratio between -0.26 and 0.26). Missing SILAC ratios are indicated by asterisks. Mean values that do not reach the respective threshold due to outlier values are indicated by triangles. (B-D) Proteins specifically enriched in the Asc1p-neighborhood (B) at glucose starvation, (C) at heat-stress, or (D) of the DE-variant were assigned to functional groups in a non-exclusive manner. Proteome-corrected candidates of the respective groups are listed within the bar chart, those that are exclusively enriched in these specific experiments are listed in bold. The number of proteins per group is given by the x-axis. Further proteins that do not belong to the chosen groups are listed below the diagrams.

3.1.9 During mild heat stress mRNA-binding proteins remain high frequent Asc1p-neighbors

As mentioned above the Asc1 protein is part of a signaling system that protects cells against a variety of stresses resulting in growth defects of Asc1p-depleted cells. Amongst others these cells are sensitive to heat shock apparent as slow growth at 37°C (Fig. 10; Auesukaree et al., 2009; Sinha et al., 2008). Therefore, with BioID alterations in the proteinaceous Asc1-BirA*p-neighborhood induced by mild heat shock were analyzed. In order to unravel heat-dependent changes, *ASC1-birA** cells were exposed to 37°C and directly compared to *ASC1-birA** reference cells permanently cultivated at 30°C. Asc1p-independent biotinylations and enrichments were filtered by the comparison to the *birA** negative control strain grown equally at 37°C. Initially, all strains were cultivated at 30°C until they reached an optical culture density of 0.6. Then, the cultures were shifted to the respective temperatures. Excess biotin was added after adjustment to the elevated temperature and the cultures were cultivated at 30°C or 37°C for one further hour. This BioID set-up was performed in three biological replicates. One replicate was performed with a label swap. In contrast to the indications in Fig. 14B, the *ASC1-birA** strain cultivated at 37°C was in this case labeled with *heavy* isotopic amino acids, the *ASC1-birA** reference strain with *medium* and the *birA** negative control strain with *light* lysine and arginine. LC-MS/MS2 data processing was performed as described in Tab. S5. On the whole proteome level several heat-shock proteins, members of the HSP70 family, and further HSP-associated proteins were up-regulated in the *ASC1-birA** strain cultivated at 37°C in comparison to the reference culture cultivated at 30°C reflecting the heat response of yeast cells

at 37°C (Tab. S10). The heat treatment caused alterations in the proximity of Asc1p, however, less substantial than glucose deprivation. Proteins with log$_2$ SILAC enrichment ratio ≥ 0.26 against the reference culture and negative control were defined as heat-dependently enriched in the Asc1p-neighborhood, which applied for in total eleven proteome-corrected proteins (Tab. 6, and in more detail in Tab. S11; biotin site positions are listed in Tab. S12). Further candidates that were identified without a proteome value for normalization are listed in Tab. S11.

Tab. 6: Dynamics in the Asc1p-neighborhood during heat stress. Proteins that were enriched from *ASC1-birA** cells cultivated at 37°C with a log$_2$ SILAC ratio ≥ 0.26 against the *ASC1-birA** reference strain (30°C) and against the *birA** negative control strain in at least two out of three biological replicates were considered as heat-specifically enriched in the Asc1p-neighborhood. The ratios were normalized against the respective proteome value. A two-sample t-test with a p-value of 0.05 indicated the enrichment as statistically significant. Standard deviations (SD) and the number of identified biotinylation sites are listed. Proteins that were already identified as Asc1p-neighbors during exponential growth are listed in bold. The colors represent the values of the mean SILAC ratios. SILAC quantification and statistical analyses were performed with the MaxQuant/Perseus software. Biotinylated lysine residues were identified with the MaxQuant/Perseus and the Proteome Discoverer™ software. Exceptions of the described thresholds are indicated as follows: ^{T} p-value above the threshold in the t-test; $^\Delta$ mean value does not reach the respective threshold due to an outlier value.

Protein	enriched /ASC1-birA*		enriched /birA* (37°C)		number of biotin sites
	ratio	SD	ratio	SD	
proteome-corrected and biotin site(s) identified					
Scp160	**0.85**	0.11	**3.00**	0.02	3
Stm1	**0.70**	0.07	**0.88**	0.05	4
Psp2	**0.68**	0.22	**0.66**	0.42	2
Sro9	**0.32**	0.04	**1.64**	0.10	1
Rps20	**0.27**	0.04	**0.70**	0.22	2
Def1	**0.25** $^\Delta$	0.24^T	**3.55**	0.73	2
proteome-corrected, but no biotin site identified					
Hek2	**1.06**	0.29	**0.22**	0.16^T	-
Xrn1	**0.60**	0.08	**0.27**	0.32^T	-
Rpg1	**0.52**	0.05	**0.80**	0.22	-
New1	**0.46**	0.09	**0.50**	0.12	-
Pst2	**0.25** $^\Delta$	0.13^T	**0.64**	0.29	-

0   0.5   1.0   > 1.5

The eleven candidates included eight neighbors already identified with BioID during exponential growth: Scp160p, Stm1p, Xrn1p, Rpg1p, Sro9p, Rps20p, Pst2p and Def1p located in proximity to Asc1p during heat stress and were increasingly enriched from cells cultivated at 37°C (Fig. 16A). Additionally, three heat-specific Asc1p-neighbors, Hek2p (or Khd1p), Psp2p and New1p, were identified at elevated temperature (Tab. 6, Fig. 16C). Among the eleven candidates eight proteins feature mRNA-binding activity (Fig. 16C). The enrichment of natural biotinylation targets like Acc1p, Hfa1p or Arc1p was not affected by heat indicating that general biotinylation was mainly temperature-independent (Tab. S13). These data show that in contrast to glucose starvation heat shock at 37°C maintains the Asc1p-neighborhood substantially and rather enriches for proteins with mRNA-binding activity.

3.1.10 Asc1^{DE}p locates to ribosomes *in vivo*, but is presumably shifted from its natural position

The proposed function of the Asc1 protein in cellular signaling and translation most probably goes along with its exposed position at the head region of the 40S ribosomal subunit. The *asc1^{DE}* strain expresses an Asc1p variant that showed a decreased affinity to ribosomes during sucrose density gradient ultracentrifugation due to two amino acid exchanges (Coyle et al., 2009). Both residues, R38 and K40, are located at the interface to the 18S rRNA and replacement by negatively charged amino acids was believed to repel Asc1p off the ribosome. The R38D and K40E exchanges, however, cause only mild phenotypic abnormalities (Coyle et al., 2009; Schmitt et al., 2017) suggesting that ribosome-dissociation might be an *in vitro* artefact.

With an *asc1^{DE}-birA** fusion, also expressed from a high-copy number plasmid in the Δ*asc1* strain, the *in vivo* neighborhood of the Asc1^{DE}p variant was quantitatively analyzed. To account for alterations caused by the two amino acid exchanges, three biological replicates of BioID experiments were performed with the *ASC1-birA** strain as reference and the *birA** strain as negative control strain (Fig. 14B). Data processing was performed as described in Tab. S5. Proteins with a log$_2$ SILAC enrichment ratio ≥ 0.26 for the *asc1^{DE}-birA*/ASC1-birA** comparison were considered as Asc1^{DE}p-specific neighbor candidates, whereas proteins with a log$_2$ SILAC enrichment ratio ≤ -0.26 were defined as Asc1p-neighbors that locate to a lesser extent proximal to Asc1^{DE}p. A log$_2$ SILAC enrichment ratio ≥ 0.26 in comparison to the negative control was required in both cases (Tab. 7, and in more detail in Tab. S14; positions of biotinylated lysine residues are listed in Tab. S15). The following paragraph focuses only on proteome-corrected candidates due to their higher reliability, however, further candidates that were identified without a proteome value for normalization are listed in Tab. S14.

Tab. 7: The proteinaceous neighborhood of Asc1^{DE}p in comparison to wt-Asc1p. Proteins that were enriched from the *asc1^{DE}-birA** strain with a log$_2$ SILAC ratio ≥ 0.26 against the *ASC1-birA** reference strain were considered as DE-specifically enriched in the Asc1p-neighborhood; proteins with a log$_2$ SILAC ratio $\leq$ -0.26 were considered as migrated from the Asc1^{DE}p-neighborhood. A log$_2$ SILAC ratio ≥ 0.26 against the *birA** negative control strain was required in both cases in at least two out of three biological replicates. The ratios were normalized against the respective proteome value. A two-sample t-test with a p-value of 0.05 indicated the enrichment as statistically significant. Standard deviations and the number of identified biotinylation sites are listed. Proteins that were identified as wt-Asc1p-neighbors are listed in bold. The colors represent the values of the mean SILAC ratios. SILAC quantification and statistical analyses were performed with the MaxQuant/Perseus software. Biotinylated lysine residues were identified with the MaxQuant/Perseus and the Proteome Discoverer™ software. Exceptions of the described thresholds are indicated as follows: [T] p-value above the threshold in the t-test; [Δ] mean value does not reach the respective threshold due to an outlier value.

Protein	enriched /ASC1-birA*		enriched /birA*		number of biotin sites
	ratio	SD	ratio	SD	
proteome-corrected and biotin site(s) identified					
Asc1	**2.90**	0.29	**5.67**	0.45	14
Ssa1	**1.17**	0.17	**0.70**	0.11	1
Imd3	**0.42**	0.14	**0.36**	0.26[T]	2
Cdc33	**-0.28**	0.10	**0.67**	0.09	2
Lsm12	**-0.77**	0.07	**0.59**	0.13	1
proteome-corrected, but no biotin site identified					
Fmp52	**1.50**	0.28	**1.57**	0.37	-
Ham1	**1.42**	0.25	**0.89**	0.26	-
Pre9	**1.13**	0.20	**0.00**[Δ]	0.55[T]	-
Gcd1	**1.10**	0.19	**0.52**	0.09[T]	-
Sec14	**1.08**	0.15	**0.37**	0.14	-
Trr1	**1.05**	0.11	**0.42**	0.26[T]	-
Tma20	**0.81**	0.11	**0.46**	0.04	-
Rpt3	**0.74**	0.23	**0.79**	0.39	-
Por1	**0.65**	0.12	**0.33**	0.36[T]	-
Tif6	**0.63**	0.30	**1.37**	0.46	-
Ynk1	**0.53**	0.34	**0.42**	0.29[T]	-
Rpt6	**0.40**	0.27[T]	**0.43**	0.29[T]	-
Rpl10	**0.40**	0.15	**0.34**	0.12	-
Rps11	**0.30**	0.03	**0.41**	0.29[T]	-
Pst2	**-0.38**	0.07	**0.56**	0.17	-
Atp7	**-0.45**	0.47[T]	**0.73**	0.21	-

< -1.5   -1.0   -0.5   0   0.5   1.0   > 1.5

The comparison with the proteinaceous neighborhood of the wt-Asc1 protein verified ribosome association of the Asc1^{DE} protein, since most of the wt-Asc1p-neighbors were likewise found for Asc1^{DE}p, reflected by a log$_2$ SILAC enrichment ratio between -0.26 and 0.26 (Fig. 16A). These included among others the ribosomal proteins Rps3, Rps26A and Rps2 confirming physical proximity to ribosomes. This is further supported by ribosome-associated candidates like e.g. Pbp4p, Scp160p and Sro9p. Still, the Asc1^{DE}p microenvironment was not totally identical with the Asc1p-neighborhood: Four proteins were less captured from the *asc1^{DE}-birA** strain, namely Cdc33p, Pst2p, Lsm12p and Atp7p (Tab. 7, Fig. 16A).

Asc1^{DE}p itself was even more enriched from *asc1^{DE}-birA** cells than Asc1-BirA*p from *ASC1-birA** cells (Tab. 7, Fig. 16A). The total protein abundance of the Asc1p variants was, however, not altered. This hints to a more efficient self-biotinylation or to an increased frequency of neighboring Asc1^{DE}p molecules, possibly through Asc1^{DE}p-dimer formation. Altogether, 17 proteins were proteome-corrected and exclusively identified as Asc1^{DE}p neighbors (Tab. 7). These included further ribosome-associated proteins, NTPases, proteins involved in nucleotide metabolism, and two additional ribosomal proteins (Fig. 16D). These candidates suggest a twisted position of Asc1^{DE}p at ribosomes and/or even ribosome dissociation for a fraction of all Asc1^{DE}p molecules. It can be concluded that the R38D K40E exchange does not lead to a total dissociation of Asc1^{DE}p from the ribosome *in vivo*. Together with the knowledge about a decreased affinity to ribosomes during sucrose density gradient ultracentrifugation *in vitro*, the BioID data suggest that the Asc1^{DE}p mutant is still incorporated into ribosomes, but to some extent shifted from its natural position.

3.1.11 Asc1p/*ASC1* genetically interacts with high-confident BioID-neighbors

Dynamics in the Asc1p microenvironment were studied with BioID *in vivo* and various proteins were identified in the proximity of the scaffold protein at different growth conditions. A functional relation between Asc1p and its close neighbors is possible, but not necessary. Indeed, genetic interactions of Asc1p/*ASC1* with Not3p, Xrn1p and Smy2p, identified with BioID in the proximity of Asc1p at exponential growth, were reported previously (Sezen et al., 2009; Wilmes et al., 2008). To evaluate whether there are further genetic interactions of Asc1p with its proximal proteins, especially with the highest scoring candidates found with BioID, double deletion strains were constructed. *DEF1*, *STM1, SCP160*, *GIS2* and *HEK2*, encoding the RNAPII degradation factor, the ribosomal clamping factor or mRNA-binding proteins, respectively, were knocked-out each in the wt-*ASC1* and the Asc1p-depleted *asc1$^-$* strain backgrounds.

The *ASC1* ORF not only comprises the coding sequence for Asc1p, but also contains an intron, which bears the *SNR24* gene. A complete *ASC1* knock-out additionally leads to deletion of *SNR24* coding for the U24 snoRNA. The *asc1⁻* strain is characterized by a *loxP* insertion within the first exon, which creates a TAG stop codon (Rachfall et al., 2013). Thus, translation of the *ASC1* mRNA is abrogated. Splicing of the mRNA, however, is still functional leading to intact *SNR24* mRNA and hence U24 snoRNA (Rachfall et al., 2013). Therefore, the *asc1⁻* strain is most suitable for the investigation of Asc1p-dependent phenotypes, since it excludes U24-dependent effects.

The deletion of genes encoding Asc1p-proximal proteins was obtained by replacing the respective ORFs with an *URA3* marker cassette (Gueldener et al., 2002). At least two independent positive clones per knock-out were used for phenotypical analyses. Conditions that were known to affect the growth of Asc1p-depleted cells were used to score for genetic interactions. These included growth in the presence of the translational inhibitors cycloheximide and canavanine as well as in the presence of the cell wall damaging agent congo red. Hyper-osmotic stress was induced by high concentrations of NaCl, and 2% glycerol instead of glucose were used as non-fermentable carbon source to analyze the respiratory capacity of the double mutants. Additionally, the growth at 37°C was monitored.

The *DEF1* ORF was deleted in the wt-*ASC1* background resulting in clones with a strong slow-growth phenotype. No transformants with a *DEF1* deletion in the *asc1⁻* strain background were obtained hinting to synthetic lethality, which, however, remains to be confirmed. Yeast cells bearing the *asc1⁻* Δ*gis2* double mutation were viable and behaved like the *asc1⁻* single mutant at all tested conditions (Fig. S2A). This also applied for the *asc1⁻* Δ*stm1* double mutant strain in case of most, but not all monitored growth conditions. The *asc1⁻* and Δ*stm1* single mutant strains exhibit slow growth at 37°C, and deletion of the *STM1* gene in the *asc1⁻* strain further decreased fitness of the yeast cells to almost no growth (Fig. 17A; see also Fig. S2C). The expression of plasmid-borne wt-*ASC1* in the double mutant restored growth as it was observed for the *STM1* single deletion (Fig. 17A). Deletion of the *HEK2* ORF in the *asc1⁻* strain did not alter the behavior on the tested growth conditions (Fig. S2D). The growth of the *asc1⁻* Δ*scp160* double mutant on agar plates containing elevated levels of NaCl suggests a genetic interaction of *ASC1* and *SCP160* in response to osmotic stress. Asc1p-depleted cells demonstrated a growth defect in the presence of 70 mM NaCl. The additional deletion of *SCP160*, however, rescued this phenotype, hinting to a suppressor function of *SCP160* on *asc1⁻* sensitivity for osmotic stress (Fig. 17B; see also Fig. S2B). With the expression of plasmid-borne wt-*ASC1* in the double mutant the growth behavior of the *SCP160* single deletion was restored (Fig. 17B).

Other *asc1*⁻ phenotypes were unaffected by the deletion of *SCP160* (Fig. S2B). In summary, the *ASC1* gene genetically interacts with the genes encoding the ribosomal clamping factor Stm1p and the mRNA-binding protein Scp160p in response to heat stress and osmotic stress, respectively.
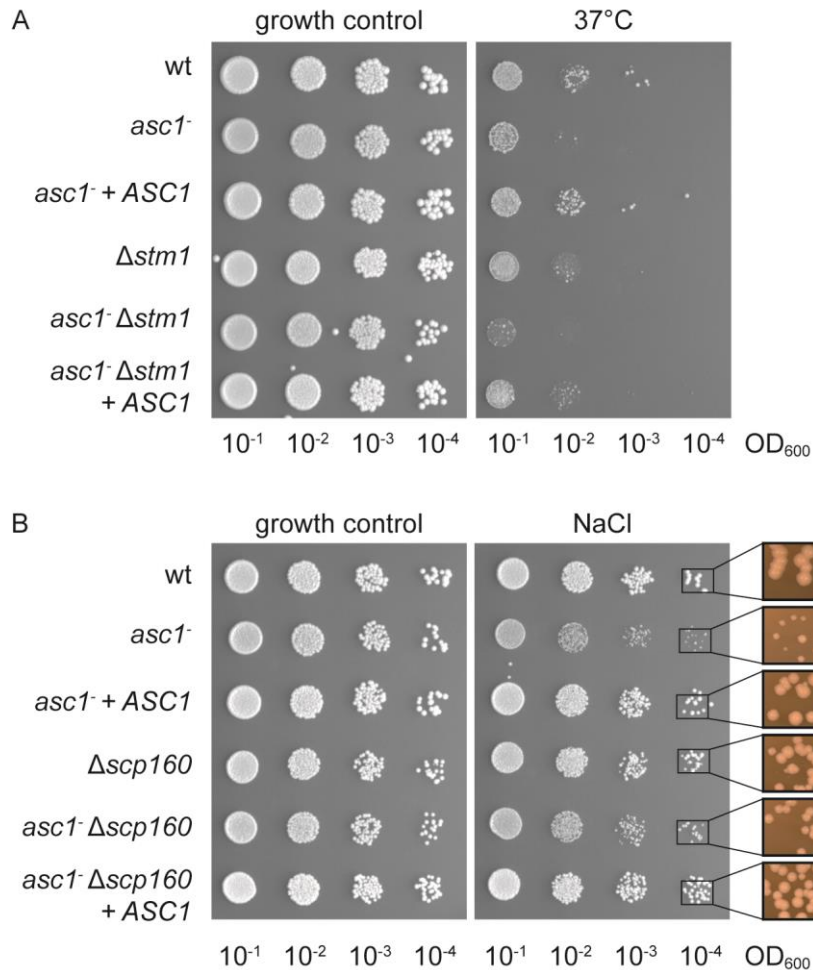
Fig. 17: Deletion of the *STM1* or *SCP160* gene in *asc1*⁻ cells reveals genetic interactions with *ASC1* at heat stress or osmotic stress, respectively. For drop dilution assays 20 µl of 10-fold dilution series of cell suspensions containing the indicated strains were spotted on YNB agar plates. The *asc1*⁻ strain and double mutant strains were complemented with wt-*ASC1* expressed from a CEN plasmid with the endogenous *ASC1*-promoter. wt-*ASC1*, *asc1*⁻ and Δ*stm1* or Δ*scp160* single mutant cells were transformed with the respective empty vectors (pME2789 and pME2791). The plates were photographed after three or five days of growth. (A) The heat sensitivity of *asc1*⁻ and Δ*stm1* single and double mutants was scored on YNB agar plates incubated at 37°C instead of 30°C. (B) YNB agar plates containing osmotic stress inducing amounts of NaCl (70 mM) were used to analyze the sensitivity of *asc1*⁻ and Δ*scp160* single and double mutants. Yeast colonies of the last spot were 8.4-fold magnified with a binocular microscope.

3.1.12 P-body formation is decreased in Asc1p-depleted cells during heat stress

Among the 40 proteins identified in the proximity of Asc1p during exponential growth several were described as components or regulators of stress granules and P-bodies. The proximity of Asc1p to these proteins hints to a regulative impact on the formation of mRNP granules. Indeed, it has been reported that Asc1p is required for P-body assembly in response to replication stress induced by hydroxyurea (Tkach et al., 2012). The same study showed that Asc1p does not affect P-body formation when cells were shifted to water representing several kinds of stress including glucose starvation, nitrogen starvation and osmotic stress amongst others (Tkach et al., 2012). To investigate the impact of Asc1p on P-body formation specifically during heat stress and glucose starvation, wt-*ASC1* and *asc1⁻* strains were transformed with a plasmid expressing the mCherry-tagged P-body marker protein Edc3 (Buchan et al., 2008; kindly provided by Prof. Dr. Heike Krebber, Georg-August-University Göttingen). P-bodies are naturally occurring to some extend in unstressed yeast cells. Fluorescence microscopy revealed Edc3p-mCherry foci in about 14% and 11% of all wt-*ASC1* and *asc1⁻* cells, respectively, indicating that the basic level of foci is Asc1p-independent (Fig. 18).
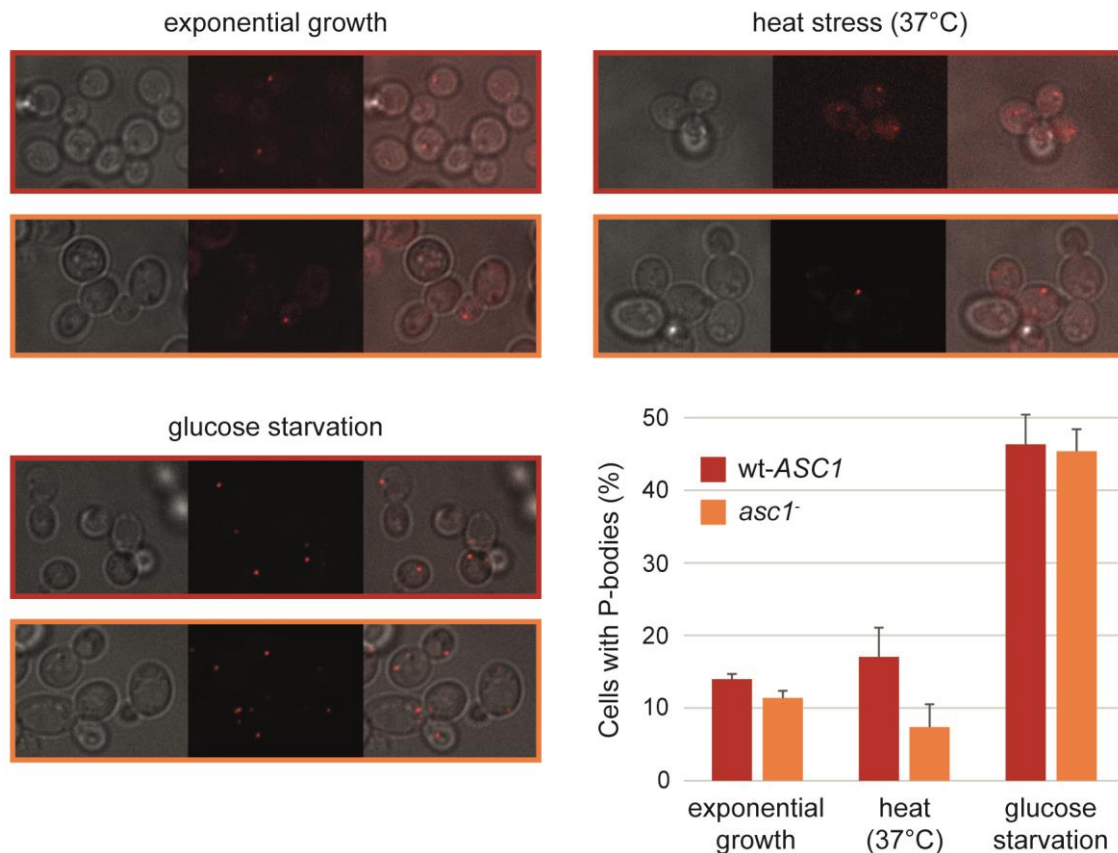
Fig. 18: P-body formation at exponential growth, heat stress and glucose starvation. The number of cells with P-bodies in wt-*ASC1* and *asc1⁻* cultures was determined during exponential growth, at 37°C or in the absence of glucose. The diagram gives the percentage of all cells with P-bodies per condition.

When shifted to 37°C for one hour, which corresponds to a rather mild heat shock as applied in the BioID analysis, P-bodies were observed in about 17% of all wt-*ASC1* cells, but only 7% of the *asc1⁻* cells (Fig. 18). Thus, P-body formation is lower in cells lacking Asc1p. The cultivation of both strains in the absence of glucose for 15-30 min results in P-body formation in about 45% of all cells in both strain backgrounds (Fig. 18). In summary, these data show that Asc1p is not essential for P-body formation in general, but that it might play a regulatory role in the formation of P-bodies in response to heat.

3.2 Strategy and plasmid construction for the analysis of physical Asc1p protein-protein interactions with Bpa-mediated cross-link experiments

Multiple proteins were identified in the proximity of Asc1p at different growth conditions with BioID potentially being also physical Asc1p interaction partners. Covalent protein cross-linking with artificial amino acids is an emerging technique for the structural analysis of protein-protein interactions. It is based on the genetic code expansion system, developed by Peter Schultz and coworkers, that enables the site-specific incorporation of unnatural amino acids, e.g. the photo-reactive amino acid ρ-benzoyl-phenylalanine (Bpa), into a bait protein at any position during translation (Chin et al., 2003; Wang et al., 2001). Bpa is a benzophenone and covalently cross-links to carbon-hydrogen bonds of nearby peptides upon UV-activation at 350-360 nm, a wavelength that does not cause any harm to proteins or DNA (reviewed in Dormán and Prestwich, 1994). Genetic code expansion and Bpa-mediated photo-reactive cross-linking allow to screen for protein-protein interactions *in vivo*, but can also be used *in vitro* for more targeted protein interaction analyses. In this study, Bpa incorporation was intended at several positions in C-terminally Strep-tagged Asc1p. Initially, the Strep-tag was supposed to enable affinity purification of the Asc1^{Bpa}p variants for *in vitro* Bpa cross-link experiments with likewise purified Asc1p-neighboring proteins identified with BioID.

The integration of Bpa at a desired amino acid residue position requires the exchange of the respective codon to the amber stop codon (UAG) and the additional expression of a Bpa-specific aminoacyl-tRNA synthetase/tRNA$_{CUA}$ pair (Fig. 19), which is orthogonal to the host system (Chin et al., 2003; Wang et al., 2001). In *S. cerevisiae*, the usage of an aminoacyl-tRNA synthetase/tRNA pair from *E. coli* was established, which sufficiently differs from the yeast system and does not aminoacylate endogenous tRNAs (Chin et al., 2003). Mutagenesis of the *E. coli* tRNA$_{CUA}$ resulted in a Bpa-specific adapter molecule (Chin et al., 2003). Additional to these components Bpa needs to be sufficiently taken up by the cell. Usage of the amber stop codon for Bpa incorporation decreases the translational efficiency of the UAG-containing

mRNA to 10% and less as this codon still mediates translational stops at high frequency. Therefore, overexpression of the Strep-tagged Asc1[Bpa]p variants from a high-copy number plasmid was intended to overcome the lowered translation rate.
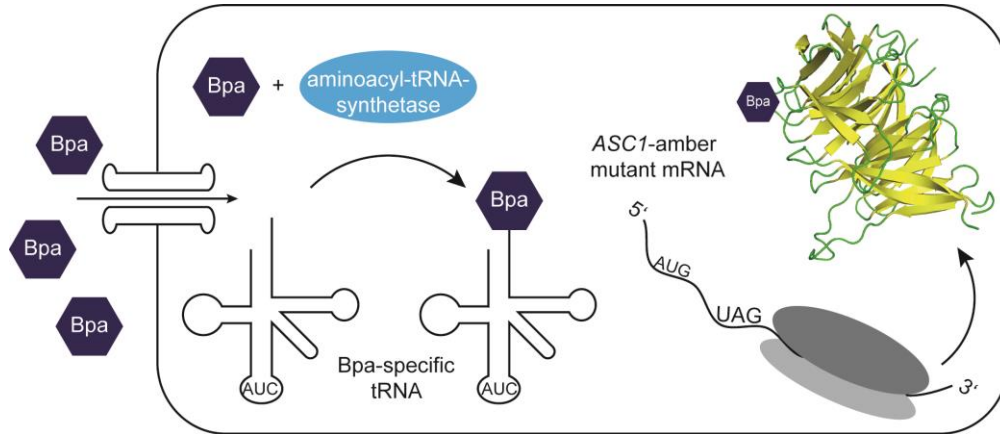
Fig. 19: *In vivo* **Bpa-incorporation into Asc1p during translation.** For amino acid substitutions within Asc1p the codon of the desired position is replaced by the amber stop codon. The additional expression of a Bpa-specific plasmid-borne aminoacyl-tRNA synthetase/tRNA pair as well as sufficient supply and subsequent uptake of Bpa into the cells enables the incorporation of Bpa into the Asc1 protein during translation.

3.2.1 The Asc1p loop structures provide suitable sites for Bpa-incorporation

The β-propeller structure of the scaffold Asc1p provides several surfaces for protein-protein interactions, and each of the seven propeller blades has been described to bind various proteins in *S. cerevisiae* or higher eukaryotes. Because it is unknown whether the BioID-identified Asc1p-neighbors physically interact with the scaffold protein, and if they do, at which site of the propeller, Bpa-incorporation at multiple positions, both at the ribosome-averted and ribosome-facing site of the WD40 protein were intended (Fig. 20). Amino acids within the structurally important β-sheets of the Asc1p core were not primarily considered for the exchange to avoid damages to the overall β-propeller shape. Similarly, highly conserved amino acids, which might be required to maintain Asc1p functionality were not exchanged. Rather, amino acids within the flexible loop structures exposed for UV-induced cross-linking were chosen to be replaced by Bpa. In total, 17 alleles encoding C-terminally Strep-tagged Asc1p variants with amino acid exchanges at the ribosome-averted site, and 16 at the ribosome-facing site of Asc1p were realized. For these amino acid substitutions, the respective nucleotide triplets were replaced by the amber stop codon by site-directed mutagenesis.
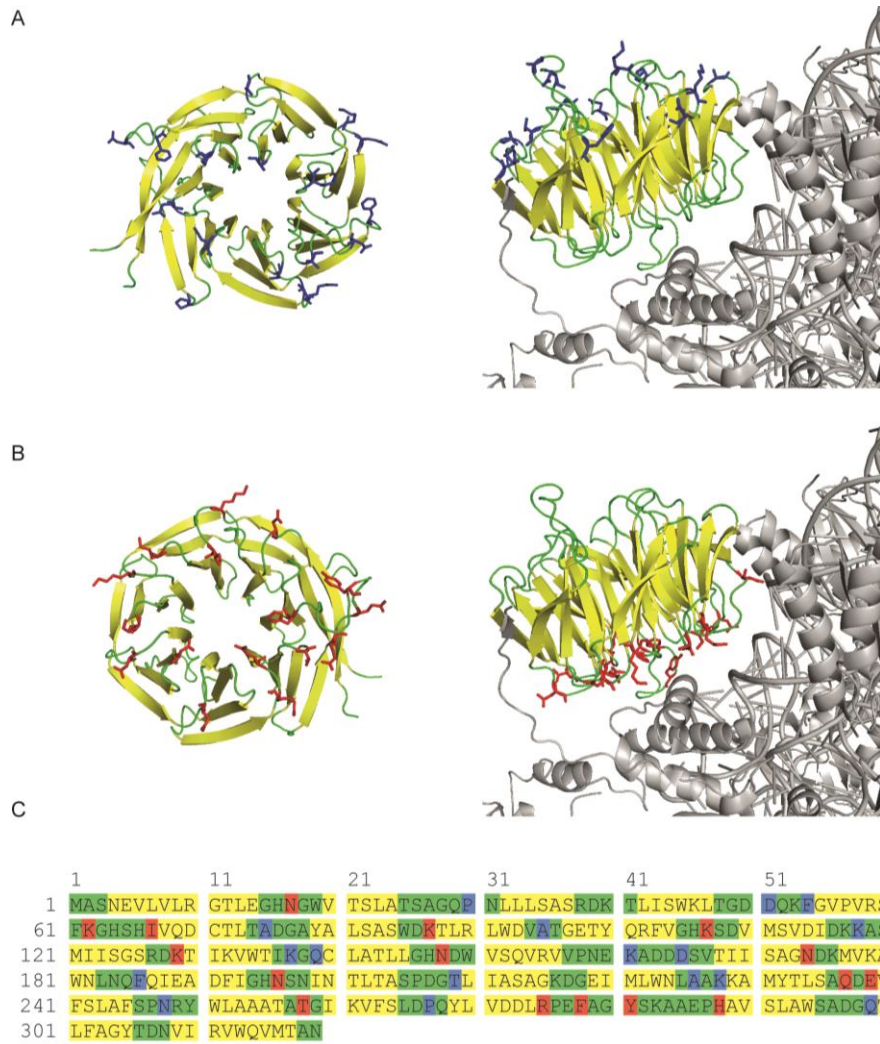
Fig. 20: Amino acids chosen for the exchange to Bpa within the Asc1p structure and amino acid sequence. Bpa was intended to be incorporated at various sites within the Asc1p amino acid sequence. (A) 17 amino acids at the ribosome-averted site of Asc1p, and (B) 16 residues at the ribosome-facing site were chosen. (C) Loops (green) and β-sheets (yellow) within the Asc1p amino acid sequence are color-coded. Sites chosen for Bpa-incorporation are colored in blue (ribosome-averted site) or red (ribosome-facing site). The crystal structure data of the *S. cerevisiae* 80S ribosome derives from the PDB entry 4V88 (Ben-Shem et al., 2011) and was used for visualization with the *PyMOL Molecular Graphics System* software.

3.2.2 Asc1[Amber]p variants with amino acid exchanges within the N-terminal half of the untagged protein are observed in the expected range

The genetic code expansion system is highly variable: Aminoacyl-tRNA synthetase/tRNA$_{CUA}$ pairs specific for multiple unnatural or natural amino acids are available, which are incorporated into bait proteins with similar rates. A Tyr-specific set is used to analyze the efficiency of

Amber-mutant protein synthesis at low costs before actual Bpa-incorporation and subsequent cross-linking.

S. cerevisiae Δ*asc1* cells were transformed with the different high-copy number plasmids bearing *asc1^Amber^-Strep* mutant alleles and simultaneously with a plasmid encoding a Tyr-specific aminoacyl-tRNA synthetase/tRNA$_{CUA}$ pair to analyze the efficiency of protein biosynthesis for the Asc1^Amber^p variants. Tyr was added to the growth medium to increase its incorporation into the Asc1^Amber^ proteins. Western blot analyses of protein extracts derived from these *asc1^Amber^-Strep* mutants, however, did not detect any of the Asc1^Amber^p-Strep variants (Fig. 21A, and data not shown).
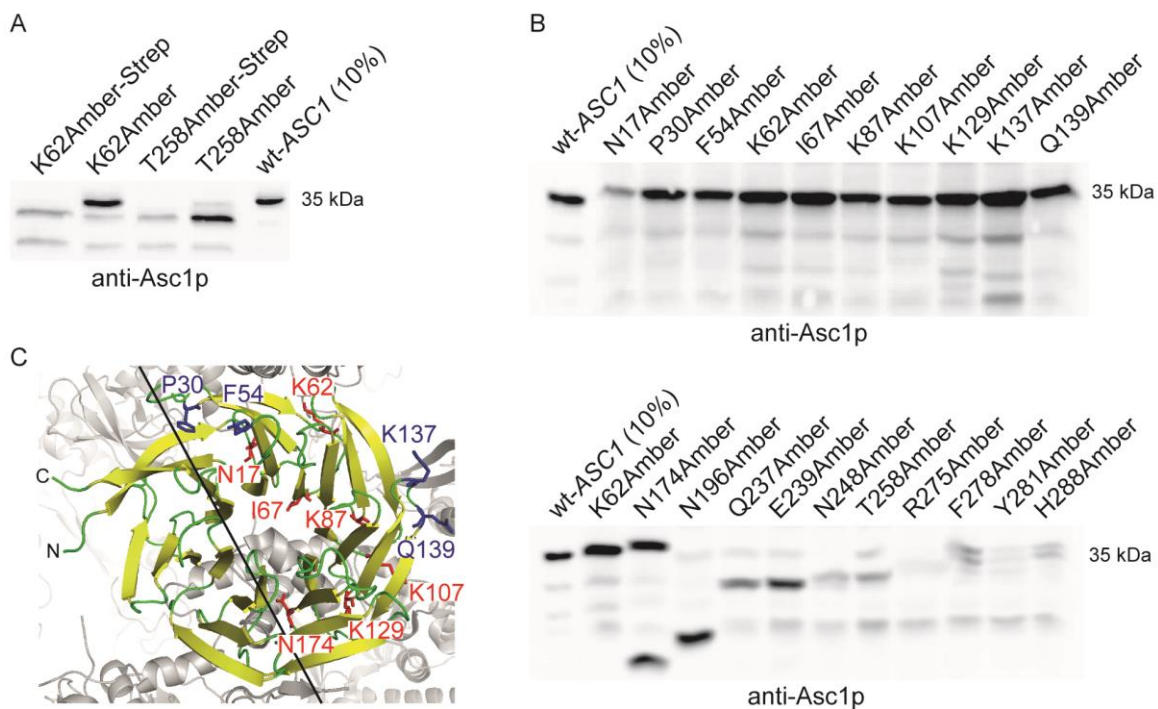
Fig. 21: The incorporation of Tyr in response to the Amber stop codon is most efficient in the N-terminal half of untagged Asc1p. (A) Western blot analyses of protein extracts derived from *asc1^Amber^-Strep* and untagged *asc1^Amber^* mutants with an Asc1p-specific antibody revealed a more efficient biosynthesis of the untagged proteins. 10% of a wt-*ASC1* cell extract were loaded as reference. (B) Mutants bearing the codon exchange within the 5'-region of the DNA sequence resulting in amino acid substitutions in the N-terminal part of the protein were detected at higher levels compared to mutated proteins with rather C-terminal amino acid exchanges. (C) The amino acids that were efficiently substituted by Tyr are depicted in the crystal structure. They are located in the rather N-terminal part of the protein. The crystal structure data of the *S. cerevisiae* 80S ribosome derives from the PDB entry 4V88 (Ben-Shem et al., 2011) and was used for visualization with the *PyMOL Molecular Graphics System* software.

The Strep-tag was intended to enable the purification of Asc1p for UV-induced *in vitro* cross-linking, however, it was observed in the past that the Strep-tagged version of Asc1p is less efficiently expressed than untagged Asc1p, even though both were encoded on high copy number plasmids. Therefore, the same codon exchanges were inserted into wt-*ASC1*. Indeed, expression of the untagged Asc1[Amber] proteins was higher compared to the tagged variants (Fig. 21A, and data not shown).

The efficiency of Tyr incorporation instead of translational stops, however, also depends on the position of the Amber codon within the sequence. Codon exchanges within the first half of the coding sequence affect Asc1[Amber]p formation in the expected range (~10% of wt-Asc1p), whereas Asc1p variants with rather C-terminal amino acid residues substituted by Tyr (or Bpa) were observed at even lower rates or were not detectable (Fig. 21B and C, and data not shown). This might hint to a more frequent translational stop when the Amber stop codon is placed near the 3'-end of the mRNA or to a decreased stability of the protein product carrying a rather C-terminal amino acid exchange. Interestingly, ubiquitylation sites are highly abundant within the N-terminal part of Asc1p, but almost absent in the C-terminal part. In summary, not all sites are suitable for Bpa incorporation and subsequent UV-induced cross-linking. For the purification of efficiently expressed Bpa-containing Asc1p variants a Strep-tag-independent purification method needs to be established. Alternatively, recombinant expression of the Strep-tagged Asc1[Amber]p mutants in *E. coli* might result in increased protein yields and might thus be suitable for future Bpa-based protein-protein interaction analyses. *In vivo* Bpa-mediated cross-link experiments can be considered to further screen for Asc1p-interacting proteins.

4. Discussion

4.1 Approaching the head region of the 40S subunit of the ribosome: *In vivo* labeling of Asc1p-proximal proteins with quantitative BioID

As mediators for protein-protein interactions scaffolds are required for the dynamic organization of protein proximities and the arrangement of multiprotein complexes with a major impact on cellular signaling. The highly conserved Gβ-like Asc1 protein belongs to the WD40 repeat family and serves as scaffold at the exposed head region of ribosomes (Ben-Shem et al., 2011; Chantrel et al., 1998; Sengupta et al., 2004). The β-propeller was proposed to function as central hub that communicates cellular signaling events to the translational machinery (Coyle et al., 2009). As such, the dynamic organization of local protein proximities at the ribosome is of major importance.

With a combination of BioID and SILAC the molecular microenvironment of Asc1p at the head region of ribosomes was quantitatively studied *in vivo*. With this approach 40 potential Asc1p-neighbors were identified at exponential growth. Beyond established interaction partners, like Scp160p, Smy2p, Ubp3p, and Bre5p (Baum et al., 2004; Ossareh-Nazari et al., 2010; Sezen et al., 2009), new ones, like Def1p, Sro9p and Stm1p were found. Four ribosomal proteins, namely Rps26A, Rps20, Rps3, and Rps2, were confirmed as Asc1p-neighbors with BioID according to the 80S crystal structure. Rps3p is a physical Asc1p-interaction partner that embraces the scaffold with its highly unstructured C-terminal arm, and Rps2p and Rps20p are indeed situated in close proximity to Asc1p (Fig. 22A; Ben-Shem et al., 2011). Rps3p and Rps20p are arranged near the mRNA entry channel, and the interaction of Rps20p with the translation initiation factor eIF4B was reported to result in a structural reorganization of the channel for mRNA loading (Walker et al., 2013). Thus, Asc1p resides at a highly regulative area of the ribosome for mRNA translation. Although Rps26Ap was demonstrated to co-purify with Tap-tagged Asc1p (Schütz et al., 2014), it seems to be shielded from direct Asc1p contact within the 40S structure (Fig. 22A). The last 21 C-terminal amino acids of the protein, however, were not resolved within the crystal (Ben-Shem et al., 2011). Rps26Ap was biotinylated by the biotin ligase BirA*p at residues Lys116 and Lys117, two C-terminal amino acids that were not resolved (Fig. 22B). Thus, it seems that Rps26Ap approaches Asc1p with its very C-terminus. However, it is possible that proximity of Asc1-BirA*p to Rps26Ap is established between two neighboring ribosomes and not within one ribosome. Rps26p is a mainly solvent exposed ribosomal protein that was described as important surface for the binding of mRNAs to ribosomes (Min et al., 2013; Sharifulin et al., 2012). Thus, Asc1p co-localizes with ribosomal proteins of importance for mRNA association to the translational machinery.
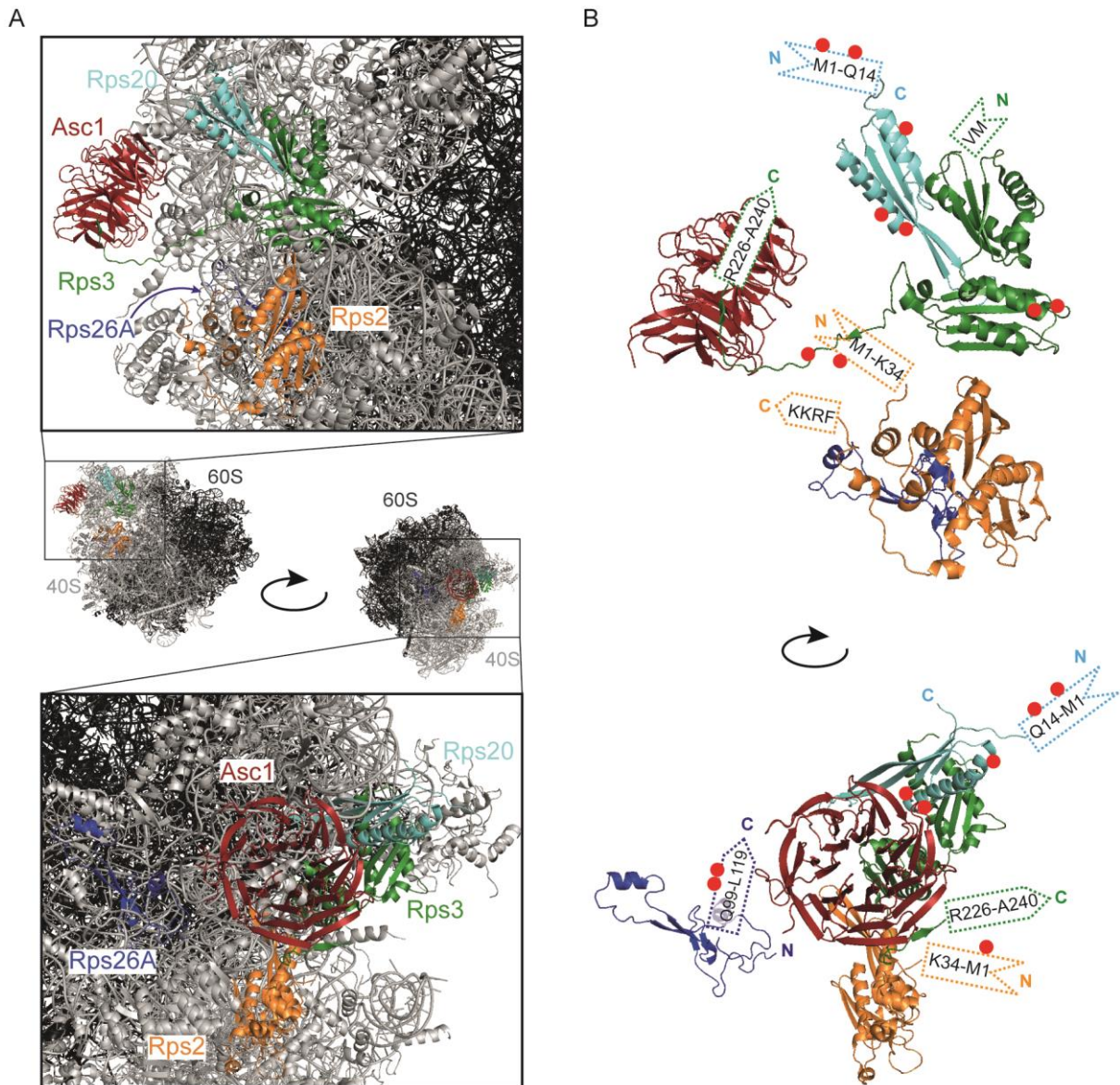
Fig. 22: Asc1p locates close to structural components of the 40S ribosome. (A) Asc1p physically interacts with the exposed unstructured C-terminal arm of the ribosomal protein Rps3 and is located in close proximity to Rps2p and Rps20p. Rps26Ap seems to be shielded from direct Asc1p contact within the 40S structure, however, it was highly enriched from the Asc1p-neighborhood by BioID. (B) Asc1p and the four ribosomal proteins are depicted as organized within the 40S subunit. Unresolved amino acids within the structures of the Asc1p-neighboring ribosomal proteins are indicated. The sites of protein biotinylation are labeled with red dots. The crystal structure data derive from the PDB entry 4V88 (Ben-Shem et al., 2011) and were used for visualization with the *PyMOL Molecular Graphics System* software.

Both Rps26p and Asc1p are eukaryote specific ribosomal proteins and are missing within the 40S pre-ribosome, which is exported from the nucleus into the cytoplasm (Strunk et al., 2012). Full 40S maturation requires the formation of a non-translating 80S pre-ribosome. Asc1p was

observed within these 80S pre-structures, Rps26p seems to be incorporated after pre-80S disassembly at one of the last maturation steps (Strunk et al., 2012). Thus, proximity between both proteins might even be established during 40S maturation.

Furthermore, Rps26p interacts with Upf1p, a major regulator of the nonsense-mediated decay (NMD) of mRNA and thus binds an important quality control component at the ribosome (Min et al., 2013). NMD targets aberrant mRNAs to degradation by the exonuclease Xrn1p (Muhlrad and Parker, 1994), also an Asc1p-neighboring protein. Asc1p has been described to be involved in the regulation of endonucleolytic cleavage of mRNAs as part of the mRNA quality control system (Kuroha et al., 2010). A connection between Asc1p, Rps26p and Xrn1p in quality control is, however, not known. Rps26Ap is moreover crucial for pseudohyphal and invasive growth of diploid or haploid yeast cells, respectively, as it is required for efficient expression of the cell surface flocculin Flo11p during starvation (Strittmatter et al., 2006). Similarly, the absence of pseudohyphae formation and adhesive growth of a Δasc1 strain can be traced back to decreased Flo11p levels (Valerius et al., 2007). A cooperative mechanism in *FLO11* expression should be further considered.

4.2 mRNA-binding proteins locate to the head region close to Asc1p

Besides the core protein constituents of ribosomes further ribosome-associated proteins were identified in the direct environment of Asc1p with BioID. One major group comprises proteins with mRNA-binding activity. mRNAs associate with distinct mRNA-binding proteins that are required for their export from the nucleus and for their recruitment to ribosomes to enable translation of the message (Frey et al., 2001; Scherrer et al., 2011; Sobel and Wolin, 1999). The multi-KH domain-containing mRNA-binding protein Scp160 is required for the localization of specific mRNAs to the ribosome and was reported to associate to translating ribosomes in an Asc1p-dependent manner (Baum et al., 2004; Coyle et al., 2009; Frey et al., 2001; Hirschmann et al., 2014). The BioID analysis confirmed this interaction and identified two further constituents of an extended complex, namely Smy2p and Eap1p. The so-called SESA network (Smy2p, Eap1p, Scp160p, and Asc1p) regulates the *POM34* mRNA translation required for spindle pole body duplication (Sezen et al., 2009). Also in human cells a complex consisting of RACK1, the Scp160p orthologue vigilin and the Smy2p orthologue GIGYF2, which responds to stress conditions was mentioned (Belozerov et al., 2014).

Scp160p preferentially locates to the endoplasmatic reticulum (ER) in association with polysomes, which might be required for the localized translation of specific mRNAs (Frey et al., 2001). Besides the *POM34* mRNA, Scp160p was further described to associate to polarity

factor and mating pathway mRNAs, e.g. *SRO7*, *FUS3* or *ASH1* to regulate their localized translation at bud and shmoo tips (Irie et al., 2002; Gelin-Licht et al., 2012). Consistently, Scp160p is involved in the pheromone response pathway by interacting with the active form of the pheromone receptor Gpa1p (Guo et al., 2003). Cells depleted of Asc1p show an increased sensitivity to pheromone implicating a role in the mating response as well (Chasse et al., 2006; Zeller et al., 2007). Thus, the local proximity of Asc1p to Scp160p might be functionally required for pheromone sensing and signaling.

In total, Scp160p binds more than 1000 messages, encoding proteins of the cellular periphery (cell wall and plasma membrane) as well as proteins of the nucleolus and proteins involved in mRNA-processing (Hogan et al., 2008). In this study, also a genetic interaction between Scp160p and Asc1p was observed during the osmotic stress response. Asc1p-depleted cells are highly sensitive against high salt levels. The additional deletion of the *SCP160* gene diminished this growth defect (Fig. 17B and Fig. S2B). Among the 1000 messages Scp160p might bind mRNAs whose translation is crucial to cope with elevated salt levels. In the absence of Asc1p, however, these mRNAs would not be efficiently translated, since Scp160p binds ribosomes in an Asc1p-dependent manner. In the absence of Scp160p Asc1p-independent mRNA-binding proteins could take over, resulting in increased translation of the required mRNAs.

With BioID the two paralogous mRNA-binding proteins Sro9p and Slf1p were identified in the proximity of Asc1p. They bind distinct, but also overlapping mRNAs, and associate to polysomes (Kershaw et al., 2015; Schenk et al., 2012; Sobel and Wolin, 1999). Both proteins bind amongst others mRNAs encoding ribosomal proteins and histones (Schenk et al., 2012). Furthermore, Sro9p specifically associates with mRNAs encoding proteins of the RNA polymerase II complex, whereas Slf1p binds those of the RNA polymerase I complex (Schenk et al., 2012). Sro9p binds to nascent mRNAs in the nucleus and accompanies them into the cytoplasm for translation (Röther et al., 2010). Furthermore, it is a component of the high molecular weight complex that regulates the activity of the heme-dependent transcription factor Hap1p (Hon et al., 2001; Lan et al., 2004). As a co-chaperone Sro9p stably associates to Hap1p and represses its activity together with Ssa and Yjd1p. In the presence of heme Hsp90p joins the complex and induces activity of the transcription factor (Hon et al., 2001; Lan et al., 2004). Asc1p was initially identified in a suppressor screen for gene deletions that rescue the no growth phenotype of cells depleted of both, Hap1p and Hem1p, the latter required for heme biosynthesis (Chantrel et al., 1998). Thus, both Asc1p and Sro9p, are closely connected to heme-dependent Hap1p-signaling.

In that line, Sro9p and Slf1p are also required to protect yeast cells against oxidative stress and toxic amounts of copper (Kershaw et al., 2015; Yu et al., 1996). Slf1p is a Pab1p-binding protein and was described to stabilize its associated mRNAs by preventing mRNA decay (Richardson et al., 2012; Schenk et al., 2012). It e.g. stabilizes mRNAs encoding important regulators of copper homeostasis, especially those required to protect the cell from increased copper levels (Schenk et al., 2012). Moreover, Slf1p binds mRNAs encoding proteins required for the oxidative stress response, specifically during oxidative stress, and seems to be required for their translation (Kershaw et al., 2015). Appositely, Asc1p is required to protect yeast cells against oxidative and nitrosative stress (Rachfall et al., 2013). The nitric oxide (NO) reductase Yhb1p and the putative nitroreductase Hbn1p are both highly up-regulated in Asc1p-depleted cells (Rachfall et al., 2013). *YHB1* and *HBN1* are, however, no described targets of Sro9p or Slf1p. Interestingly, Sro9p expression is highly up-regulated in Asc1p-depleted cells implying a further interplay between Asc1p and its BioID-neighbor (Schmitt et al., 2017).

Gis2p, another mRNA-binding protein that was found within the Asc1p-neighborhood, locates to stress granules and P-bodies during glucose deprivation (Rojas et al., 2012). The zinc-finger motif protein interacts with Pab1p and eIF4G and has been reported to bind a rather specific subset of mRNAs (Scherrer et al., 2011). Among these, messages encoding ribosomal proteins, GTPases, and proteins required for chromatin organization and rRNA processing were enriched (Scherrer et al., 2011). Additional to canonical mRNAs, Gis2p was described as activator of internal ribosomal entry site (IRES)-containing mRNAs in cap-independent translation when expressed in HEK293T cells, equally as its human orthologue ZNF9 (Sammons et al., 2011). Also, the Asc1p orthologue RACK1 from *D. melanogaster* is required for the translation of IRES-containing mRNAs of viruses (Majzoub et al., 2014). Thus, a cooperative mechanism of Asc1p/RACK1 together with Gis2p/ZNF9 in cap-independent translation should be further considered. Furthermore, Gis2p was reported to interact with the mRNA-binding protein Sro9p (Sammons et al., 2011) indicating related spatial organization of Asc1p-neighboring mRNA-binding proteins.

The translation of individual mRNAs depends on mRNA-specific associated multiprotein complexes, which influence mRNA stability, localization and finally decide about translation initiation or translational repression (Angenstein et al., 2002). Therefore, the associated proteins need to be strictly regulated according to cellular signals, which happens e.g. via protein phosphorylation. Adjusting proximities of several mRNA-binding proteins near the scaffold Asc1p appears suitable to control mRNA translation in a spatiotemporal manner probably in coordination with further regulatory components at the ribosome.

4.3 Translation initiation factors converge the Asc1p β-propeller

In accordance with Asc1p's implication in translation, a number of proteins required for the initiation of transcript decoding were revealed in the Asc1p microenvironment during exponential growth. Translation initiation is facilitated by the closed loop formation of mRNAs mediated by the poly(A)-binding protein (Pab1p) and the cap-binding protein eIF4E. The latter is encoded by *CDC33* in the budding yeast and was found in the proximity of Asc1p in this study. Also in mammals RACK1 interacts with eIF4E and regulates the phosphorylation of the initiation factor by PKCβII (Ruan et al., 2012).

Furthermore, the eIF4E-associated protein Eap1 was identified as Asc1p-neighbor with BioID. Eap1p was described as repressor of translation initiation that competes with eIF4G for eIF4E binding. The lack of Eap1p results in 329 differently translated mRNAs (Cridge et al., 2010). Furthermore, it physically interacts with specific proteins of the Pumilio-homology domain family (Puf), which might be required to repress the translation of specific mRNAs (Cridge et al., 2010). Indeed, the interaction between Puf5p and Eap1p is required to prevent translation of specific mRNAs. The phosphorylation of another Puf protein, namely Puf3p, was described to depend on Asc1p expression at one residue (Schmitt et al., 2017). This further supports that the appropriate translational efficiency for certain mRNAs might be Asc1p-dependent. Eap1p moreover promotes mRNA decay by recruiting the decapping activator Dhh1p to targeted Puf5p-associated mRNAs (Blewett and Goldstrohm, 2012). Thus, Cdc33p and Eap1p have a major impact on mRNA translation and degradation.

Cdc33p depletion results in the loss of pseudohyphae formation and the absence of adhesive growth (Ross et al., 2012) as does the depletion of Asc1p (Valerius et al., 2007). Also, cells missing its negative regulator Eap1p or the decapping activator Dhh1p were demonstrated to fail to form pseudohyphae and to grow adhesively (Ibrahimo et al., 2006; Park et al., 2006). Thus, Asc1p and its neighboring proteins represent a hotspot target for the regulation through the respective signal transduction pathways. Furthermore, Eap1p regulates the general amino acid control pathway in an eIF4E-independent manner by attenuating *GCN4* mRNA translation upon TOR inactivation (Matsuo et al., 2005).

Another Asc1p-neighbor is Pbp1p, a Pab1p-binding protein on translated and non-translated mRNAs (Mangus et al., 1998). Pab1p is required for efficient initiation by mediating the closed loop formation of mRNAs, and is thus essential for viability of yeast cells. Pbp1p-depletion in a Δ*pab1* strain, however, suppresses its lethality (Mangus et al., 1998). The double deletion strain exhibits an accumulation of 80S ribosomes and a strong reduction of polysomes indicating decreased rates of translation initiation (Mangus et al., 1998). Pbp1p further

associates with the poly(A) nuclease (PAN) complex required for the posttranscriptional trimming of the nascent poly(A) tail of mRNAs for maturation (Mangus et al., 2004a). Depletion of Pbp1p results in diminished poly(A) tail length of mRNAs suggesting that the protein functions as negative regulator of the PAN-complex (Mangus et al., 2004b). Additionally, Pbp1p interacts with the decapping activator Dhh1p to promote mRNA decay. The proximity to Pbp1p hints to a general impact of Asc1p on the fate of mRNAs from maturation to subsequent mRNA translation and mRNA decay.

Pbp1p was repeatedly identified in a complex with the Pbp1p-binding protein Pbp4 and the RNA-binding domain-containing protein Lsm12 (Fleischer et al., 2006; Mangus et al., 2004b), and both were found in the Asc1p-neighborhood in this study. All three proteins were identified as components of stress granules. Additionally, deletion of *PBP1* suppresses the growth defect of a Δ*ccr4* Δ*hek2* double deletion mutant encoding a deadenlyase and a mRNA-binding protein, respectively (Kimura et al., 2013). This implicates a genetic interaction of *PBP1* with the heat-specific Asc1p-neighbor Hek2p/*HEK2*. Pbp1p is further involved in mating type switching of mother cells by regulating the expression of the *HO* endonuclease post-transcriptionally via its 3'UTR (Tadauchi et al., 2004). Accordingly, Hek2p is required to prevent *HO* transcription in daughter cells by localizing *ASH1* mRNA to the distal tip of daughter cells (Irie et al., 2002).

Pbp1p also shuttles into the nucleus where it acts as suppressor of RNA-DNA hybrid formation at repetitive ribosomal DNA (rDNA) sequences. Thereby, it stabilizes the rDNA repeats required for genome stability and lifespan maintenance (Salvi et al., 2014). Moreover, Pbp1p interacts with the Asc1p-neighboring protein Stm1, which promotes rDNA destabilization and subsequent lifespan shortening in Pbp1p-depleted cells (Salvi et al., 2014).

Furthermore, a physical interaction of Asc1p with the multi-subunit initiation factor eIF3 was reported, specifically with the b- and c-subunits Prt1p and Nip1p (Kouba et al., 2012a; Sengupta et al., 2004). In this study the eIF3/a-subunit Rpg1p was identified as Asc1p-neighbor supporting the eIF3 arrangement as described from the crystal structure by Llácer et al. (2015; Fig. 23A). However, the biotinylated lysine residue of Rpg1p is located in some distance to Asc1p (Fig. 23B) hinting to an altered arrangement of eIF3/a during mRNA translation. All three initiation factors were further described to be phosphorylated in an Asc1p-dependent manner (Schmitt et al., 2017) suggesting a regulatory impact of Asc1p on translation initiation. The eIF3/a-subunit contains a PCI-domain required to bridge the interaction of mRNAs with the ribosome for translation initiation and to maintain the eIF3 core by contacting the eIF3/c-subunit Nip1p with this domain (Khoshnevis et al., 2014). Rpg1p further interacts with Rps0p thereby promoting eIF3 complex binding to the 40S subunit (Kouba et al., 2012b), and it binds

the ribosomal proteins Rps2 and Rps3 with its C-terminal domain (Chiu et al., 2010). The network of Asc1p, Rpg1p and Rps3p (Fig. 23B) might be able to allosterically communicate signals into the decoding center of the ribosome for translational regulation.
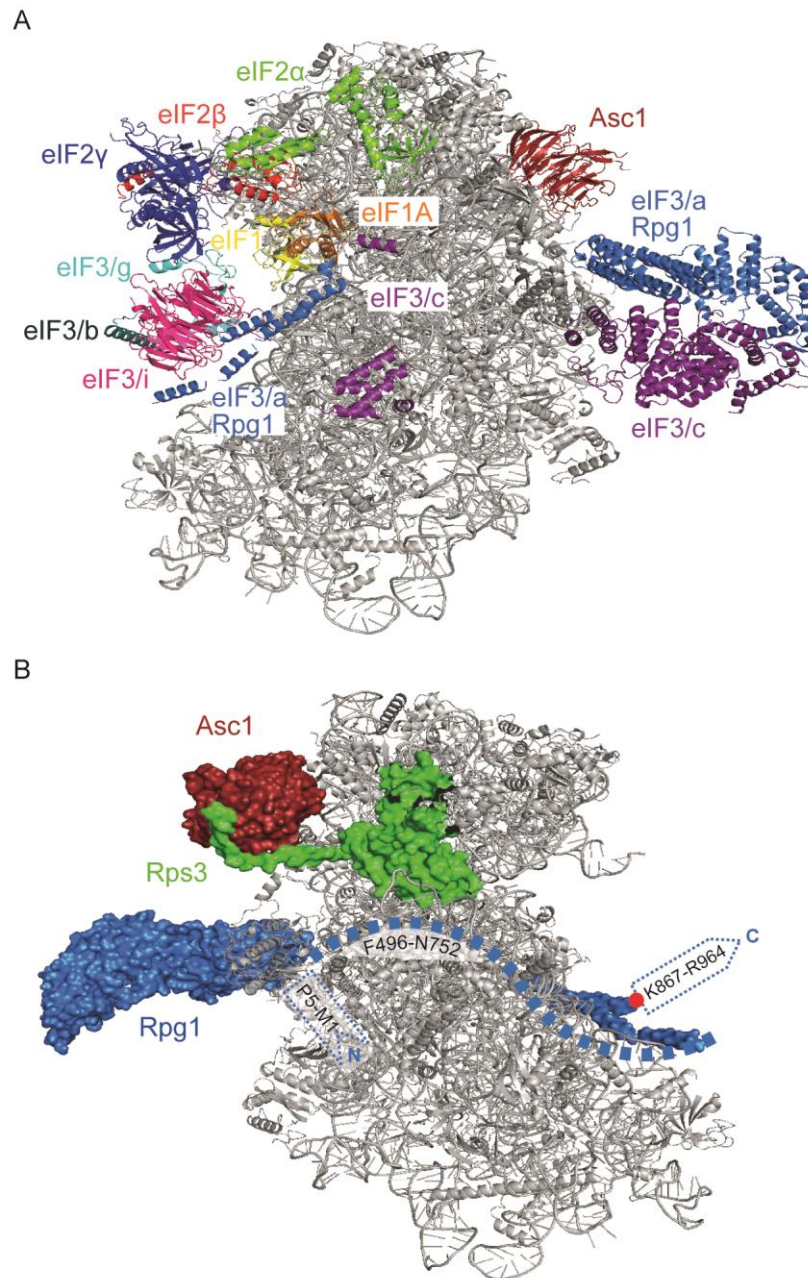
Fig. 23: Rpg1p is an Asc1p-neighboring protein during exponential growth. (A) Translation initiation factors are visualized at the 40S ribosomal subunit as resolved by Llácer et al. (2015). Asc1p neighbors the translation initiation factor Rpg1p (eIF3/a) as observed with BioID. (B) Asc1p, Rps3p and Rpg1p build a network at the 40S ribosomal subunit during exponential growth. Rpg1p was not fully resolved, however, its interaction with Rps3p was described. Unresolved N- and C-terminal amino acids as well as an unresolved area within the protein are indicated, and the biotinylated lysine residue is labeled with a red dot. The crystal structure data derive from the PDB entry 3JAP (Llácer et al., 2015) and were used for visualization with the *PyMOL Molecular Graphics System* software.

Interestingly, Rpg1p is also involved in the general control of amino acid biosynthesis by regulating the translation of *GCN4* mRNA: To avoid *GCN4* translation at non-starvation conditions, translation attenuates at the first of 4 upstream ORFs (uORFs). Rpg1p is essential to reinitiate translation at the actual *GCN4* ORF for *GCN4* translation in response to nitrogen starvation (Munzarová et al., 2011; Szamecz et al., 2008). This mechanism is tightly regulated via phosphorylation of eIF2α by the general control sensor kinase Gcn2p (reviewed in Hinnebusch, 2005). Deletion of *GCN2* results in increased sensitivity to amino acid starvation conditions. The additional knock-out of *ASC1* suppresses this growth phenotype (Hoffmann et al., 1999). Furthermore, Asc1p is required to prevent eIF2α phosphorylation at non-starvation conditions (Valerius et al., 2007). Thus, both Asc1p and Rpg1p affect *GCN4* mRNA translation and subsequent amino acid biosynthesis at distinct regulative steps.

Strikingly, Rpg1p moreover interacts with cytoskeletal components (Hasek et al., 2000; Palecek et al., 2001) and might thus be involved in the localized translation of specific mRNAs. Together, these data reveal Asc1p in a key position within the area of translation initiation, a dynamic control center for the spatiotemporal regulation of gene expression at the ribosome.

4.4 The multifaceted ribosome-clamping factor Stm1p co-localizes with Asc1p in dependence of glucose availability

Translation attenuation and re-initiation in response to nutritional stimuli is tightly regulated. Stm1p, known as VIG2 or SERBP1 in *D. melanogaster* and mammals (Anger et al., 2013), respectively, locates to non-translating 80S ribosomes and polysomes and is required to allow for efficient translation re-initiation after nutritionally poor conditions (Van Dyke et al., 2006). Stm1p functions as ribosome clamping factor and its position within the 80S ribosome during nutrient starvation extends from the 40S into the 60S ribosomal subunit (Fig. 24A; Ben-Shem et al., 2011; Van Dyke et al., 2013). It protrudes through both subunits and follows in part the path that is normally occupied by mRNA during translation (Ben-Shem et al., 2011). Thus, transcript decoding at the ribosome and Stm1p localization within the decoding center are mutually exclusive events. During challenging growth conditions like e.g. nutrient deprivation global translation is massively slowed down, and a pool of non-translating 80S ribosomes is kept in readiness to facilitate translation re-initiation as soon as nutrients are available (van den Elzen et al., 2014). As a preservation factor for ribosomes Stm1p is required to prevent subunit disassembly in the absence of translated mRNAs during times of deficiency (Van Dyke et al., 2013). To re-initiate translation after harms went by, a Dom34p-Hbs1p complex promotes subunit-disassembly (van den Elzen et al., 2014).

The BioID analysis of cells during exponential growth revealed Stm1p as an Asc1p-proximal protein with several biotinylated lysine residues. None of the identified biotin-labeled residues within Stm1p is exposed to the proximity of Asc1p according to the 80S ribosome crystal structure (Fig. 24B). Crystallization of the 80S ribosome was performed with purified ribosomes derived from yeast cells at glucose deprivation (Ben-Shem et al., 2011). At starvation Stm1p seems to shift its position into the 80S ribosome. The BioID analyses suggest that Stm1p directly neighbors Asc1p at the 40S ribosomal head when mRNAs are actively translated and kept there in storage until starvation signaling shifts it into its clamping position. Consistently, Stm1p was not identified in the Asc1p proximity during glucose deprivation. During starvation Asc1p, Stm1p and Rps3p form a network at the ribosome (Fig. 24A; Ben-Shem et al., 2011). Wolf and Grayhack (2015) suggested, that the interaction between Asc1p and Rps3p could mediate ribosome stalling. Correspondingly, the Asc1p-Rps3p-Stm1p network appears suitable to talk a signal as e.g. glucose shortage to Stm1p inducing its dynamic relocation for ribosome preservation.
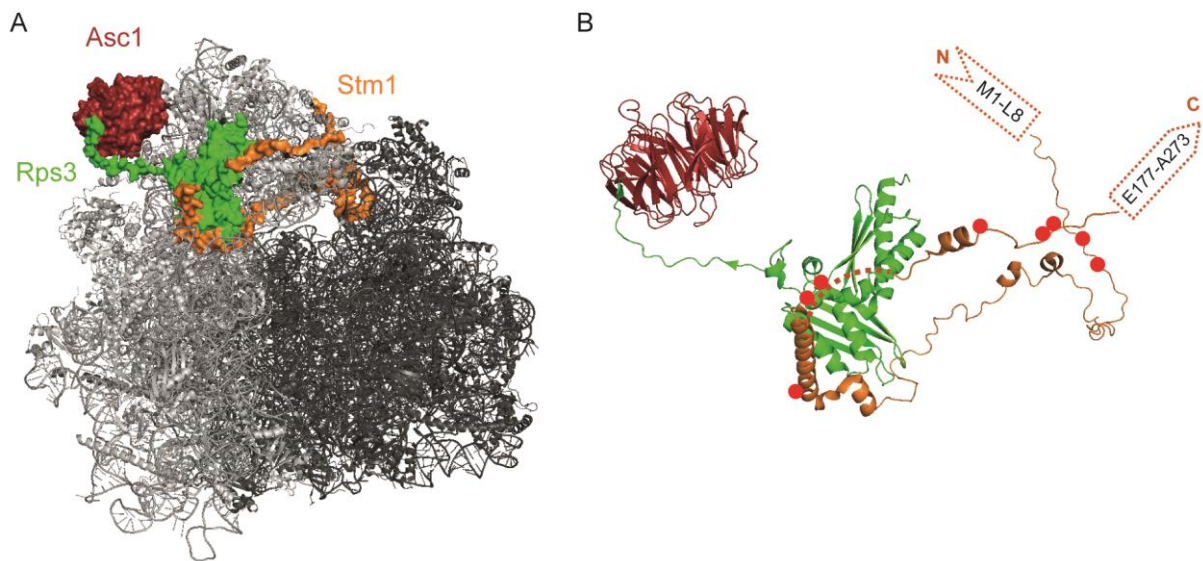
Fig. 24: Stm1p functions as ribosome preservation factor during glucose starvation, but locates proximal to Asc1p at exponential growth. (A) At glucose deprivation the ribosomal clamping factor Stm1p is located in between the 40S and 60S subunits and prevents mRNA translation. At this condition Asc1p, Rps3p and Stm1p form a tightly connected network at the ribosome. (B) Stm1p appears as a protein without intrinsic structure during glucose starvation. Its structural organization and localization during exponential growth are unknown. BioID analyses, however, suggest a localization near Asc1p. The unresolved N- and C-terminal amino acids as well as an unresolved stretch within the protein are indicated. Biotinylated lysine residues are labeled with red dots. The crystal structure data derive from the PDB entry 4V88 (Ben-Shem et al., 2011) and were used for visualization with the *PyMOL Molecular Graphics System* software.

Additionally, Stm1p was demonstrated to physically and genetically interact with the mRNA decapping activator Dhh1p and to promote its accumulation within P-bodies (Balagopal and Parker, 2009; Mitchell et al., 2013). Therefore, Stm1p might also affect mRNA decay during glucose shortage. In mammalian cells, the Stm1p orthologue SERBP1 interacts with eIF3 and with the hepatitis C virus IRES (Anger et al., 2013) suggesting an extended network for translational regulation in response to environmental stimuli. Stm1p mainly localizes to ribosomes in the cytoplasm, however, a fraction of Stm1p was additionally identified in the nucleus. It is also a DNA-binding protein that specifically interacts with G4 quadruplex and purine motif triplex DNA structures (Frantz and Gilbert, 1995; Nelson et al., 2000). It was demonstrated to bind Cdc13p, a protein involved in telomere replication and to associate with subtelomeric regions (Hayashi and Murakami, 2002; Van Dyke et al., 2004). Overexpression of the Stm1p orthologue Oga1p of *S. pombe* results in increased chronological lifespan (Ohtsuka et al., 2013). Yeast Stm1p interacts with Pbp1p most likely in the nucleus, and it contributes to the destabilization of rDNA sequences in Pbp1p-depleted cells resulting in lifespan shortening (Salvi et al., 2014). Thus, in addition to translation-related processes Asc1p-neighboring proteins play important roles within the nucleus, thereby enabling communication between nuclear and cytoplasmic gene expression events, possibly in part mediated by Asc1p.

4.5 Def1p, the RNA polymerase II degradation factor, co-localizes with Asc1p during exponential growth

A highly biotinylated Asc1-BirA*p-neighbor identified with BioID is the RNA polymerase (RNAP) II degradation factor Def1p. An interaction between the two proteins is suggested also from co-purification experiments with Asc1p-Strep (Schmitt, 2015). After ubiquitylation through Rsp5p in response to transcription stress, Def1p is truncated C-terminally prior to amino acid 530 in a proteasome-dependent manner within the cytosol (Wilson et al., 2013). The remaining N-terminal part of the protein was described to translocate into the nucleus where it binds the RNAPII subunit Rbp1p at stalled elongation complexes, thereby mediating the poly-ubiquitylation of Rbp1p by the Elongin-Cullin ubiquitin ligase complex and its subsequent degradation (Fig. 25B; Wilson et al., 2013; Woudstra et al., 2002). The identification of a C-terminal Def1p peptide ranging from N631 to K661 with the BioID experiment (beyond other peptides; Fig. 25A) therefore suggests that the proximity of both proteins is established in the cytoplasm prior to the Def1p truncation. Phospho-proteome analyses demonstrated that Def1p is Asc1p-dependently phosphorylated. Phosphorylation of T258 and S260 is downregulated in Asc1p-depleted cells (Schmitt et al., 2017). Hence, Asc1p seems to be involved in signaling to

Def1p, thereby possibly affecting its processing and migration into the nucleus for RNAPII degradation. The ubiquitin-specific protease Ubp3p reverses the ubiquitylation of RNAPII in the nucleus and can thus be considered as Def1p antagonist (Kvint et al., 2008). It was demonstrated that Ubp3p co-purifies with Def1p, both RNAPII subunits (Rbp1p and Rbp2p) and the translation elongation factor Spt5p (Kvint et al., 2008). Strikingly, both Ubp3p and Spt5p were identified as Asc1p-neighboring proteins in this study. Thus, a group of proteins involved in nuclear RNAPII regulation is located in proximity to Asc1p most probably during their cytosolic stage. Whether the processing of Def1p and the subsequent degradation of RNAPII are Asc1p-dependently regulated will be of major interest in on-going studies.
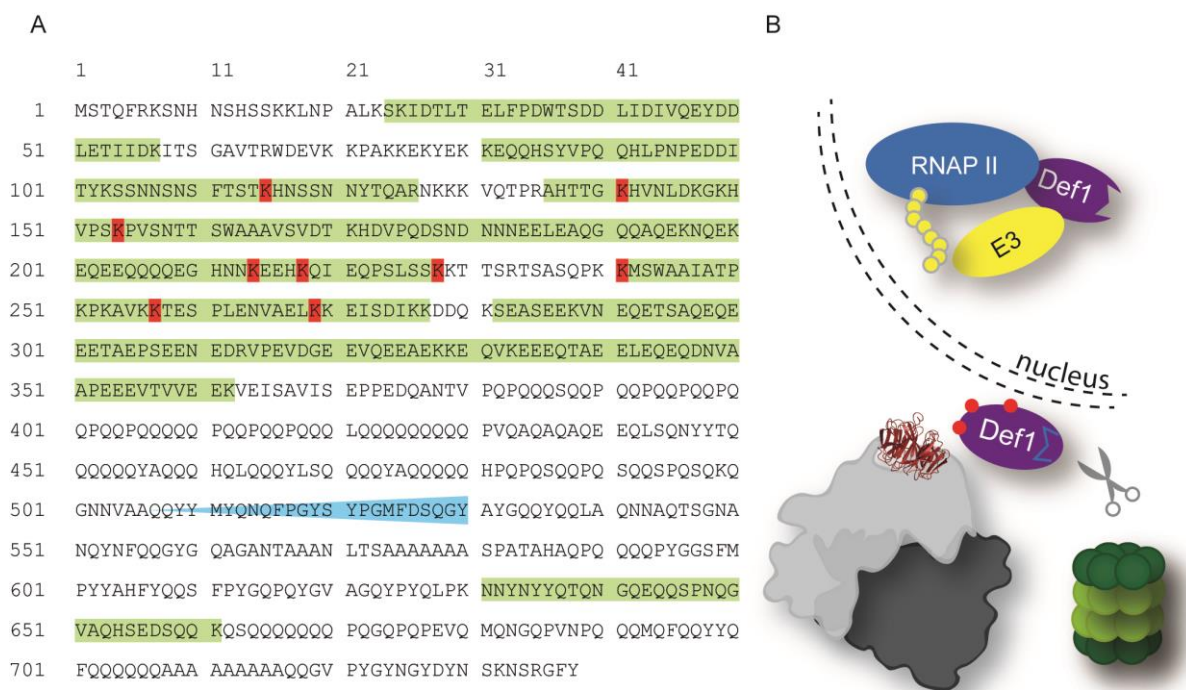
Fig. 25: The unprocessed Def1 protein locates close to cytoplasmic Asc1p. (A) Def1p is highly biotinylated by the Asc1-BirA* fusion protein, mainly in the N-terminal half of the protein. Proteasome-dependent processing of Def1p in response to transcription stress occurs prior to amino acid 530 and the presence of a C-terminal peptide confirms cytoplasmic proximity of Def1p to Asc1p. Biotinylated lysine residues are colored in red. The area of Def1p-processing is indicated in blue and peptides identified by LC-MS analysis are highlighted in green. (B) After proteasomal cleavage truncated Def1p translocates into the nucleus and mediates RNAPII polyubiquitylation (yellow chain) by an Elongin-Cullin E3 complex for subsequent degradation.

Similar to Stm1p, Def1p interacts with telomeric DNA and is further required for efficient telomere extension (Chen et al., 2005b). Its deletion in cells additionally depleted of fully functional Pif1p, a protein crucial for telomere maintenance and damage control at G4 quadruplex structures, moreover results in a synthetic sick phenotype suggesting shared functions in telomere stability (Stundon and Zakian, 2015). Also Asc1p-depletion has been described to result in aberrant telomere length, precisely in elongated telomere structures compared to wild type cells (Askree et al., 2004). If telomere maintenance requires a physical or genetic interaction of Def1p and Stm1p in the nucleus, or Asc1p-mediated regulation of these candidates in the cytoplasm remains to be studied.

4.6 Regulators of transcription temporarily co-localize with Asc1p during feast

With BioID several transcriptional regulators were identified in the proximity of Asc1p. Spt5p is a universally conserved transcription elongation factor (Harris et al., 2003) that forms a complex with Spt4p. Together they associate mainly to RNAPII, but also to RNAPI (Tardiff et al., 2007; Viktorovskaya et al., 2011) and are described to be required for efficient transcription elongation (Hartzog and Fu, 2013). Furthermore, the complex affects co-transcriptional mRNA-processing while binding the nascent transcript and recruiting pre-mRNA capping enzymes and the 3'-RNA cleavage factor I (Lindstrom et al., 2003; Mayer et al., 2012). Spt5p also assists the mRNA-binding protein She2p with its association to elongating RNAPII and subsequently to nascent transcripts (e.g. *ASH1*), and it is crucial for their localization at distal bud tips (Shen et al., 2010). Consistently, Spt5p was described as a binding platform at the RNAPII for the recruitment of further transcriptional regulators (Mayer et al., 2012). A temporal proximity of this nuclear scaffold protein to the ribosomal scaffold Asc1p regulatory connects the two fundamental processes of nuclear mRNA synthesis and cytosolic mRNA translation.

Pob3p is another transcriptional regulator located in close proximity to Asc1p during exponential growth. It is part of the facilitates chromatin transcription (FACT) complex, which is implicated in transcription initiation and elongation (Brewster et al., 2001; Formosa et al., 2001; Schlesinger and Formosa, 2000; Schwabish and Struhl, 2004). It is required for nucleosome organization and thereby provides access for polymerases to enable DNA transcription and replication (Formosa et al., 2001; Schlesinger and Formosa, 2000; Wittmeyer and Formosa, 1997). Another Asc1p-neighbor found with BioID is Not3p, part of the Ccr4-NOT complex that functions as transcriptional regulator, locates to translating ribosomes and it is required for mRNA deadenylation (Basquin et al., 2012; Collart et al., 2013; Panasenko and

Collart, 2012). Thus, this complex has a broad impact on mRNA fate through connecting nuclear and cytoplasmic regulation of gene expression.

Mbf1p was identified as Asc1p-neighboring protein at exponential growth and is a transcriptional coactivator that bridges the interaction of Gcn4p with the TATA-binding protein Spt15p to promote Gcn4p-dependent transcriptional activation of amino acid biosynthesis-related genes (Takemaru et al., 1998). Mbf1p further contains a RNA-binding domain that is clearly independent from its DNA-binding domain (Klass et al., 2013). This hints to a connection between transcriptional regulation and post-transcriptional control of the nascent mRNA within the cytoplasm (Klass et al., 2013). Indeed, archaeal MBF1 associates with 30S and translating 70S ribosomes (Blombach et al., 2014). Beyond Gcn4p itself, Mbf1p in proximity to Asc1p might connect translational with transcriptional aspects of the general control of amino acid biosynthesis in yeast.

Transcriptional regulation through these proteins takes place in the nucleus of the cell. Asc1p/RACK1 contains no nuclear entry or export sequences. Still, mammalian RACK1 has been described to enter the nucleus, where it associates to promoter regions of DNA in an indirect manner (He et al., 2010). In the nuclei of neuronal cells RACK1 rhythmically forms a complex with protein kinase C and the transcription factor BMAL1 and thereby regulates the circadian clock as it synchronizes transcriptional activity with the oscillatory cycle (Robles et al., 2010). Most of the transcription-related proteins identified proximal to Asc1p with BioID allocate to both the nucleus and to the cytoplasm of a cell. For yeast Asc1p there is so far no evidence for nuclear localization suggesting that proximity to the transcriptional regulators takes place in the cytoplasm. In conclusion, Asc1p might not only connect cellular signaling to ribosomal activity for protein biosynthesis, but might also synchronize mRNA synthesis in the nucleus with cytoplasmic mRNA translation (summarized in Fig. 26A).

4.7 Asc1p-proximal proteins are components and regulators of stress granules and P-bodies

Proteinaceous components of mRNP granules build another group of proteins enriched by Asc1p-mediated BioID. There are at least two distinct types of mRNP granules in the budding yeast *S. cerevisiae*: P-bodies and stress granules. P-bodies contain mRNAs and their associated proteins as well as proteins of the mRNA degradation machinery like Xrn1p or Dhh1p (Kulkarni et al., 2010). They are considered as separated compartments for mRNA degradation and can be observed in cells of cultures in steady state growth phases. However, their number and size increases upon environmental stresses as e.g. heat stress or glucose deprivation

(reviewed in Decker and Parker, 2012). Constituents of P-bodies that were identified in the proximity of Asc1p include the 5'-3' exonuclease Xrn1p and the mRNA-binding protein Gis2. The mRNA-binding protein Scp160 was reported to negatively regulate P-body formation in unstressed yeast cells (Weidner et al., 2014). An Asc1p-dependent formation of P-bodies was observed specifically upon treatment with hydroxyurea that induces replication stress (Tkach et al., 2012) and in response to mild heat stress as demonstrated in this study (Fig. 18). The assembly of mRNP granules was described to rely on proteins with self-interaction domains (Buchan, 2014; Decker et al., 2007). The Asc1/RACK1 protein, at least in higher eukaryotes, was described to form homodimers *in vivo* (Liu et al., 2007b, 2007a; Thornton et al., 2004), and yeast Asc1p, recombinantly expressed in *E. coli*, was shown to dimerize *in vitro* (Yatime et al., 2011). Thus, the region close to Asc1p might be the aggregation area for the formation of P-bodies or stress granules.

Stress granules were described to contain stalled pre-initiation complexes in higher eukaryotes, and they are defined by the presence of 40S ribosomal subunits, various translation initiation factors and mRNP complexes. In yeast, these granule like structures are mainly named EGP granules according to their major components eIF4<u>E</u>, eIF4<u>G</u> and <u>P</u>ab1p (Hoyle, 2007). Stress granule components identified in the Asc1p-neighborhood include proteins of the translational machinery (Cdc33p, Eap1p), mRNA-binding proteins (Slf1p, Gis2p), and the ubiquitin-specific protease Ubp3p as well as its cofactor Bre5p. The latter were demonstrated to co-localize with stress granules and to affect stress granule assembly during stationary phase (Nostramo et al., 2016). The Asc1p-BioID candidates Pbp1p, Pbp4p and Lsm12p were described as stress granule components, and Pbp1p is further required for efficient stress granule assembly (Swisher and Parker, 2010), a function that is conserved for its human orthologue ATAXIN-2 (Nonhoff, 2007). The sequestration of proteins into these mRNP granules has also a major impact on cellular signaling. Induction of stress granule formation in response to Pbp1p phosphorylation by the nutrient kinase Psk1p results in the sequestration of the growth controlling nutrient kinase complex TORC1 into stress granules (DeMille et al., 2015; Takahara and Maeda, 2012). Similarly, human RACK1 is sequestered into stress granules resulting in decreased activation of the apoptosis-mediating MAPK MTK1 (Arimoto et al., 2008). Yeast EGP granules do not contain 40S ribosomal proteins or further initiation factors like eIF3. Only severe heat stress and ethanol treatment were reported to result in the formation of stress granules with major similarity to mammalian structures including 40S ribosomal subunits and eIF3 (Grousl et al., 2009, 2013; Kato et al., 2011). Accordingly, yeast Asc1p has not been reported as stress granule or P-body component. It can be assumed that the proteins found near

Asc1p do not co-localize with Asc1p within stress granules but primarily prior to granule formation at the ribosomes. This is further supported by the fact that stress granules are formed specifically upon severe stresses in contrast to P-bodies, which are present also in unstressed yeast cells. The proximity of Asc1p to multiple stress granules and P-body components and regulators suggest an impact on mRNA fate in response to cellular signaling through guiding them into the mRNA stabilizing stress granules or mRNA degrading P-bodies, respectively.

4.8 Asc1p-neighboring proteins determine ribosome homeostasis

The regulation of protein biosynthesis in response to varying stimuli occurs on multiple stages including transcription and translation and is affected by factors like mRNA-binding proteins or the sequestration of mRNAs into mRNP granules for translational repression. The cellular adaptation to carbon source starvation includes an even more fundamental response: the degradation of ribosomes. In exponentially growing cells a high percentage of all proteins comprises ribosomal core constituents (Warner, 1999). Hence, their decay delivers huge amounts of proteins. Ribophagy targets mature ribosomes to vacuoles for degradation in an autophagy-like mechanism upon nutrient starvation (Kraft et al., 2008). The Asc1p-neighbors Ubp3p and Bre5p form a heterotetrameric complex that is specifically required for the regulation of 60S subunit degradation in response to glucose deprivation (Cohen et al., 2003; Kraft et al., 2008; Ossareh-Nazari et al., 2014). It was demonstrated that Rpl25p is ubiquitylated by the E3 ubiquitin ligase Ltn1p, a modification that protect the 60S subunit from degradation. Deubiquitylation by the Ubp3p/Bre5p complex subsequently mediates the engulfment of the 60S subunit for vacuolar degradation (Kraft et al., 2008; Ossareh-Nazari et al., 2014). The deubiquitylating activity of Ubp3p/Bre5p further affects several signal transduction pathways, e.g. the pheromone response (Hurst and Dohlman, 2013; Wang and Dohlman, 2002), cell wall integrity (Wang et al., 2008), glucose signaling (Li and Wang, 2013) and the osmotic stress response (Solé et al., 2011), pathways also affected by Asc1p.

Besides ribosome degradation factors, Asc1p-neighbors identified with BioID are involved in ribosome biogenesis. Nan1p and Nob1p are both required for 18S rRNA maturation (Dragon et al., 2002; Fatica et al., 2003). Nan1p is part of the small subunit processome and supports nuclear events of rRNA processing (Dragon et al., 2002). The processed, but still immature pre-rRNA is joined by most 40S ribosomal proteins in the nucleus to build the pre-40S complex that translocates into the cytoplasm for further maturation. Ribosome assembly factors such as Nob1p prevent pre-mature translation in the cytoplasm by occupying the binding sites for translation initiation factors (Strunk and Karbstein, 2009; Strunk et al., 2011). Asc1p joins the

40S ribosomes in the cytoplasm (Strunk et al., 2012). It was identified in non-translating 80S pre-ribosomes that assemble in the course of 40S maturation (Strunk et al., 2012). In a following step rRNA cleavage at the 3'-end is executed by the endonuclease Nob1p yielding in mature 18S rRNA (Lamanna and Karbstein, 2009; Pertschy et al., 2009). Since both proteins are situated at the head region of the 40S ribosomal subunit, proximity between Nob1p and Asc1p might occur during maturation of the 40S ribosome.

The multifaceted 5'-3' exonuclease Xrn1p is involved in 25S rRNA cleavage for 60S ribosome maturation (Geerlings et al., 2000) and plays a role in different mRNA-degradation pathways (reviewed in Nagarajan et al., 2013). Additionally, Xrn1p binds to G4 quadruplex DNA structures and cleaves single stranded DNA regions downstream of the G4 structures (Liu and Gilbert, 1994; Liu et al., 1995). Thereby, it affects telomere length, evident by shortened telomeres and senescence in *xrn1* mutant cells (Lew et al., 1998; Liu et al., 1995). The BioID analyses revealed proteins within the proximity of Asc1p that are important regulators of both ribosome biogenesis and decay (Fig. 26A), and thus affect the fate of ribosomes in response to environmental and cellular stimuli.

4.9 Glucose starvation provokes extensive rearrangements in the Asc1p-neighborhood

Poor growth conditions like glucose shortage lead to major adaptations in the cell. Changes in the microenvironment of Asc1p at the head region of the 40S ribosomal subunit were recorded with BioID in this work (summarized in Fig. 26B). Stm1p, proximal to Asc1p during exponential growth, relocated upon glucose deprivation consistent with its described clamping position within the 80S complex of non-translating monosomes (Ben-Shem et al., 2011). Translational repression during starvation further results in the migration of major translational regulators like eIF4E or Pab1p and associated mRNA-binding proteins into stress granules or EGP bodies (Hoyle et al., 2007). Accordingly, many of the proteins identified in the proximity of Asc1p during exponential growth, especially proteins implicated in translation and transcription, leave the Asc1p-neighborhood during glucose starvation. This goes along with general alterations in the translational and transcriptional activity.

Ribosomal proteins, both from the small and large ribosomal subunits, accumulate within the Asc1p microenvironment during glucose shortage suggesting a ribosome condensation process. In the stationary growth phase of *E. coli* cells, fractions of hibernating 70S dimers were observed (Wada et al., 1990). Translationally repressed 80S dimers as well as 80S-60S heterodimers were also reported in rat glioma cells in response to varying stresses (Krokowski et al., 2011). In yeast cells, the level of polysomes rapidly decreases upon glucose deprivation,

whereas inactive monosomes accumulate upon glucose deprivation (Ashe et al., 2000). These Stm1p-clamped non-translating monosomes might aggregate thereby providing proximity of Asc1p to proteins of the 60S subunit and further 40S subunit constituents. These Asc1p-surrounding ribosomal proteins might shield against Asc1-BirA*p-mediated self-biotinylation leading to the observed reduction in Asc1p enrichment from glucose starved cells with BioID in comparison to exponentially grown cells.

Upon glucose deprivation metabolic proteins are increasingly enriched with BioID in the vicinity of Asc1p. The remaining actively translating ribosomes seem to be engaged preferentially in primary metabolism of a cell, possibly at local hotspots where these metabolic processes take place. Additionally, Coq5p, a mitochondrial protein implicated in ubiquinone biosynthesis, is highly enriched in proximity to Asc1p during glucose starvation. The protein was identified as Asc1p-neighbor already during exponential growth, but shows an enormous enrichment upon glucose deprivation. Coq5p is a methyltransferase that locates to the matrix site of the inner mitochondrial membrane where it is involved in the biosynthesis of the ubiquinone (or coenzyme Q) complex (Dibrov et al., 1997). Its 19 N-terminal amino acids are required for mitochondrial import of the protein and are processed after the import. As a constituent of the electron transfer chain, ubiquinone is required for cellular respiration. Coq5p seems to be of special importance during glucose deprivation possibly by the enforcement of increased ubiquinone production and respiration to efficiently generate energy. The strong BioID enrichment of Coq5p upon glucose starvation suggests that Coq5p together with ribosomes accumulates at the cytosolic face of mitochondria.

A connection of Asc1p to respiration is documented in several studies: The deletion of the *ASC1* gene was described to suppress the growth defect of a *hap1$^-$ hem1$^-$* strain required for heme signaling (Chantrel et al., 1998). Furthermore, Asc1p-depletion results in a reduced translational efficiency specifically for mitochondrial ribosomal proteins and an accordingly decreased respiratory capacity (Rachfall et al., 2013; Thompson et al., 2016). The NO reductase Yhb1p is moreover highly up-regulated in Asc1p-depleted cells, both at the protein and the mRNA level (Rachfall et al., 2013). The protein promotes NO detoxification and is thus required to maintain efficient cellular respiration (Liu et al., 2000). Altogether, Asc1p is part of a network that connects the regulation of respiration with ribosomal activity, possibly in cooperation with or affected by the ubiquinone biosynthetic protein Coq5.

In summary, the Asc1p-BioID analysis of glucose-starved yeast cells suggests an extensive rearrangement within the head region of the 40S ribosomal subunit that reflects adaptation processes taking place during energy-low conditions.
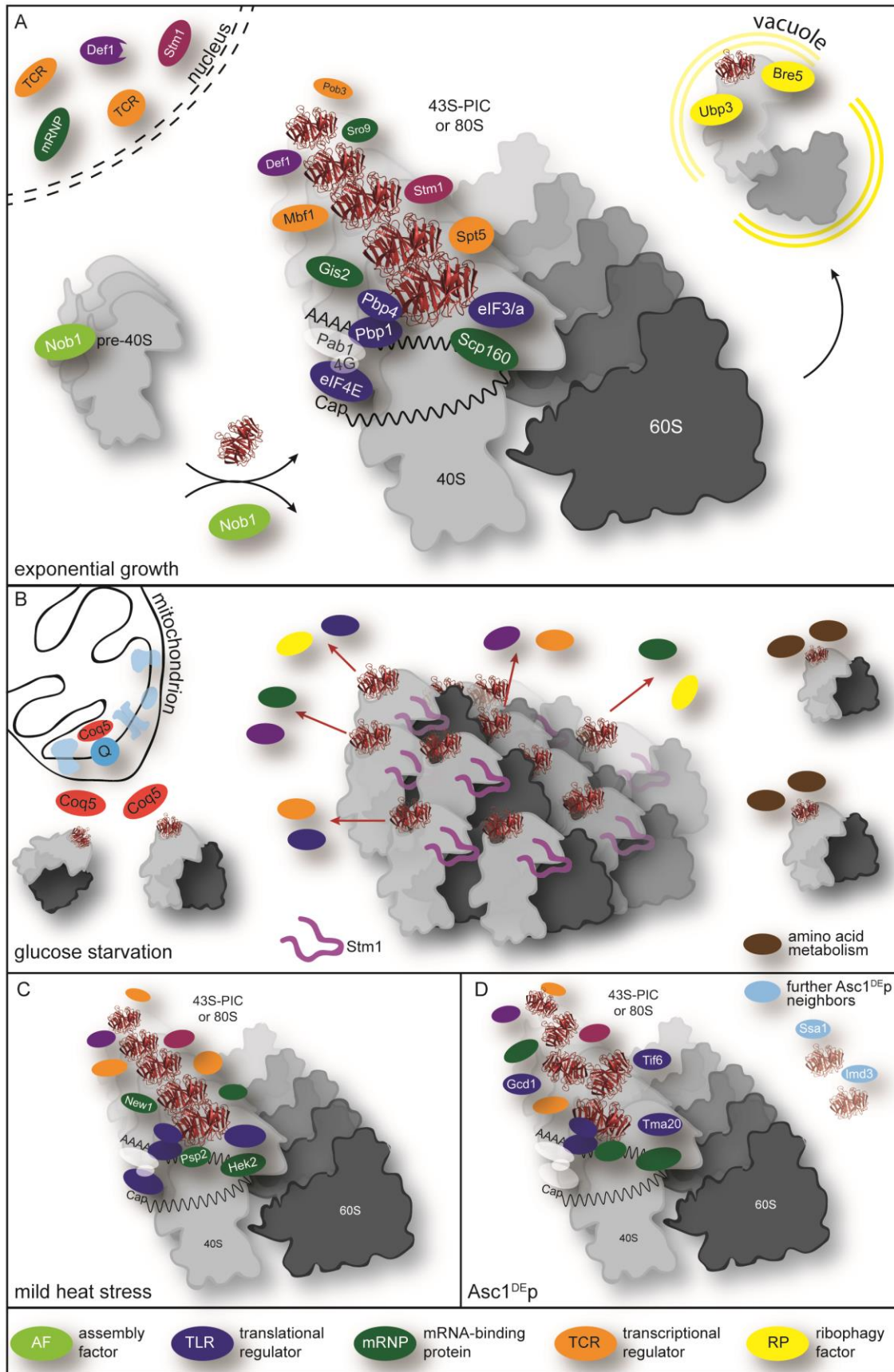
Fig. 26: Dynamics in the Asc1p-neighborhood. (A) During exponential growth Asc1p locates in close proximity to the ribosome assembly factor Nob1p, to the ribosomal clamping factor Stm1p, to the RNAPII degradation factor Def1p, to mRNA-binding proteins, translational as well as

nucleocytoplasmic transcriptional regulators and proteins involved in ribophagy. (B) In response to glucose starvation most of these proteins leave the Asc1p-neighborhood, whereas ribosomal proteins of the small and the large subunit accumulate in the proximity of Asc1p hinting to ribosome aggregation. Non-translating ribosomes are clamped by Stm1p, which does not locate close to Asc1p during starvation. Proteins required for amino acid biosynthesis and the mitochondrial protein Coq5 are enriched in the proximity of Asc1p, the latter reflecting the increased energy requirement during starvation. (C) Mild heat stress results in an Asc1p-neighborhood similar to that in yeast cells at exponential growth, however, additional mRNA-binding proteins appear close to Asc1p. (D) The proteins located in proximity of the Asc1^{DE}p variant resemble those of the wt-Asc1p-neighborhood suggesting ribosome-binding *in vivo*. Additional ribosomal or ribosome-associated proteins indicate a shifted position at the ribosome. Also partial ribosome dissociation should be considered.

4.10 The microenvironment of Asc1p is maintained during mild heat

In contrast to glucose starvation, the exposure of yeast cells to mild heat stress caused only few alterations in the Asc1p proximity. Def1p, Stm1p, but also the mRNA-binding proteins that were identified as Asc1p-neighbors during exponential growth were again enriched in the proximity of Asc1p when cells were cultivated at 37°C. Three additional proteins with mRNA-binding activity located proximal to Asc1p specifically during mild heat stress: Hek2p, New1p and Psp2p (summarized in Fig. 26C).

Hek2p (also named Khd1p) binds hundreds of mRNAs comprising about 20% of the yeast transcriptome (Hasegawa et al., 2008). Many of the associated messages encode nuclear transcriptional regulators, as well as cell wall and plasma membrane proteins (Hasegawa et al., 2008). Accordingly, Hek2p is involved in cell wall integrity and genetically interacts with Pbp1p in this regard (Ito et al., 2011; Kimura et al., 2013). Furthermore, Hek2p binds the *ASH1* mRNA and is required for its proper localization to bud tips (Irie et al., 2002), but also for its translational repression, probably by the simultaneous interaction with eIF4G (Paquin et al., 2007). Phosphorylation of Hek2p at the distal tip releases the translational repression (Paquin et al., 2007). Hek2p was further described to bind subtelomeric regions and to affect telomere length and silencing (Denisenko and Bomsztyk, 2002, 2008). Psp2p and the prion protein New1 were also specifically enriched with BioID through Asc1-BirA*p during mild heat stress and were both reported as mRNA-binding proteins (Inoue et al., 2011; Mitchell et al., 2013). Overexpression of Psp2p was further described to overcome aging-dependent cell death in response to mitochondrial damage as does the overexpression of Cdc33p and Pbp1p (Wang and Chen, 2015).

After the growth of yeast cells at 37°C many proteins that appeared proximal to Asc1p during exponential growth were even more enriched by Asc1p-BioID. This specifically applied to Stm1p and mRNA-binding proteins like Scp160 and Sro9. Thus, a temperature-specific accumulation of mRNA-binding proteins takes place at the head region of ribosomes. Furthermore, growth of the *ascl⁻ Δstm1* strains at 37°C revealed a severe growth defect suggesting a genetic interaction of these proteins during the heat response. It was reported that the *E. coli* derived biotin ligase BirA*p is increasingly active during growth at 37°C (Kim et al., 2016), so that the increased enrichment of Asc1p-proximal proteins might be a side-effect of the biotinylation activity. However, the visualization of total protein biotinylation with HRP-coupled streptavidin of protein extracts derived from cells cultivated at 30°C or 37°C revealed no obvious difference (see Fig. S1). It will be of interest to perform these experiments with cells from more elevated temperatures at or beyond 42°C when more severe translational responses are expected, however, this would require faster or more efficient biotinylation through BirA*p.

4.11 Asc1^{DE}-BirA*p binds less efficiently to ribosomes, but does not leave the ribosome completely

As an integral constituent of the mRNA translational machinery the functionality of Asc1p was presumed to depend on its binding to the ribosome. Surprisingly, the Asc1^{DE}p variant, which features an obvious ribosome-binding defect during ultracentrifugation of cell extracts in sucrose density gradients, showed only very mild phenotypes (Coyle et al., 2009; Schmitt et al., 2017). A recent study revealed that Asc1^{DE}p still associates with ribosomes *in vivo* by formaldehyde cross-linking prior to ultracentrifugation (Thompson et al., 2016), however, without knowledge about the extend and the integrity of its positioning at the ribosome. The quantitative BioID analyses of the Asc1^{DE}-BirA* fusion protein provided insight in the *in vivo* microenvironment of this mutated version of the scaffold protein. Proximal proteins of Asc1^{DE}-BirA*p clearly resembled those of the wt-Asc1-BirA*p neighborhood during exponential growth. Therefore, we can confirm with BioID that the mutated protein is still positioned at the ribosome as suggested by Thompson et al. (2016). However, additional proteins were enriched and identified in the proximity of Asc1^{DE}p. These include further ribosome associated proteins (e.g. Gcd1 and Tif6) and ribosomal core constituents, namely Rps11p and Rpl10p. Thus, it can be assumed that (1) Asc1^{DE}p is less rigidly placed in its precise ribosomal position and that it occupies a more flexible orientation at the ribosome, and (2) that a small subpopulation of Asc1^{DE}p might indeed dissociate from the ribosome (summarized in Fig. 26D). In mammalian cells, RACK1 is recruited to stress granules in response to specific stresses together with 40S

ribosomal subunits, whereas RACK1^{DE} was not found there suggesting an *in vivo* binding defect of the mammalian mutated Asc1p orthologue (Arimoto et al., 2008). In our study, components of the 26S proteasome and the protease Pre9p were identified in the proximity of Asc1^{DE}p. The Asc1^{DE} protein itself was, however, stable and highly enriched with BioID, even more efficiently than wt-Asc1p. This might hint to a structural rearrangement of the mutated protein at the ribosome or to ribosome-dissociation leading to a more efficient self-biotinylation. Alternatively, a possible accumulation as Asc1^{DE}-molecules or even homodimer formation might explain the increased rate of BirA*p-mediated self-biotinylation. It remains to be shown whether the artificial Asc1^{DE}p version resembles any physiological status of an Asc1 protein with altered ribosome-binding characteristics, e.g. as consequence of post-translational modifications or structural dynamics within the ribosome.

4.12 Quantitative BioID – An *in vivo* tool to study dynamic microenvironments

Proximity-dependent <u>Bio</u>tin <u>ID</u>entification, short BioID, was first described by Burke and co-workers (2012) and was developed as an *in vivo* screen for interacting and proximal proteins of a bait protein in mammalian cells. The method was meanwhile adapted for a few other organisms including *T. brucei*, *Toxoplasma gondii*, or *Dictyostelium amoebae* (Batsios et al., 2016; Chen et al., 2015; Morriswood et al., 2013). In this study, the *in vivo* labeling technique was applied for the yeast *S. cerevisiae* to analyze the proteinaceous microenvironment of the ribosomal scaffold protein Asc1p. Here, the BioID approach was for the first time performed quantitatively with SILAC labeling enabling a direct comparison of the *ASC1-birA** strain to fundamental negative controls, but also to differential growth conditions. This approach will be further exploited to study dynamic changes of the Asc1p microenvironment in response to environmental stimuli and in dependence of post-translational Asc1p modifications. UV-inducible Bpa cross-link experiment with Asc1p and its proximal proteins identified with BioID should allow us to distinguish between protein neighbors and physical interaction partners in future studies. A covalent cross-link could reveal structural aspects of protein-protein interactions as it enables the mapping of the interaction site within two proteins. The BioID experiments performed in this work provide a new insight into the proteinaceous Asc1p microenvironment and allow us to study functional relationships of Asc1p with the identified candidates in future projects. The quantitative design of the BioID approach as presented here can be generally considered to analyze the dynamics of molecular microenvironments *in vivo* depending on environmental stimuli or post-translational modifications.

5. References

Angenstein, F., Evans, A.M., Settlage, R.E., Moran, S.T., Ling, S.-C., Klintsova, A.Y., Shabanowitz, J., Hunt, D.F., and Greenough, W.T. (2002). A Receptor for Activated C Kinase Is Part of Messenger Ribonucleoprotein Complexes Associated with PolyA-mRNAs in Neurons. J. Neurosci. *22*, 8827–8837.

Anger, A.M., Armache, J.-P., Berninghausen, O., Habeck, M., Subklewe, M., Wilson, D.N., and Beckmann, R. (2013). Structures of the human and Drosophila 80S ribosome. Nature *497*, 80–85.

Arimoto, K., Fukuda, H., Imajoh-Ohmi, S., Saito, H., and Takekawa, M. (2008). Formation of stress granules inhibits apoptosis by suppressing stress-responsive MAPK pathways. Nat. Cell Biol. *10*, 1324–1332.

Ashe, M.P., De Long, S.K., and Sachs, A.B. (2000). Glucose depletion rapidly inhibits translation initiation in yeast. Mol. Biol. Cell *11*, 833–848.

Ashique, A.M., Kharazia, V., Yaka, R., Phamluong, K., Peterson, A.S., and Ron, D. (2006). Localization of the scaffolding protein RACK1 in the developing and adult mouse brain. Brain Res. *1069*, 31–38.

Askree, S.H., Yehuda, T., Smolikov, S., Gurevich, R., Hawk, J., Coker, C., Krauskopf, A., Kupiec, M., and McEachern, M.J. (2004). A genome-wide screen for Saccharomyces cerevisiae deletion mutants that affect telomere length. Proc. Natl. Acad. Sci. U. S. A. *101*, 8658–8663.

Auesukaree, C., Damnernsawad, A., Kruatrachue, M., Pokethitiyook, P., Boonchird, C., Kaneko, Y., and Harashima, S. (2009). Genome-wide identification of genes involved in tolerance to various environmental stresses in Saccharomyces cerevisiae. J. Appl. Genet. *50*, 301–310.

Balagopal, V., and Parker, R. (2009). Stm1 modulates mRNA decay and Dhh1 function in Saccharomyces cerevisiae. Genetics *181*, 93–103.

Basquin, J., Roudko, V.V., Rode, M., Basquin, C., Séraphin, B., and Conti, E. (2012). Architecture of the nuclease module of the yeast Ccr4-not complex: the Not1-Caf1-Ccr4 interaction. Mol. Cell *48*, 207–218.

Batsios, P., Meyer, I., and Gräf, R. (2016). Proximity-Dependent Biotin Identification (BioID) in Dictyostelium Amoebae. Methods Enzymol. *569*, 23–42.

Battaini, F., Pascale, A., Lucchi, L., Pasinetti, G.M., and Govoni, S. (1999). Protein kinase C anchoring deficit in postmortem brains of Alzheimer's disease patients. Exp. Neurol. *159*, 559–564.

Baum, S., Bittins, M., Frey, S., and Seedorf, M. (2004). Asc1p, a WD40-domain containing adaptor protein, is required for the interaction of the RNA-binding protein Scp160p with polysomes. Biochem. J. *380*, 823–830.

Belozerov, V.E., Ratkovic, S., McNeill, H., Hilliker, A.J., and McDermott, J.C. (2014). In vivo interaction proteomics reveal a novel p38 mitogen-activated protein kinase/Rack1 pathway regulating proteostasis in Drosophila muscle. Mol. Cell. Biol. *34*, 474–484.

Benoit, R.M., Wilhelm, R.N., Scherer-Becker, D., and Ostermeier, C. (2006). An improved method for fast, robust, and seamless integration of DNA fragments into multiple plasmids. Protein Expr. Purif. *45*, 66–71.

Ben-Shem, A., Garreau de Loubresse, N., Melnikov, S., Jenner, L., Yusupova, G., and Yusupov, M. (2011). The structure of the eukaryotic ribosome at 3.0 Å resolution. Science *334*, 1524–1529.

Bhattacharyya, R.P., Reményi, A., Good, M.C., Bashor, C.J., Falick, A.M., and Lim, W.A. (2006). The Ste5 scaffold allosterically modulates signaling output of the yeast mating pathway. Science *311*, 822–826.

Bird, R.J., Baillie, G.S., and Yarwood, S.J. (2010). Interaction with receptor for activated C-kinase 1 (RACK1) sensitizes the phosphodiesterase PDE4D5 towards hydrolysis of cAMP and activation by protein kinase C. Biochem. J. *432*, 207–216.

Blewett, N.H., and Goldstrohm, A.C. (2012). A eukaryotic translation initiation factor 4E-binding protein promotes mRNA decapping and is required for PUF repression. Mol. Cell. Biol. *32*, 4181–4194.

Blombach, F., Launay, H., Snijders, A.P.L., Zorraquino, V., Wu, H., de Koning, B., Brouns, S.J.J., Ettema, T.J.G., Camilloni, C., Cavalli, A., et al. (2014). Archaeal MBF1 binds to 30S and 70S ribosomes via its helix-turn-helix domain. Biochem. J. *462*, 373–384.

Brandman, O., Stewart-Ornstein, J., Wong, D., Larson, A., Williams, C.C., Li, G.-W., Zhou, S., King, D., Shen, P.S., Weibezahn, J., et al. (2012). A ribosome-bound quality control complex triggers degradation of nascent peptides and signals translation stress. Cell *151*, 1042–1054.

Brandon, N.J., Uren, J.M., Kittler, J.T., Wang, H., Olsen, R., Parker, P.J., and Moss, S.J. (1999). Subunit-specific association of protein kinase C and the receptor for activated C kinase with GABA type A receptors. J. Neurosci. Off. J. Soc. Neurosci. *19*, 9228–9234.

Brandon, N.J., Jovanovic, J.N., Smart, T.G., and Moss, S.J. (2002). Receptor for activated C kinase-1 facilitates protein kinase C-dependent phosphorylation and functional modulation of GABA(A) receptors with the activation of G-protein-coupled receptors. J. Neurosci. Off. J. Soc. Neurosci. *22*, 6353–6361.

Breitkreutz, A., Choi, H., Sharom, J.R., Boucher, L., Neduva, V., Larsen, B., Lin, Z.-Y., Breitkreutz, B.-J., Stark, C., Liu, G., et al. (2010). A global protein kinase and phosphatase interaction network in yeast. Science *328*, 1043–1046.

Brewster, N.K., Johnston, G.C., and Singer, R.A. (2001). A bipartite yeast SSRP1 analog comprised of Pob3 and Nhp6 proteins modulates transcription. Mol. Cell. Biol. *21*, 3491–3502.

Buchan, J.R. (2014). mRNP granules. Assembly, function, and connections with disease. RNA Biol. *11*, 1019–1030.

Buchan, J.R., and Parker, R. (2009). Eukaryotic stress granules: the ins and outs of translation. Mol. Cell *36*, 932–941.

Buchan, J.R., Muhlrad, D., and Parker, R. (2008). P bodies promote stress granule assembly in Saccharomyces cerevisiae. J. Cell Biol. *183*, 441–455.

Burnette, W.N. (1981). "Western blotting": electrophoretic transfer of proteins from sodium dodecyl sulfate--polyacrylamide gels to unmodified nitrocellulose and radiographic detection with antibody and radioiodinated protein A. Anal. Biochem. *112*, 195–203.

Cai, Z., Chai, Y., Zhang, C., Qiao, W., Sang, H., and Lu, L. (2015). The Gβ-like protein CpcB is required for hyphal growth, conidiophore morphology and pathogenicity in Aspergillus fumigatus. Fungal Genet. Biol. FG B *81*, 120–131.

Cao, X.-X., Xu, J.-D., Xu, J.-W., Liu, X.-L., Cheng, Y.-Y., Wang, W.-J., Li, Q.-Q., Chen, Q., Xu, Z.-D., and Liu, X.-P. (2010). RACK1 promotes breast carcinoma proliferation and invasion/metastasis in vitro and in vivo. Breast Cancer Res. Treat. *123*, 375–386.

Carthew, R.W., and Sontheimer, E.J. (2009). Origins and Mechanisms of miRNAs and siRNAs. Cell *136*, 642–655.

Ceci, M., Gaviraghi, C., Gorrini, C., Sala, L.A., Offenhäuser, N., Marchisio, P.C., and Biffo, S. (2003). Release of eIF6 (p27BBP) from the 60S subunit allows 80S ribosome assembly. Nature *426*, 579–584.

Ceci, M., Welshhans, K., Ciotti, M.T., Brandi, R., Parisi, C., Paoletti, F., Pistillo, L., Bassell, G.J., and Cattaneo, A. (2012). RACK1 is a ribosome scaffold protein for β-actin mRNA/ZBP1 complex. PloS One *7*, e35034.

Chang, B.Y., Conroy, K.B., Machleder, E.M., and Cartwright, C.A. (1998). RACK1, a receptor for activated C kinase and a homolog of the beta subunit of G proteins, inhibits activity of src tyrosine kinases and growth of NIH 3T3 cells. Mol. Cell. Biol. *18*, 3245–3256.

Chang, B.Y., Chiang, M., and Cartwright, C.A. (2001). The interaction of Src and RACK1 is enhanced by activation of protein kinase C and tyrosine phosphorylation of RACK1. J. Biol. Chem. *276*, 20346–20356.

Chang, B.Y., Harte, R.A., and Cartwright, C.A. (2002). RACK1: a novel substrate for the Src protein-tyrosine kinase. Oncogene *21*, 7619–7629.

Chang, I.-F., Szick-Miranda, K., Pan, S., and Bailey-Serres, J. (2005). Proteomic characterization of evolutionarily conserved and variable proteins of Arabidopsis cytosolic ribosomes. Plant Physiol. *137*, 848–862.

Chantrel, Y., Gaisne, M., Lions, C., and Verdière, J. (1998). The transcriptional regulator Hap1p (Cyp1p) is essential for anaerobic or heme-deficient growth of Saccharomyces cerevisiae: Genetic and molecular characterization of an extragenic suppressor that encodes a WD repeat protein. Genetics *148*, 559–569.

Chapman-Smith, A., and Cronan, J.E. (1999). The enzymatic biotinylation of proteins: a post-translational modification of exceptional specificity. Trends Biochem. Sci. *24*, 359–363.

Chasse, S.A., Flanary, P., Parnell, S.C., Hao, N., Cha, J.Y., Siderovski, D.P., and Dohlman, H.G. (2006). Genome-scale analysis reveals Sst2 as the principal regulator of mating pheromone signaling in the yeast Saccharomyces cerevisiae. Eukaryot. Cell *5*, 330–346.

Chen, A.L., Kim, E.W., Toh, J.Y., Vashisht, A.A., Rashoff, A.Q., Van, C., Huang, A.S., Moon, A.S., Bell, H.N., Bentolila, L.A., et al. (2015). Novel components of the Toxoplasma inner membrane complex revealed by BioID. MBio *6*, e02357-02314.

Chen, J.-G., Ullah, H., Temple, B., Liang, J., Guo, J., Alonso, J.M., Ecker, J.R., and Jones, A.M. (2006). RACK1 mediates multiple hormone responsiveness and developmental processes in Arabidopsis. J. Exp. Bot. *57*, 2697–2708.

Chen, S., Dell, E.J., Lin, F., Sai, J., and Hamm, H.E. (2004). RACK1 regulates specific functions of Gbetagamma. J. Biol. Chem. *279*, 17861–17868.

Chen, S., Lin, F., and Hamm, H.E. (2005a). RACK1 binds to a signal transfer region of G betagamma and inhibits phospholipase C beta2 activation. J. Biol. Chem. *280*, 33445–33452.

Chen, Y.-B., Yang, C.-P., Li, R.-X., Zeng, R., and Zhou, J.-Q. (2005b). Def1p is involved in telomere maintenance in budding yeast. J. Biol. Chem. *280*, 24784–24791.

Cheng, Z., Li, J.-F., Niu, Y., Zhang, X.-C., Woody, O.Z., Xiong, Y., Djonović, S., Millet, Y., Bush, J., McConkey, B.J., et al. (2015). Pathogen-secreted proteases activate a novel plant immune pathway. Nature *521*, 213–216.

Chiabudini, M., Tais, A., Zhang, Y., Hayashi, S., Wölfle, T., Fitzke, E., and Rospert, S. (2014). Release factor eRF3 mediates premature translation termination on polylysine-stalled ribosomes in Saccharomyces cerevisiae. Mol. Cell. Biol. *34*, 4062–4076.

Chin, J.W., Cropp, T.A., Anderson, J.C., Mukherji, M., Zhang, Z., and Schultz, P.G. (2003). An expanded eukaryotic genetic code. Science *301*, 964–967.

Chiu, W.-L., Wagner, S., Herrmannová, A., Burela, L., Zhang, F., Saini, A.K., Valásek, L., and Hinnebusch, A.G. (2010). The C-terminal region of eukaryotic translation initiation factor 3a (eIF3a) promotes mRNA recruitment, scanning, and, together with eIF3j and the eIF3b RNA recognition motif, selection of AUG start codons. Mol. Cell. Biol. *30*, 4415–4434.

Cho, W. (2006). Building signaling complexes at the membrane. Sci. STKE Signal Transduct. Knowl. Environ. *2006*, pe7.

Choi, D.-S., Young, H., McMahon, T., Wang, D., and Messing, R.O. (2003). The mouse RACK1 gene is regulated by nuclear factor-kappa B and contributes to cell survival. Mol. Pharmacol. *64*, 1541–1548.

Chou, Y.C., Chou, C.C., Chen, Y.K., Tsai, S., Hsieh, F.M., Liu, H.J., and Hseu, T.H. (1999). Structure and genomic organization of porcine RACK1 gene. Biochim. Biophys. Acta *1489*, 315–322.

Choudhury, K., Cardenas, D., Pullikuth, A.K., Catling, A.D., Aiyar, A., and Kelly, B.L. (2011). Trypanosomatid RACK1 orthologs show functional differences associated with translation despite similar roles in Leishmania pathogenesis. PloS One *6*, e20710.

Cohen, M., Stutz, F., Belgareh, N., Haguenauer-Tsapis, R., and Dargemont, C. (2003). Ubp3 requires a cofactor, Bre5, to specifically de-ubiquitinate the COPII protein, Sec23. Nat. Cell Biol. *5*, 661–667.

Collart, M.A., Panasenko, O.O., and Nikolaev, S.I. (2013). The Not3/5 subunit of the Ccr4-Not complex: a central regulator of gene expression that integrates signals between the cytoplasm and the nucleus in eukaryotic cells. Cell. Signal. *25*, 743–751.

Cox, J., and Mann, M. (2008). MaxQuant enables high peptide identification rates, individualized p.p.b.-range mass accuracies and proteome-wide protein quantification. Nat. Biotechnol. *26*, 1367–1372.

Cox, E.A., Bennin, D., Doan, A.T., O'Toole, T., and Huttenlocher, A. (2003). RACK1 regulates integrin-mediated adhesion, protrusion, and chemotactic cell migration via its Src-binding site. Mol. Biol. Cell *14*, 658–669.

Coyle, S.M., Gilbert, W.V., and Doudna, J.A. (2009). Direct link between RACK1 function and localization at the ribosome in vivo. Mol. Cell. Biol. *29*, 1626–1634.

Cridge, A.G., Castelli, L.M., Smirnova, J.B., Selley, J.N., Rowe, W., Hubbard, S.J., McCarthy, J.E.G., Ashe, M.P., Grant, C.M., and Pavitt, G.D. (2010). Identifying eIF4E-binding protein translationally-controlled transcripts reveals links to mRNAs bound by specific PUF proteins. Nucleic Acids Res. *38*, 8039–8050.

De Silva, D., Tu, Y.-T., Amunts, A., Fontanesi, F., and Barrientos, A. (2015). Mitochondrial ribosome assembly in health and disease. Cell Cycle Georget. Tex *14*, 2226–2250.

Decker, C.J., and Parker, R. (2012). P-bodies and stress granules: possible roles in the control of translation and mRNA degradation. Cold Spring Harb. Perspect. Biol. *4*, a012286.

Decker, C.J., Teixeira, D., and Parker, R. (2007). Edc3p and a glutamine/asparagine-rich domain of Lsm4p function in processing body assembly in Saccharomyces cerevisiae. J. Cell Biol. *179*, 437–449.

Dell, E.J., Connor, J., Chen, S., Stebbins, E.G., Skiba, N.P., Mochly-Rosen, D., and Hamm, H.E. (2002). The betagamma subunit of heterotrimeric G proteins interacts with RACK1 and two other WD repeat proteins. J. Biol. Chem. *277*, 49888–49895.

Demarco, R.S., and Lundquist, E.A. (2010). RACK-1 acts with Rac GTPase signaling and UNC-115/abLIM in Caenorhabditis elegans axon pathfinding and cell migration. PLoS Genet. *6*, e1001215.

DeMille, D., Badal, B.D., Evans, J.B., Mathis, A.D., Anderson, J.F., and Grose, J.H. (2015). PAS kinase is activated by direct SNF1-dependent phosphorylation and mediates inhibition of TORC1 through the phosphorylation and activation of Pbp1. Mol. Biol. Cell *26*, 569–582.

Denisenko, O., and Bomsztyk, K. (2002). Yeast hnRNP K-like genes are involved in regulation of the telomeric position effect and telomere length. Mol. Cell. Biol. *22*, 286–297.

Denisenko, O., and Bomsztyk, K. (2008). Epistatic interaction between the K-homology domain protein HEK2 and SIR1 at HMR and telomeres in yeast. J. Mol. Biol. *375*, 1178–1187.

Dibrov, E., Robinson, K.M., and Lemire, B.D. (1997). The COQ5 gene encodes a yeast mitochondrial protein necessary for ubiquinone biosynthesis and the assembly of the respiratory chain. J. Biol. Chem. *272*, 9175–9181.

Doan, A.T., and Huttenlocher, A. (2007). RACK1 regulates Src activity and modulates paxillin dynamics during cell migration. Exp. Cell Res. *313*, 2667–2679.

Dohlman, H.G. (2002). G proteins and pheromone signaling. Annu. Rev. Physiol. *64*, 129–152.

Dormán, G., and Prestwich, G.D. (1994). Benzophenone photophores in biochemistry. Biochemistry (Mosc.) *33*, 5661–5673.

Dragon, F., Gallagher, J.E.G., Compagnone-Post, P.A., Mitchell, B.M., Porwancher, K.A., Wehner, K.A., Wormsley, S., Settlage, R.E., Shabanowitz, J., Osheim, Y., et al. (2002). A large nucleolar U3 ribonucleoprotein required for 18S ribosomal RNA biogenesis. Nature *417*, 967–970.

Dresios, J., Panopoulos, P., and Synetos, D. (2006). Eukaryotic ribosomal proteins lacking a eubacterial counterpart: important players in ribosomal function. Mol. Microbiol. *59*, 1651–1663.

Elion, E.A. (2001). The Ste5p scaffold. J. Cell Sci. *114*, 3967–3978.

van den Elzen, A.M.G., Schuller, A., Green, R., and Séraphin, B. (2014). Dom34-Hbs1 mediated dissociation of inactive 80S ribosomes promotes restart of translation after stress. EMBO J. *33*, 265–276.

Ero, R., Dimitrova, V.T., Chen, Y., Bu, W., Feng, S., Liu, T., Wang, P., Xue, C., Tan, S.M., and Gao, Y.-G. (2015). Crystal structure of Gib2, a signal-transducing protein scaffold associated with ribosomes in Cryptococcus neoformans. Sci. Rep. *5*, 8688.

Farley, A.R., Powell, D.W., Weaver, C.M., Jennings, J.L., and Link, A.J. (2011). Assessing the components of the eIF3 complex and their phosphorylation status. J. Proteome Res. *10*, 1481–1494.

Fatica, A., Oeffinger, M., Dlakić, M., and Tollervey, D. (2003). Nob1p is required for cleavage of the 3' end of 18S rRNA. Mol. Cell. Biol. *23*, 1798–1807.

Feng, J., Cai, X., Zhao, J., and Yan, Z. (2001). Serotonin receptors modulate GABA(A) receptor channels through activation of anchored protein kinase C in prefrontal cortical neurons. J. Neurosci. Off. J. Soc. Neurosci. *21*, 6502–6511.

Fleischer, T.C., Weaver, C.M., McAfee, K.J., Jennings, J.L., and Link, A.J. (2006). Systematic identification and functional screens of uncharacterized proteins associated with eukaryotic ribosomal complexes. Genes Dev. *20*, 1294–1307.

Formosa, T., Eriksson, P., Wittmeyer, J., Ginn, J., Yu, Y., and Stillman, D.J. (2001). Spt16-Pob3 and the HMG protein Nhp6 combine to form the nucleosome-binding factor SPN. EMBO J. *20*, 3506–3517.

Frantz, J.D., and Gilbert, W. (1995). A yeast gene product, G4p2, with a specific affinity for quadruplex nucleic acids. J. Biol. Chem. *270*, 9413–9419.

Frey, S., Pool, M., and Seedorf, M. (2001). Scp160p, an RNA-binding, Polysome-associated Protein, Localizes to the Endoplasmic Reticulum of Saccharomyces cerevisiae in a Microtubule-dependent Manner. J. Biol. Chem. *276*, 15905–15912.

Gandin, V., Senft, D., Topisirovic, I., and Ronai, Z.A. (2013a). RACK1 Function in Cell Motility and Protein Synthesis. Genes Cancer *4*, 369–377.

Gandin, V., Gutierrez, G.J., Brill, L.M., Varsano, T., Feng, Y., Aza-Blanc, P., Au, Q., McLaughlan, S., Ferreira, T.A., Alain, T., et al. (2013b). Degradation of newly synthesized polypeptides by ribosome-associated RACK1/c-Jun N-terminal kinase/eukaryotic elongation factor 1A2 complex. Mol. Cell. Biol. *33*, 2510–2526.

Gavin, A.-C., Bösche, M., Krause, R., Grandi, P., Marzioch, M., Bauer, A., Schultz, J., Rick, J.M., Michon, A.-M., Cruciat, C.-M., et al. (2002). Functional organization of the yeast proteome by systematic analysis of protein complexes. Nature *415*, 141–147.

Geerlings, T.H., Vos, J.C., and Raué, H.A. (2000). The final step in the formation of 25S rRNA in Saccharomyces cerevisiae is performed by 5'-->3' exonucleases. RNA N. Y. N *6*, 1698–1703.

Gelin-Licht, R., Paliwal, S., Conlon, P., Levchenko, A., and Gerst, J.E. (2012). Scp160-dependent mRNA trafficking mediates pheromone gradient sensing and chemotropism in yeast. Cell Rep. *1*, 483–494.

Gerbasi, V.R., Weaver, C.M., Hill, S., Friedman, D.B., and Link, A.J. (2004). Yeast Asc1p and mammalian RACK1 are functionally orthologous core 40S ribosomal proteins that repress gene expression. Mol. Cell. Biol. *24*, 8276–8287.

Ghaemmaghami, S., Huh, W.-K., Bower, K., Howson, R.W., Belle, A., Dephoure, N., O'Shea, E.K., and Weissman, J.S. (2003). Global analysis of protein expression in yeast. Nature *425*, 737–741.

Giaever, G., Chu, A.M., Ni, L., Connelly, C., Riles, L., Véronneau, S., Dow, S., Lucau-Danila, A., Anderson, K., André, B., et al. (2002). Functional profiling of the Saccharomyces cerevisiae genome. Nature *418*, 387–391.

Grosso, S., Volta, V., Vietri, M., Gorrini, C., Marchisio, P.C., and Biffo, S. (2008b). Eukaryotic ribosomes host PKC activity. Biochem. Biophys. Res. Commun. *376*, 65–69.

Grosso, S., Volta, V., Sala, L.A., Vietri, M., Marchisio, P.C., Ron, D., and Biffo, S. (2008a). PKCbetaII modulates translation independently from mTOR and through RACK1. Biochem. J. *415*, 77–85.

Grousl, T., Ivanov, P., Frýdlová, I., Vasicová, P., Janda, F., Vojtová, J., Malínská, K., Malcová, I., Nováková, L., Janosková, D., et al. (2009). Robust heat shock induces eIF2alpha-phosphorylation-independent assembly of stress granules containing eIF3 and 40S ribosomal subunits in budding yeast, Saccharomyces cerevisiae. J. Cell Sci. *122*, 2078–2088.

Grousl, T., Ivanov, P., Malcova, I., Pompach, P., Frydlova, I., Slaba, R., Senohrabkova, L., Novakova, L., and Hasek, J. (2013). Heat shock-induced accumulation of translation elongation and termination factors precedes assembly of stress granules in S. cerevisiae. PloS One *8*, e57083.

Gueldener, U., Heinisch, J., Koehler, G.J., Voss, D., and Hegemann, J.H. (2002). A second set of loxP marker cassettes for Cre-mediated multiple gene knockouts in budding yeast. Nucleic Acids Res. *30*, e23.

Guo, J., Wang, J., Xi, L., Huang, W.-D., Liang, J., and Chen, J.-G. (2009). RACK1 is a negative regulator of ABA responses in Arabidopsis. J. Exp. Bot. *60*, 3819–3833.

Guo, J., Wang, S., Valerius, O., Hall, H., Zeng, Q., Li, J.-F., Weston, D.J., Ellis, B.E., and Chen, J.-G. (2011a). Involvement of Arabidopsis RACK1 in protein translation and its regulation by abscisic acid. Plant Physiol. *155*, 370–383.

Guo, J., Jin, Z., Yang, X., Li, J.-F., and Chen, J.-G. (2011b). Eukaryotic initiation factor 6, an evolutionarily conserved regulator of ribosome biogenesis and protein translation. Plant Signal. Behav. *6*, 766–771.

Guo, M., Aston, C., Burchett, S.A., Dyke, C., Fields, S., Rajarao, S.J.R., Uetz, P., Wang, Y., Young, K., and Dohlman, H.G. (2003). The yeast G protein alpha subunit Gpa1 transmits a signal through an RNA binding effector protein Scp160. Mol. Cell *12*, 517–524.

Guo, Y., Wang, W., Wang, J., Feng, J., Wang, Q., Jin, J., Lv, M., Li, X., Li, Y., Ma, Y., et al. (2013). Receptor for activated C kinase 1 promotes hepatocellular carcinoma growth by enhancing mitogen-activated protein kinase kinase 7 activity. Hepatol. Baltim. Md *57*, 140–151.

Harris, J.K., Kelley, S.T., Spiegelman, G.B., and Pace, N.R. (2003). The genetic core of the universal ancestor. Genome Res. *13*, 407–412.

Hartzog, G.A., and Fu, J. (2013). The Spt4-Spt5 complex: a multi-faceted regulator of transcription elongation. Biochim. Biophys. Acta *1829*, 105–115.

Hasegawa, Y., Irie, K., and Gerber, A.P. (2008). Distinct roles for Khd1p in the localization and expression of bud-localized mRNAs in yeast. RNA N. Y. N *14*, 2333–2347.

Hasek, J., Kovarik, P., Valásek, L., Malínská, K., Schneider, J., Kohlwein, S.D., and Ruis, H. (2000). Rpg1p, the subunit of the Saccharomyces cerevisiae eIF3 core complex, is a microtubule-interacting protein. Cell Motil. Cytoskeleton *45*, 235–246.

Hayashi, N., and Murakami, S. (2002). STM1, a gene which encodes a guanine quadruplex binding protein, interacts with CDC13 in Saccharomyces cerevisiae. Mol. Genet. Genomics MGG *267*, 806–813.

He, D.-Y., Neasta, J., and Ron, D. (2010). Epigenetic regulation of BDNF expression via the scaffolding protein RACK1. J. Biol. Chem. *285*, 19043–19050.

Hermanto, U., Zong, C.S., Li, W., and Wang, L.-H. (2002). RACK1, an insulin-like growth factor I (IGF-I) receptor-interacting protein, modulates IGF-I-dependent integrin signaling and promotes cell spreading and contact with extracellular matrix. Mol. Cell. Biol. *22*, 2345–2365.

Hinnebusch, A.G. (2005). Translational regulation of GCN4 and the general amino acid control of yeast. Annu. Rev. Microbiol. *59*, 407–450.

Hinnebusch, A.G., and Lorsch, J.R. (2012). The mechanism of eukaryotic translation initiation: new insights and challenges. Cold Spring Harb. Perspect. Biol. *4*.

Hirschmann, W.D., Westendorf, H., Mayer, A., Cannarozzi, G., Cramer, P., and Jansen, R.-P. (2014). Scp160p is required for translational efficiency of codon-optimized mRNAs in yeast. Nucleic Acids Res. *42*, 4043–4055.

Ho, Y., Gruhler, A., Heilbut, A., Bader, G.D., Moore, L., Adams, S.-L., Millar, A., Taylor, P., Bennett, K., Boutilier, K., et al. (2002). Systematic identification of protein complexes in Saccharomyces cerevisiae by mass spectrometry. Nature *415*, 180–183.

Hoffman, C.S., and Winston, F. (1987). A ten-minute DNA preparation from yeast efficiently releases autonomous plasmids for transformation of Escherichia coli. Gene *57*, 267–272.

Hoffmann, B., Mösch, H.U., Sattlegger, E., Barthelmess, I.B., Hinnebusch, A., and Braus, G.H. (1999). The WD protein Cpc2p is required for repression of Gcn4 protein activity in yeast in the absence of amino-acid starvation. Mol. Microbiol. *31*, 807–822.

Hogan, D.J., Riordan, D.P., Gerber, A.P., Herschlag, D., and Brown, P.O. (2008). Diverse RNA-binding proteins interact with functionally related sets of RNAs, suggesting an extensive regulatory system. PLoS Biol. *6*, e255.

Hon, T., Lee, H.C., Hach, A., Johnson, J.L., Craig, E.A., Erdjument-Bromage, H., Tempst, P., and Zhang, L. (2001). The Hsp70-Ydj1 molecular chaperone represses the activity of the heme activator protein Hap1 in the absence of heme. Mol. Cell. Biol. *21*, 7923–7932.

de Hoog, C.L., Foster, L.J., and Mann, M. (2004). RNA and RNA binding proteins participate in early stages of cell spreading through spreading initiation centers. Cell *117*, 649–662.

Hoyle, N.P., Castelli, L.M., Campbell, S.G., Holmes, L.E.A., and Ashe, M.P. (2007). Stress-dependent relocalization of translationally primed mRNPs to cytoplasmic granules that are kinetically and spatially distinct from P-bodies. J. Cell Biol. *179*, 65–74.

Hurst, J.H., and Dohlman, H.G. (2013). Dynamic ubiquitination of the mitogen-activated protein kinase kinase (MAPKK) Ste7 determines mitogen-activated protein kinase (MAPK) specificity. J. Biol. Chem. *288*, 18660–18671.

Ibrahimo, S., Holmes, L.E.A., and Ashe, M.P. (2006). Regulation of translation initiation by the yeast eIF4E binding proteins is required for the pseudohyphal response. Yeast Chichester Engl. *23*, 1075–1088.

Inada, T., Winstall, E., Tarun, S.Z., Yates, J.R., Schieltz, D., and Sachs, A.B. (2002). One-step affinity purification of the yeast ribosome and its associated proteins and mRNAs. RNA N. Y. N *8*, 948–958.

Inoue, H., Nojima, H., and Okayama, H. (1990). High efficiency transformation of Escherichia coli with plasmids. Gene *96*, 23–28.

Inoue, Y., Kawai-Noma, S., Koike-Takeshita, A., Taguchi, H., and Yoshida, M. (2011). Yeast prion protein New1 can break Sup35 amyloid fibrils into fragments in an ATP-dependent manner. Genes Cells Devoted Mol. Cell. Mech. *16*, 545–556.

Irie, K., Tadauchi, T., Takizawa, P.A., Vale, R.D., Matsumoto, K., and Herskowitz, I. (2002). The Khd1 protein, which has three KH RNA-binding motifs, is required for proper localization of ASH1 mRNA in yeast. EMBO J. *21*, 1158–1167.

Ishida, S., Takahashi, Y., and Nagata, T. (1993). Isolation of cDNA of an auxin-regulated gene encoding a G protein beta subunit-like protein from tobacco BY-2 cells. Proc. Natl. Acad. Sci. U. S. A. *90*, 11152–11156.

Islas-Flores, T., Guillén, G., Islas-Flores, I., San Román-Roque, C., Sánchez, F., Loza-Tavera, H., Bearer, E.L., and Villanueva, M.A. (2009). Germination behavior, biochemical features and sequence analysis of the RACK1/arcA homolog from Phaseolus vulgaris. Physiol. Plant. *137*, 264–280.

Islas-Flores, T., Rahman, A., Ullah, H., and Villanueva, M.A. (2015). The Receptor for Activated C Kinase in Plant Signaling: Tale of a Promiscuous Little Molecule. Front. Plant Sci. *6*, 1090.

Ito, H., Fukuda, Y., Murata, K., and Kimura, A. (1983). Transformation of intact yeast cells treated with alkali cations. J. Bacteriol. *153*, 163–168.

Ito, W., Li, X., Irie, K., Mizuno, T., and Irie, K. (2011). RNA-binding protein Khd1 and Ccr4 deadenylase play overlapping roles in the cell wall integrity pathway in Saccharomyces cerevisiae. Eukaryot. Cell *10*, 1340–1347.

Iwasaki, Y., Komano, M., Ishikawa, A., Sasaki, T., and Asahi, T. (1995). Molecular cloning and characterization of cDNA for a rice protein that contains seven repetitive segments of the Trp-Asp forty-amino-acid repeat (WD-40 repeat). Plant Cell Physiol. *36*, 505–510.

Jannot, G., Bajan, S., Giguère, N.J., Bouasker, S., Banville, I.H., Piquet, S., Hutvagner, G., and Simard, M.J. (2011). The ribosomal protein RACK1 is required for microRNA function in both C. elegans and humans. EMBO Rep. *12*, 581–586.

Jeong, H.T., Oowatari, Y., Abe, M., Tanaka, K., Matsuda, H., and Kawamukai, M. (2004). Interaction between a negative regulator (Msa2/Nrd1) and a positive regulator (Cpc2) of sexual differentiation in Schizosaccharomyces pombe. Biosci. Biotechnol. Biochem. *68*, 1621–1626.

Kadrmas, J.L., Smith, M.A., Pronovost, S.M., and Beckerle, M.C. (2007). Characterization of RACK1 function in Drosophila development. Dev. Dyn. Off. Publ. Am. Assoc. Anat. *236*, 2207–2215.

Kang, D., Gho, Y.S., Suh, M., and Kang, C.K. (2002). Highly Sensitive and Fast Protein Detection with Coomassie Brilliant Blue in Sodium Dodecyl Sulfate-Polyacrylamide Gel Electrophoresis. Bull. Korean Chem. Soc. *23*, 1511–1512.

Kato, K., Yamamoto, Y., and Izawa, S. (2011). Severe ethanol stress induces assembly of stress granules in Saccharomyces cerevisiae. Yeast Chichester Engl. *28*, 339–347.

Kershaw, C.J., Costello, J.L., Castelli, L.M., Talavera, D., Rowe, W., Sims, P.F.G., Ashe, M.P., Hubbard, S.J., Pavitt, G.D., and Grant, C.M. (2015). The yeast La related protein Slf1p is a key activator of translation during the oxidative stress response. PLoS Genet. *11*, e1004903.

Khoshnevis, S., Gunišová, S., Vlčková, V., Kouba, T., Neumann, P., Beznosková, P., Ficner, R., and Valášek, L.S. (2014). Structural integrity of the PCI domain of eIF3a/TIF32 is required for mRNA recruitment to the 43S pre-initiation complexes. Nucleic Acids Res. *42*, 4123–4139.

Kiely, P.A., Sant, A., and O'Connor, R. (2002). RACK1 is an insulin-like growth factor 1 (IGF-1) receptor-interacting protein that can regulate IGF-1-mediated Akt activation and protection from cell death. J. Biol. Chem. *277*, 22581–22589.

Kiely, P.A., Leahy, M., O'Gorman, D., and O'Connor, R. (2005). RACK1-mediated integration of adhesion and insulin-like growth factor I (IGF-I) signaling and cell migration are defective in cells expressing an IGF-I receptor mutated at tyrosines 1250 and 1251. J. Biol. Chem. *280*, 7624–7633.

Kiely, P.A., O'Gorman, D., Luong, K., Ron, D., and O'Connor, R. (2006). Insulin-like growth factor I controls a mutually exclusive association of RACK1 with protein phosphatase 2A and beta1 integrin to promote cell migration. Mol. Cell. Biol. *26*, 4041–4051.

Kiely, P.A., Baillie, G.S., Lynch, M.J., Houslay, M.D., and O'Connor, R. (2008). Tyrosine 302 in RACK1 is essential for insulin-like growth factor-I-mediated competitive binding of PP2A and beta1 integrin and for tumor cell proliferation and migration. J. Biol. Chem. *283*, 22952–22961.

Kiely, P.A., Baillie, G.S., Barrett, R., Buckley, D.A., Adams, D.R., Houslay, M.D., and O'Connor, R. (2009). Phosphorylation of RACK1 on tyrosine 52 by c-Abl is required for insulin-like growth factor I-mediated regulation of focal adhesion kinase. J. Biol. Chem. *284*, 20263–20274.

Kim, D.I., Jensen, S.C., Noble, K.A., Kc, B., Roux, K.H., Motamedchaboki, K., and Roux, K.J. (2016). An improved smaller biotin ligase for BioID proximity labeling. Mol. Biol. Cell *27*, 1188–1196.

Kim, S.W., Joo, Y.J., and Kim, J. (2010). Asc1p, a ribosomal protein, plays a pivotal role in cellular adhesion and virulence in Candida albicans. J. Microbiol. Seoul Korea *48*, 842–848.

Kimura, Y., Irie, K., and Irie, K. (2013). Pbp1 is involved in Ccr4- and Khd1-mediated regulation of cell growth through association with ribosomal proteins Rpl12a and Rpl12b. Eukaryot. Cell *12*, 864–874.

Kiss-László, Z., Henry, Y., Bachellerie, J.P., Caizergues-Ferrer, M., and Kiss, T. (1996). Site-specific ribose methylation of preribosomal RNA: a novel function for small nucleolar RNAs. Cell *85*, 1077–1088.

Kiss-László, Z., Henry, Y., and Kiss, T. (1998). Sequence and structural elements of methylation guide snoRNAs essential for site-specific ribose methylation of pre-rRNA. EMBO J. *17*, 797–807.

Klass, D.M., Scheibe, M., Butter, F., Hogan, G.J., Mann, M., and Brown, P.O. (2013). Quantitative proteomic analysis reveals concurrent RNA-protein interactions and identifies new RNA-binding proteins in Saccharomyces cerevisiae. Genome Res. *23*, 1028–1038.

Kleinschmidt, M., Schulz, R., and Braus, G.H. (2006). The yeast CPC2/ASC1 gene is regulated by the transcription factors Fhl1p and Ifh1p. Curr. Genet. *49*, 218–228.

Kong, Q., Wang, L., Liu, Z., Kwon, N.-J., Kim, S.C., and Yu, J.-H. (2013). Gβ-like CpcB plays a crucial role for growth and development of Aspergillus nidulans and Aspergillus fumigatus. PloS One *8*, e70355.

Kouba, T., Rutkai, E., Karásková, M., and Valášek, L.S. (2012a). The eIF3c/NIP1 PCI domain interacts with RNA and RACK1/ASC1 and promotes assembly of translation preinitiation complexes. Nucleic Acids Res. *40*, 2683–2699.

Kouba, T., Dányi, I., Gunišová, S., Munzarová, V., Vlčková, V., Cuchalová, L., Neueder, A., Milkereit, P., and Valášek, L.S. (2012b). Small ribosomal protein RPS0 stimulates translation initiation by mediating 40S-binding of eIF3 via its direct contact with the eIF3a/TIF32 subunit. PloS One *7*, e40464.

Kraft, C., Deplazes, A., Sohrmann, M., and Peter, M. (2008). Mature ribosomes are selectively degraded upon starvation by an autophagy pathway requiring the Ubp3p/Bre5p ubiquitin protease. Nat. Cell Biol. *10*, 602–610.

Kraus, S., Gioeli, D., Vomastek, T., Gordon, V., and Weber, M.J. (2006). Receptor for activated C kinase 1 (RACK1) and Src regulate the tyrosine phosphorylation and function of the androgen receptor. Cancer Res. *66*, 11047–11054.

Krokowski, D., Gaccioli, F., Majumder, M., Mullins, M.R., Yuan, C.L., Papadopoulou, B., Merrick, W.C., Komar, A.A., Taylor, D., and Hatzoglou, M. (2011). Characterization of hibernating ribosomes in mammalian cells. Cell Cycle Georget. Tex *10*, 2691–2702.

Kulak, N.A., Pichler, G., Paron, I., Nagaraj, N., and Mann, M. (2014). Minimal, encapsulated proteomic-sample processing applied to copy-number estimation in eukaryotic cells. Nat. Methods *11*, 319–324.

Kulkarni, M., Ozgur, S., and Stoecklin, G. (2010). On track with P-bodies. Biochem. Soc. Trans. *38*, 242–251.

Kuroha, K., Akamatsu, M., Dimitrova, L., Ito, T., Kato, Y., Shirahige, K., and Inada, T. (2010). Receptor for activated C kinase 1 stimulates nascent polypeptide-dependent translation arrest. EMBO Rep. *11*, 956–961.

Kvint, K., Uhler, J.P., Taschner, M.J., Sigurdsson, S., Erdjument-Bromage, H., Tempst, P., and Svejstrup, J.Q. (2008). Reversal of RNA polymerase II ubiquitylation by the ubiquitin protease Ubp3. Mol. Cell *30*, 498–506.

Kwon, H.J., Bae, S., Son, Y.H., and Chung, H.M. (2001). Expression of the Xenopus homologue of the receptor for activated C-kinase 1 (RACK1) in the Xenopus embryo. Dev. Genes Evol. *211*, 195–197.

Laemmli, U.K. (1970). Cleavage of structural proteins during the assembly of the head of bacteriophage T4. Nature *227*, 680–685.

Lamanna, A.C., and Karbstein, K. (2009). Nob1 binds the single-stranded cleavage site D at the 3'-end of 18S rRNA with its PIN domain. Proc. Natl. Acad. Sci. U. S. A. *106*, 14259–14264.

Lan, C., Lee, H.C., Tang, S., and Zhang, L. (2004). A novel mode of chaperone action: heme activation of Hap1 by enhanced association of Hsp90 with the repressed Hsp70-Hap1 complex. J. Biol. Chem. *279*, 27607–27612.

Lane, M.D., Rominger, K.L., Young, D.L., and Lynen, F. (1964). THE ENZYMATIC SYNTHESIS OF HOLOTRANSCARBOXYLASE FROM APOTRANSCARBOXYLASE AND (+)-BIOTIN. II. INVESTIGATION OF THE REACTION MECHANISM. J. Biol. Chem. *239*, 2865–2871.

Lemmon, M.A., and Ferguson, K.M. (2000). Signal-dependent membrane targeting by pleckstrin homology (PH) domains. Biochem. J. *350 Pt 1*, 1–18.

Letzring, D.P., Wolf, A.S., Brule, C.E., and Grayhack, E.J. (2013). Translation of CGA codon repeats in yeast involves quality control components and ribosomal protein L1. RNA N. Y. N *19*, 1208–1217.

Lew, J.E., Enomoto, S., and Berman, J. (1998). Telomere length regulation and telomeric chromatin require the nonsense-mediated mRNA decay pathway. Mol. Cell. Biol. *18*, 6121–6130.

Li, J.-J., and Xie, D. (2015). RACK1, a versatile hub in cancer. Oncogene *34*, 1890–1898.

Li, Y., and Wang, Y. (2013). Ras protein/cAMP-dependent protein kinase signaling is negatively regulated by a deubiquitinating enzyme, Ubp3, in yeast. J. Biol. Chem. *288*, 11358–11365.

Li, S., Esterberg, R., Lachance, V., Ren, D., Radde-Gallwitz, K., Chi, F., Parent, J.-L., Fritz, A., and Chen, P. (2011). Rack1 is required for Vangl2 membrane localization and planar cell polarity signaling while attenuating canonical Wnt activity. Proc. Natl. Acad. Sci. U. S. A. *108*, 2264–2269.

Liedtke, C.M., Yun, C.H.C., Kyle, N., and Wang, D. (2002). Protein kinase C epsilon-dependent regulation of cystic fibrosis transmembrane regulator involves binding to a receptor for activated C kinase (RACK1) and RACK1 binding to Na+/H+ exchange regulatory factor. J. Biol. Chem. *277*, 22925–22933.

Liliental, J., and Chang, D.D. (1998). Rack1, a receptor for activated protein kinase C, interacts with integrin beta subunit. J. Biol. Chem. *273*, 2379–2383.

Lindstrom, D.L., Squazzo, S.L., Muster, N., Burckin, T.A., Wachter, K.C., Emigh, C.A., McCleery, J.A., Yates, J.R., and Hartzog, G.A. (2003). Dual roles for Spt5 in pre-mRNA processing and transcription elongation revealed by identification of Spt5-associated proteins. Mol. Cell. Biol. *23*, 1368–1378.

Link, A.J., Eng, J., Schieltz, D.M., Carmack, E., Mize, G.J., Morris, D.R., Garvik, B.M., and Yates, J.R. (1999). Direct analysis of protein complexes using mass spectrometry. Nat. Biotechnol. *17*, 676–682.

Liu, Z., and Gilbert, W. (1994). The yeast KEM1 gene encodes a nuclease specific for G4 tetraplex DNA: implication of in vivo functions for this novel DNA structure. Cell *77*, 1083–1092.

Liu, L., Zeng, M., Hausladen, A., Heitman, J., and Stamler, J.S. (2000). Protection from nitrosative stress by yeast flavohemoglobin. Proc. Natl. Acad. Sci. U. S. A. *97*, 4672–4676.

Liu, X., Nie, X., Ding, Y., and Chen, J. (2010). Asc1, a WD-repeat protein, is required for hyphal development and virulence in Candida albicans. Acta Biochim. Biophys. Sin. *42*, 793–800.

Liu, Y.V., Baek, J.H., Zhang, H., Diez, R., Cole, R.N., and Semenza, G.L. (2007a). RACK1 competes with HSP90 for binding to HIF-1alpha and is required for O(2)-independent and HSP90 inhibitor-induced degradation of HIF-1alpha. Mol. Cell *25*, 207–217.

Liu, Y.V., Hubbi, M.E., Pan, F., McDonald, K.R., Mansharamani, M., Cole, R.N., Liu, J.O., and Semenza, G.L. (2007b). Calcineurin promotes hypoxia-inducible factor 1alpha expression by dephosphorylating RACK1 and blocking RACK1 dimerization. J. Biol. Chem. *282*, 37064–37073.

Liu, Z., Lee, A., and Gilbert, W. (1995). Gene disruption of a G4-DNA-dependent nuclease in yeast leads to cellular senescence and telomere shortening. Proc. Natl. Acad. Sci. U. S. A. *92*, 6002–6006.

Llácer, J.L., Hussain, T., Marler, L., Aitken, C.E., Thakur, A., Lorsch, J.R., Hinnebusch, A.G., and Ramakrishnan, V. (2015). Conformational Differences between Open and Closed States of the Eukaryotic Translation Initiation Complex. Mol. Cell *59*, 399–412.

López-Bergami, P., Habelhah, H., Bhoumik, A., Zhang, W., Wang, L.-H., and Ronai, Z. (2005). RACK1 mediates activation of JNK by protein kinase C [corrected]. Mol. Cell *19*, 309–320.

Lopez-Bergami, P., Huang, C., Goydos, J.S., Yip, D., Bar-Eli, M., Herlyn, M., Smalley, K.S.M., Mahale, A., Eroshkin, A., Aaronson, S., et al. (2007). Rewired ERK-JNK signaling pathways in melanoma. Cancer Cell *11*, 447–460.

Lu, J., and Deutsch, C. (2008). Electrostatics in the ribosomal tunnel modulate chain elongation rates. J. Mol. Biol. *384*, 73–86.

Lykke-Andersen, J., and Bennett, E.J. (2014). Protecting the proteome: Eukaryotic cotranslational quality control pathways. J. Cell Biol. *204*, 467–476.

Majzoub, K., Hafirassou, M.L., Meignin, C., Goto, A., Marzi, S., Fedorova, A., Verdier, Y., Vinh, J., Hoffmann, J.A., Martin, F., et al. (2014). RACK1 controls IRES-mediated translation of viruses. Cell *159*, 1086–1095.

Mamidipudi, V., Chang, B.Y., Harte, R.A., Lee, K.C., and Cartwright, C.A. (2004). RACK1 inhibits the serum- and anchorage-independent growth of v-Src transformed cells. FEBS Lett. *567*, 321–326.

Mamidipudi, V., Dhillon, N.K., Parman, T., Miller, L.D., Lee, K.C., and Cartwright, C.A. (2007). RACK1 inhibits colonic cell growth by regulating Src activity at cell cycle checkpoints. Oncogene *26*, 2914–2924.

Mangus, D.A., Amrani, N., and Jacobson, A. (1998). Pbp1p, a factor interacting with Saccharomyces cerevisiae poly(A)-binding protein, regulates polyadenylation. Mol. Cell. Biol. *18*, 7383–7396.

Mangus, D.A., Evans, M.C., Agrin, N.S., Smith, M., Gongidi, P., and Jacobson, A. (2004a). Positive and negative regulation of poly(A) nuclease. Mol. Cell. Biol. *24*, 5521–5533.

Mangus, D.A., Smith, M.M., McSweeney, J.M., and Jacobson, A. (2004b). Identification of factors regulating poly(A) tail synthesis and maturation. Mol. Cell. Biol. *24*, 4196–4206.

Matsuda, R., Ikeuchi, K., Nomura, S., and Inada, T. (2014). Protein quality control systems associated with no-go and nonstop mRNA surveillance in yeast. Genes Cells Devoted Mol. Cell. Mech. *19*, 1–12.

Matsuo, R., Kubota, H., Obata, T., Kito, K., Ota, K., Kitazono, T., Ibayashi, S., Sasaki, T., Iida, M., and Ito, T. (2005). The yeast eIF4E-associated protein Eap1p attenuates GCN4 translation upon TOR-inactivation. FEBS Lett. *579*, 2433–2438.

Mattijssen, S., and Maraia, R.J. (2015). LARP4 Is Regulated by Tumor Necrosis Factor Alpha in a Tristetraprolin-Dependent Manner. Mol. Cell. Biol. *36*, 574–584.

Mayer, A., Schreieck, A., Lidschreiber, M., Leike, K., Martin, D.E., and Cramer, P. (2012). The spt5 C-terminal region recruits yeast 3' RNA cleavage factor I. Mol. Cell. Biol. *32*, 1321–1331.

McLeod, M., Shor, B., Caporaso, A., Wang, W., Chen, H., and Hu, L. (2000). Cpc2, a fission yeast homologue of mammalian RACK1 protein, interacts with Ran1 (Pat1) kinase To regulate cell cycle progression and meiotic development. Mol. Cell. Biol. *20*, 4016–4027.

Melamed, D., Bar-Ziv, L., Truzman, Y., and Arava, Y. (2010). Asc1 supports cell-wall integrity near bud sites by a Pkc1 independent mechanism. PloS One *5*, e11389.

Miller, L.D., Lee, K.C., Mochly-Rosen, D., and Cartwright, C.A. (2004). RACK1 regulates Src-mediated Sam68 and p190RhoGAP signaling. Oncogene *23*, 5682–5686.

Min, E.E., Roy, B., Amrani, N., He, F., and Jacobson, A. (2013). Yeast Upf1 CH domain interacts with Rps26 of the 40S ribosomal subunit. RNA N. Y. N *19*, 1105–1115.

Mitchell, S.F., Jain, S., She, M., and Parker, R. (2013). Global analysis of yeast mRNPs. Nat. Struct. Mol. Biol. *20*, 127–133.

Morriswood, B., Havlicek, K., Demmel, L., Yavuz, S., Sealey-Cardona, M., Vidilaseris, K., Anrather, D., Kostan, J., Djinovic-Carugo, K., Roux, K.J., et al. (2013). Novel bilobe components in Trypanosoma brucei identified using proximity-dependent biotinylation. Eukaryot. Cell *12*, 356–367.

Mourton, T., Hellberg, C.B., Burden-Gulley, S.M., Hinman, J., Rhee, A., and Brady-Kalnay, S.M. (2001). The PTPmu protein-tyrosine phosphatase binds and recruits the scaffolding protein RACK1 to cell-cell contacts. J. Biol. Chem. *276*, 14896–14901.

Muhlrad, D., and Parker, R. (1994). Premature translational termination triggers mRNA decapping. Nature *370*, 578–581.

Mukherjee, A., Roy, S., Saha, B., and Mukherjee, D. (2016). Spatio-Temporal Regulation of PKC Isoforms Imparts Signaling Specificity. Front. Immunol. *7*, 45.

Müller, F., Krüger, D., Sattlegger, E., Hoffmann, B., Ballario, P., Kanaan, M., and Barthelmess, I.B. (1995). The cpc-2 gene of Neurospora crassa encodes a protein entirely composed of WD-repeat segments that is involved in general amino acid control and female fertility. Mol. Gen. Genet. MGG *248*, 162–173.

Mumberg, D., Müller, R., and Funk, M. (1994). Regulatable promoters of Saccharomyces cerevisiae: comparison of transcriptional activity and their use for heterologous expression. Nucleic Acids Res. *22*, 5767–5768.

Munzarová, V., Pánek, J., Gunišová, S., Dányi, I., Szamecz, B., and Valášek, L.S. (2011). Translation reinitiation relies on the interaction between eIF3a/TIF32 and progressively folded cis-acting mRNA elements preceding short uORFs. PLoS Genet. *7*, e1002137.

Nagarajan, V.K., Jones, C.I., Newbury, S.F., and Green, P.J. (2013). XRN 5'→3' exoribonucleases: structure, mechanisms and functions. Biochim. Biophys. Acta *1829*, 590–603.

Nakashima, A., Chen, L., Thao, N.P., Fujiwara, M., Wong, H.L., Kuwano, M., Umemura, K., Shirasu, K., Kawasaki, T., and Shimamoto, K. (2008). RACK1 functions in rice innate immunity by interacting with the Rac1 immune complex. Plant Cell *20*, 2265–2279.

Neasta, J., Kiely, P.A., He, D.-Y., Adams, D.R., O'Connor, R., and Ron, D. (2012). Direct interaction between scaffolding proteins RACK1 and 14-3-3ζ regulates brain-derived neurotrophic factor (BDNF) transcription. J. Biol. Chem. *287*, 322–336.

Nelson, L.D., Musso, M., and Van Dyke, M.W. (2000). The yeast STM1 gene encodes a purine motif triple helical DNA-binding protein. J. Biol. Chem. *275*, 5573–5581.

Nilsson, J., Sengupta, J., Frank, J., and Nissen, P. (2004). Regulation of eukaryotic translation by the RACK1 protein: a platform for signalling molecules on the ribosome. EMBO Rep. *5*, 1137–1141.

van Nocker, S., and Ludwig, P. (2003). The WD-repeat protein superfamily in Arabidopsis: conservation and divergence in structure and function. BMC Genomics *4*, 50.

Nostramo, R., Varia, S.N., Zhang, B., Emerson, M.M., and Herman, P.K. (2016). The Catalytic Activity of the Ubp3 Deubiquitinating Protease Is Required for Efficient Stress Granule Assembly in Saccharomyces cerevisiae. Mol. Cell. Biol. *36*, 173–183.

Núñez, A., Franco, A., Madrid, M., Soto, T., Vicente, J., Gacto, M., and Cansado, J. (2009). Role for RACK1 orthologue Cpc2 in the modulation of stress response in fission yeast. Mol. Biol. Cell *20*, 3996–4009.

Núñez, A., Franco, A., Soto, T., Vicente, J., Gacto, M., and Cansado, J. (2010). Fission yeast receptor of activated C kinase (RACK1) ortholog Cpc2 regulates mitotic commitment through Wee1 kinase. J. Biol. Chem. *285*, 41366–41373.

Ohn, T., Kedersha, N., Hickman, T., Tisdale, S., and Anderson, P. (2008). A functional RNAi screen links O-GlcNAc modification of ribosomal proteins to stress granule and processing body assembly. Nat. Cell Biol. *10*, 1224–1231.

Ohsugi, M., and Imanishi, Y. (1985). Microbiological activity of biotin-vitamers. J. Nutr. Sci. Vitaminol. (Tokyo) *31*, 563–572.

Ohtsuka, H., Ogawa, S., Kawamura, H., Sakai, E., Ichinose, K., Murakami, H., and Aiba, H. (2013). Screening for long-lived genes identifies Oga1, a guanine-quadruplex associated protein that affects the chronological lifespan of the fission yeast Schizosaccharomyces pombe. Mol. Genet. Genomics MGG *288*, 285–295.

Omosigho, N.N., Swaminathan, K., Plomann, M., Müller-Taubenberger, A., Noegel, A.A., and Riyahi, T.Y. (2014). The Dictyostelium discoideum RACK1 orthologue has roles in growth and development. Cell Commun. Signal. CCS *12*, 37.

Ong, S.-E., Blagoev, B., Kratchmarova, I., Kristensen, D.B., Steen, H., Pandey, A., and Mann, M. (2002). Stable isotope labeling by amino acids in cell culture, SILAC, as a simple and accurate approach to expression proteomics. Mol. Cell. Proteomics *1*, 376–386.

Onishi, I., Lin, P.J.C., Diering, G.H., Williams, W.P., and Numata, M. (2007). RACK1 associates with NHE5 in focal adhesions and positively regulates the transporter activity. Cell. Signal. *19*, 194–203.

Oowatari, Y., Jeong, H., Tanae, K., Nakagawa, T., and Kawamukai, M. (2011). Regulation and role of an RNA-binding protein Msa2 in controlling the sexual differentiation of fission yeast. Curr. Genet. *57*, 191–200.

Ossareh-Nazari, B., Bonizec, M., Cohen, M., Dokudovskaya, S., Delalande, F., Schaeffer, C., Van Dorsselaer, A., and Dargemont, C. (2010). Cdc48 and Ufd3, new partners of the ubiquitin protease Ubp3, are required for ribophagy. EMBO Rep. *11*, 548–554.

Ossareh-Nazari, B., Niño, C.A., Bengtson, M.H., Lee, J.-W., Joazeiro, C.A.P., and Dargemont, C. (2014). Ubiquitylation by the Ltn1 E3 ligase protects 60S ribosomes from starvation-induced selective autophagy. J. Cell Biol. *204*, 909–917.

Otsuka, M., Takata, A., Yoshikawa, T., Kojima, K., Kishikawa, T., Shibata, C., Takekawa, M., Yoshida, H., Omata, M., and Koike, K. (2011). Receptor for activated protein kinase C: requirement for efficient microRNA function and reduced expression in hepatocellular carcinoma. PloS One *6*, e24359.

Padanilam, B.J., and Hammerman, M.R. (1997). Ischemia-induced receptor for activated C kinase (RACK1) expression in rat kidneys. Am. J. Physiol. *272*, F160-166.

Palecek, J., Hasek, J., and Ruis, H. (2001). Rpg1p/Tif32p, a subunit of translation initiation factor 3, interacts with actin-associated protein Sla2p. Biochem. Biophys. Res. Commun. *282*, 1244–1250.

Palmer, D.A., Thompson, J.K., Li, L., Prat, A., and Wang, P. (2006). Gib2, a novel Gbeta-like/RACK1 homolog, functions as a Gbeta subunit in cAMP signaling and is essential in Cryptococcus neoformans. J. Biol. Chem. *281*, 32596–32605.

Pan, C.Q., Sudol, M., Sheetz, M., and Low, B.C. (2012). Modularity and functional plasticity of scaffold proteins as p(l)acemakers in cell signaling. Cell. Signal. *24*, 2143–2165.

Panasenko, O.O., and Collart, M.A. (2012). Presence of Not5 and ubiquitinated Rps7A in polysome fractions depends upon the Not4 E3 ligase. Mol. Microbiol. *83*, 640–653.

Paquin, N., Ménade, M., Poirier, G., Donato, D., Drouet, E., and Chartrand, P. (2007). Local activation of yeast ASH1 mRNA translation through phosphorylation of Khd1p by the casein kinase Yck1p. Mol. Cell *26*, 795–809.

Park, Y.-U., Hur, H., Ka, M., and Kim, J. (2006). Identification of translational regulation target genes during filamentous growth in Saccharomyces cerevisiae: regulatory role of Caf20 and Dhh1. Eukaryot. Cell *5*, 2120–2127.

Parsons, A.B., Brost, R.L., Ding, H., Li, Z., Zhang, C., Sheikh, B., Brown, G.W., Kane, P.M., Hughes, T.R., and Boone, C. (2004). Integration of chemical-genetic and genetic interaction data links bioactive compounds to cellular target pathways. Nat. Biotechnol. *22*, 62–69.

Pascale, A., Fortino, I., Govoni, S., Trabucchi, M., Wetsel, W.C., and Battaini, F. (1996). Functional impairment in protein kinase C by RACK1 (receptor for activated C kinase 1) deficiency in aged rat brain cortex. J. Neurochem. *67*, 2471–2477.

Pertschy, B., Schneider, C., Gnädig, M., Schäfer, T., Tollervey, D., and Hurt, E. (2009). RNA helicase Prp43 and its co-factor Pfa1 promote 20 to 18 S rRNA processing catalyzed by the endonuclease Nob1. J. Biol. Chem. *284*, 35079–35091.

Phalip, V., Kuhn, I., Lemoine, Y., and Jeltsch, J.M. (1999). Characterization of the biotin biosynthesis pathway in Saccharomyces cerevisiae and evidence for a cluster containing BIO5, a novel gene involved in vitamer uptake. Gene *232*, 43–51.

Qu, L.H., Henry, Y., Nicoloso, M., Michot, B., Azum, M.C., Renalier, M.H., Caizergues-Ferrer, M., and Bachellerie, J.P. (1995). U24, a novel intron-encoded small nucleolar RNA with two 12 nt long, phylogenetically conserved complementarities to 28S rRNA. Nucleic Acids Res. *23*, 2669–2676.

Rabl, J., Leibundgut, M., Ataide, S.F., Haag, A., and Ban, N. (2011). Crystal structure of the eukaryotic 40S ribosomal subunit in complex with initiation factor 1. Science *331*, 730–736.

Rachfall, N., Schmitt, K., Bandau, S., Smolinski, N., Ehrenreich, A., Valerius, O., and Braus, G.H. (2013). RACK1/Asc1p, a ribosomal node in cellular signaling. Mol. Cell. Proteomics *12*, 87–105.

Rappsilber, J., Ishihama, Y., and Mann, M. (2003). Stop and go extraction tips for matrix-assisted laser desorption/ionization, nanoelectrospray, and LC/MS sample pretreatment in proteomics. Anal. Chem. *75*, 663–670.

Rappsilber, J., Mann, M., and Ishihama, Y. (2007). Protocol for micro-purification, enrichment, pre-fractionation and storage of peptides for proteomics using StageTips. Nat. Protoc. *2*, 1896–1906.

Regmi, S., Rothberg, K.G., Hubbard, J.G., and Ruben, L. (2008). The RACK1 signal anchor protein from Trypanosoma brucei associates with eukaryotic elongation factor 1A: a role for translational control in cytokinesis. Mol. Microbiol. *70*, 724–745.

Richardson, R., Denis, C.L., Zhang, C., Nielsen, M.E.O., Chiang, Y.-C., Kierkegaard, M., Wang, X., Lee, D.J., Andersen, J.S., and Yao, G. (2012). Mass spectrometric

identification of proteins that interact through specific domains of the poly(A) binding protein. Mol. Genet. Genomics MGG *287*, 711–730.

Rigas, A.C., Ozanne, D.M., Neal, D.E., and Robson, C.N. (2003). The scaffolding protein RACK1 interacts with androgen receptor and promotes cross-talk through a protein kinase C signaling pathway. J. Biol. Chem. *278*, 46087–46093.

Robles, M.S., Boyault, C., Knutti, D., Padmanabhan, K., and Weitz, C.J. (2010). Identification of RACK1 and protein kinase Calpha as integral components of the mammalian circadian clock. Science *327*, 463–466.

Rojas, M., Farr, G.W., Fernandez, C.F., Lauden, L., McCormack, J.C., and Wolin, S.L. (2012). Yeast Gis2 and its human ortholog CNBP are novel components of stress-induced RNP granules. PloS One *7*, e52824.

Ron, D., Chen, C.H., Caldwell, J., Jamieson, L., Orr, E., and Mochly-Rosen, D. (1994). Cloning of an intracellular receptor for protein kinase C: a homolog of the beta subunit of G proteins. Proc. Natl. Acad. Sci. U. S. A. *91*, 839–843.

Ron, D., Luo, J., and Mochly-Rosen, D. (1995). C2 region-derived peptides inhibit translocation and function of beta protein kinase C in vivo. J. Biol. Chem. *270*, 24180–24187.

Ron, D., Jiang, Z., Yao, L., Vagts, A., Diamond, I., and Gordon, A. (1999). Coordinated movement of RACK1 with activated betaIIPKC. J. Biol. Chem. *274*, 27039–27046.

Rosdahl, J.A., Mourton, T.L., and Brady-Kalnay, S.M. (2002). Protein kinase C delta (PKCdelta) is required for protein tyrosine phosphatase mu (PTPmu)-dependent neurite outgrowth. Mol. Cell. Neurosci. *19*, 292–306.

Ross, D., Saxena, M., and Altmann, M. (2012). eIF4E is an important determinant of adhesion and pseudohyphal growth of the yeast S. cerevisiae. PloS One *7*, e50773.

Rothberg, K.G., Burdette, D.L., Pfannstiel, J., Jetton, N., Singh, R., and Ruben, L. (2006). The RACK1 homologue from Trypanosoma brucei is required for the onset and progression of cytokinesis. J. Biol. Chem. *281*, 9781–9790.

Röther, S., Burkert, C., Brünger, K.M., Mayer, A., Kieser, A., and Strässer, K. (2010). Nucleocytoplasmic shuttling of the La motif-containing protein Sro9 might link its nuclear and cytoplasmic functions. RNA N. Y. N *16*, 1393–1401.

Roux, K.J., Kim, D.I., Raida, M., and Burke, B. (2012). A promiscuous biotin ligase fusion protein identifies proximal and interacting proteins in mammalian cells. J. Cell Biol. *196*, 801–810.

Ruan, Y., Sun, L., Hao, Y., Wang, L., Xu, J., Zhang, W., Xie, J., Guo, L., Zhou, L., Yun, X., et al. (2012). Ribosomal RACK1 promotes chemoresistance and growth in human hepatocellular carcinoma. J. Clin. Invest. *122*, 2554–2566.

Ruiz Carrillo, D., Chandrasekaran, R., Nilsson, M., Cornvik, T., Liew, C.W., Tan, S.M., and Lescar, J. (2012). Structure of human Rack1 protein at a resolution of 2.45 Å. Acta Crystallograph. Sect. F Struct. Biol. Cryst. Commun. *68*, 867–872.

Sabila, M., Kundu, N., Smalls, D., and Ullah, H. (2016). Tyrosine Phosphorylation Based Homo-dimerization of Arabidopsis RACK1A Proteins Regulates Oxidative Stress Signaling Pathways in Yeast. Front. Plant Sci. *7*, 176.

Saiki, R.K., Scharf, S., Faloona, F., Mullis, K.B., Horn, G.T., Erlich, H.A., and Arnheim, N. (1985). Enzymatic amplification of beta-globin genomic sequences and restriction site analysis for diagnosis of sickle cell anemia. Science *230*, 1350–1354.

Salvi, J.S., Chan, J.N.Y., Szafranski, K., Liu, T.T., Wu, J.D., Olsen, J.B., Khanam, N., Poon, B.P.K., Emili, A., and Mekhail, K. (2014). Roles for Pbp1 and caloric restriction in genome and lifespan maintenance via suppression of RNA-DNA hybrids. Dev. Cell *30*, 177–191.

Sammons, M.A., Samir, P., and Link, A.J. (2011). Saccharomyces cerevisiae Gis2 interacts with the translation machinery and is orthogonal to myotonic dystrophy type 2 protein ZNF9. Biochem. Biophys. Res. Commun. *406*, 13–19.

Satoh, R., Tanaka, A., Kita, A., Morita, T., Matsumura, Y., Umeda, N., Takada, M., Hayashi, S., Tani, T., Shinmyozu, K., et al. (2012). Role of the RNA-binding protein Nrd1 in stress granule formation and its implication in the stress response in fission yeast. PloS One *7*, e29683.

Schenk, L., Meinel, D.M., Strässer, K., and Gerber, A.P. (2012). La-motif-dependent mRNA association with Slf1 promotes copper detoxification in yeast. RNA N. Y. N *18*, 449–461.

Scherrer, T., Femmer, C., Schiess, R., Aebersold, R., and Gerber, A.P. (2011). Defining potentially conserved RNA regulons of homologous zinc-finger RNA-binding proteins. Genome Biol. *12*, R3.

Schlesinger, M.B., and Formosa, T. (2000). POB3 is required for both transcription and replication in the yeast Saccharomyces cerevisiae. Genetics *155*, 1593–1606.

Schmitt, K. (2015). Ribosomal Asc1p/RACK1 in the phosphorylation signaling network of Saccharomyces cerevisiae. Dissertation, Georg-August-University Göttingen.

Schmitt, K., Smolinski, N., Neumann, P., Schmaul, S., Hofer-Pretz, V., Braus, G.H., and Valerius, O. (2017). Asc1p/RACK1 Connects Ribosomes to Eukaryotic Phosphosignaling. Mol. Cell. Biol. *37,* e00279-16.

Schütz, S., Fischer, U., Altvater, M., Nerurkar, P., Peña, C., Gerber, M., Chang, Y., Caesar, S., Schubert, O.T., Schlenstedt, G., et al. (2014). A RanGTP-independent mechanism allows ribosomal protein nuclear import for ribosome assembly. ELife *3*, e03473.

Schwabish, M.A., and Struhl, K. (2004). Evidence for eviction and rapid deposition of histones upon transcriptional elongation by RNA polymerase II. Mol. Cell. Biol. *24*, 10111–10117.

Sengupta, J., Nilsson, J., Gursky, R., Spahn, C.M.T., Nissen, P., and Frank, J. (2004). Identification of the versatile scaffold protein RACK1 on the eukaryotic ribosome by cryo-EM. Nat. Struct. Mol. Biol. *11*, 957–962.

Serrels, B., Sandilands, E., Serrels, A., Baillie, G., Houslay, M.D., Brunton, V.G., Canel, M., Machesky, L.M., Anderson, K.I., and Frame, M.C. (2010). A complex between FAK, RACK1, and PDE4D5 controls spreading initiation and cancer cell polarity. Curr. Biol. CB *20*, 1086–1092.

Sezen, B., Seedorf, M., and Schiebel, E. (2009). The SESA network links duplication of the yeast centrosome with the protein translation machinery. Genes Dev. *23*, 1559–1570.

Sharifulin, D., Khairulina, Y., Ivanov, A., Meschaninova, M., Ven'yaminova, A., Graifer, D., and Karpova, G. (2012). A central fragment of ribosomal protein S26 containing the eukaryote-specific motif YxxPKxYxK is a key component of the ribosomal binding site of mRNA region 5' of the E site codon. Nucleic Acids Res. *40*, 3056–3065.

Sharma, G., Pallesen, J., Das, S., Grassucci, R., Langlois, R., Hampton, C.M., Kelly, D.F., des Georges, A., and Frank, J. (2013). Affinity grid-based cryo-EM of PKC binding to RACK1 on the ribosome. J. Struct. Biol. *181*, 190–194.

Shaw, A.S., and Filbert, E.L. (2009). Scaffold proteins and immune-cell signalling. Nat. Rev. Immunol. *9*, 47–56.

Shen, Z., St-Denis, A., and Chartrand, P. (2010). Cotranscriptional recruitment of She2p by RNA pol II elongation factor Spt4-Spt5/DSIF promotes mRNA localization to the yeast bud. Genes Dev. *24*, 1914–1926.

Shevchenko, A., Wilm, M., Vorm, O., and Mann, M. (1996). Mass spectrometric sequencing of proteins silver-stained polyacrylamide gels. Anal. Chem. *68*, 850–858.

Shor, B., Calaycay, J., Rushbrook, J., and McLeod, M. (2003). Cpc2/RACK1 is a ribosome-associated protein that promotes efficient translation in Schizosaccharomyces pombe. J. Biol. Chem. *278*, 49119–49128.

Sinha, H., David, L., Pascon, R.C., Clauder-Münster, S., Krishnakumar, S., Nguyen, M., Shi, G., Dean, J., Davis, R.W., Oefner, P.J., et al. (2008). Sequential elimination of major-effect contributors identifies additional quantitative trait loci conditioning high-temperature growth in yeast. Genetics *180*, 1661–1670.

Smith, T.F., Gaitatzes, C., Saxena, K., and Neer, E.J. (1999). The WD repeat: a common architecture for diverse functions. Trends Biochem. Sci. *24*, 181–185.

Sobel, S.G., and Wolin, S.L. (1999). Two Yeast La Motif-containing Proteins Are RNA-binding Proteins that Associate with Polyribosomes. Mol. Biol. Cell *10*, 3849–3862.

Solé, C., Nadal-Ribelles, M., Kraft, C., Peter, M., Posas, F., and de Nadal, E. (2011). Control of Ubp3 ubiquitin protease activity by the Hog1 SAPK modulates transcription upon osmostress. EMBO J. *30*, 3274–3284.

Sonenberg, N., and Hinnebusch, A.G. (2009). Regulation of translation initiation in eukaryotes: mechanisms and biological targets. Cell *136*, 731–745.

Southern, E.M. (1975). Detection of specific sequences among DNA fragments separated by gel electrophoresis. J. Mol. Biol. *98*, 503–517.

Speth, C., Willing, E.-M., Rausch, S., Schneeberger, K., and Laubinger, S. (2013). RACK1 scaffold proteins influence miRNA abundance in Arabidopsis. Plant J. Cell Mol. Biol. *76*, 433–445.

Steele, M.R., McCahill, A., Thompson, D.S., MacKenzie, C., Isaacs, N.W., Houslay, M.D., and Bolger, G.B. (2001). Identification of a surface on the beta-propeller protein RACK1 that interacts with the cAMP-specific phosphodiesterase PDE4D5. Cell. Signal. *13*, 507–513.

Stirnimann, C.U., Petsalaki, E., Russell, R.B., and Müller, C.W. (2010). WD40 proteins propel cellular networks. Trends Biochem. Sci. *35*, 565–574.

Stolz, J., Hoja, U., Meier, S., Sauer, N., and Schweizer, E. (1999). Identification of the plasma membrane H+-biotin symporter of Saccharomyces cerevisiae by rescue of a fatty acid-auxotrophic mutant. J. Biol. Chem. *274*, 18741–18746.

Strittmatter, A.W., Fischer, C., Kleinschmidt, M., and Braus, G.H. (2006). FLO11 mediated filamentous growth of the yeast Saccharomyces cerevisiae depends on the expression of the ribosomal RPS26 genes. Mol. Genet. Genomics MGG *276*, 113–125.

Strunk, B.S., and Karbstein, K. (2009). Powering through ribosome assembly. RNA N. Y. N *15*, 2083–2104.

Strunk, B.S., Loucks, C.R., Su, M., Vashisth, H., Cheng, S., Schilling, J., Brooks, C.L., Karbstein, K., and Skiniotis, G. (2011). Ribosome assembly factors prevent premature translation initiation by 40S assembly intermediates. Science *333*, 1449–1453.

Strunk, B.S., Novak, M.N., Young, C.L., and Karbstein, K. (2012). A translation-like cycle is a quality control checkpoint for maturing 40S ribosome subunits. Cell *150*, 111–121.

Stundon, J.L., and Zakian, V.A. (2015). Identification of Saccharomyces cerevisiae Genes Whose Deletion Causes Synthetic Effects in Cells with Reduced Levels of the Nuclear Pif1 DNA Helicase. G3 Bethesda Md *5*, 2913–2918.

Swisher, K.D., and Parker, R. (2010). Localization to, and effects of Pbp1, Pbp4, Lsm12, Dhh1, and Pab1 on stress granules in Saccharomyces cerevisiae. PloS One *5*, e10006.

Szamecz, B., Rutkai, E., Cuchalová, L., Munzarová, V., Herrmannová, A., Nielsen, K.H., Burela, L., Hinnebusch, A.G., and Valášek, L. (2008). eIF3a cooperates with sequences 5' of uORF1 to promote resumption of scanning by post-termination ribosomes for reinitiation on GCN4 mRNA. Genes Dev. *22*, 2414–2425.

Tadauchi, T., Inada, T., Matsumoto, K., and Irie, K. (2004). Posttranscriptional regulation of HO expression by the Mkt1-Pbp1 complex. Mol. Cell. Biol. *24*, 3670–3681.

Takahara, T., and Maeda, T. (2012). Transient sequestration of TORC1 into stress granules during heat stress. Mol. Cell *47*, 242–252.

Takemaru, K., Harashima, S., Ueda, H., and Hirose, S. (1998). Yeast Coactivator MBF1 Mediates GCN4-Dependent Transcriptional Activation. Mol. Cell. Biol. *18*, 4971–4976.

Tardiff, D.F., Abruzzi, K.C., and Rosbash, M. (2007). Protein characterization of Saccharomyces cerevisiae RNA polymerase II after in vivo cross-linking. Proc. Natl. Acad. Sci. U. S. A. *104*, 19948–19953.

Tarnowski, K., Fituch, K., Szczepanowski, R.H., Dadlez, M., and Kaus-Drobek, M. (2014). Patterns of structural dynamics in RACK1 protein retained throughout evolution: a hydrogen-deuterium exchange study of three orthologs. Protein Sci. Publ. Protein Soc. *23*, 639–651.

Thompson, M.K., Rojas-Duran, M.F., Gangaramani, P., and Gilbert, W.V. (2016). The ribosomal protein Asc1/RACK1 is required for efficient translation of short mRNAs. ELife *5*, e11154.

Thornton, C., Tang, K.-C., Phamluong, K., Luong, K., Vagts, A., Nikanjam, D., Yaka, R., and Ron, D. (2004). Spatial and temporal regulation of RACK1 function and N-methyl-D-aspartate receptor activity through WD40 motif-mediated dimerization. J. Biol. Chem. *279*, 31357–31364.

Tkach, J.M., Yimit, A., Lee, A.Y., Riffle, M., Costanzo, M., Jaschob, D., Hendry, J.A., Ou, J., Moffat, J., Boone, C., et al. (2012). Dissecting DNA damage response pathways by analysing protein localization and abundance changes during DNA replication stress. Nat. Cell Biol. *14*, 966–976.

Ullah, H., Scappini, E.L., Moon, A.F., Williams, L.V., Armstrong, D.L., and Pedersen, L.C. (2008). Structure of a signal transduction regulator, RACK1, from Arabidopsis thaliana. Protein Sci. Publ. Protein Soc. *17*, 1771–1780.

Valerius, O., Kleinschmidt, M., Rachfall, N., Schulze, F., López Marín, S., Hoppert, M., Streckfuss-Bömeke, K., Fischer, C., and Braus, G.H. (2007). The Saccharomyces homolog of mammalian RACK1, Cpc2/Asc1p, is required for FLO11-dependent adhesive growth and dimorphism. Mol. Cell. Proteomics *6*, 1968–1979.

Van Dyke, M.W., Nelson, L.D., Weilbaecher, R.G., and Mehta, D.V. (2004). Stm1p, a G4 quadruplex and purine motif triplex nucleic acid-binding protein, interacts with ribosomes and subtelomeric Y' DNA in Saccharomyces cerevisiae. J. Biol. Chem. *279*, 24323–24333.

Van Dyke, N., Baby, J., and Van Dyke, M.W. (2006). Stm1p, a ribosome-associated protein, is important for protein synthesis in Saccharomyces cerevisiae under nutritional stress conditions. J. Mol. Biol. *358*, 1023–1031.

Van Dyke, N., Chanchorn, E., and Van Dyke, M.W. (2013). The Saccharomyces cerevisiae protein Stm1p facilitates ribosome preservation during quiescence. Biochem. Biophys. Res. Commun. *430*, 745–750.

Vani, K., Yang, G., and Mohler, J. (1997). Isolation and cloning of a Drosophila homolog to the mammalian RACK1 gene, implicated in PKC-mediated signalling. Biochim. Biophys. Acta *1358*, 67–71.

Viktorovskaya, O.V., Appling, F.D., and Schneider, D.A. (2011). Yeast transcription elongation factor Spt5 associates with RNA polymerase I and RNA polymerase II directly. J. Biol. Chem. *286*, 18825–18833.

Volta, V., Beugnet, A., Gallo, S., Magri, L., Brina, D., Pesce, E., Calamita, P., Sanvito, F., and Biffo, S. (2013). RACK1 depletion in a mouse model causes lethality, pigmentation deficits and reduction in protein synthesis efficiency. Cell. Mol. Life Sci. CMLS *70*, 1439–1450.

Vomastek, T., Iwanicki, M.P., Schaeffer, H.-J., Tarcsafalvi, A., Parsons, J.T., and Weber, M.J. (2007). RACK1 targets the extracellular signal-regulated kinase/mitogen-activated protein kinase pathway to link integrin engagement with focal adhesion disassembly and cell motility. Mol. Cell. Biol. *27*, 8296–8305.

Vondriska, T.M., Pass, J.M., and Ping, P. (2004). Scaffold proteins and assembly of multiprotein signaling complexes. J. Mol. Cell. Cardiol. *37*, 391–397.

Voss, S., and Skerra, A. (1997). Mutagenesis of a flexible loop in streptavidin leads to higher affinity for the Strep-tag II peptide and improved performance in recombinant protein purification. Protein Eng. *10*, 975–982.

Wada, A., Yamazaki, Y., Fujita, N., and Ishihama, A. (1990). Structure and probable genetic location of a "ribosome modulation factor" associated with 100S ribosomes in stationary-phase Escherichia coli cells. Proc. Natl. Acad. Sci. U. S. A. *87*, 2657–2661.

Walker, S.E., Zhou, F., Mitchell, S.F., Larson, V.S., Valasek, L., Hinnebusch, A.G., and Lorsch, J.R. (2013). Yeast eIF4B binds to the head of the 40S ribosomal subunit and promotes mRNA recruitment through its N-terminal and internal repeat domains. RNA N. Y. N *19*, 191–207.

Wang, X., and Chen, X.J. (2015). A cytosolic network suppressing mitochondria-mediated proteostatic stress and cell death. Nature *524*, 481–484.

Wang, Y., and Dohlman, H.G. (2002). Pheromone-dependent ubiquitination of the mitogen-activated protein kinase kinase Ste7. J. Biol. Chem. *277*, 15766–15772.

Wang, L., Brock, A., Herberich, B., and Schultz, P.G. (2001). Expanding the genetic code of Escherichia coli. Science *292*, 498–500.

Wang, L., Berndt, P., Xia, X., Kahnt, J., and Kahmann, R. (2011). A seven-WD40 protein related to human RACK1 regulates mating and virulence in Ustilago maydis. Mol. Microbiol. *81*, 1484–1498.

Wang, S., Chen, J.-Z., Zhang, Z., Gu, S., Ji, C., Tang, R., Ying, K., Xie, Y., and Mao, Y. (2003). Cloning, expression and genomic structure of a novel human GNB2L1 gene, which encodes a receptor of activated protein kinase C (RACK). Mol. Biol. Rep. *30*, 53–60.

Wang, Y., Zhu, M., Ayalew, M., and Ruff, J.A. (2008). Down-regulation of Pkc1-mediated signaling by the deubiquitinating enzyme Ubp3. J. Biol. Chem. *283*, 1954–1961.

Wang, Y., Shen, G., Gong, J., Shen, D., Whittington, A., Qing, J., Treloar, J., Boisvert, S., Zhang, Z., Yang, C., et al. (2014). Noncanonical Gβ Gib2 is a scaffolding protein promoting cAMP signaling through functions of Ras1 and Cac1 proteins in Cryptococcus neoformans. J. Biol. Chem. *289*, 12202–12216.

Warner, J.R. (1999). The economics of ribosome biosynthesis in yeast. Trends Biochem. Sci. *24*, 437–440.

Wehner, P., Shnitsar, I., Urlaub, H., and Borchers, A. (2011). RACK1 is a novel interaction partner of PTK7 that is required for neural tube closure. Dev. Camb. Engl. *138*, 1321–1327.

Weidner, J., Wang, C., Prescianotto-Baschong, C., Estrada, A.F., and Spang, A. (2014). The polysome-associated proteins Scp160 and Bfr1 prevent P body formation under normal growth conditions. J. Cell Sci. *127*, 1992–2004.

van Werven, F.J., and Timmers, H.T.M. (2006). The use of biotin tagging in Saccharomyces cerevisiae improves the sensitivity of chromatin immunoprecipitation. Nucleic Acids Res. *34*, e33.

Wessel, D., and Flügge, U.I. (1984). A method for the quantitative recovery of protein in dilute solution in the presence of detergents and lipids. Anal. Biochem. *138*, 141–143.

Wilmes, G.M., Bergkessel, M., Bandyopadhyay, S., Shales, M., Braberg, H., Cagney, G., Collins, S.R., Whitworth, G.B., Kress, T.L., Weissman, J.S., et al. (2008). A genetic interaction map of RNA-processing factors reveals links between Sem1/Dss1-containing complexes and mRNA export and splicing. Mol. Cell *32*, 735–746.

Wilson, K.P., Shewchuk, L.M., Brennan, R.G., Otsuka, A.J., and Matthews, B.W. (1992). Escherichia coli biotin holoenzyme synthetase/bio repressor crystal structure delineates the biotin- and DNA-binding domains. Proc. Natl. Acad. Sci. U. S. A. *89*, 9257–9261.

Wilson, M.D., Harreman, M., Taschner, M., Reid, J., Walker, J., Erdjument-Bromage, H., Tempst, P., and Svejstrup, J.Q. (2013). Proteasome-mediated processing of Def1, a critical step in the cellular response to transcription stress. Cell *154*, 983–995.

Wittmeyer, J., and Formosa, T. (1997). The Saccharomyces cerevisiae DNA polymerase alpha catalytic subunit interacts with Cdc68/Spt16 and with Pob3, a protein similar to an HMG1-like protein. Mol. Cell. Biol. *17*, 4178–4190.

Wolf, A.S., and Grayhack, E.J. (2015). Asc1, homolog of human RACK1, prevents frameshifting in yeast by ribosomes stalled at CGA codon repeats. RNA N. Y. N *21*, 935–945.

Won, M., Park, S.K., Hoe, K.L., Jang, Y.J., Chung, K.S., Kim, D.U., Kim, H.B., and Yoo, H.S. (2001). Rkp1/Cpc2, a fission yeast RACK1 homolog, is involved in actin cytoskeleton organization through protein kinase C, Pck2, signaling. Biochem. Biophys. Res. Commun. *282*, 10–15.

Woodcock, D.M., Crowther, P.J., Doherty, J., Jefferson, S., DeCruz, E., Noyer-Weidner, M., Smith, S.S., Michael, M.Z., and Graham, M.W. (1989). Quantitative evaluation of Escherichia coli host strains for tolerance to cytosine methylation in plasmid and phage recombinants. Nucleic Acids Res. *17*, 3469–3478.

Woudstra, E.C., Gilbert, C., Fellows, J., Jansen, L., Brouwer, J., Erdjument-Bromage, H., Tempst, P., and Svejstrup, J.Q. (2002). A Rad26-Def1 complex coordinates repair and RNA pol II proteolysis in response to DNA damage. Nature *415*, 929–933.

Xu, C., and Min, J. (2011). Structure and function of WD40 domain proteins. Protein Cell *2*, 202–214.

Yaka, R., Thornton, C., Vagts, A.J., Phamluong, K., Bonci, A., and Ron, D. (2002). NMDA receptor function is regulated by the inhibitory scaffolding protein, RACK1. Proc. Natl. Acad. Sci. U. S. A. *99*, 5710–5715.

Yaka, R., He, D.-Y., Phamluong, K., and Ron, D. (2003). Pituitary adenylate cyclase-activating polypeptide (PACAP(1-38)) enhances N-methyl-D-aspartate receptor function and brain-derived neurotrophic factor expression via RACK1. J. Biol. Chem. *278*, 9630–9638.

Yarwood, S.J., Steele, M.R., Scotland, G., Houslay, M.D., and Bolger, G.B. (1999). The RACK1 signaling scaffold protein selectively interacts with the cAMP-specific phosphodiesterase PDE4D5 isoform. J. Biol. Chem. *274*, 14909–14917.

Yatime, L., Hein, K.L., Nilsson, J., and Nissen, P. (2011). Structure of the RACK1 dimer from Saccharomyces cerevisiae. J. Mol. Biol. *411*, 486–498.

Yu, J., Zhu, D., Chang, Y., and Zhao, Q. (2014). Maize ZmRACK1 is involved in the plant response to fungal phytopathogens. Int. J. Mol. Sci. *15*, 9343–9359.

Yu, W., Farrell, R.A., Stillman, D.J., and Winge, D.R. (1996). Identification of SLF1 as a new copper homeostasis gene involved in copper sulfide mineralization in Saccharomyces cerevisiae. Mol. Cell. Biol. *16*, 2464–2472.

Zeller, C.E., Parnell, S.C., and Dohlman, H.G. (2007). The RACK1 ortholog Asc1 functions as a G-protein beta subunit coupled to glucose responsiveness in yeast. J. Biol. Chem. *282*, 25168–25176.

Zhang, D., Chen, L., Li, D., Lv, B., Chen, Y., Chen, J., XuejiaoYan, null, and Liang, J. (2014). OsRACK1 is involved in abscisic acid- and H2O2-mediated signaling to regulate seed germination in rice (Oryza sativa, L.). PloS One *9*, e97120.

Zhang, W., Zong, C.S., Hermanto, U., Lopez-Bergami, P., Ronai, Z., and Wang, L.-H. (2006). RACK1 recruits STAT3 specifically to insulin and insulin-like growth factor 1 receptors for activation, which is important for regulating anchorage-independent growth. Mol. Cell. Biol. *26*, 413–424.

Online databases

http://www.yeastgenome.org

http://smart.embl-heidelberg.de

http://www.uniprot.org

http://www.rcsb.org

http://www.genome.jp/kegg/pathway.html

Online databases

6. Supplementary Material

Tab. S1: Oligonucleotides used as primers in this study.

identifier	sequence	application
NS90	AAGGATAACACCGTGCCACT (fw)	*ASC1-birA** cloning
NS91	ATTACATGACTCGAGTTATTTTTCTGCACTACGCA (rv)	
NS93	CCGCTCGAGTCATGTAATTA (fw)	
NS94	AGTGGCACGGTGTTATCCTTAGAAGAACCAGAAGAACCA GAAGAACCAGAAGAACCGTTAGCAGTCATAACTTGCC (rv)	
NS96	ATGAAGGATAACACCGTGCCACT (fw)	*birA** cloning
NS97	GGTGTTATCCTTCATGAATTCCTGCAGCCCGGGGG (rv)	
NS152	GTTGTCCGCTTCCGATGATGAAACTTTGATCTCCTGG (fw)	*asc1^DE^-birA** cloning
NS153	CCAGGAGATCAAAGTTTCATCATCGGAAGCGGACAAC (rv)	
BP24*	TGGCCACTTTGTTGGGTCAC (fw)	*ASC1* sequencing
NS32	TCATCAGAGATCTTGGTGATAATTGG (rv)	
NS95	GCAGGAAGCGGGGATCAATC (fw)	*birA** sequencing
NS98	CGATCGAGATTGATCCCCGC (rv)	
ASC1_ natP**	CAGAGCTCATTAGCATTATGAATTGGAACC (fw)	cloning of pME4481
NS03	TGTCACGCTTACATTCACGCCCTC (rv)	
NS58	TTGGAAGGTCACTAGGGTTGGGTCACA (fw)	N17Amber
NS59	TGTGACCCAACCCTAGTGACCTTCCAA (rv)	
NS107	TCTGCTGGTCAATAGAACCTATTGTTG (fw)	P30Amber
NS108	CAACAATAGGTTCTATTGACCAGCAGA (rv)	
NS109	TTGACTGGTGACTAGCAAAAGTTTGGT (fw)	D51Amber
NS110	ACCAAACTTTTGCTAGTCACCAGTCAA (rv)	
NS111	GACGACCAAAAGTAGGGTGTCCCAGTT (fw)	F54Amber
NS112	AACTGGGACACCCTACTTTTGGTCGTC (rv)	
NS60	GTTAGATCTTTCTAGGGTCACAGTCAC (fw)	K62Amber
NS61	GTGACTGTGACCCTAGAAAGATCTAAC (rv)	
NS62	GGTCACAGTCACTAGGTCCAAGACTGT (fw)	I67Amber
NS63	ACAGTCTTGGACCTAGTGACTGTGACC (rv)	
NS113	TGTACTTTGACTTAGGACGGTGCTTAC (fw)	A75Amber
NS114	GTAAGCACCGTCCTAAGTCAAAGTACA (rv)	
NS64	GCTTCTTGGGACTAGACCTTGAGATTA (fw)	K87Amber
NS65	TAATCTCAAGGTCTAGTCCCAAGAAGC (rv)	
NS115	TTATGGGATGTTTAGACCGGTGAAACC (fw)	A95Amber
NS116	GGTTTCACCGGTCTAAACATCCCATAA (rv)	
NS66	TTCGTCGGTCACTAGTCCGATGTTATG (fw)	K107Amber
NS67	CATAACATCGGACTAGTGACCGACGAA (rv)	
NS117	GACATTGACAAGTAGGCTTCCATGATT (fw)	K118Amber
NS118	AATCATGGAAGCCTACTTGTCAATGTC (rv)	
NS68	GGTTCCCGTGACTAGACCATCAAGGTC (fw)	K129Amber
NS69	GACCTTGATGGTCTAGTCACGGGAACC (rv)	
NS119	GTCTGGACCATCTAGGGTCAATGTTTG (fw)	K137Amber
NS120	CAAACATTGACCCTAGATGGTCCAGAC (rv)	
NS121	ACCATCAAAGGTTAGTGTTTGGCCACT (fw)	Q139Amber
NS122	AGTGGCCAAACACTAACCTTTGATGGT (rv)	

amino acid exchanges in Asc1p and Asc1p-Strep for Bpa cross-linking

Tab. S1: Continued.

identifier	sequence	application	
NS70	TTGTTGGGTCACTAGGACTGGGTTTCC (fw)	N148Amber	amino acid exchanges in Asc1p and Asc1p-Strep for Bpa cross-linking
NS71	GGAAACCCAGTCCTAGTGACCCAACAA (rv)		
NS123	GTTCCAAACGAATAGGCTGATGATGAC (fw)	K161Amber	
NS124	GTCATCATCAGCCTATTCGTTTGGAAC (rv)		
NS125	AAAGCTGATGATTAGTCTGTCACCATC (fw)	D165Amber	
NS126	GATGGTGACAGACTAATCATCAGCTTT (rv)		
NS72	ATTTCTGCCGGTTAGGACAAAATGGTT (fw)	N174Amber	
NS73	AACCATTTTGTCCTAACCGGCAGAAAT (rv)		
NS127	AACTTAAACCAATAGCAAATTGAAGCT (fw)	F186Amber	
NS128	AGCTTCAATTTGCTATTGGTTTAAGTT (rv)		
NS74	TTCATCGGTCACTAGTCCAACATCAAC (fw)	N196Amber	
NS75	GTTGATGTTGGACTAGTGACCGATGAA (rv)		
NS129	TCCCCAGACGGATAGTTGATTGCTTCC (fw)	T209Amber	
NS130	GGAAGCAATCAACTATCCGTCTGGGGA (rv)		
NS131	TTGTGGAACTTGTAGGCTAAGAAGGCT (fw)	A226Amber	
NS132	AGCCTTCTTAGCCTACAAGTTCCACAA (rv)		
NS133	AACTTGGCTGCTTAGAAGGCTATGTAC (fw)	K228Amber	
NS134	GTACATAGCCTTCTAAGCAGCCAAGTT (rv)		
NS76	ACTTTGTCTGCCTAGGATGAAGTTTTC (fw)	Q237Amber	
NS77	GAAAACTTCATCCTAGGCAGACAAAGT (rv)		
NS78	TCTGCCCAAGATTAGGTTTTCTCTTTG (fw)	E239Amber	
NS79	CAAAGAGAAAACCTAATCTTGGGCAGA (rv)		
NS135	GCTTTCTCTCCATAGAGATACTGGTTG (fw)	N248Amber	
NS136	CAACCAGTATCTCTATGGAGAGAAAGC (rv)		
NS80	GCTGCCACTGCTTAGGGTATTAAGGTC (fw)	T258Amber	
NS81	GACCTTAATACCCTAAGCAGTGGCAGC (rv)		
NS137	TTTTCTTTGGACTAGCAATACTTGGTC (fw)	P267Amber	
NS138	GACCAAGTATTGCTAGTCCAAAGAAAA (rv)		
NS82	GTCGATGACTTGTAGCCAGAATTTGCT (fw)	R275Amber	
NS83	AGCAAATTCTGGCTACAAGTCATCGAC (rv)		
NS84	TTGAGACCAGAATAGGCTGGTTACAGC (fw)	F278Amber	
NS85	GCTGTAACCAGCCTATTCTGGTCTCAA (rv)		
NS86	GAATTTGCTGGTTAGAGCAAGGCCGCT (fw)	Y281Amber	
NS87	AGCGGCCTTGCTCTAACCAGCAAATTC (rv)		
NS88	GCCGCTGAACCATAGGCTGTTTCTTTG (fw)	H288Amber	
NS89	CAAAGAAACAGCCTATGGTTCAGCGGC (rv)		
NS139	TCTGCTGACGGTTAGACTTTGTTTGCC (fw)	Q299Amber	
NS140	GGCAAACAAAGTCTAACCGTCAGCAGA (rv)		
NS174	AGAAAGCATACACATTTTATTCTCAATGTCCAA CCCATTTGATTTCAGCTGAAGCTTCGTACGC (fw)	*STM1* knock-out	
NS175	CACTGTTATTGGATTCTTTCAGTTGGAATTATTCA TATATAAGGCGCATAGGCCACTAGTGGATCTG (rv)		
NS176	CCTTCGCTTGTTTTAGTTGT (fw)	Δ*stm1* verification	
NS177	TCTCGATTGGATGTCAACCC (rv)		
NS178	GCTTTCCCTTCAGAAATCAGGAAAAAAGAAAAG AATACGAAAAAGCAGCTGAAGCTTCGTACGC (fw)	*GIS2* knock-out	
NS179	CATGATAAGTGATTGTTCCTTTGTTTTTTTCAGTG GATGTTTCACGCATAGGCCACTAGTGGATCTG (rv)		

Tab. S1: Continued.

identifier	sequence	application
NS180	CTATTCCAGCAGGAGATGGC (fw)	Δ*gis2* verification
NS181	CGTGTATTGGTTTCGGCAGC (rv)	
NS186	GCTTAAAATATACTTCCCACACCCCCTCCTTCC ATTATAACTGCACAGCTGAAGCTTCGTACGC (fw)	*SCP160* knock-out
NS187	AAAGCCAAAATCTATATTGAAAAAAATTGGTTTCA AAGAGCTTGTGCATAGGCCACTAGTGGATCTG (rv)	
NS188	CACAACAGCACTTTCTATTT (fw)	Δ*scp160* verification
NS189	CCGCCTTATAACGAAGACTC (rv)	
NS190	GTTTGGTCGTTTTCTCAATATAATCTACATCATCA TATATATATACAGCTGAAGCTTCGTACGC (fw)	*DEF1* knock-out
NS191	ATTCCCCATTTCGTTTTTTATGTGGGAGGTTCTAC TTCTCCCTTAGCATAGGCCACTAGTGGATCTG (rv)	
NS192	GTAGTGGCGGGAAAAGGAAA (fw)	Δ*def1* verification
NS193	CCGCAAAATAAAGACACAGC (rv)	
NS194	AACTTATCGGGTAACTTAGAGACAGCATTAGTAT ATATACCAGCCCAGCTGAAGCTTCGTACGC (fw)	*HEK2* knock-out
NS195	TAGTTTGTTTTGTCTGTGTGGGACGTGCGCACGC ACACGTATATAGCATAGGCCACTAGTGGATCTG (rv)	
NS196	CAAACAAGACTATAATCTGG (fw)	Δ*hek2* verification
NS197	CCTCTAGCCGGCGATGCGCG (rv)	
NS205	TGAGCTTTATAGTAAGAACTGC (fw)	*GIS2* Southern probe
NS206	GGAAACTTAATAGAACAAATCA (rv)	
NS29	GCCAGCAACAATACCAGCACC (fw)	Southern probe for other KOs
NS30	CCAATTTGTGTGCTTCTCTTGACG (rv)	

* kindly provided by Dr. Blagovesta Popova   ** kindly provided by Kerstin Schmitt

Tab. S2: Perseus workflow for MaxQuant LC-MS data analysis as performed for the "exponential growth" BioID analysis. At step 6 processing was branched and is described as branch a and b. Branch a describes the data analysis for candidates with proteome values for the normalization of enrichment effects, branch b describes the data analysis for candidates without proteome values.

Step	Command	Function	
		ASC1-birA* BioID analyses	*asc1^{DE}-birA** BioID analyses
1	Generic matrix upload	upload of proteinGroups.txt file: normalized SILAC ratios (*birA*/ASC1-birA** and wt-*ASC1/ASC1-birA**), biotin site positions, etc.	upload of proteinGroups.txt file: normalized SILAC ratios (*birA*/ASC1-birA** ratios only) and biotin site positions, etc.
2.1	Filter rows based on categorical columns	remove candidates "Only identified by site"	
2.2		remove candidates identified with a "Reverse" database	
2.3		remove "Potential contaminants"	
3	Transform	inverse ratios (1/x), resulting in *ASC1-birA*/birA** and *ASC1-birA*/wt-ASC1*	inverse ratios (1/x), resulting in *ASC1-birA*/birA**
4	Transform	$\log_2(x)$	
5	Matching rows by name	merge *ASC1-birA** experiment with *asc1^{DE}-birA** experiment	

Tab. S2: Continued.

Step	Command	Function
6	Combine expression columns	proteome correction of enrichment ratios: subtract proteome ratios from enrichment ratios (E-P)
7a	Categorical annotation rows	group biological replicates (enrichment ratios and proteome ratios): *ASC1-birA*/birA**
8a	Two-samples test	1. group: enrichment ratios, 2. group: proteome ratios; t-test side: both; p-value threshold: 0.05
9a	Categorical annotation rows	group biological replicates (enrichment ratios and proteome ratios): *ASC1-birA**/wt-*ASC1*
10a	Two-samples test	1. group: enrichment ratios, 2. group: proteome ratios; t-test side: both; p-value threshold: 0.05
11a	Categorical annotation rows	group biological replicates (E-P ratios): *ASC1-birA*/birA**
12a	Categorical annotation rows	group biological replicates (E-P ratios): *ASC1-birA**/wt-*ASC1*
13a	Filter rows based on valid values	minimal number of values: 2; in each group (as defined in step 11a), values should be greater or equal 0.26; reduce matrix
14a	Filter rows based on valid values	minimal number of values: 2; in each group (as defined in step 12a), values should be greater or equal 1; reduce matrix
15a	select rows manually	remove rows with only 2 or 3 values ≥ 0.26 for *ASC1-birA*/birA**, but at least 5 available quantification values
16a	average group	calculate mean of *ASC1-birA*/birA** and *ASC1-birA**/wt-*ASC1* SILAC ratios in groups defined in step 11a and 12a
7b	Categorical annotation rows	group biological replicates (E-P ratios): *ASC1-birA*/birA** and *ASC1-birA**/wt-*ASC1*
8b	Filter rows based on valid values	minimal number of values: 2; in each group (as defined in step 7b), values should be valid; add categorical row ("keep" or "discard")
9b	Filter rows based on categorical column	filter for "discard", remove columns with "keep" (obtained from 8b)
10b	One-sample test	columns: *ASC1-birA*/birA** (6 replicates); p-value threshold: 0.05
11b	One-sample test	columns: *ASC1-birA**/wt-*ASC1* (3 replicates); p-value threshold: 0.05
12b	Categorical annotation rows	group biological replicates (enrichment ratios): *ASC1-birA*/birA**
13b	Categorical annotation rows	group biological replicates (enrichment ratios): *ASC1-birA**/wt-*ASC1*
14b	Filter rows based on valid values	minimal number of values: 2; in each group (as defined in 12b), values should be greater or equal 0.26; reduce matrix
15b	Filter rows based on valid values	minimal number of values: 2; in each group (as defined in 13b), values should be greater or equal 1; reduce matrix
16b	select rows manually	remove rows with only 2 or 3 values ≥ 0.26 for *ASC1-birA*/birA**, but at least 5 available quantification values
17b	average group	calculate mean of *ASC1-birA*/birA** and *ASC1-birA**/wt-*ASC1* SILAC ratios in groups defined in step 12b and 13b
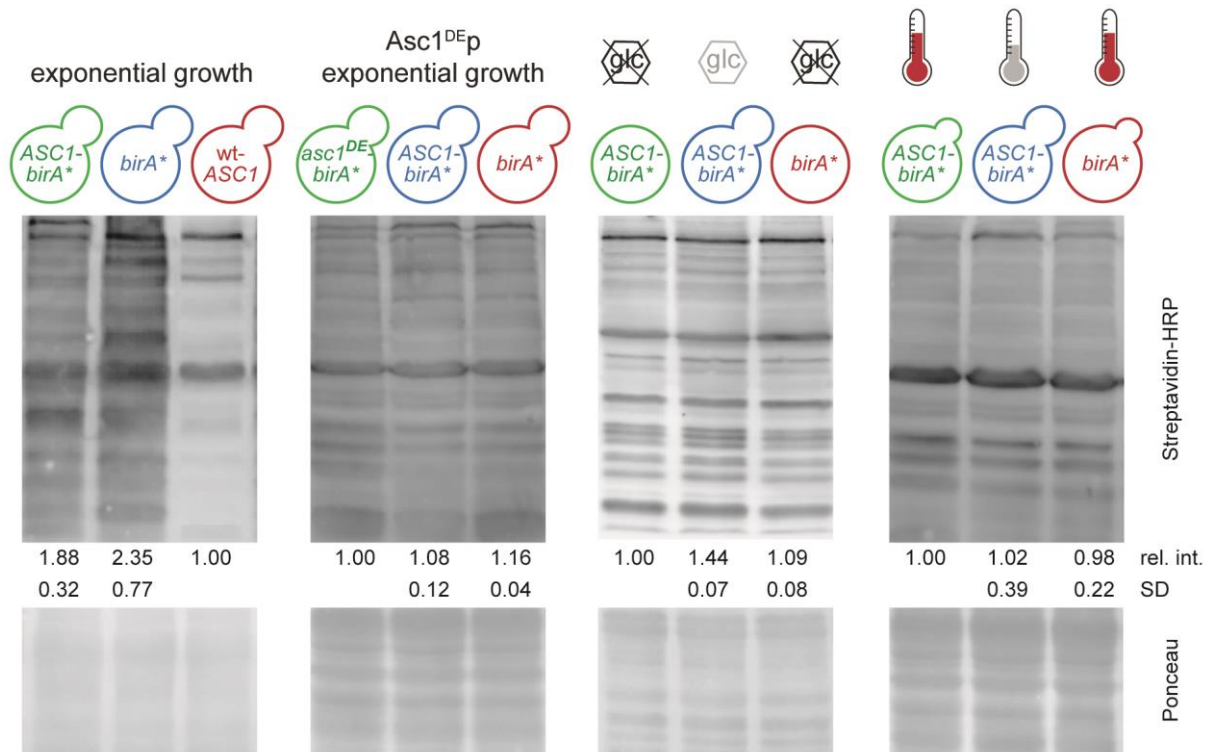
Fig. S1: Overall protein biotinylation visualized for strains and conditions used for BioID analyses. Prior to combining cells of three strains/conditions of a BioID experiment and before biotin affinity capture an aliquot from each culture was taken to compare the level of biotinylation. Biotinylated proteins were visualized with Streptavidin-HRP after Western blotting. The level of biotinylation was normalized according to the Ponceau-stained proteins of the whole proteome. The relative intensities (rel.int.) are indicated with standard deviation (SD).

Tab. S3: SILAC-based identification of Asc1p-neighbors during exponential growth with BioID.
Proteins that were enriched from cells of the *ASC1-birA** strain with a log$_2$ SILAC-ratio ≥ 0.26 against
the *birA** negative control in at least 4 out of 6 replicates and against the wt-*ASC1* negative control with
a log$_2$ SILAC-ratio ≥ 1.00 in at least 2 out of 3 replicates are listed. The ratios were normalized against
the respective proteome value (if available). Mean values and standard deviations (SD) of log$_2$ SILAC
ratios are listed. Additionally, SILAC ratios (enrichment ratio, proteome ratio and enrichment-proteome
ratio (E-P)) are given for each replicate individually. Candidates are listed according to the mean *ASC1-
birA**/*birA** ratio in a descending mode and according to the availability of a proteome value and biotin
site(s). The colors represent the values of the mean SILAC ratios. SILAC quantification and statistical
analyses were performed with the MaxQuant/Perseus software. Abbreviations: NaN = Not a Number.
The depicted color-code applies for all following tables.

Tab. S3.

Protein	/birA	SD	/wt	SD	E-P 1	E-P 2	E-P 3	E-P 4	E-P 5	E-P 6	/wt E-P 1	/wt E-P 2	/wt E-P 3	enr 1	enr 2	enr 3	enr 4	enr 5	enr 6	/wt enr 1	/wt enr 2	/wt enr 3	prot 1	prot 2	prot 3	prot 4	prot 5	prot 6	/wt prot 1	/wt prot 2	/wt prot 3
proteome-corrected and biotin site(s) identified																															
Def1	3.22	0.37	3.38	0.06	2.82	2.79	3.08	3.50	3.43	3.68	3.33	3.38	3.45	2.62	2.68	2.80	3.24	3.17	3.33	3.29	3.36	3.26	-0.20	-0.11	-0.28	-0.26	-0.26	-0.35	-0.03	-0.02	-0.18
Rps26A	3.10	0.28	4.57	0.27	3.52	2.95	3.21	2.90	3.27	2.75	4.79	4.27	4.66	3.52	2.99	3.25	2.95	3.28	2.71	4.76	4.15	4.64	0.00	0.03	0.04	0.05	0.00	-0.05	-0.03	-0.12	-0.02
Pbp4	2.91	0.49	5.08	0.09	NaN	2.57	3.26	NaN	NaN	NaN	NaN	5.14	5.02	2.54	2.16	2.71	3.14	3.15	2.81	3.96	4.80	4.75	NaN	-0.40	-0.54	NaN	NaN	NaN	NaN	-0.35	-0.27
Scp160	2.84	0.14	6.72	0.74	2.98	2.76	2.90	2.93	2.89	2.60	6.92	5.91	7.34	2.88	2.64	2.78	2.75	2.77	2.44	6.89	5.83	7.28	-0.10	-0.12	-0.12	-0.19	-0.12	-0.15	-0.03	-0.08	-0.06
Asc1	2.84	0.58	4.77	0.45	3.06	2.36	2.44	3.37	2.23	3.59	5.26	4.37	4.68	1.67	1.73	2.61	2.95	2.44	4.07	1.20	1.20	2.33	-1.39	-0.63	0.17	-0.42	0.21	0.48	-4.06	-3.17	-2.35
Sro9	2.00	0.29	3.84	0.26	1.99	1.69	1.68	2.26	2.40	2.00	4.01	3.54	3.96	2.23	2.29	2.30	2.61	2.77	2.53	4.21	3.78	4.42	0.24	0.60	0.62	0.35	0.36	0.52	0.20	0.24	0.46
Lsm12	1.30	0.15	4.62	0.67	1.27	1.14	1.18	1.43	1.53	1.26	4.18	4.29	5.39	1.24	1.19	1.14	1.55	1.58	1.27	4.18	4.31	5.35	-0.02	0.05	-0.04	0.11	0.05	0.01	0.00	0.02	-0.04
Ubp3	1.23	0.17	3.08	0.51	1.34	1.31	NaN	NaN	1.04	NaN	2.72	3.44	NaN	0.92	0.87	0.92	1.02	1.14	1.04	2.72	3.26	3.74	-0.42	-0.44	NaN	NaN	0.10	NaN	0.00	-0.19	NaN
Rps20	0.81	0.19	6.65	1.33	1.00	0.50	0.95	0.83	0.87	0.68	5.11	7.41	7.42	0.98	0.50	0.93	0.90	0.94	0.74	5.09	7.35	7.42	-0.02	0.00	-0.02	0.07	0.07	0.05	-0.02	-0.06	-0.01
Rps3	0.78	0.04	2.55	0.07	0.75	0.79	0.81	0.82	0.80	0.72	2.56	2.62	2.48	0.82	0.83	0.82	0.92	0.86	0.73	2.56	2.63	2.48	0.07	0.04	0.01	0.09	0.06	0.01	0.01	0.01	-0.01
Stm1	0.68	0.17	3.66	0.34	0.48	0.56	0.66	0.92	0.84	0.64	3.76	3.28	3.94	0.26	0.40	0.60	0.72	0.63	0.47	3.73	3.24	4.05	-0.23	-0.16	-0.06	-0.21	-0.21	-0.17	-0.03	-0.05	0.11
Cdc33	0.66	0.65	2.96	2.26	0.37	-0.53	0.89	1.13	1.15	0.95	4.20	4.33	0.35	0.36	-0.48	0.97	1.10	1.17	1.01	4.18	4.23	0.37	-0.02	0.05	0.07	-0.03	0.02	0.06	-0.02	-0.09	0.02
Spt5	0.61	0.24	2.35	0.17	0.58	0.85	0.63	NaN	0.76	0.21	2.27	NaN	2.54	0.66	0.56	0.72	0.71	0.81	0.78	2.12	2.25	2.70	0.08	-0.29	0.08	NaN	0.05	0.06	-0.11	-0.02	0.16
Gis2	0.61	0.19	3.81	0.45	0.85	0.42	0.52	0.47	0.77	NaN	4.13	NaN	3.50	0.83	0.47	0.49	0.70	0.89	0.78	4.11	NaN	3.44	-0.02	0.05	-0.03	0.23	0.12	NaN	-0.02	-0.03	-0.06
Rpg1	0.54	0.61	1.01	2.10	0.96	-0.33	-0.15	0.90	0.94	0.93	3.44	-0.18	-0.23	1.29	-0.05	0.12	0.99	1.11	1.10	3.64	-0.02	-0.07	0.33	0.28	0.27	0.09	0.17	0.17	0.21	0.16	0.16
Mbf1	0.53	0.26	4.85	0.42	0.63	0.01	0.66	0.67	0.67	0.56	4.96	5.20	4.39	1.01	0.40	0.98	0.84	0.97	0.70	5.17	5.56	4.69	0.38	0.39	0.31	0.17	0.30	0.14	0.21	0.35	0.30
Pob3	0.50	0.21	2.79	0.26	0.52	0.68	0.38	0.16	0.74	0.54	3.06	2.77	2.54	0.65	0.94	0.55	0.45	0.84	0.79	3.21	2.97	2.77	0.13	0.26	0.17	0.29	0.10	0.25	0.15	0.20	0.23
Rps2	0.37	0.16	1.72	0.24	0.37	0.13	0.26	0.56	0.43	0.46	1.97	1.69	1.49	0.45	0.23	0.33	0.60	0.47	0.45	1.99	1.72	1.51	0.08	0.10	0.06	0.04	0.04	-0.01	0.02	0.04	0.02
proteome-corrected, but no biotin site identified																															
Coq5	1.76	2.90	3.55	1.31	2.70	2.56	4.24	NaN	-2.44	NaN	2.85	2.73	5.06	2.50	2.45	4.07	NaN	-3.19	-1.40	2.79	2.72	5.03	-0.20	-0.11	-0.17	-0.59	-0.75	NaN	-0.06	-0.02	-0.04
Atp7	1.25	0.37	2.23	0.06	0.85	0.93	1.57	1.22	1.79	1.16	2.19	2.28	NaN	0.64	0.87	1.36	0.95	1.62	0.94	2.60	2.78	NaN	-0.21	-0.05	-0.21	-0.26	-0.17	-0.22	0.41	0.50	0.26
Cnb1	1.06	0.41	2.08	0.33	NaN	1.37	1.22	NaN	0.60	NaN	NaN	2.31	1.85	NaN	1.65	1.63	NaN	1.05	NaN	NaN	2.29	1.82	0.43	0.28	0.41	0.39	0.45	NaN	0.07	-0.03	-0.03
Pst2	1.02	0.11	4.14	0.32	1.02	0.98	0.94	1.13	1.17	0.90	3.78	4.38	4.25	0.87	0.76	0.85	1.17	1.16	0.97	3.69	4.31	4.12	-0.16	-0.22	-0.09	0.04	0.00	0.07	-0.09	-0.07	-0.13
Not3	0.65	0.27	2.55	0.69	NaN	0.46	0.84	NaN	NaN	NaN	NaN	2.06	3.04	0.51	0.17	0.11	0.04	0.25	0.17	2.96	2.05	2.65	NaN	-0.29	-0.73	NaN	NaN	NaN	0.16	NaN	-0.39
Pbp1	0.64	0.30	3.03	0.69	1.02	NaN	0.57	0.68	0.29	NaN	2.54	NaN	3.52	0.41	0.36	0.38	0.48	0.50	0.35	2.70	2.46	3.25	-0.61	NaN	-0.19	-0.20	0.21	NaN	0.16	NaN	-0.27
Xrn1	0.62	0.22	2.70	0.07	0.61	0.51	0.39	0.58	1.05	0.58	2.73	2.74	2.62	0.51	0.43	0.49	0.53	0.85	0.60	2.78	2.86	2.84	-0.09	-0.08	0.10	-0.05	-0.19	0.02	0.05	0.11	0.22
Nan1	0.32	0.29	1.37	0.71	0.32	0.04	0.61	NaN	NaN	NaN	1.31	0.69	2.11	0.82	0.78	0.55	1.20	1.00	0.16	1.82	1.19	1.99	0.50	0.74	-0.06	NaN	NaN	NaN	0.50	0.50	-0.12
no proteome value, but biotin site(s) identified																															
Syh1	1.64	0.11	2.84	0.16	NaN	NaN	NaN	NaN	NaN	NaN	NaN	NaN	NaN	1.60	1.56	1.72	1.81	1.67	1.50	2.91	2.60	2.68	NaN	NaN	NaN	NaN	NaN	NaN	NaN	NaN	NaN
Hel2	1.64	0.66	2.58	0.90	NaN	NaN	NaN	NaN	NaN	NaN	NaN	NaN	NaN	1.83	1.73	2.29	NaN	0.72	NaN	2.58	1.66	0.78	NaN	NaN	NaN	NaN	NaN	NaN	NaN	0.50	NaN
Bre5	-0.01	2.51	3.55	0.41	1.60	-4.69	NaN	NaN	NaN	NaN	3.75	3.82	NaN	0.98	-5.13	0.84	1.24	1.12	0.88	3.75	3.08	3.81	-0.62	-0.44	NaN	NaN	NaN	NaN	0.00	-0.74	NaN
Ubp2	0.68	0.39	1.42	0.05	NaN	NaN	NaN	NaN	NaN	NaN	NaN	NaN	NaN	1.01	0.89	0.88	0.79	-0.04	0.54	1.44	1.36	1.47	NaN	NaN	NaN	NaN	NaN	NaN	NaN	NaN	NaN
Nob1	0.67	0.37	3.25	0.34	NaN	NaN	0.58	NaN	0.32	0.77	NaN	NaN	3.74	0.72	0.04	0.56	1.16	0.88	0.67	2.89	3.29	3.57	NaN	NaN	-0.02	NaN	0.56	-0.10	NaN	NaN	-0.17
Smy2	0.62	0.82	3.24	0.36	NaN	NaN	NaN	NaN	NaN	NaN	NaN	NaN	NaN	0.91	-0.70	-0.11	1.26	1.25	1.09	3.36	2.84	3.53	NaN	NaN	NaN	NaN	NaN	NaN	NaN	NaN	NaN
Slf1	0.44	0.18	2.19	0.45	NaN	NaN	NaN	NaN	NaN	NaN	NaN	NaN	NaN	0.52	0.24	0.35	0.66	NaN	NaN	1.91	1.95	2.71	NaN	NaN	NaN	NaN	NaN	NaN	NaN	NaN	NaN
Hsm3	0.43	0.60	2.79	0.20	NaN	NaN	NaN	NaN	NaN	NaN	NaN	NaN	NaN	0.50	0.34	-0.66	1.00	0.92	0.50	2.95	2.56	2.85	NaN	NaN	NaN	NaN	NaN	NaN	NaN	NaN	NaN
Eap1	-0.09	0.91	1.93	0.44	NaN	NaN	NaN	NaN	NaN	NaN	NaN	NaN	NaN	0.40	-1.91	-0.02	0.42	0.14	0.43	1.52	1.88	2.39	NaN	NaN	NaN	NaN	NaN	NaN	NaN	NaN	NaN
neither proteome value nor biotin site identified																															
Shs1	1.65	0.24	2.84	0.11	NaN	NaN	NaN	NaN	NaN	NaN	NaN	NaN	NaN	1.58	1.54	2.09	1.39	1.72	1.56	2.85	2.95	2.73	NaN	NaN	NaN	NaN	NaN	NaN	NaN	NaN	NaN
Rim11	1.37	0.33	2.58	0.95	NaN	NaN	NaN	NaN	NaN	NaN	NaN	NaN	NaN	1.36	0.95	1.44	1.75	NaN	NaN	NaN	1.91	3.26	NaN	NaN	NaN	NaN	NaN	NaN	NaN	NaN	NaN
Nab6	0.65	0.36	1.82	0.20	NaN	NaN	NaN	NaN	NaN	NaN	NaN	NaN	NaN	0.86	0.24	0.85	NaN	NaN	NaN	2.03	1.80	1.64	NaN	NaN	NaN	NaN	NaN	NaN	NaN	NaN	NaN
Yor385W	0.50	0.32	2.34	0.57	NaN	NaN	NaN	NaN	NaN	NaN	NaN	NaN	NaN	0.32	0.37	0.10	1.04	0.67	0.52	1.68	2.60	2.74	NaN	NaN	NaN	NaN	NaN	NaN	NaN	NaN	NaN
Ypk1	0.36	0.43	2.49	0.58	0.84	NaN	NaN	NaN	NaN	0.26	1.76	NaN	NaN	0.65	0.08	-0.24	0.78	0.52	NaN	1.89	3.06	2.51	-0.19	NaN	NaN	NaN	NaN	0.26	0.13	NaN	NaN

Column groups: mean and SD of log2 SILAC ratios (/birA, SD, /wt, SD); ASC1-birA*/birA* E-P (1–6); ASC1-birA*/wt E-P (1–3); ASC1-birA*/birA* enrichment (1–6); ASC1-birA*/wt enrichment (1–3); ASC1-birA*/birA* proteome (1–6); ASC1-birA*/wt proteome (1–3).

Tab. S4: Positions of biotinylated lysine residues of identified Asc1p-neighbors during exponential growth. The position(s) of biotinylated lysine residues within the amino acid sequence of the identified Asc1p-neighbors are listed. Modified lysine residues only identified with the MaxQuant/Perseus software are labeled in red, those only identified with the Proteome Discoverer™ software in blue.

Protein	biotinylated lysine residues
normalized to proteome value and biotin site(s) identified	
Def1	115; 141; 154; 214; 218; 228; 241; 257; 269
Rps26A	116; 117
Pbp4	39; 41; 65; 77; 79
Scp160	48; 56; 71; 79
Asc1	40; 46; 53; 62; 87; 107; 117; 118; 137; 161; 176; 179; 228; 229; 283
Sro9	25; 27; 59; 84; 116
Lsm12	80; 134
Ubp3	397; 405
Rps20	6; 8; 30; 32; 101
Rps3	106; 108; 212
Stm1	23; 27; 121; 143; 145; 165; 170; 171; 184; 192; 194; 204; 244; 260
Cdc33	8; 9; 24; 36
Spt5	770
Gis2	91
Rpg1	866
Mbf1	46; 127; 135
Pob3	115
Rps2	10
no proteome value, but biotin site(s) identified	
Syh1	555; 565; 581
Hel2	496
Bre5	214; 366; 414
Ubp2	1141; 1145
Nob1	184
Smy2	442; 471
Slf1	11
Hsm3	466
Eap1	290

Tab. S5: Perseus workflow for MaxQuant LC-MS data analysis as performed for the "glucose starvation", "heat stress" and "Asc1^{DE}p" BioID analyses. The workflow for the BioID analyses investigating the neighborhood of *asc1^{DE}-birA** is shown as representative. The number of biological replicates differs between the three BioID analyses. At step 6 processing was branched and is described as branch a and b. Branch a describes the data analysis for candidates with proteome values for the normalization of enrichment effects, branch b describes the data analysis for candidates without proteome values.

Step	Command	Function
1	Generic matrix upload	upload of proteinGroups.txt file: normalized SILAC ratios (*ASC1-birA*/asc1^{DE}-birA** and *birA*/asc1^{DE}-birA**), biotin site positions, etc.
2.1	Filter rows based on categorical columns	remove candidates "Only identified by site"
2.2		remove candidates identified with a "Reverse" database
2.3		remove "Potential contaminants"

Tab. S5: Continued.

Step	Command	Function
3	Transform	inverse ratios (1/x), resulting in *asc1^{DE}-birA*/ASC1-birA** and *asc1^{DE}-birA*/birA** (in the "heat stress" experiment this step was not required for the label swap replicate)
4	Transform	$\log_2(x)$
5	Combine expression columns	proteome correction of enrichment ratios: subtract proteome ratios from enrichment ratios (E-P)
6a	Categorical annotation rows	group biological replicates (enrichment ratios and proteome ratios): *asc1^{DE}-birA*/ASC1-birA**
7a	Two-samples test	1. group: enrichment ratios, 2. group: proteome ratios; t-test side: both; p-value threshold: 0.05
8a	Categorical annotation rows	group biological replicates (enrichment ratios and proteome ratios): *asc1^{DE}-birA*/birA**
9a	Two-samples test	1. group: enrichment ratios, 2. group: proteome ratios; t-test side: both; p-value threshold: 0.05
10a	Categorical annotation rows	group biological replicates (E-P ratios): *asc1^{DE}-birA*/ASC1-birA**
11a	Categorical annotation rows	group biological replicates (E-P ratios): *asc1^{DE}-birA*/birA**
12a	Filter rows based on valid values	minimal number of values: 2 (or 3 if 5 replicates); in each group (as defined in step 11a), values should be greater or equal 0.26; reduce matrix
13a	Filter rows based on valid values	minimal number of values: 2 (or 3 if 5 replicates); in each group (as defined in step 10a), values should be outside -0.26 and 0.26; reduce matrix
14a	average group	calculate mean of *asc1^{DE}-birA*/ASC1-birA** and *asc1^{DE}-birA*/birA** SILAC ratios in groups defined in step 10a and 11a
6b	Categorical annotation rows	group biological replicates (E-P ratios): *asc1^{DE}-birA*/ASC1-birA** and *asc1^{DE}-birA*/ birA**
7b	Filter rows based on valid values	minimal number of values: 2; in at least one group (as defined in step 6b), values should be valid; add categorical row ("keep" or "discard")
8b	Filter rows based on categorical column	filter for "discard", remove columns with "keep" (obtained from 7b)
9b	One-sample test	columns: *asc1^{DE}-birA*/ASC1-birA**; p-value threshold: 0.05
10b	One-sample test	columns: *asc1^{DE}-birA*/ birA**; p-value threshold: 0.05
11b	Categorical annotation rows	group biological replicates (enrichment ratios): *asc1^{DE}-birA*/ASC1-birA**
12b	Categorical annotation rows	group biological replicates (enrichment ratios): *asc1^{DE}-birA*/ birA**
13b	Filter rows based on valid values	minimal number of values: 2 (or 3 if 5 replicates); in each group (as defined in step 12b), values should be greater or equal 0.26; reduce matrix
14b	Filter rows based on valid values	minimal number of values: 2 (or 3 if 5 replicates); in at least one group (as defined in step 11b), values should be outside -0.26 and 0.26; reduce matrix
15b	average group	calculate mean of *asc1^{DE}-birA*/ASC1-birA** and *asc1^{DE}-birA*/birA** SILAC ratios in groups defined in step 11b and 12b

Tab. S6: Alterations of total cellular protein abundances in the glucose-starved *ASC1-birA** strain in comparison to its equivalent grown exponentially reflect glucose depletion. Total cellular protein abundances were compared from the glucose-starved *ASC1-birA** strain against the same strain grown exponentially. Proteins with a $\log_2$ SILAC ratio ≥ 0.26 or ≤ -0.26 in at least three out of five biological replicates were considered as starvation-specifically up- or down-regulated on the whole proteome level, respectively. The colors represent the values of the mean SILAC ratios. A selection of respective proteins is listed with their elemental molecular function according to the Gene Ontology assignment. SILAC quantification was performed with the MaxQuant/Perseus software. Abbreviations: SD = standard deviation; NaN = Not a Number.

Protein	*ASC1-birA**(-glc)/*ASC1-birA** proteome							Gene ontology (molecular function)
	mean	SD	1	2	3	4	5	
Hxt6; Hxt7	**3.99**	1.14	5.94	3.54	3.99	3.50	3.00	sugar transport
Hxt2	**1.23**	0.27	1.14	1.18	1.00	1.62	NaN	sugar transport
Hxk1	**0.75**	0.54	1.61	0.60	0.63	0.12	0.78	sugar import; glycolytic process; hexokinase activity
Emi2	**0.63**	0.33	1.12	0.76	0.23	0.53	0.49	glycolytic process; glucokinase activity
Hsp104	**0.41**	0.11	0.58	0.46	0.38	0.30	0.34	ATP catabolic process
Sco1	**0.37**	0.17	0.58	NaN	0.35	0.38	0.17	copper ion transport; respiratory chain complex IV assembly
Ndi1	**0.33**	0.07	0.32	0.22	0.40	0.34	0.37	mitochondrial electron transport
Gpm2	**0.32**	0.18	0.48	0.49	0.21	0.07	0.35	intramolecular transferase activity; glycolytic process
Hca4	**-0.48**	0.12	-0.56	-0.32	-0.60	-0.44	NaN	ATP-dependent RNA helicase activity
Fks1	**-0.51**	0.09	-0.47	-0.44	-0.67	-0.50	-0.46	1.3-beta-D-glucan synthase activity
Nog2	**-0.53**	0.21	-0.70	-0.48	-0.68	NaN	-0.26	GTP binding; GTPase activity
Kre2	**-0.83**	0.25	-0.88	-0.53	-1.16	-0.95	-0.63	alpha-1.2-mannosyltransferase activity
Itr1	**-1.05**	0.19	-1.25	-0.82	-1.22	-0.91	-1.07	myo-inositol transmembrane transporter activity
Ktr1	**-1.07**	0.16	-1.01	-1.13	-1.26	-1.10	-0.83	alpha-1.2-mannosyltransferase activity
Dip5	**-1.54**	0.28	-1.87	NaN	-1.39	-1.36	NaN	amino acid transmembrane transporter activity
Mup1	**-1.98**	0.48	-2.00	-1.70	-2.80	-1.70	-1.70	L-methionine transmembrane transporter activity

Tab. S7: SILAC-based identification of dynamic Asc1p-neighbors during glucose starvation. Proteins enriched from glucose starved *ASC1-birA** cells with a log$_2$ SILAC ratio $\geq$ 0.26 against the *ASC1-birA** reference strain (2% glucose) were considered as starvation-specifically enriched in the Asc1p-neighborhood; proteins with a log$_2$ SILAC ratio $\leq$ -0.26 as distanced from Asc1p. A log$_2$ SILAC ratio $\geq$ 0.26 against the *birA** negative control strain was required in both cases in at least three out of five biological replicates. The ratios were normalized against the respective proteome value (if available). Mean values and standard deviations (SD) of log$_2$ SILAC ratios are listed. Additionally, SILAC ratios (enrichment ratio, proteome ratio and enrichment-proteome ratio (E-P)) are given for each replicate. Candidates are listed according to the mean *ASC1-birA**(-glc)/*ASC1-birA** ratio in a descending mode and according to the availability of a proteome value and biotin site(s). Asc1p-neighbors at exponential growth are listed in bold. The colors represent the values of the mean SILAC ratios. SILAC quantification and statistical analyses were performed with the MaxQuant/Perseus software. Abbreviations: NaN = Not a Number.

Tab. S7.

Protein	mean and SD of log₂ SILAC ratios				ASC1-birA*(-glc)/ ASC1-birA* E-P					ASC1-birA*(-glc)/ birA*(-glc) E-P					ASC1-birA*(-glc)/ASC1-birA* enrichment				
	/ASC1-birA*	SD	/birA*(-glc)	SD	1	2	3	4	5	1	2	3	4	5	1	2	3	4	5
proteome-corrected and biotin site(s) identified																			
Rpl12	0.55	0.45	0.57	0.53	1.20	0.46	0.78	0.04	0.28	1.28	0.53	0.91	-0.01	0.15	1.15	0.45	0.70	0.09	0.17
Eft1	0.37	0.35	0.32	0.32	0.90	0.35	0.41	-0.07	0.28	0.83	0.30	0.37	-0.02	0.13	0.78	0.25	0.27	-0.09	0.14
Lsm12	-0.32	0.07	0.99	0.08	-0.39	-0.40	-0.28	-0.24	-0.30	0.97	0.90	1.07	1.07	0.96	-0.36	-0.37	-0.19	-0.21	-0.32
Rpa190	-0.47	0.21	0.35	0.09	-0.51	-0.67	-0.66	-0.33	-0.19	0.22	0.35	0.48	0.36	0.34	-0.68	-0.82	-0.86	-0.41	-0.36
Rps20	-0.49	0.08	0.85	0.13	-0.42	-0.57	-0.40	-0.54	-0.54	1.06	0.80	0.84	0.73	0.80	-0.45	-0.60	-0.47	-0.55	-0.55
Stm1	-0.70	0.07	0.87	0.16	-0.61	-0.75	-0.80	-0.67	-0.67	1.09	0.91	0.69	0.75	0.91	-0.58	-0.78	-0.75	-0.54	-0.63
Rpg1	-0.90	0.16	1.42	0.39	-0.68	-1.01	-1.10	-0.92	-0.81	1.86	1.27	1.60	0.85	1.54	-0.74	-1.13	-1.14	-0.93	-0.80
Sro9	-1.11	0.20	2.57	0.68	-0.79	-1.11	-1.19	-1.35	-1.11	3.62	2.53	2.08	1.88	2.77	-0.98	-1.33	-1.33	-1.23	-1.05
Psp2	-1.14	0.28	0.81	0.46	-1.03	-1.54	-0.85	-1.31	-0.96	1.23	1.26	0.39	0.29	0.87	-0.86	-1.20	-0.99	-1.24	-1.01
Asc1	-1.50	0.18	1.90	0.52	-1.36	-1.74	-1.63	-1.37	-1.37	2.38	2.36	2.06	1.24	1.48	-1.51	-1.83	-1.89	-1.43	-1.53
Bre5	-1.50	0.16	1.67	0.41	-1.38	-1.35	-1.64	NaN	-1.64	1.81	2.14	1.58	NaN	1.16	-1.59	-2.07	-1.95	-2.13	-1.65
Def1	-1.53	0.75	3.34	0.90	-0.79	-1.20	-1.40	-2.79	-1.48	4.05	4.23	2.43	2.33	3.66	-0.94	-1.46	-1.56	-2.67	-1.29
Pbp4	-1.70	0.22	2.85	0.46	-1.45	-1.65	NaN	-1.97	-1.75	3.15	3.30	NaN	2.30	2.65	-1.53	-1.96	-1.52	-1.95	-1.85
Scp160	-1.76	0.20	2.50	0.56	-1.53	-1.90	-1.90	-1.94	-1.56	3.27	2.62	2.65	1.78	2.16	-1.43	-1.93	-1.90	-1.97	-1.58
proteome-corrected, but no biotin site identified																			
Coq5	5.67	1.41	5.61	1.36	NaN	5.36	4.03	7.44	5.84	NaN	5.07	4.06	7.25	6.05	NaN	5.37	3.50	7.50	5.78
Fpr1	1.01	0.53	0.72	0.45	1.84	1.05	1.03	0.43	0.69	1.44	0.82	0.67	0.29	0.39	2.11	1.00	1.21	-0.03	0.72
Rpl18	0.97	0.77	0.60	0.70	1.76	1.10	1.61	0.07	0.29	1.55	0.65	0.95	-0.04	-0.11	1.79	1.06	1.64	0.16	0.37
Sec26	0.96	0.87	0.66	0.79	2.26	0.37	NaN	0.52	0.70	1.81	0.27	NaN	0.07	0.47	2.27	0.44	NaN	0.42	0.80
Shb17	0.95	0.48	0.70	0.55	1.54	1.11	1.19	0.53	0.40	1.33	0.52	1.23	0.27	0.14	1.49	1.09	1.02	0.27	0.14
Cpr1	0.88	0.64	0.66	0.64	1.83	1.09	0.87	0.24	0.37	1.61	0.85	0.72	0.05	0.07	2.12	1.19	0.98	0.22	0.51
Rpl23	0.86	0.58	0.54	0.51	1.63	0.95	1.17	0.22	0.35	1.30	0.63	0.64	0.07	0.06	1.54	0.93	1.11	0.22	0.36
Chc1	0.81	0.81	0.57	0.57	2.04	0.93	0.95	0.01	0.13	1.55	0.47	0.41	0.11	0.30	2.15	0.95	0.91	-0.05	0.21
Lys9	0.74	0.63	0.56	0.44	1.70	1.00	0.59	0.18	0.22	1.15	0.68	0.73	0.09	0.15	2.36	1.43	0.90	0.12	0.44
Thr1	0.73	0.73	0.62	0.63	1.65	0.85	1.14	-0.10	0.09	1.50	0.63	0.91	-0.11	0.18	1.76	0.92	1.34	-0.01	0.10
Act1	0.71	0.55	0.52	0.55	1.55	0.84	0.73	0.19	0.23	1.42	0.60	0.40	0.06	0.13	1.53	0.84	0.72	0.18	0.20
Rps5	0.70	0.50	0.53	0.51	1.37	0.80	0.92	0.11	0.30	1.27	0.51	0.74	0.05	0.07	1.33	0.77	0.86	0.07	0.25
Rps11	0.68	0.50	0.52	0.45	1.28	0.80	0.98	0.08	0.27	1.18	0.43	0.74	0.08	0.18	1.27	0.73	0.98	0.17	0.29
Ura2	0.67	0.69	0.60	0.68	1.77	0.73	0.69	0.03	0.13	1.71	0.60	0.60	0.02	0.08	1.66	0.66	0.63	0.08	0.08
Rps4	0.59	0.42	0.35	0.33	1.24	0.62	0.66	0.16	0.29	0.91	0.29	0.35	0.12	0.08	1.20	0.56	0.61	0.13	0.25
Sah1	0.58	0.54	0.34	0.44	1.44	0.58	0.59	0.05	0.22	1.08	0.28	0.33	-0.03	0.06	1.34	0.56	0.54	0.01	0.11
Rps14	0.55	0.44	0.44	0.51	1.27	0.42	0.65	0.22	0.20	1.28	0.28	0.51	0.12	0.00	1.26	0.40	0.62	0.18	0.21
Ura6	0.54	0.41	0.54	0.47	1.24	0.39	0.52	0.22	0.34	1.23	0.57	0.67	-0.01	0.23	1.20	0.39	0.51	-0.09	0.12
Tif11	0.54	0.30	0.53	0.44	NaN	0.96	0.48	0.26	0.45	NaN	0.55	1.12	0.37	0.07	NaN	0.84	0.52	0.36	0.31
Rpl9A	0.51	0.41	0.32	0.42	1.16	0.57	0.49	0.11	0.22	1.00	0.32	0.32	-0.06	0.01	1.10	0.51	0.45	0.15	0.19
Rpl10	0.50	0.34	0.48	0.43	1.02	0.52	0.55	0.13	0.26	1.15	0.51	0.53	0.08	0.14	0.95	0.51	0.52	0.17	0.26
Rpl11	0.46	0.38	0.34	0.34	0.97	0.47	0.62	-0.06	0.29	0.84	0.27	0.49	-0.01	0.12	0.89	0.44	0.58	-0.01	0.27
Adi1	0.44	0.25	0.65	0.46	0.78	0.16	0.22	0.57	0.49	1.28	0.74	0.82	0.34	0.08	0.98	0.22	0.26	0.36	0.67
Rpl1	0.43	0.31	0.31	0.31	0.85	0.46	0.55	0.05	0.23	0.83	0.27	0.29	0.05	0.09	0.76	0.35	0.49	0.13	0.16
Rps0	0.40	0.27	0.54	0.40	0.83	0.35	0.44	0.11	0.25	1.11	0.67	0.58	0.17	0.15	0.77	0.35	0.36	0.07	0.17
Mvd1	0.36	0.34	0.27	0.28	0.90	0.47	0.26	0.10	0.06	0.69	0.26	0.35	-0.03	0.08	0.90	0.44	0.30	0.03	0.01
Pex11	0.35	0.17	0.30	0.20	0.39	0.37	0.59	0.15	0.25	0.45	0.18	0.53	0.32	0.03	0.60	0.37	0.72	0.25	0.33
Hek2	-0.28	0.08	0.56	0.19	-0.17	-0.30	NaN	-0.27	-0.36	0.81	0.37	NaN	0.58	0.47	-0.18	-0.60	NaN	-0.29	-0.56
Bfr1	-0.55	0.09	0.30	0.07	-0.41	-0.63	-0.60	-0.59	-0.51	0.38	0.19	0.28	0.35	0.31	-0.38	-0.68	-0.57	-0.38	-0.40
Ret2	-0.69	0.31	0.25	0.24	-0.35	-0.80	-1.15	-0.59	-0.54	0.31	-0.01	0.44	0.50	0.02	-0.35	-0.87	-1.29	-0.59	-0.66
Dia1	-0.81	0.30	0.52	0.12	-0.49	-1.07	-1.06	-0.64	NaN	0.40	0.68	0.51	0.49	NaN	-0.52	-1.13	-1.17	-0.79	-0.77
Ccr4	-0.83	0.15	0.27	0.32	-0.70	NaN	-0.86	-0.73	-1.03	0.38	NaN	0.59	0.30	-0.18	-0.78	-1.05	-0.76	-0.94	-0.99
Xrn1	-0.93	0.15	0.40	0.14	-0.91	-1.10	-1.03	-0.92	-0.71	0.38	0.22	0.55	0.32	0.52	-0.81	-1.10	-1.03	-0.92	-0.83
Srp1	-0.95	0.49	0.45	0.28	-0.90	-1.65	NaN	-0.65	-0.59	0.83	0.46	NaN	0.31	0.20	-0.88	-1.68	NaN	-0.67	-0.62
Gis2	-1.10	0.26	0.34	0.15	-0.83	-1.43	NaN	-0.97	-1.18	0.53	0.17	NaN	0.34	0.34	-1.49	-1.73	NaN	-1.25	-1.38
His6	-1.33	0.99	0.31	0.47	-0.71	-2.42	-2.40	-0.48	-0.65	0.96	0.42	-0.35	0.14	0.38	-0.89	-2.51	-2.26	-0.54	-0.51
Shs1	-1.54	0.17	0.91	0.23	-1.49	-1.66	-1.68	NaN	-1.32	0.86	0.68	0.85	NaN	1.24	-1.48	-1.54	-1.73	-1.48	-1.63
Mbf1	-1.64	0.24	0.46	0.14	-1.61	-1.77	-1.87	-1.24	-1.70	0.64	0.54	0.38	0.28	0.47	-1.50	-1.61	-1.72	-1.15	-1.39
Spt5	-1.90	0.33	0.52	0.39	-2.00	-1.60	-2.11	-1.53	-2.28	0.39	1.21	0.34	0.32	0.32	-2.13	-1.65	-2.19	-1.58	-2.36
New1	-2.43	0.42	0.35	0.43	-2.40	-2.80	-2.91	-2.08	-1.98	0.86	0.42	0.63	0.03	-0.20	-2.58	-2.96	-3.02	-2.26	-2.27
Ent3	-2.79	0.12	0.64	0.16	-2.59	-2.82	-2.89	-2.81	-2.86	0.80	0.45	0.64	0.82	0.51	-2.79	-2.88	-2.76	-2.76	-2.87
no proteome value, but biotin site(s) identified																			
Syh1	-2.33	0.58	**0.55**	0.25	NaN	NaN	NaN	NaN	NaN	NaN	NaN	NaN	NaN	NaN	-1.36	-2.77	-2.73	-2.53	-2.28
neither proteome value nor biotin site identified																			
Smy2	-3.93	2.36	**0.51**	0.20	NaN	NaN	NaN	NaN	NaN	NaN	NaN	NaN	NaN	NaN	-2.72	-8.08	-3.37	-2.34	-3.13
Hel2	-1.86	0.28	**0.90**	0.73	NaN	NaN	NaN	NaN	NaN	NaN	NaN	NaN	NaN	NaN	-2.07	-2.12	NaN	-1.75	-1.52
Sas10	-1.28	0.20	1.33	0.33	NaN	NaN	NaN	NaN	NaN	NaN	NaN	NaN	NaN	NaN	-1.08	-1.47	-1.29	NaN	NaN
Rsc58	**-0.46**	0.25	**0.81**	0.27	NaN	-0.85	NaN	NaN	NaN	NaN	0.81	NaN	NaN	NaN	NaN	-0.77	-0.41	-0.17	-0.48

Tab. S7: Continued.

Protein	ASC1-birA*(-glc)/birA*(-glc) enrichment					ASC1-birA*(-glc)/ASC1-birA* proteome					ASC1-birA*(-glc)/birA*(-glc) proteome				
	1	2	3	4	5	1	2	3	4	5	1	2	3	4	5
proteome-corrected and biotin site(s) identified															
Rpl12	1.19	0.50	0.90	0.02	0.13	-0.05	-0.02	-0.08	0.05	-0.11	-0.09	-0.03	-0.01	0.03	-0.02
Eft1	0.76	0.28	0.38	-0.05	0.10	-0.12	-0.10	-0.14	-0.01	-0.14	-0.07	-0.02	0.01	-0.03	-0.03
Lsm12	1.06	1.01	1.04	1.08	1.04	0.03	0.03	0.09	0.03	-0.02	0.08	0.12	-0.04	0.01	0.08
Rpa190	0.16	0.25	0.48	0.39	0.31	-0.17	-0.15	-0.20	-0.08	-0.17	-0.06	-0.10	0.00	0.03	-0.03
Rps20	1.17	0.78	0.83	0.70	0.81	-0.03	-0.03	-0.07	-0.01	-0.01	0.11	-0.02	-0.01	-0.03	0.00
Stm1	1.09	0.66	0.61	0.68	0.79	0.03	-0.03	0.05	0.13	0.03	0.00	-0.24	-0.09	-0.07	-0.12
Rpg1	2.11	1.47	1.78	1.02	1.77	-0.06	-0.11	-0.04	-0.02	0.00	0.25	0.20	0.18	0.17	0.23
Sro9	4.00	3.00	2.74	2.53	3.39	-0.19	-0.22	-0.14	0.13	0.06	0.38	0.47	0.66	0.66	0.62
Psp2	1.62	1.19	0.91	1.03	1.23	0.17	0.34	-0.14	0.07	-0.05	0.40	-0.07	0.52	0.74	0.36
Asc1	-0.23	0.38	0.36	0.10	-0.46	-0.15	-0.09	-0.25	-0.05	-0.16	-2.61	-1.98	-1.70	-1.14	-1.94
Bre5	1.71	1.36	1.04	0.96	1.39	-0.22	-0.72	-0.31	NaN	0.00	-0.09	-0.78	-0.54	NaN	0.23
Def1	4.18	4.18	2.06	2.09	3.75	-0.15	-0.26	-0.16	0.13	0.19	0.13	-0.05	-0.37	-0.24	0.09
Pbp4	3.19	2.90	2.42	2.15	2.60	-0.08	-0.31	NaN	0.02	-0.10	0.05	-0.39	NaN	-0.15	-0.05
Scp160	3.28	2.47	2.50	1.62	2.07	0.09	-0.03	0.00	-0.03	-0.02	0.01	-0.15	-0.15	-0.16	-0.10
proteome-corrected, but no biotin site identified															
Coq5	NaN	5.26	4.04	7.26	6.28	0.08	0.01	-0.52	0.06	-0.06	-0.02	0.19	-0.03	0.01	0.23
Fpr1	1.49	0.72	0.65	-0.38	0.23	0.27	-0.05	0.18	-0.46	0.03	0.04	-0.10	-0.02	-0.67	-0.16
Rpl18	1.53	0.63	0.94	0.02	-0.01	0.02	-0.04	0.03	0.10	0.09	-0.02	-0.03	-0.02	0.06	0.09
Sec26	1.84	0.14	NaN	0.01	0.50	0.02	0.06	0.10	-0.10	0.10	0.03	-0.13	-0.02	-0.06	0.03
Shb17	1.28	0.69	1.26	0.27	0.27	-0.04	-0.01	-0.17	-0.26	-0.25	-0.05	0.18	0.04	0.01	0.13
Cpr1	1.12	0.30	0.17	-0.56	-0.35	0.29	0.10	0.12	-0.02	0.14	-0.49	-0.55	-0.54	-0.61	-0.42
Rpl23	1.24	0.57	0.68	0.08	0.05	-0.09	-0.02	-0.06	0.00	0.01	-0.06	-0.06	0.04	0.01	-0.01
Chc1	1.68	0.56	0.45	0.21	0.44	0.11	0.01	-0.04	-0.06	0.07	0.13	0.09	0.04	0.10	0.14
Lys9	1.59	0.46	-0.33	-0.52	-0.07	0.66	0.43	0.30	-0.05	0.22	0.44	-0.22	-1.05	-0.61	-0.22
Thr1	1.39	0.60	0.88	-0.15	0.13	0.11	0.07	0.20	0.09	0.01	-0.11	-0.03	-0.03	-0.04	-0.05
Act1	1.31	0.55	0.39	-0.01	0.08	-0.02	0.00	-0.01	-0.01	-0.03	-0.11	-0.05	-0.01	-0.06	-0.05
Rps5	1.41	0.60	0.79	0.05	0.12	-0.04	-0.03	-0.06	0.04	-0.04	0.14	0.09	0.05	0.00	0.05
Rps11	1.36	0.49	0.77	0.18	0.21	-0.01	-0.07	0.00	0.09	0.02	0.18	0.07	0.03	0.10	0.03
Ura2	1.60	0.88	0.92	0.14	0.18	-0.11	-0.07	-0.07	0.05	-0.05	-0.11	0.27	0.32	0.11	0.10
Rps4	1.02	0.35	0.38	0.09	0.12	-0.05	-0.05	-0.05	-0.03	-0.04	0.11	0.06	0.03	-0.02	0.04
Sah1	1.08	0.32	0.42	0.03	0.06	-0.11	-0.02	-0.05	-0.03	-0.11	0.00	0.04	0.09	0.06	0.00
Rps14	1.44	0.32	0.50	0.16	0.11	-0.02	-0.02	-0.03	-0.05	0.01	0.16	0.04	-0.01	0.04	0.11
Ura6	1.00	0.53	0.54	-0.25	0.04	-0.04	0.00	-0.01	-0.31	-0.21	-0.22	-0.03	-0.13	-0.24	-0.19
Tif11	NaN	0.46	1.23	0.33	-0.02	-0.26	-0.12	0.04	0.09	-0.14	-0.08	-0.09	0.11	-0.04	-0.08
Rpl9A	1.00	0.29	0.41	-0.01	0.02	-0.06	-0.06	-0.04	0.04	-0.03	0.01	-0.03	0.09	0.05	0.01
Rpl10	1.15	0.48	0.57	0.08	0.13	-0.07	-0.01	-0.04	0.04	0.00	0.00	-0.02	0.04	0.01	-0.02
Rpl11	0.85	0.27	0.47	-0.01	0.09	-0.07	-0.03	-0.04	0.05	-0.02	0.01	0.00	-0.01	0.00	-0.03
Adi1	1.37	0.65	0.70	0.07	0.23	0.20	0.05	0.05	-0.21	0.17	0.09	-0.09	-0.12	-0.27	0.15
Rpl1	0.86	0.22	0.31	0.04	0.07	-0.09	-0.11	-0.06	0.07	-0.07	0.03	-0.05	0.02	-0.02	-0.01
Rps0	1.20	0.70	0.60	0.12	0.20	-0.06	0.00	-0.08	-0.05	-0.08	0.09	0.03	0.02	-0.05	0.04
Mvd1	0.68	0.33	0.34	0.06	0.17	0.00	-0.03	0.03	-0.08	-0.05	-0.01	0.07	-0.02	0.09	0.09
Pex11	0.94	0.10	0.16	0.18	-0.03	0.22	0.00	0.13	0.10	0.08	0.49	-0.08	-0.37	-0.14	-0.07
Hek2	0.54	0.12	NaN	0.30	0.18	-0.01	-0.31	-0.23	-0.02	-0.20	-0.27	-0.24	-0.04	-0.29	-0.29
Bfr1	0.34	0.01	0.11	0.28	0.09	0.03	-0.05	0.03	0.22	0.11	-0.04	-0.18	-0.18	-0.07	-0.22
Ret2	0.21	0.06	0.29	0.31	0.10	0.00	-0.07	-0.14	0.01	-0.12	-0.10	0.07	-0.16	-0.19	0.08
Dia1	0.64	0.69	0.42	0.25	0.09	-0.03	-0.06	-0.11	-0.16	NaN	0.24	0.00	-0.10	-0.25	NaN
Ccr4	0.10	-0.14	0.08	0.05	-0.09	-0.08	NaN	0.10	-0.20	0.03	-0.28	NaN	-0.51	-0.24	0.08
Xrn1	0.43	0.15	0.34	0.27	0.25	0.09	0.00	-0.01	0.00	-0.11	0.05	-0.07	-0.22	-0.05	-0.27
Srp1	0.98	0.42	NaN	0.39	0.30	0.02	-0.03	0.04	-0.03	-0.03	0.15	-0.04	-0.05	0.08	0.10
Gis2	0.25	0.08	NaN	0.40	0.12	-0.66	-0.30	-0.36	-0.28	-0.20	-0.28	-0.10	-0.02	0.06	-0.21
His6	0.73	0.43	-0.04	0.30	0.33	-0.18	-0.09	0.14	-0.06	0.15	-0.22	0.02	0.31	0.15	-0.05
Shs1	0.72	0.72	0.41	0.68	0.71	0.01	0.12	-0.05	NaN	-0.31	-0.14	0.03	-0.44	NaN	-0.53
Mbf1	0.97	0.89	0.76	0.66	0.82	0.11	0.15	0.15	0.10	0.31	0.33	0.35	0.38	0.38	0.35
Spt5	0.39	0.92	0.32	0.10	0.37	-0.13	-0.04	-0.08	-0.05	-0.08	0.00	-0.30	-0.02	-0.22	0.05
New1	0.85	0.49	0.63	0.00	0.02	-0.19	-0.16	-0.11	-0.18	-0.29	-0.01	0.07	-0.01	-0.04	0.22
Ent3	0.70	0.86	1.07	1.20	0.73	-0.20	-0.06	0.13	0.04	-0.01	-0.10	0.40	0.44	0.39	0.22
no proteome value, but biotin site(s) identified															
Syh1	0.67	0.58	0.23	0.39	0.87	NaN	NaN	NaN	NaN	NaN	NaN	NaN	NaN	NaN	NaN
neither proteome value nor biotin site identified															
Smy2	0.33	0.47	0.30	0.70	0.73	NaN	NaN	NaN	NaN	NaN	NaN	NaN	NaN	NaN	NaN
Hel2	1.62	0.99	NaN	-0.11	1.08	NaN	NaN	NaN	NaN	NaN	NaN	NaN	NaN	NaN	NaN
Sas10	1.67	1.01	1.32	NaN	NaN	NaN	NaN	NaN	-0.17	NaN	NaN	NaN	NaN	-0.24	NaN
Rsc58	NaN	0.49	0.93	0.72	1.12	-0.55	0.08	NaN	NaN	NaN	-0.23	-0.31	NaN	NaN	NaN

Tab. S8: Positions of biotinylated lysine residues of dynamic Asc1p-neighbors during glucose starvation. The position(s) of biotinylated lysine residues within the amino acid sequence of dynamic Asc1p-neighbors during glucose starvation are listed. Modified lysine residues only identified with the MaxQuant/Perseus software are labeled in red, those only identified with the Proteome Discoverer™ software in blue.

Protein	biotinylated lysine residue(s)
proteome-corrected and biotin site(s) identified	
Rpl12	31
Eft1	50
Lsm12	80
Rpa190	877
Rps20	6; 8; 30; 32
Stm1	23; 27; 171; 184; 192; 260
Rpg1	599; 709
Sro9	25; 27
Psp2	193; 290; 295
Asc1	40; 53; 62; 87; 107; 117; 118; 137; 161; 176; 179; 228; 229
Bre5	214
Def1	141; 200; 214; 228; 257
Pbp4	65
Scp160	79; 890; 1000
no proteome value, but biotin site identified	
Syh1	555

Tab. S9: SILAC-based comparison of natural biotinylation targets in glucose starved and non-starved *S. cerevisiae* cells. The enrichment of natural biotinylation targets was compared from the *ASC1-birA** strain cultivated in the absence of glucose against the same strain grown exponentially. The colors represent the values of the mean SILAC ratios (white = Not a Number). All naturally biotinylated *S. cerevisiae* proteins were unaffected by glucose starvation with a $\log_2$ SILAC ratio between -0.26 and 0.26. SILAC quantification was performed with the MaxQuant/Perseus software. Abbreviations: SD = standard deviation; E-P = enrichment value - proteome value.

Protein	mean	SD	*ASC1-birA*(-glc)/ ASC1-birA*(+glc)* E-P					*ASC1-birA*(-glc)/ ASC1-birA*(+glc)* enrichment					*ASC1-birA*(-glc)/ ASC1-birA*(+glc)* proteome					Biotin site position(s)
			1	2	3	4	5	1	2	3	4	5	1	2	3	4	5	
Acc1	0.04	0.09																735; 2061
Ade2	-0.11	0.29																388; 558
Arc1	0.02	0.10																86; 89; 218
Dur1,2	-0.09	0.39																1798
Hfa1	0.06	0.23																804
Pyc1	0.07	0.06																19; 1124; 1135
Pyc2	0.08	0.10																20; 1125; 1136

Tab. S10: Alterations of total cellular protein abundances in the heat-stressed *ASC1-birA** strain in comparison to its equivalent grown at 30°C reflect the elevated temperature. Total cellular protein abundances were compared from the heat-stressed *ASC1-birA** strain against the same strain grown at 30°C. Proteins with a $\log_2$ SILAC ratio ≥ 0.26 in at least two out of three biological replicates in this comparison were considered as heat-specifically up-regulated on the whole proteome level. The colors represent the values of the mean SILAC ratios. A selection of respective proteins is listed with their elemental molecular function according to the Gene Ontology assignment. SILAC quantification was performed with the MaxQuant/Perseus software. Abbreviations: SD = standard deviation; NaN = Not a Number.

Protein	*ASC1-birA**(37°C)/ *ASC1-birA** proteome					Gene ontology (molecular function)
	mean	SD	1	2	3	
Hsp26	**2.71**	0.41	2.50	3.18	2.44	unfolded protein binding; mRNA-binding
Hsp82	**1.57**	0.10	1.69	1.54	1.49	unfolded protein binding; ATP binding
Hsp104	**1.56**	0.08	1.65	1.56	1.49	chaperone binding; unfolded protein binding; ATP binding
Ssa1	**1.56**	0.08	1.60	1.62	1.47	unfolded protein binding; ATPase activity
Aha1	**1.14**	0.13	1.29	1.04	1.09	chaperone binding
Cpr6	**0.97**	0.06	0.99	1.02	0.91	unfolded protein binding
Hsp78	**0.87**	0.11	0.75	0.95	0.92	misfolded protein binding; ATPase activity
Hch1	**0.75**	0.14	0.61	0.76	0.88	chaperone binding; ATPase activator activity
Sti1	**0.70**	0.04	0.73	0.66	0.71	Hsp70 protein binding; Hsp90 protein binding
Hsp10	**0.65**	0.15	0.68	0.49	0.78	chaperone binding; unfolded protein binding; ATP binding
Hsc82	**0.63**	0.07	0.70	0.58	0.60	unfolded protein binding; ATPase activity
Hsp60	**0.62**	0.02	0.62	0.64	0.60	chaperone binding; unfolded protein binding; ATPase activity
Kar2	**0.61**	0.08	0.57	0.70	0.57	unfolded protein binding; ATPase activity
Ssa2	**0.61**	0.04	0.64	0.62	0.57	unfolded protein binding; ATPase activity
Sis1	**0.53**	0.05	0.59	0.52	0.49	misfolded protein binding; DNA binding
Ubc4	**0.47**	0.26	0.43	0.74	0.22	protein binding; ubiquitin binding

Tab. S11: SILAC-based identification of dynamic Asc1p-neighbors during heat stress. Proteins enriched from heat-stressed *ASC1-birA** cells with a log$_2$ SILAC ratio ≥ 0.26 against the *ASC1-birA** reference strain (30°C) and against the *birA** negative control strain in at least two out of three biological replicates were considered as heat-specifically enriched in the Asc1p-neighborhood. The ratios were normalized against the respective proteome value (if available). Mean values and standard deviations (SD) of log$_2$ SILAC ratios are listed. Additionally, SILAC ratios (enrichment ratio, proteome ratio and enrichment-proteome ratio (E-P)) are given for each replicate individually. Candidates are listed according to the mean *ASC1-birA**(37°C)/*ASC1-birA**(30°C) ratio in a descending mode and according to the availability of a proteome value and biotin site(s). Proteins that were identified as Asc1p-neighbors during exponential growth are listed in bold. The colors represent the values of the mean SILAC ratios. SILAC quantification and statistical analyses were performed with the MaxQuant/Perseus software. Abbreviations: NaN = Not a Number.

Tab. S11.

Protein	mean and SD of log₂ SILAC ratios				ASC1-birA*(37°C)/ ASC1-birA*(30°C) E-P			ASC1-birA*(37°C)/ birA*(37°C) E-P			ASC1-birA*(37°C)/ ASC1-birA*(30°C) enrichment			ASC1-birA*(37°C)/ birA*(37°C) enrichment			ASC1-birA*(37°C)/ ASC1-birA*(30°C) proteome			ASC1-birA*(37°C)/ birA*(37°C) proteome		
	/ASC1-birA*	SD	/birA*(37°C)	SD	1	2	3	1	2	3	1	2	3	1	2	3	1	2	3	1	2	3
proteome-corrected and biotin site(s) identified																						
Scp160	0.85	0.11	3.00	0.02	0.90	0.93	0.73	3.01	3.00	2.98	0.91	0.90	0.72	2.85	2.85	2.87	0.00	-0.03	-0.01	-0.15	-0.16	-0.11
Stm1	0.70	0.07	0.88	0.05	0.76	0.62	0.73	0.85	0.93	0.84	0.74	0.48	0.76	0.60	0.52	0.67	-0.02	-0.14	0.03	-0.42	-0.25	-0.17
Psp2	0.68	0.22	0.66	0.42	NaN	0.83	0.52	NaN	0.95	0.36	0.61	0.64	0.55	1.05	1.19	0.81	NaN	-0.19	0.03	0.24	NaN	0.44
Sro9	0.32	0.04	1.64	0.10	0.35	0.34	0.28	1.65	1.74	1.53	0.37	0.23	0.22	2.16	1.94	1.88	0.02	-0.11	-0.06	0.20	0.51	0.35
Rps20	0.27	0.04	0.70	0.22	0.30	0.23	0.30	0.79	0.45	0.86	0.22	0.19	0.29	0.76	0.51	0.86	-0.08	-0.04	0.00	0.06	-0.03	0.00
Def1	0.25	0.24	3.55	0.73	0.44	-0.02	0.32	4.22	2.77	3.67	0.47	0.35	0.22	3.35	2.90	3.42	0.03	0.37	-0.10	0.13	-0.86	-0.25
proteome-corrected, but no biotin site identified																						
Hek2	1.06	0.29	0.22	0.16	1.31	0.75	1.12	0.34	0.28	0.03	1.12	0.70	1.19	0.22	0.08	-0.19	-0.19	-0.04	0.08	-0.20	-0.12	-0.22
Xrn1	0.60	0.08	0.27	0.32	0.67	0.62	0.52	0.27	0.58	-0.05	0.58	0.63	0.65	-0.05	0.33	0.19	-0.09	0.01	0.13	-0.25	-0.32	0.24
Rpg1	0.52	0.05	0.80	0.22	0.55	0.47	0.55	0.60	0.76	1.04	0.50	0.48	0.47	0.89	0.90	1.19	-0.05	0.02	-0.08	0.14	0.29	0.15
New1	0.46	0.09	0.50	0.12	0.38	0.55	0.47	0.54	0.60	0.36	0.28	0.46	0.35	0.45	0.48	0.32	-0.10	-0.09	-0.12	-0.12	-0.08	-0.04
Pst2	0.25	0.13	0.64	0.29	0.38	0.11	0.26	0.52	0.43	0.97	0.62	0.30	0.55	0.31	0.23	0.79	0.25	0.19	0.28	-0.20	-0.21	-0.18
no proteome value, but biotin site(s) identified																						
Ubp2	0.45	0.15	0.74	0.24	NaN	NaN	NaN	NaN	NaN	NaN	0.59	0.47	0.30	1.01	0.66	0.54	NaN	NaN	NaN	NaN	NaN	NaN
Bre5	0.45	0.17	0.69	0.04	NaN	NaN	NaN	NaN	NaN	NaN	0.64	0.30	0.41	0.65	0.73	0.68	NaN	NaN	NaN	NaN	NaN	NaN
neither proteome value nor biotin site identified																						
Tma46	0.60	0.10	0.46	0.14	NaN	NaN	NaN	NaN	NaN	NaN	0.66	0.53	NaN	0.36	0.55	NaN	NaN	NaN	NaN	NaN	NaN	NaN
Sas10	0.57	0.06	1.13	0.11	NaN	NaN	NaN	NaN	NaN	NaN	0.62	0.53	NaN	1.06	1.21	NaN	NaN	NaN	NaN	NaN	NaN	NaN
Syh1	0.52	0.08	1.72	0.06	NaN	NaN	NaN	NaN	NaN	NaN	0.50	0.60	0.45	1.65	1.73	1.77	NaN	NaN	NaN	NaN	NaN	NaN
Smy2	0.47	0.21	1.41	0.18	NaN	NaN	NaN	NaN	NaN	NaN	0.37	0.70	0.32	1.24	1.60	1.38	NaN	NaN	NaN	NaN	NaN	NaN
Spt5	0.44	0.04	0.39	0.09	0.66	NaN	NaN	0.63	NaN	NaN	0.47	0.42	NaN	0.33	0.46	NaN	-0.18	NaN	NaN	-0.30	NaN	NaN
Ubp3	0.36	0.09	0.81	0.13	0.11	NaN	NaN	1.36	NaN	NaN	0.25	0.44	0.38	0.76	0.96	0.72	0.15	NaN	NaN	-0.60	NaN	NaN
Dia1	0.30	0.15	0.65	0.55	NaN	NaN	NaN	NaN	NaN	NaN	0.15	0.46	0.29	0.12	1.22	0.59	NaN	NaN	NaN	NaN	NaN	NaN
Pbp4	0.29	0.01	2.40	0.30	0.57	NaN	NaN	3.11	NaN	NaN	0.28	0.28	0.30	2.73	2.28	2.17	-0.29	NaN	NaN	-0.37	NaN	NaN
Gis2	0.25	0.12	0.34	0.11	0.55	NaN	NaN	0.48	NaN	NaN	0.31	0.11	0.33	0.41	0.39	0.21	-0.25	NaN	NaN	-0.06	NaN	NaN

Tab. S12: Positions of biotinylated lysine residues of dynamic Asc1p-neighbors during heat stress.
The position(s) of biotinylated lysine residues within the amino acid sequence of dynamic Asc1p-neighbors during heat stress are listed. Modified lysine residues only identified with the MaxQuant/Perseus software are labeled in red, those only identified with the Proteome Discoverer™ software in blue.

Protein	biotinylated lysine residue(s)
proteome-corrected and biotin site(s) identified	
Scp160	71; 79; 890
Stm1	23; 27; 184; 260
Psp2	290; 295
Sro9	27
Rps20	6; 8
Def1	141; 214
no proteome value, but biotin site(s) identified	
Ubp2	1145
Bre5	214

Tab. S13: SILAC-based comparison of natural biotinylation targets in heat-stressed and non-stressed *S. cerevisiae* cells. The enrichment of natural biotinylation targets was compared from the *ASC1-birA** strain cultivated at 37°C against the same strain grown at 30°C. The colors represent the values of the mean SILAC ratios (white = Not a Number). All naturally biotinylated proteins of *S. cerevisiae* were unaffected by heat stress with $\log_2$ SILAC ratios between -0.26 and 0.26. SILAC quantification was performed with the MaxQuant/Perseus software. Abbreviations: SD = standard deviation; E-P = enrichment value - proteome value.

Protein	mean	SD	*ASC1-birA**(37°C)/ *ASC1-birA**(30°C) E-P			*ASC1-birA**(37°C)/ *ASC1-birA**(30°C) enrichment			*ASC1-birA**(37°C)/ *ASC1-birA**(30°C) proteome			Biotin site position(s)
			1	2	3	1	2	3	1	2	3	
Acc1	-0.03	0.05										735
Ade2	0.13	0.06										
Arc1	0.01	0.08										86; 89
Dur1,2	0.07	0.10										1798; 1807
Hfa1	0.03	0.08										804
Pyc1	0.08	0.06										1135
Pyc2	-0.01	0.12										1125; 1136

Tab. S14: SILAC-based analysis of the proteinaceous Asc1^DEp-neighborhood in comparison to wt-Asc1p. Proteins enriched from *asc1^DE-birA** cells with a $\log_2$ SILAC ratio ≥ 0.26 against the *ASC1-birA** reference strain were considered as DE-specific neighbors; proteins with a $\log_2$ SILAC ratio ≤ -0.26 as distanced from Asc1^DEp compared to wt-Asc1p. A $\log_2$ SILAC ratio ≥ 0.26 against the *birA**

negative control strain was required in both cases in at least three out of five biological replicates. The ratios were normalized against the respective proteome value (if available). Mean values and standard deviations (SD) of $\log_2$ SILAC ratios are listed. Additionally, SILAC ratios (enrichment ratio, proteome ratio and enrichment-proteome ratio (E-P)) are given for each replicate individually. Candidates are listed according to the mean $asc1^{DE}$-birA*/ASC1-birA* ratio in a descending mode and according to the availability of a proteome value and biotin site(s). Proteins that were identified as Asc1p-neighbors during exponential growth are listed in bold. The colors represent the values of the mean SILAC ratios. SILAC quantification and statistical analyses were performed with the MaxQuant/Perseus software. Abbreviations: NaN = Not a Number.

Protein	mean and SD of log₂ SILAC ratios				$asc1^{DE}$-birA*/ASC1-birA* E-P			$asc1^{DE}$-birA*/birA* E-P			$asc1^{DE}$-birA*/ASC1-birA* enrichment			$asc1^{DE}$-birA*/birA* enrichment			$asc1^{DE}$-birA*/ASC1-birA* proteome			$asc1^{DE}$-birA*/birA* proteome		
	/ASC1-birA*	SD	/birA*	SD	1	2	3	1	2	3	1	2	3	1	2	3	1	2	3	1	2	3
proteome-corrected and biotin site(s) identified																						
Asc1	**2.90**	0.29	**5.67**	0.45	3.15	2.96	2.58	6.06	5.18	5.76	2.68	2.58	2.14	5.20	4.93	5.92	-0.47	-0.38	-0.44	-0.86	-0.25	0.16
Ssa1	**1.17**	0.17	**0.70**	0.11	1.08	1.07	1.37	0.62	0.77	NaN	1.48	1.28	1.64	1.45	1.63	NaN	0.40	0.21	0.28	0.83	0.85	0.82
Imd3	**0.42**	0.14	**0.36**	0.26	0.26	0.51	0.50	0.35	0.63	0.10	0.37	0.53	0.56	0.38	0.56	0.12	0.10	0.02	0.06	0.03	-0.07	0.02
Cdc33	**-0.28**	0.10	**0.67**	0.09	-0.30	-0.17	-0.36	0.78	0.64	0.60	-0.31	-0.10	-0.28	0.77	0.71	0.65	-0.01	0.07	0.08	-0.01	0.07	0.05
Lsm12	**-0.77**	0.07	**0.59**	0.13	-0.70	-0.78	-0.84	0.73	0.54	0.48	-0.79	-0.81	-0.80	0.75	0.59	0.52	-0.09	-0.03	0.04	0.02	0.05	0.04
proteome-corrected, but no biotin site(s) identified																						
Fmp52	**1.50**	0.28	**1.57**	0.37	1.21	1.76	1.54	1.38	1.99	1.34	1.14	1.84	1.36	1.29	2.00	1.11	-0.07	0.08	-0.18	-0.09	0.01	-0.22
Ham1	**1.42**	0.25	**0.89**	0.26	1.20	1.69	1.37	1.13	0.91	0.62	1.16	1.69	1.39	1.33	1.20	0.94	-0.03	0.00	0.02	0.20	0.29	0.32
Pre9	**1.13**	0.20	**0.00**	0.55	1.06	1.36	0.98	0.32	0.31	-0.63	1.08	1.41	1.06	0.35	0.64	-0.45	0.02	0.05	0.09	0.03	0.33	0.18
Gcd1	**1.10**	0.19	**0.52**	0.09	1.23	0.97	NaN	0.46	0.58	NaN	1.01	1.18	1.25	0.48	0.58	0.05	-0.22	0.22	NaN	0.02	0.00	NaN
Sec14	**1.08**	0.15	**0.37**	0.14	0.95	1.05	1.25	0.29	0.53	0.28	0.91	0.98	1.11	0.36	0.61	0.32	-0.05	-0.07	-0.14	0.08	0.08	0.04
Trr1	**1.05**	0.11	**0.42**	0.26	0.92	1.14	1.08	0.47	0.65	0.13	0.94	1.16	0.94	0.44	0.66	0.06	0.02	0.02	-0.15	-0.03	0.01	-0.07
Tma20	**0.81**	0.11	**0.46**	0.04	0.89	0.73	NaN	0.48	0.43	NaN	0.90	0.80	NaN	0.54	0.67	NaN	0.01	0.07	-0.15	0.06	0.24	0.05
Rpt3	**0.74**	0.23	**0.79**	0.39	0.87	0.88	0.48	0.84	1.14	0.37	0.72	1.04	0.55	0.82	1.22	0.31	-0.15	0.16	0.08	-0.02	0.08	-0.06
Por1	**0.65**	0.12	**0.33**	0.36	0.63	0.78	0.53	0.42	0.64	-0.06	0.52	0.73	0.44	0.14	0.36	-0.24	-0.10	-0.05	-0.10	-0.28	-0.27	-0.18
Tif6	**0.63**	0.30	**1.37**	0.46	0.42	0.84	NaN	1.05	1.69	NaN	0.32	0.73	NaN	1.27	1.88	NaN	-0.09	-0.11	-0.12	0.23	0.18	0.15
Ynk1	**0.53**	0.34	**0.42**	0.29	0.59	0.84	0.18	0.59	0.59	0.08	0.46	0.72	0.18	0.42	0.45	-0.02	-0.13	-0.12	0.00	-0.17	-0.14	-0.10
Rpt6	**0.40**	0.27	**0.43**	0.29	0.18	0.71	0.33	0.10	0.67	0.52	0.37	0.96	0.47	0.13	0.77	0.18	0.20	0.25	0.13	0.02	0.11	-0.34
Rpl10	**0.40**	0.15	**0.34**	0.12	0.27	0.56	0.38	0.31	0.48	0.25	0.22	0.55	0.38	0.32	0.45	0.24	-0.05	-0.01	0.00	0.01	-0.03	-0.02
Rps11	**0.30**	0.03	**0.41**	0.29	0.33	0.30	0.27	0.74	0.19	0.30	0.26	0.25	0.25	0.76	0.22	0.37	-0.07	-0.05	-0.02	0.02	0.03	0.07
Pst2	**-0.38**	0.07	**0.56**	0.17	-0.35	-0.33	-0.46	0.70	0.59	0.37	-0.35	-0.49	-0.54	0.69	0.51	0.36	0.00	-0.16	-0.08	-0.01	-0.08	-0.01
Atp7	**-0.45**	0.47	**0.73**	0.21	0.07	-0.83	-0.59	0.54	0.95	0.70	-0.03	-1.02	-0.78	0.30	0.70	0.27	-0.10	-0.19	-0.19	-0.24	-0.26	-0.43
no proteome value, but biotin site(s) identified																						
Dur1,2	**0.71**	0.09	**1.14**	0.16	NaN	NaN	NaN	NaN	NaN	NaN	0.69	0.81	0.64	1.26	1.20	0.96	NaN	NaN	NaN	NaN	NaN	NaN
Not3	**0.19**	0.13	**0.24**	0.38	NaN	NaN	NaN	NaN	NaN	NaN	0.27	0.27	0.04	0.41	0.50	-0.19	NaN	NaN	NaN	NaN	NaN	NaN
neither proteome value nor biotin site identified																						
Coq5	**6.75**	0.54	**4.34**	0.41	NaN	1.17	NaN	NaN	-1.18	NaN	NaN	7.13	6.37	NaN	4.05	4.63	6.11	5.97	NaN	4.38	5.23	NaN
Rtt10	**1.35**	0.36	**1.11**	0.54	NaN	NaN	NaN	NaN	NaN	NaN	1.01	1.32	1.72	1.18	1.61	0.54	NaN	NaN	NaN	NaN	NaN	NaN
Mot2	**0.29**	0.45	**0.83**	0.43	NaN	NaN	NaN	NaN	NaN	NaN	0.57	0.53	-0.23	0.96	1.17	0.35	NaN	NaN	NaN	NaN	NaN	NaN
Yor385W	**-0.40**	0.15	**0.47**	0.32	NaN	NaN	NaN	NaN	NaN	NaN	-0.35	-0.57	-0.29	0.83	0.37	0.21	NaN	NaN	NaN	NaN	NaN	NaN
Nan1	**-0.48**	0.45	**0.42**	0.21	NaN	NaN	NaN	NaN	NaN	NaN	-0.94	-0.46	-0.04	0.35	0.65	0.25	NaN	NaN	NaN	NaN	NaN	NaN

Tab. S15: Positions of biotinylated lysine residues of Asc1^{DE}p-neighbors. The position(s) of biotinylated lysine residues within the amino acid sequence of Asc1^{DE}p-neighbors are listed. Modified lysine residues only identified with the MaxQuant/Perseus software are labeled in red, those only identified with the Proteome Discoverer^{TM} software in blue.

| Protein	biotinylated lysine residue(s)
proteome-corrected and biotin site(s) identified	
Asc1	53; 62; 87; 107; 117; 118; 132; 137; 161; 176; 179; 228; 229; 283
Ssa1	504
Imd3	426; 430
Cdc33	8; 24
Lsm12	80
no proteome value, but biotin site(s) identified	
Dur1,2	1798; 1807
Not3	816; 823

Fig. S2.

150
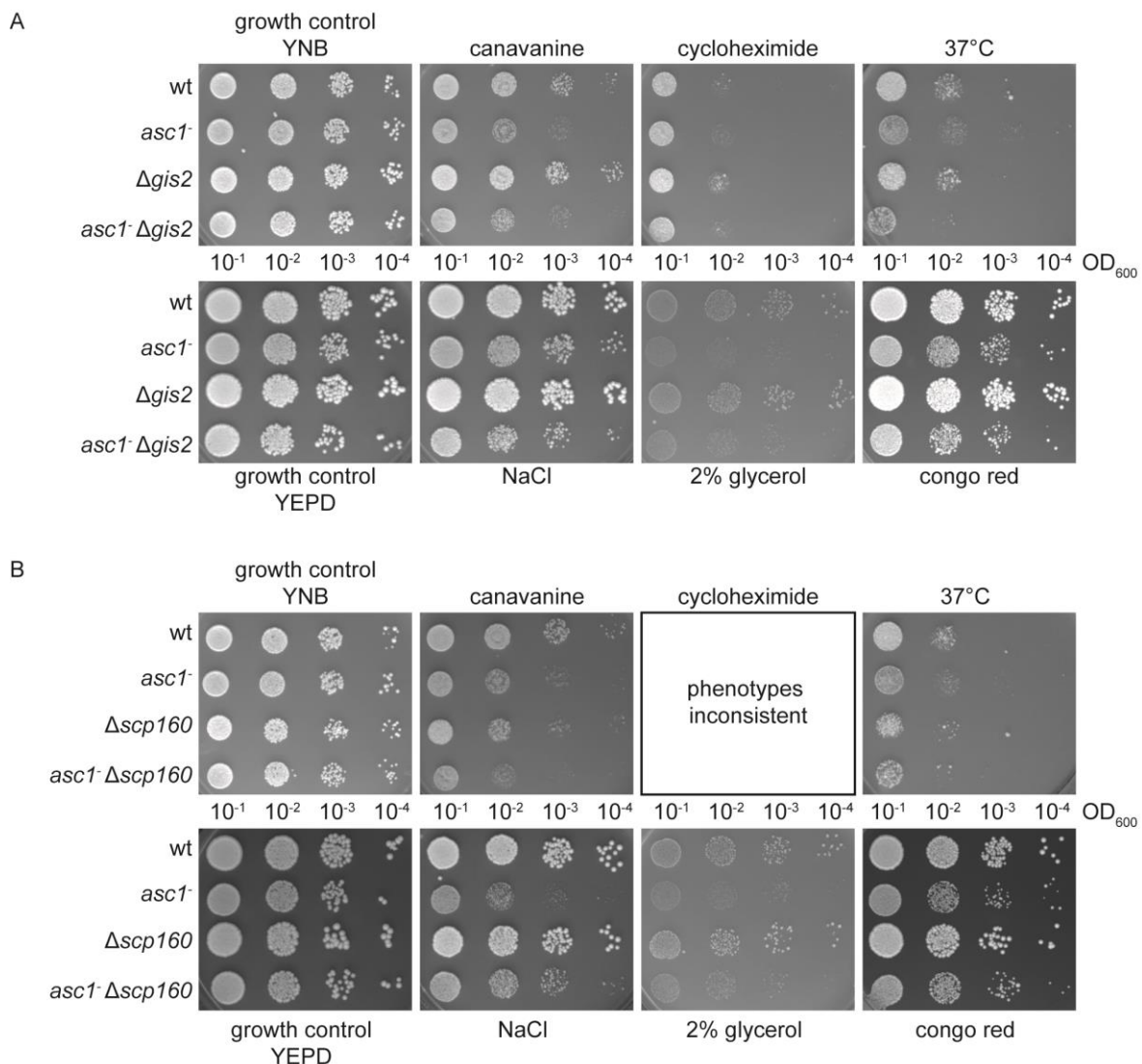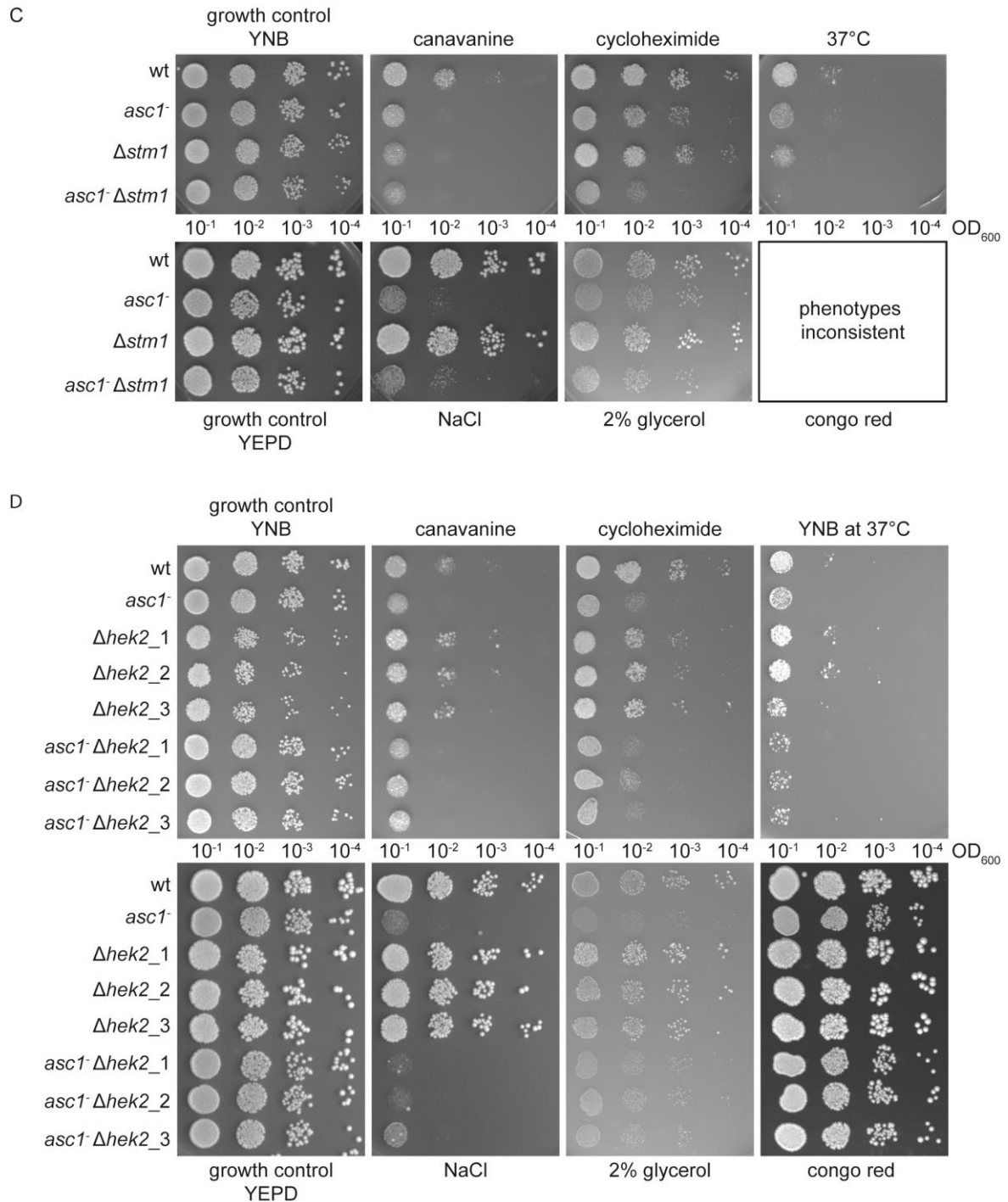
Fig. S2: Double mutant strains lacking Asc1p and Gis2p, Scp160p, Stm1p or Hek2p, respectively, are mostly unobtrusive regarding *asc1⁻*-phenotypes. For drop dilution assays 10-fold dilution series of cell suspensions from the wt-*ASC1*, *asc1⁻*, (A) Δ*gis2*, (B) Δ*scp160*, (C) Δ*stm1,* (D) Δ*hek2*, and the respective double mutant strains were spotted on YNB agar plates containing canavanine (600 ng/ml), cycloheximide (0.15 µg/ml), and on YNB plates that were incubated at 37°C. Cells were also dropped on YEPD plates with NaCl (75 mM) or with congo red (125 µg/ml) and on YEP plates with 2% glycerol instead of glucose. A YNB and a YEPD agar plate were used for growth control and all plates were photographed after three to five days of growth. For each single and double mutant strain at least 3 individual clones were tested, however, only one is depicted in A-C, all three are shown in D.

Abbreviations

3-AT	3-amino-1,2,4-triazole
3D	3-dimensional
ABA	abscisic acid
AMP	adenosine monophosphat
ATP	adenosine triphosphat
bp	base pair(s)
BioID	proximity-dependent biotin identification
BirA*	BirA^{R118G}
Bpa	ρ-benzoyl-phenylalanine
BSA	bovine serum albumin
cAMP	cyclic adenosine monophosphat
cDNA	complementary DNA
CID	collision-induced dissociation
C-terminus/-terminal	Carboxy-terminus/-terminal
DAPA	7,8-diaminopelargonic acid
DE	R38D K40E
DNA	deoxyribonucleic acid
DTB	desthiobiotin
DTT	dithiothreitol
EDTA	ethylenediaminetetraacetic acid
e.g.	for example
EGP granule	eIF4E, eIF4G, Pab1p granule
EGTA	ethylene glycol tetraacetic acid
eIF	eukaryotic initiation factor
EM	electron micscroscopy
ER	endoplasmatic reticulum
et al.	et alii
FACT	facilitates chromatin transcription
Fig.	figure
FT	fourier transform
fw	forward
G_1/G_2	gap phase 1/gap phase 2
GDP	guanosine diphosphate

glc	glucose
GPCR	G-protein coupled receptor
GTP	guanosine triphosphate
h	hour(s)
HRP	horseradish peroxidase
IP	interaction partner
IRES	internal ribosomal entry site
KAPA	7-keto-8-aminopelargonic acid
KH domain	K-homology domain
LB	lysogeny broth
LC	liquid chromatography
M	mitosis
MAPK	mitogen activated protein kinase
MAP2K	mitogenn activated protein kinase kinase
MAP3K	mitogen activated protein kinase kinase kinase
MAP4K	mitogen activated protein kinase kinase kinase kinase
min	minute(s)
miRISC	miRNA-induced silencing complex
miRNA	micro RNA
mRNA	messenger RNA
mRNP	messenger ribonucleoprotein
MS	mass spectrometry
NaN	not a number
NMD	nonsense mediated decay
NMDA	*N*-methyl-D-aspartate
NMDAR	*N*-methyl-D-aspartate receptor
NO	nitric oxide
N-terminus/terminal	amino-terminus/-terminal
NTP	nucleoside-triphosphate
OD	optical density
o/n	overnight
ORF	open reading frame
PABP	poly(A)-binding protein
PAGE	polyacrylamide gel electrophoresis

PAN	poly(A) nuclease
P-body	processing body
PBS	phosphate buffered saline
PCR	polymerase chain reaction
PEG	polyethylene glycol
PIC	pre-initiation complex
PKA	protein kinase A
PKC	protein kinase C
PMSF	phenylmethanesulfonyl fluoride
PSM	peptide sequence match
rDNA	ribosomal DNA
RNA	ribonucleic acid
RNAP	RNA polymerase
rpm	rounds per minute
RQC	ribosomal quality control
rRNA	ribosomal RNA
rv	reverse
SD	standard deviation
SDS	sodium dodecyl sulfate
sec	seconds
SESA	Scp160p, Eap1p, Smy2p, Asc1p
SILAC	stable isotope labeling with amino acids in cell culture
snoRNA	small nucleolar RNA
SOB	super optimal broth
Tab.	table
TAE	tris base, acetic acid, EDTA
TB	transformation buffer
TBS	tris buffered saline
TC	ternary complex
TCA	trichloracetic acid
TE	tris, EDTA
TFA	trifluoracetic acid
Tris	tris(hydroxymethyl)aminomethane
tRNA	transfer RNA

tRNA$_i$	initiator tRNA
uORF	upstream open reading frame
UTR	untranslated region
UV	ultraviolet
V	volume
WD	tryptophane aspartate
wt	wild type
YEPD	yeast extract peptone dextrose
YNB	yeast nitrogen base